Non-minimal supersymmetric models: LHC phenomenology and model discrimination

Dissertation zur Erlangung des
naturwissenschaftlichen Doktorgrades
der Julius-Maximillians-Universität Würzburg

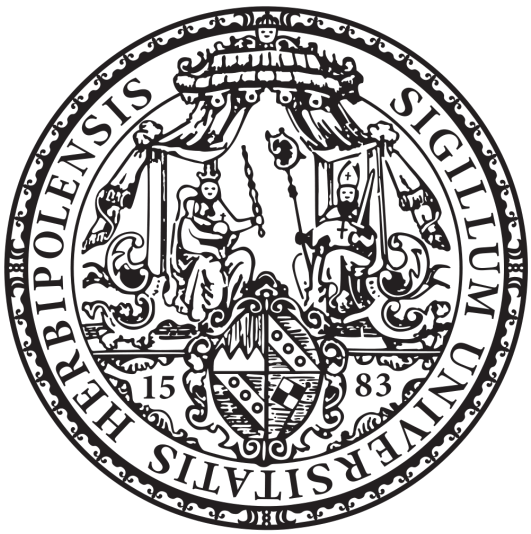

vorgelegt von

Manuel Ernst Krauß

aus Ochsenfurt

Würzburg, 2015

Eingereicht am 22. September 2015

bei der Fakultät für Physik und Astronomie

1. Gutachter: Prof. Dr. Werner Porod

2. Gutachter: Prof. Dr. Raimund Ströhmer

3. Gutachter: _____

der Dissertation

Vorsitzende(r): Prof. Dr. Randolf Hanke

1. Prüfer: Prof. Dr. Werner Porod

2. Prüfer: Prof. Dr. Raimund Ströhmer

3. Prüfer: Prof. Dr. Matthias Kadler

im Promotionskolloquium

Tag des Promotionskolloquiums: 18. Dezember 2015

Doktorurkunde ausgehändigt am: _____

Wo kämen wir hin, wenn jeder sagte,
wo kämen wir hin und keiner ginge,
um zu sehen, wohin wir kämen, wenn
wir gingen.

Kurt Marti

LIST OF PUBLICATIONS

In the context of the present thesis, the following papers were published.

Journal articles

1. M. E. Krauss and W. Porod, *Is the CMS eejj excess a hint for light supersymmetry?*, *Phys.Rev.* **D92**, 055019 (2015), [arXiv:1507.04349].

2. M. D. Goodsell, M. E. Krauss, T. Müller, W. Porod, and F. Staub, *Dark matter scenarios in a UV-complete model with Dirac gauginos*, *JHEP* **1510**, 132 (2015), [arXiv:1507.01010].

3. L. Basso, B. Fuks, M. E. Krauss, and W. Porod, *Doubly-charged Higgs and vacuum stability in left-right supersymmetry*, *JHEP* **1507**, 147 (2015), [arXiv:1503.08211].

4. A. Abada, M. E. Krauss, W. Porod, F. Staub, A. Vicente, and C. Weiland, *Lepton flavor violation in low-scale seesaw models: SUSY and non-SUSY contributions*, *JHEP* **1411**, 048 (2014), [arXiv:1408.0138].

5. M. E. Krauss, W. Porod, F. Staub, A. Abada, A. Vicente, and C. Weiland, *Decoupling of heavy sneutrinos in low-scale seesaw models*, *Phys.Rev.* **D90**, 013008 (2014), [arXiv:1312.5318].

6. M. E. Krauss, W. Porod, and F. Staub, $SO(10)$ *inspired gauge-mediated supersymmetry breaking*, *Phys.Rev.* **D88**, 015014 (2013), [arXiv:1304.0769].

Working group reports

1. G. Brooijmans, R. Contino, B. Fuks, F. Moortgat *et. al*, *Les Houches 2013: Physics at TeV colliders – New Physics working group report*
   Contribution **15**: A. Alloul, L. Basso, B. Fuks, M. E. Krauss, and W. Porod, *Reviving Minimal Left-Right Supersymmetry in the Light of LHC Data*, [arXiv:1405.1617].

KURZZUSAMMENFASSUNG

Man ist sich einig darüber, dass das Standardmodell der Teilchenphysik in seiner aktuellen Form nicht der Weisheit letzter Schluss ist – zu viele grundlegende Fragen lässt es offen. Lediglich die genaue Form der nötigen Erweiterung wird heiß debattiert. Supersymmetrische Modelle gehören zu den vielversprechendsten Ansätzen zu Physik jenseits des Standardmodells, da sie gleichzeiting das Hierarchieproblem lösen und die Dichte der beobachteten dunklen Materie im Universum erklären können. Obwohl das minimale supersymmetrische Modell weitere Vorzüge vorzuweisen hat – hierzu gehört die Vereinheitlichung der Eichkopplungen an großen Skalen sowie radiative elektroschwache Symmetriebrechung – sprechen die aktuellen Messungen am LHC eine andere Sprache. Zudem sind auch in diesem Modell die Neutrinos masselos, sodass es nicht die endgültige Theorie darstellen kann. Dies mindert jedoch nicht die Schönheit des Konzepts der Supersymmetrie, weshalb es an der Zeit ist, nichtminimale supersymmetrische Modelle zu untersuchen, welche die o. g. Probleme nicht aufweisen. Diese Modelle müssen auf Herz und Nieren geprüft werden, bevor man sie mit experimentellen Daten vergleichen und Vorhersagen für zukünftige Experimente treffen kann.

Das Ziel dieser Arbeit ist es, zu diesem wichtigen Prozess beizutragen. Hierzu soll die besonders aussichtsreiche Klasse von supersymmetrischen Modellen, welche auf einer links-rechts-Eichsymmetrie basieren, genau untersucht werden. Diese Modelle sind deutlich weniger von LHC-Ausschlussgrenzen betroffen und sagen zudem rechtshändige Neutrinos voraus, mit welchen die leichten Neutrinomassen erklärt werden können.

Zu Beginn wenden wir uns einem links-rechts-supersymmetrischen Modell an der TeV-Skala zu, in welchem $SU(2)_R$-Tripletts sowohl für die Brechung der Links-Rechts-Symmetrie als auch für die Generation von Neutrinomassen verantwortlich sind. Zur führenden Ordnung in der Störungstheorie beinhaltet diese Art von Modellen ein tachyonisches doppelt geladenes Skalarfeld. Wir wenden uns der Ermittlung der zugehörigen Masse auf dem Einschleifenniveau zu und zeigen erstmals in einer konsistenten, vollständigen Berechnung derselben, dass die Masse im Allgemeinen reell ist. Anschließend werden die Beschränkungen an die Links-Rechts-Brechungsskala aus aktuellen LHC-Daten ermittelt. Wir zeigen, dass unser Modell gewisse Signal-Überschüsse in jenen Daten erklären kann – der aktuelle LHC-Lauf wird klären, ob diese tatsächlich neuer Physik oder doch nur statistischen Fluktuationen entsprechen. Schließlich bestimmen wir in einer Untersuchung

der Vakuumstruktur auf dem Einschleifenniveau diejenigen Parameterregionen, in welchen die phänomenologisch korrekte elektroschwache Symmetriebrechung angenommen wird. Passenderweise werden Regionen bevorzugt, welche messbare Signale am LHC vorhersagen.

In einem leicht unterschiedlichen Modell, in dem eine $U(1)_R \times U(1)_{B-L}$ bis herunter an die TeV-Skala überleben kann, implementieren wir einen über Eichwechselwirkungen vermittelten Supersymmetrie-Brechungsmechanismus, mit besonderem Augenmerk auf die eichkinetische Mischung in den Randbedingungen. Durch die erweiterte Eichgruppe wird die Higgsmasse bereits auf führender Ordnung erhöht. Wir ermitteln die Konsequenzen für die Skala der Supersymmetrie-Brechungsskala. Anschließend untersuchen wir die am LHC zu erwartende Phänomenologie und zeigen auf, in welchen Prozessen sich dieses Modell von Standard-Szenarien unterscheidet.

Durch diese Arbeit hinweg nehmen wir an, dass die leichten Neutrinomassen duch einen Seesaw-Mechanismus an der TeV-Skala erklärt werden. Dass dies zu potentiell höchst interessanten Signalen in Niederenergieexperimenten führt, wird im letzten Teil dieser Arbeit thematisiert. Der Fokus liegt hierbei auf Lepton-Flavour-verletzenden Prozessen wie $\mu \to e\,\gamma$, $\mu \to 3\,e$ oder die $\mu - e$-Umwandlung in Atomkernen, welche wir im Rahmen eines supersymmetrischen Modells mit inversem Seesaw-Mechanismus genauer untersuchen. Insbesondere widerlegen wir Behauptungen von nichtentkoppelnden Z-Pinguin-Diagrammen und untersuchen die Aussichten, Signale an zukünftigen Experimenten zu messen sowie Rückschlüsse auf das zugrundeliegende Modell ziehen zu können. In diesem Zusammenhang demonstrieren wir die Möglichkeit, durch die relativen Verhältnisse von Verzweigungsverhältnissen wie $\mathrm{BR}(\tau \to 3\,\mu)/\mathrm{BR}(\tau \to \mu\,e^+e^-)$ unterscheiden zu können, ob die zugehörigen Prozesse hauptsächlich durch supersymmetrische oder durch $W - \nu$-Diagramme herbeigeführt wurden.

ABSTRACT

It is generally agreed upon the fact that the Standard Model of particle physics can only be viewed as an effective theory that needs to be extended as it leaves some essential questions unanswered. The exact realization of the necessary extension is subject to discussion. Supersymmetry is among the most promising approaches to physics beyond the Standard Model as it can simultaneously solve the hierarchy problem and provide an explanation for the dark matter abundance in the universe. Despite further virtues like gauge coupling unification and radiative electroweak symmetry breaking, minimal supersymmetric models cannot be the ultimate answer to the open questions of the Standard Model as they still do not incorporate neutrino masses and are besides heavily constrained by LHC data. This does, however, not derogate the beauty of the concept of supersymmetry. It is therefore time to explore non-minimal supersymmetric models which are able to close these gaps, review their consistency, test them against experimental data and provide prospects for future experiments.

The goal of this thesis is to contribute to this process by exploring an extraordinarily well motivated class of models which bases upon a left-right symmetric gauge group. While relaxing the tension with LHC data, those models automatically include the ingredients for neutrino masses.

We start with a left-right supersymmetric model at the TeV scale in which scalar $SU(2)_R$ triplets are responsible for the breaking of left-right symmetry as well as for the generation of neutrino masses. Although a tachyonic doubly-charged scalar is present at tree-level in this kind of models, we show by performing the first complete one-loop evaluation that it gains a real mass at the loop level. The constraints on the predicted additional charged gauge bosons are then evaluated using LHC data, and we find that we can explain small excesses in the data of which the current LHC run will reveal if they are actual new physics signals or just background fluctuations. In a careful evaluation of the loop-corrected scalar potential we then identify parameter regions in which the vacuum with the phenomenologically correct symmetry-breaking properties is stable. Conveniently, those regions favour low left-right symmetry breaking scales which are accessible at the LHC.

In a slightly modified version of this model where a $U(1)_R \times U(1)_{B-L}$ gauge symmetry survives down to the TeV scale, we implement a minimal gauge-mediated supersymmetry

breaking mechanism for which we calculate the boundary conditions in the presence of gauge kinetic mixing. We show how the presence of the extended gauge group raises the tree-level Higgs mass considerably so that the need for heavy supersymmetric spectra is relaxed. Taking the constraints from the Higgs sector into account, we then explore the LHC phenomenology of this model and point out where the expected collider signatures can be distinguished from standard scenarios.

In particular if neutrino masses are explained by low-scale seesaw mechanisms as is done throughout this work, there are potentially spectacular signals at low-energy experiments which search for charged lepton flavour violation. The last part of this thesis is dedicated to the detailed exploration of processes like $\mu \to e\,\gamma$, $\mu \to 3\,e$ or $\mu - e$ conversion in nuclei in a supersymmetric framework with an inverse seesaw mechanism. In particular, we disprove claims about a non-decoupling effect in Z-mediated three-body decays and study the prospects for discovering and distinguishing signals at near-future experiments. In this context we identify the possibility to deduce from ratios like $\mathrm{BR}(\tau \to 3\,\mu)/\mathrm{BR}(\tau \to \mu\,e^+e^-)$ whether the contributions from $\nu - W$ loops dominate over supersymmetric contributions or vice versa.

CONTENTS

CHAPTER 1

INTRODUCTION

With the start of the second run of the Large Hadron Collider (LHC) [1] at CERN, for the first time proton-proton collisions at a centre-of-mass energy of $\sqrt{s} = 13$ TeV are achieved in a laboratory. In the first run with $\sqrt{s} = 8$ TeV, the Standard Model of particle physics (SM) has been once more confirmed to be an outstandingly accurate description of high-energy physics phenomena and despite some sporadic fluctuations, so far no measurement has shown significant inconsistency with the SM predictions. Complementary to the high energies probed at the LHC, many low-energy experiments report excellent agreement with the SM.

The Standard Model is based on the gauge group $SU(3)_c \times SU(2)_L \times U(1)_Y$, where c stands for colour, L for *left* in the sense of chirality, and Y for the hypercharge. As the $SU(2)_L$ factor indicates, the SM is a chiral theory, meaning that a left-handed field transforms differently compared to its right-handed counterpart. A consequence is that, *e.g.*, the left-handed charged leptons e_L and neutrinos ν_L form a doublet under $SU(2)_L$ while the right-handed e_R are singlets. Right-handed neutrinos, which are singlets under the complete gauge group, are not included in the Standard Model. If this gauge group were exact, not only the gauge bosons but also the fermions would be massless as a Dirac mass term including the left-and right-handed fields would obviously violate gauge invariance. However, the electroweak gauge group $SU(2)_L \times U(1)_Y$ has to be broken to the electromagnetic $U(1)_{em}$ which itself is exact. The basic idea for this breakdown is the spontaneous symmetry breaking proposed in the Brout-Englert-Higgs mechanism [2, 3]. The predicted remnant, a scalar particle, has for a long time been the only missing jigsaw piece of the Standard Model, until finally a scalar with properties consistent with the Higgs boson has been discovered in the last run of the LHC [4, 5]. Therefore, the SM is now complete, and is hence the first self-consistent particle physics theory that could, in principle, be valid up to energy scales where gravity comes into play.

A justified question that one might therefore ask is what particle physicists actually expect from the higher energies that are now being probed at the LHC – and the answer is manifold as there are good reasons why the Standard Model is *not* the ultimate particle physics theory, and that instead new phenomena should show up at the TeV scale. In particular the connection to cosmology cannot be made without assuming additional

mechanisms which themselves cannot be established in the SM framework. Among these problems is the matter-antimatter asymmetry in the universe as well as the matter composition that we observe. Only a small part of the matter in the universe is of baryonic origin; the dominating portion is "dark matter" in the sense that it does not show up when doing spectroscopy. So far it has only been observed indirectly, *e.g.* in the behaviour of galaxy rotation curves or via gravitational lensing effects. The SM lacks a description of this phenomenon as no known particle exhibits the suitable properties. A convenient candidate would be an electrically neutral, weakly-interacting massive particle with a mass of $\mathcal{O}(100\ \text{GeV} \ldots 1\ \text{TeV})$[1], corresponding to non-relativistic cold dark matter. Although neutrinos are also "dark" in this respect, they would constitute hot dark matter. Being relativistic during structure formation, hot dark matter washes out the small-scale structures of the universe; judging from the structures we observe in the universe, neutrinos can thus only account for a small portion of the total amount of dark matter. The neutrinos pose a further riddle as the accommodation of neutrino masses in the theory is not possible without extending the Standard Model. In addition to this experimental evidence there is also a solid indication for physics beyond the Standard Model (BSM) from the theoretical viewpoint. This so-called hierarchy problem is related to the hierarchy between the electroweak and the Planck scale and the consequences for scalar particles; we will discuss it in some detail in the next chapter. A more philosophical question would be if there is a reason why the gauge group is as we observe it. In particular one might ask if there is a physical interpretation of the rather unattractive hypercharge or a reason for the left chirality of the interactions that we observe – or if the original theory at higher scales is left-right-symmetric, or even features a single unified gauge group.

Many theories have been proposed that partially or fully address the issues plaguing the Standard Model. Most of them predict new particles with masses within the reach of the LHC. Hence, there is plenty to explore by the two multi-purpose LHC detectors CMS and ATLAS, and a variety of different signatures from different models are searched for in the respective analyses; see *e.g.* the summary websites of the Exotics groups [6, 7]. A particularly well-motivated BSM scenario relates bosons and fermions by a symmetry, the "supersymmetry" (SUSY) [8, 9]. Minimal realizations thereof simply supersymmetrize the Standard Model and already by themselves have appealing features. However, secondary to still not incorporating neutrino masses, those scenarios are already heavily constrained by the LHC results, so that it is time to seriously consider non-minimal realizations and explore their phenomenology. We will do so for different well-motivated scenarios, mostly based on extended gauge symmetries like left-right symmetry.

The rest of this thesis is organized as follows. In chapter 2 we start by motivating supersymmetry and introduce the concept via some technical details. After a brief summary of the minimal SUSY model we point to weak spots thereof and turn to the discussion of non-minimal supersymmetric models. In chapter 3 we consider a representative of left-right-supersymmetry which automatically incorporates a mechanism to generate neutrino masses by the presence of $SU(2)_R$ triplets. Prior to the evaluation of constraints from the LHC searches we address and improve the calculation of the mass of a doubly-charged scalar in this model which has been the topic of quite some discussion in the past decades. We conclude this chapter with the discussion of the vacuum stability by the use of the one-loop

[1] In the LHC, such a particle would, if produced, carry away momentum when leaving the detector so that it could be measured as missing transverse momentum.

effective potential. In chapter 4 we consider as a gauge group a remnant of left-right symmetry where the $SU(2)_R$ is broken to a $U(1)_R$. As a consequence there are two Abelian gauge groups in the theory so that gauge kinetic mixing has to be considered. Assuming gauge mediation as the SUSY-breaking mechanism, we calculate the boundary conditions for the SUSY-breaking parameters in the presence of kinetic mixing. We then go on with exploring the model; after investigating the Higgs mass at the tree- and loop-level we turn to the collider phenomenology of the model where we discuss the impact of the boundary conditions from SUSY breaking on the signatures that we expect at the LHC. In chapter 5 we then turn to non-collider aspects. More specifically, we investigate charged lepton flavour violating (cLFV) processes such as $\mu \to e\gamma$, $\mu \to 3\,e$ as well as $\mu - e$ conversion in nuclei in the example of a model with an inverse seesaw mechanism for neutrino mass generation. After identifying the importance of different contributions to these processes, we discuss the prospects of measuring them at near-future experiments and show how to distinguish between different scenarios. In chapter 6 we conclude. In the appendix A we list the complete spectrum of the model considered in chapter 3 plus the one-loop self energy of the doubly-charged scalar as well as the one-loop tadpole corrections. In appendix B we list the formulas for the decay widths and conversion rates used in chapter 5. We furthermore describe in detail in section B.4 why it was believed for some time that Z-penguin diagrams show a non-decoupling effect and how we eventually resolved this issue.

CHAPTER 2

SUPERSYMMETRY

2.1 Motivation

The Lagrangian density can be written in its most generic form as

$$\mathcal{L} = \sum_{i,n} \frac{1}{\Lambda_i^{n-4}} \mathcal{L}_{d=n} \,, \tag{2.1}$$

where the parameters Λ_i are of mass dimension one and correspond to different scales in the theory. $\mathcal{L}_{d=n}$ contains all field-valued operators of dimension n. As the eventual Lagrangian $\mathcal{L}$ has to be of dimension four, $\mathcal{L}_{d=4}$ does not depend on any scale. For $n > 4$, the lowest scales at which these operators are generated give the most important contributions, whereas for $n < 4$ the largest scales are most relevant. The Standard Model Lagrangian contains only operators of dimension four, with the exception of one operator, the Higgs mass term $m_H^2 H^\dagger H$. Being a dimension two operator, one would "naturally" expect it to be of the order of the largest scale in the theory. Assuming that no other physics beyond the SM is present, this would be the Planck scale M_{Pl}. However, we observe that the Higgs mass is of the electroweak scale which is 17 orders of magnitude below M_{Pl}. Hence, an almost exact cancellation of completely uncorrelated parameters has to be assumed to get the correct Higgs mass, corresponding to a huge fine-tuning. This unnatural cancellation is commonly denoted as the naturalness or hierarchy problem. In terms of Feynman diagrams, one can depict that behaviour by considering quantum corrections to the Higgs mass, using a cutoff regularization at the scale Λ_{UV} (which could be M_{Pl}). The most important Standard Model contribution is given by the top loop

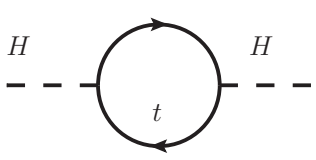

,

which gives a one-loop contribution to the Higgs mass parameter of

$$\delta m_H^2 \propto \frac{|y_t|^2}{16\pi^2}\Lambda_{UV}^2 \,, \tag{2.2}$$

with y_t denoting the top Yukawa coupling. Therefore, the scalar Higgs is sensitive to physics at the cutoff scale Λ_{UV}, ultimately giving rise to the $\Lambda_{UV}^2 H^\dagger H$ term.

One can think of this problem in different ways.

- One could simply accept that nature is fine-tuned as this "problem" is, although being extremely unnatural, no conceptual issue.

- One could assume that there is not only one universe, but that in fact we are living in a multiverse with a vast variety of different vacua and hence different parameter configurations. In that case, statistically, some of the vacua turn out to accidentally feature very large cancellations of different parameters – and we just happen to live in one of these.

Those solutions seem rather unsatisfactory since they, instead of proposing solutions, merely shift the issue into the unknown/unmeasurable or simply ignore it. Solutions can be found, however, if one demands the Higgs mass term to be technically natural in the sense of 't Hooft [10]. This means that the symmetry of the theory gets enhanced once a particular parameter vanishes, so that quantum corrections may only be driven by that symmetry-breaking parameter itself and therefore remain small.

- Rather pessimistic attempts try to argue that there is, in fact, no real hierarchy problem and that the Standard Model is valid up to arbitrarily large scales: the Higgs mass term is the only term that explicitly breaks scale invariance, so that scale symmetry gets restored in the limit $m_H^2 \to 0$ [11]. In these terms, the arguments using using cutoff regularizations are invalid as the cutoff parameter itself breaks scale invariance. However, it has been shown that, even if Planck scale physics were ignored, this scenario is unphysical since the hypercharge gauge coupling has a Landau pole at very large scales [12], hence re-introducing a scale to which the quantum corrections to the Higgs mass are sensitive. To prevent the Landau pole by imposing a different renormalization group equation (RGE) running of the gauge coupling, extra fields have to be introduced near the TeV scale.

- Other approaches regard the Higgs boson as the Nambu-Goldstone boson of a spontaneously broken approximate global symmetry. Composite Higgs as well as Little Higgs theories rely on this principle (for recent reviews, see, *e.g.*, refs. [13, 14]).

- Alternatively, one could imagine that space-time is actually $4+n$-dimensional and that the SM fields are just localized on a four-dimensional membrane while gravity acts in all dimensions. Models with large and warped extra dimensions as in ref. [15] and [16] have in common that they solve the hierarchy with the following proposal: gravity is not actually weaker than the other forces (*i.e.* the $4+n$-dimensional Planck-scale is not so much separated from the electroweak scale), but it is just experienced weak from the four-dimensional viewpoint because of the flux loss in the n extra dimensions.

- The most prominent approach instead introduces a symmetry between bosons and fermions, the so-called supersymmetry.

  Within this symmetry, femions and bosons corresponding to each other have the same mass and couplings. Thus, m_H also gives mass to fermions which by themselves do not have a naturalness problem. As δm_H^2 is an additional mass term for scalars but not for the associated fermions, it breaks supersymmetry and is naturally small. In terms of quantum corrections, for each diagram with a fermionic loop there exist diagrams with the respective bosonic partners in the loops which cancel the quadratic divergence:

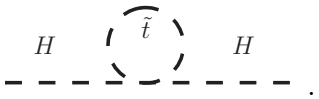

  The cancellation happens because of the relative minus sign of the respective diagrams owed to Fermi/Bose statistics. A non-zero δm_H^2 is only induced if the top quark and its superpartner have different masses, *i.e.* if supersymmetry is broken. The latter has to be the case as no scalar partner of any known fermion has been observed. However, supersymmetry can be broken "softly", *i.e.*, in a way in which no new quadratic divergences are introduced. Therefore, δm_H^2 only grows logarithmically with the mass ratio of the top quarks and their bosonic partners. Hence, the hierarchy problem is solved if supersymmetric particles exist, with masses that are not too large compared to the electroweak scale [17].

We will embark on the last possibility. In the following, we will introduce the concept of supersymmetry and its direct consequences. Before we start with some technical details we briefly mention additional virtues entailed by supersymmetric models.

Gauge coupling unification

The quest for finding a grand unified theory (GUT) in which all forces unify to a single one requires the gauge couplings of the electroweak and the strong sector to unify at a certain scale, denoted "GUT scale" in the following. The attempt to find a single GUT-scale using the RGEs of the gauge groups within the Standard Model [18], fails as the unification predicts a too small value of $\sin^2\theta_W$, θ_W being the Weinberg angle. This situation changes when supersymmetry is introduced: because of the altered particle content at the mass scale of the supersymmetric partners, the RGEs evolve differently from this scale upward. In fact, already in the minimal realization of a supersymmetric model (discussed in section 2.6), gauge coupling unification is achieved, the GUT scale being $\mathcal{O}(10^{16}$ GeV) [19–21], see also the discussion in ref. [22].

Dark matter

As mentioned in the introduction, the Standard Model cannot explain the amount of dark matter observed in the universe as it lacks a fitting particle candidate. This is not the case in supersymmetric models with conserved R-parity (see section 2.6.2) in which the fermionic partners of Higgs or gauge bosons exhibit the necessary properties [23].

2.2 Supersymmetry as a space-time symmetry

In 1967, Coleman and Mandula proved a "theorem on the impossibility of combining space-time and internal symmetries in any but a trivial way" [24]. The consequence of that theorem is that the generators of any internal symmetry of the theory must commute with the Poincaré group, and that therefore the only space-time symmetries are the known translations P_μ and Lorentz transformations $M_{\mu\nu}$. One loophole can be found in their argumentation: the theorem only applies if commutation relations are assumed. This has been exploited by Haag, Łopuszański and Sohnius who showed in ref. [25] that the only non-trivial extension of space-time symmetry consists of the addition of generators $Q_\alpha\,, Q^{\dagger\dot\alpha}$ which transform as spinors under Poincaré group operations. The corresponding (anti-) commutation relations read [8]

$$\{Q_\alpha, Q_\beta\} = \{Q^\dagger_{\dot\alpha}, Q^\dagger_{\dot\beta}\} = 0\,, \tag{2.3}$$

$$\{Q_\alpha, Q^\dagger_{\dot\beta}\} = 2\sigma^\mu_{\alpha\dot\beta} P_\mu\,, \tag{2.4}$$

$$[P^\mu, Q_\alpha] = [P^\mu, Q^\dagger_{\dot\alpha}] = 0\,, \tag{2.5}$$

where $\sigma^\mu = (\mathbf{1}_2, \vec\sigma)$, σ_i being the Pauli matrices, and α, $\dot\alpha$, β, $\dot\beta = 1, 2$. The brackets $\{\cdot\,,\cdot\}$ and $[\cdot\,,\cdot]$ denote the usual anticommutator and commutator, respectively.

Hence, a closed algebra of the known space-time symmetries and an internal symmetry can be formulated. The symmetry related to those generators is called supersymmetry. As the generators carry spinorial charge, an application to a fermionic field results in a bosonic state and vice versa:

$$Q|\text{fermion}\rangle = |\text{boson}\rangle\,, \qquad Q|\text{boson}\rangle = |\text{fermion}\rangle\,. \tag{2.6}$$

In general, there could be multiple generators Q^i_α, $Q^{i\dagger\dot\alpha}$. In this thesis, however, we will only consider one pair of Q_α, $Q^{\dagger\dot\alpha}$, corresponding to $\mathcal{N} = 1$ supersymmetry.

Superspace

To fix the notation, we mostly adopt the syntax from refs. [26,27] and deploy the Minkowski metric in the more widely-used variant in particle physics, $\eta_{\mu\nu} = \text{diag}(1, -1, -1, -1)$. We define a Dirac spinor Ψ_D in terms of the left-chiral and right-chiral Weyl spinors ξ_α and $\chi^{\dagger\dot\alpha}$:

$$\Psi_D = \begin{pmatrix} \xi_\alpha \\ \chi^{\dagger\dot\alpha} \end{pmatrix}\,, \tag{2.7}$$

where (un-) dotted indices α, β are used exclusively for (right-) left-chiral fields and all right-handed Weyl spinors carry daggers. $(\chi^{\dagger\dot\alpha})^\dagger = \chi^\alpha$ is thus a left-chiral field. The indices are raised and lowered by the antisymmetric ϵ symbol, $\xi^\alpha = \epsilon^{\alpha\beta}\xi_\beta$ etc.. Contracted terms that do not explicitly show the spinor index structure are to be read as

$$\psi\eta = \psi^\alpha\eta_\alpha = \psi^\alpha\epsilon_{\alpha\beta}\eta^\beta\,, \tag{2.8}$$

$$\psi^\dagger\eta^\dagger = \psi^\dagger_{\dot\alpha}\eta^{\dagger\dot\alpha} = \psi^\dagger_{\dot\alpha}\epsilon^{\dot\alpha\dot\beta}\eta^\dagger_{\dot\beta}\,. \tag{2.9}$$

As supersymmetry expands the space-time symmetry to the so-called superspace, also the known bosonic coordinates x^μ must be complemented by fermionic coordinates θ^α and $\bar{\theta}_{\dot{\alpha}}$. Those are two-component anticommuting Grassmann variables with mass dimension $-1/2$. Because of their anticommutation relations, $\theta_\alpha\theta_\alpha$ vanishes and consequently any power series in θ^α stops after the second-order term $\theta\theta = \theta^\alpha\epsilon_{\alpha\beta}\theta^\beta$. As a nice additional feature, derivatives and integrations turn out to be the same as they just pair with the corresponding relevant component. The derivatives read:

$$\frac{\partial}{\partial\theta^\alpha}\bar{\theta}_{\dot{\alpha}} = 0\,, \quad \frac{\partial}{\partial\theta^\alpha}\theta^\beta = \delta_\alpha^\beta \quad \Rightarrow \quad \frac{\partial}{\partial\theta^\alpha}\psi\theta = \psi_\alpha\,, \quad \frac{\partial}{\partial\theta_\alpha}\psi\theta = -\psi^\alpha\,, \quad \frac{\partial}{\partial\theta^\alpha}\theta\theta = 2\theta_\alpha \quad \text{etc.}\,. \tag{2.10}$$

A chiral covariant derivative in superspace that satisfies the SUSY algebra can then be written as [27]:

$$D_\alpha = \frac{\partial}{\partial\theta^\alpha} - i\sigma^\mu_{\alpha\dot{\alpha}}\bar{\theta}^{\dot{\alpha}}\partial_\mu\,, \qquad D^{\dagger\dot{\alpha}} = \frac{\partial}{\partial\bar{\theta}_{\dot{\alpha}}} - i\bar{\sigma}^{\mu\,\dot{\alpha}\alpha}\theta_\alpha\partial_\mu\,, \tag{2.11}$$

$$D^\alpha = -\frac{\partial}{\partial\theta_\alpha} + i\bar{\theta}_{\dot{\alpha}}\sigma^{\mu\,\dot{\alpha}\alpha}\partial_\mu\,, \qquad D^\dagger_{\dot{\alpha}} = -\frac{\partial}{\partial\bar{\theta}^{\dot{\alpha}}} + i\theta^\alpha\bar{\sigma}^\mu_{\alpha\dot{\alpha}}\partial_\mu\,. \tag{2.12}$$

2.3 Superfields

Because of the finiteness of the expansion in Grassmann coordinates, a generic scalar superfield Θ can be expressed in the following form [28]:

$$\Theta(x,\theta,\bar{\theta}) = a + \theta\xi + \bar{\theta}\chi^\dagger + \theta\theta b + \bar{\theta}\bar{\theta}c + \theta\sigma^\mu\bar{\theta}v_\mu + \bar{\theta}\bar{\theta}\theta\eta + \theta\theta\bar{\theta}\zeta^\dagger + \theta\theta\bar{\theta}\bar{\theta}d\,. \tag{2.13}$$

Chiral superfields

For constructing a theory that incorporates the Standard Model, chiral superfields $\Phi(x,\theta,\bar{\theta})$ are needed. A left-chiral superfield is defined by the requirement that the right-chiral covariant derivative annihilates it:

$$D^\dagger_{\dot{\alpha}}\Phi = 0\,. \tag{2.14}$$

Φ^*, satisfying $D_\alpha\Phi^*$, is a right-chiral superfield, accordingly. A chiral superfield can always be obtained from a generic superfield by applying $\Phi(x,\theta,\bar{\theta}) = D^\dagger_{\dot{\alpha}}D^{\dot{\alpha}\dagger}\Theta(x,\theta,\bar{\theta})$. By choosing a suitable redefinition of the coordinates, $y^\mu = x^\mu - i\theta\sigma^\mu\bar{\theta}$, eq. (2.14) is satisfied for

$$\Phi(y,\theta,\bar{\theta}) = \Phi(y,\theta) = \phi(y) + \sqrt{2}\,\theta\psi(y) + \theta\theta F(y)\,. \tag{2.15}$$

A left-chiral superfield is therefore composed of a complex scalar field ϕ, a complex left-handed Weyl spinor ψ and an auxiliary field F. As F is the coefficient of $\theta\theta$, we will name every superfield coefficient of $\theta\theta$ as "F-term" in the following.

We stress here that the number of fermionic and of bosonic degrees of freedom (DOF) within a chiral superfield is the same. On-shell, the complex scalar and the Weyl fermion each feature two DOF. Off-shell, however, the Weyl spinor has two complex components

and hence four DOF. The extra degrees of freedom from the auxiliary field F are thus needed to close the algebra off-shell. As a consequence, F does not propagate but can be eliminated by the equations of motion as will be seen in section 2.4. We further emphasize that there is a scalar "partner" for each Weyl fermion, *i.e.* for each chirality of a Dirac fermion.

Vector superfields

In addition to the matter superfields, we need to construct vector superfields $V(x, \theta, \bar{\theta})$ to incorporate the gauge bosons. They are defined by the requirement:

$$V = V^* \,, \tag{2.16}$$

which relates the coefficients of eq. (2.13) as:

$$a = a^* \,,\ \chi^\dagger = \xi^\dagger \,,\ c = b^* \,,\ v_\mu = v_\mu^* \,,\ \zeta^\dagger = \eta^\dagger \,,\ d = d^* \,. \tag{2.17}$$

One can get rid of the redundant degrees of freedom a, ξ and b by choosing a particular supergauge. In this Wess-Zumino gauge [29], the vector superfields can be written as

$$V_{WZ} = \theta\sigma^\mu\bar{\theta}A_\mu + \bar{\theta}\bar{\theta}\theta\lambda + \theta\theta\bar{\theta}\lambda^\dagger + \frac{1}{2}\theta\theta\bar{\theta}\bar{\theta}D \,. \tag{2.18}$$

A gauge supermultiplet therefore consists of a vector field A^μ, a Weyl spinor λ and an auxiliary field D which, just like F, can be expressed in terms of the physical fields when applying the equations of motion. Similar to the F-terms, we will henceforth call the coefficients of $\theta\theta\bar{\theta}\bar{\theta}$ "D-terms".

We have seen that, in the matter as well as in the gauge sector, each field known from the Standard Model gets a supersymmetric partner. The scalar partners of fermions are commonly denoted with an "s" in front of the name (*e.g.* stop, selectron), and in an abuse of notation, we talk of left (right) sfermions as superpartners of the left-chiral (right-chiral) fermion. Although those scalar particles cannot be of any chirality, the chirality information of the fermionic partner is encoded in their couplings. Fermionic superpartners of vector or scalar bosons are named with an "ino" at the end of the particle name so that we talk of gauginos and higgsinos.

2.4 The constituents of a supersymmetric model

It is convenient to write the matter interactions of a particular model in terms of the superpotential, a holomorphic function in Φ_i of mass dimension three. Its most generic form for a renormalizable theory reads:

$$W(\Phi) = L_i\Phi_i + \frac{1}{2}m_{ij}\Phi_i\Phi_j + \frac{1}{3}\lambda_{ijk}\Phi_i\Phi_j\Phi_k \,. \tag{2.19}$$

In order to be gauge invariant, each term in W has to form a gauge singlet so that L_i is zero for all but singlet fields S. The F-terms of the superpotential $\int \mathrm{d}^2\theta\, W + \text{h.c.} = [W(\Phi)]_F + \text{h.c.}$ form the non-derivative parts of the chiral Lagrangian.

The gauge self interactions are defined by constructing the supersymmetric generalization $\mathcal{W}_\alpha$ of the field-strength tensor $F^{\mu\nu}$ which is given by [26]

$$\mathcal{W}_\alpha = -\frac{1}{4} D^\dagger D^\dagger e^{-2g_a T^a V^a} D_\alpha e^{2g_a T^a V^a} , \tag{2.20}$$

a indexing the gauge group and T^a being the associated generator. The summation over repeated indices is understood. The F-terms of $\mathcal{W}^\alpha \mathcal{W}_\alpha$ eventually give the gauge self interactions

$$\mathcal{L}_{\text{gauge}} = -\frac{1}{4} F^a_{\mu\nu} F^{a,\mu\nu} + i\lambda^a \sigma^\mu \partial_\mu \lambda^{a\dagger} + \frac{1}{2} D^a D^a , \tag{2.21}$$

where a total derivative has been dropped.

The rest of the Lagrangian includes, in addition to the F-terms of the superpotential, also the gauge-matter interactions which are encoded in the D-terms of $\Phi^* e^{2g_a T^a V^a} \Phi$,

$$\mathcal{L}_{\text{matter}} = [\Phi_i^* e^{2g_a T^a V^a} \Phi_i]_D + ([W(\Phi)]_F + \text{h.c.}) . \tag{2.22}$$

Splitting that into

$$\mathcal{L}_{\text{matter}} = \mathcal{L}_{\text{chiral}} + \mathcal{L}_{\text{int}} , \tag{2.23}$$

we define $\mathcal{L}_{\text{chiral}}$ as the part which includes the covariant derivatives and the F-terms and $\mathcal{L}_{\text{int}}$ as the part which consists of the additional gauge-matter interaction terms

$$\mathcal{L}_{\text{int}} = -\left(\sqrt{2} g_a (\phi_i^* T^a \psi_i) \lambda^a + \text{h.c.}\right) + g_a (\phi_i^* T^a \phi_i) D^a . \tag{2.24}$$

Combined with eq. (2.21), the equations of motion for the auxiliary D^a can be used to eliminate those fields from the Lagrangian:

$$D^a = -g_a (\phi_i^* T^a \phi_i) . \tag{2.25}$$

Combining eqs. (2.21-2.25), the D-term contribution to the tree-level scalar potential is given by

$$V_D(\phi, \phi^*) = \frac{1}{2} D^a D_a = \frac{g_a^2}{2} (\phi_i^* T^a \phi_i)(\phi_j^* T^a \phi_j) . \tag{2.26}$$

Analogous to D^a, the auxiliary fields F_i of the chiral superfields can be eliminated from $\mathcal{L}_{\text{matter}}$. Defining the derivatives of the superpotential w.r.t. the scalar fields as

$$W^i = \frac{\partial}{\partial \Phi_i} W(\Phi)\Big|_{\Phi_i = \phi_i} , \qquad W^{ij} = \frac{\partial^2}{\partial \Phi_i \partial \Phi_j} W(\Phi)\Big|_{\Phi_i = \phi_i, \Phi_j = \phi_j} , \tag{2.27}$$

they can be expressed as

$$F_i = -W_i^* , \qquad F^{*i} = -W^i , \tag{2.28}$$

so that the chiral Lagrangian then reads

$$\mathcal{L}_{\text{chiral}} = D_\mu \phi^{i*} D^\mu \phi_i + i\psi^i \sigma^\mu D_\mu^\dagger \psi_i^\dagger - \frac{1}{2}(W^{ij}\psi_i\psi_j + \text{h.c.}) - W^i W_i^* \,, \tag{2.29}$$

D_μ being the covariant derivative. It is now clear that explicit fermion masses are represented by m_{ij} and Yukawa couplings by λ_{ijk}. The last part in eq. (2.29) is the F-term contribution to the scalar potential:

$$V_F(\phi, \phi^*) = F^{*i} F_i = W^i W_i^* = \sum_i \left| \frac{\partial W}{\partial \Phi_i} \right|^2_{\Phi_i = \phi_i} \,. \tag{2.30}$$

Note that the scalar potential V_D and V_F are both positive semidefinite, $V_i \geq 0$. In the ground state of unbroken supersymmetry both contributions vanish separately.

The full Lagrangian is given by

$$\mathcal{L} = \mathcal{L}_{\text{chiral}} + \mathcal{L}_{\text{int}} + \mathcal{L}_{\text{gauge}} \,. \tag{2.31}$$

2.5 Supersymmetry breaking

Not having observed any scalar partner of a known fermion with an identical mass makes clear that SUSY has to be broken. As mentioned in the motivation, this breaking should be "soft", *i.e.* such that no quadratic divergences are re-introduced. A necessary but not sufficient condition for this to happen is that the SUSY-breaking operators are of a mass dimension less than four. The allowed terms are [1]

$$-\mathcal{L}_{\text{soft}} = (\frac{1}{2} M_a \lambda_a \lambda_a + \xi_i \phi_i + \frac{1}{2} B_{ij} \phi_i \phi_j + \frac{1}{6} T_{ijk} \phi_i \phi_j \phi_k + \text{h.c.}) + m_{ij}^2 \phi_i^* \phi_j \,, \tag{2.32}$$

where $\xi_i \phi_i$ is only allowed by gauge invariance if ϕ_i is a singlet field. As every particular SUSY-breaking mechanism leads to different patterns of the parameters in eq. (2.32), it is often interesting to freely explore the parameter range without specifying the mechanism at work.

The above terms break supersymmetry explicitly; for a realistic breaking scenario, however, one would assume that they are generated dynamically by spontaneous symmetry breaking analogous to the Higgs mechanism. This translates to the condition that the scalar potential is minimized when either V_D or V_F are non-zero. As it turns out, particular realizations of SUSY breaking are quite intricate, and attempts to implement a tree-level SUSY breaking in the visible sector (*i.e.* induced by fields charged under the gauge group) suffer from serious problems. While D-term breaking [30,31] is ruled out as it predicts vevs for charged or coloured scalars in realistic frameworks, F-term breaking scenarios [32,33], though in principle working, are heavily constrained by the mass sum rule [34] and the consequential prediction of light charged scalars. For a comprehensive overview over the different mechanisms we refer to ref. [35].

The mentioned problems can be circumvented when SUSY is broken at a high scale in

[1] The reader might notice that, *e.g.*, no term $D_{ijk}\phi_i^*\phi_j\phi_k$ is present. This is an example of a term of $d < 4$ that does lead to a quadratic divergence and hence should not be generated by a SUSY-breaking mechanism [27].

a sector that is not directly connected to our visible world. One speaks of a "hidden sector" in the sense that it only interacts indirectly, *i.e.* via some mediation mechanism, with the superfields that we wish to describe. The two most popular mechanisms in the literature work via gravity and gauge fields as mediators. They have in common that they assume SUSY to be broken by the F-term vev $\langle F \rangle$ of a spurion superfield $\hat{X}$.

2.5.1 Gravity mediation

The probably most intuitive idea is that gravity is responsible for mediating SUSY breaking. Those models are based on the idea that SUSY is a local symmetry at high scales, the "supergravity" [36, 37], and conveniently a local SUSY Lagrangian automatically includes terms that mediate SUSY-breaking [27]. The respective operators are suppressed by the Planck scale so that the SUSY-breaking parameters are of the order

$$m_{ij}\,,\ M_a\,,\ T_{ijk} \sim \frac{\langle F \rangle}{M_{Pl}}\,. \tag{2.33}$$

Models of minimal supergravity are frequently used as the basis for simplified universal boundary conditions for the soft SUSY-breaking parameters at the GUT-scale, see section 2.6.4.

A serious drawback of Planck-scale mediated SUSY-breaking is the "SUSY flavour problem": although gravitational interactions are flavour-blind, there is no reason why the induced higher-dimensional operators which break SUSY should respect the flavour structure that we observe at experimentally accessible energies. As a consequence, the matrix-valued parameters m and T could have any flavour structure. This would in general lead to large flavour-violating effects in low-energy decays and oscillations – which is not compatible with low-energy measurements. Hence, one needs to *assume* in any realization that (at least approximately) the scalar masses are generated flavour-diagonal and that the trilinear couplings exhibit the same structure as the respective Yukawa couplings.

2.5.2 Gauge mediation

The flavour problem is solved if SUSY breaking is mediated by gauge interactions which themselves automatically preserve the flavour structure. Models with gauge-mediated supersymmetry breaking (GMSB) [38–43] introduce so-called messenger multiplets with superpotential couplings to the spurion field. As the messengers are also charged under the gauge group, they couple to the gauge bosons and gauginos so that SUSY breaking is transmitted from the secluded sector to the visible world via loop diagrams involving the messengers in the loops. See ref. [44] for a comprehensive review of GMSB scenarios. As schematically shown in figure 2.1, gauginos receive their masses M_a at one-loop whereas the scalar squared masses m^2 are generated at the two-loop order, so that both masses are of the same order of magnitude

$$M_a\,,\ m_{ij} \sim \frac{g^2}{16\pi^2}\frac{\langle F \rangle}{M}\,, \tag{2.34}$$

where M is the mass scale of the messenger fields. Trilinear couplings are not generated by these types of diagrams. In practice it turns out that this leads to difficulties with

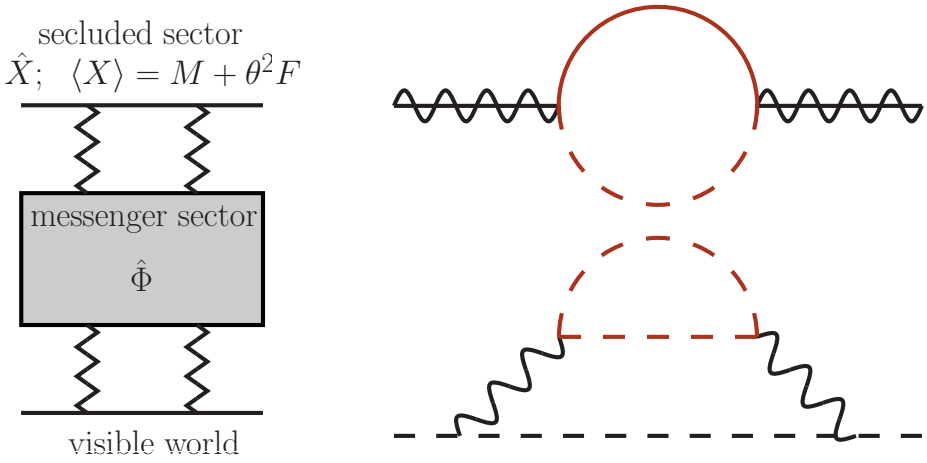

Figure 2.1: Illustration of gauge mediated supersymmetry breaking. The propagators from messenger fermions (scalars) are depicted with red solid (dashed) lines.

explaining the measured Higgs mass, see section 2.7, so that non-minimal scenarios are considered. An explicit example of a model with gauge-mediated supersymmetry breaking in an $SO(10)$ embedding will be shown in section 4.3.

2.6 The minimal supersymmetric standard model

2.6.1 Model definition

The minimal realization of a supersymmetric model must, of course, incorporate the complete SM particle content. Consequently, we need to include all left- and right-chiral fermions as well as the Higgs boson into chiral supermultiplets. Embedding the Higgs doublet into a chiral multiplet is not enough, though, for two reasons. The first reason is that the Weyl fermion associated to the Higgs field carries a hypercharge that is not opposed by any other fermion and thus leads to a gauge anomaly. The second reason is the structure of supersymmetric theories which only allow the superpotential to include either left-chiral or right-chiral superfields, not both. As a consequence, neither the term $\mu \hat{H}^* \hat{H}$ ($\hat{H}$ being the left-chiral Higgs superfield) nor a Yukawa coupling to the down-type quarks or charged leptons can be written down, which is phenomenologically unacceptable. Hence, in addition to the Higgs supermultiplet $\hat{H}_u$ giving masses to the up-type quarks we introduce a second one, $\hat{H}_d$, with the opposite hypercharge.

The superpotential of the minimal supersymmetric standard model (MSSM) [36, 45] then reads:

$$W^{\text{MSSM}} = Y_u^{ij}\, \hat{u}_i^c\, \hat{Q}_j^\alpha\, \epsilon_{\alpha\beta}\, \hat{H}_u^\beta - Y_d^{ij}\, \hat{d}_i^c\, \hat{Q}_j^\alpha\, \epsilon_{\alpha\beta}\, \hat{H}_d^\beta - Y_e^{ij}\, \hat{e}_i^c\, \hat{L}_j^\alpha\, \epsilon_{\alpha\beta}\, \hat{H}_d^\beta + \mu\, \hat{H}_u^\alpha\, \epsilon_{\alpha\beta}\, \hat{H}_d^\beta\,, \tag{2.35}$$

where $X^\alpha \epsilon_{\alpha\beta} X^\beta$ is the $SU(2)$-invariant product of fields X lying in the fundamental representation, and we have omitted colour indices. The superfields with their quantum numbers are defined in table 2.1. Following eq. (2.32), the corresponding soft SUSY-breaking terms are given by

Superfield	Spin 0	Spin $\frac{1}{2}$	# Generations	$SU(3)_c \times SU(2)_L \times U(1)_Y$
$\hat{Q}$	$\tilde{Q} = (\tilde{u}_L, \tilde{d}_L)$	$Q = (u_L, d_L)$	3	$(\mathbf{3}, \mathbf{2}, \frac{1}{6})$
$\hat{u}^c$	$\tilde{u}^c_R$	u^c_R	3	$(\bar{\mathbf{3}}, \mathbf{1}, -\frac{2}{3})$
$\hat{d}^c$	$\tilde{d}^c_R$	d^c_R	3	$(\bar{\mathbf{3}}, \mathbf{1}, \frac{1}{3})$
$\hat{L}$	$\tilde{L} = (\tilde{\nu}_L, \tilde{e}_L)$	$L = (\nu_L, e_L)$	3	$(\mathbf{1}, \mathbf{2}, -\frac{1}{2})$
$\hat{e}^c$	$\tilde{e}^c_R$	e^c_R	3	$(\mathbf{1}, \mathbf{1}, 1)$
$\hat{H}_u$	$H_u = (H_u^+, H_u^0)$	$\tilde{H}_u = (\tilde{H}_u^+, \tilde{H}_u^0)$	1	$(\mathbf{1}, \mathbf{2}, \frac{1}{2})$
$\hat{H}_d$	$H_d = (H_d^0, H_d^-)$	$\tilde{H}_d = (\tilde{H}_d^0, \tilde{H}_d^-)$	1	$(\mathbf{1}, \mathbf{2}, -\frac{1}{2})$

Table 2.1: Matter content of the MSSM with the respective quantum numbers under $SU(3)_c \times SU(2)_L \times U(1)_Y$.

$$
\begin{aligned}
-\mathcal{L}^{\text{MSSM}}_{\text{soft}} = \frac{1}{2}\Big(& M_1\, \tilde{B}\, \tilde{B} + M_2\, \tilde{W}^\alpha\, \delta_{\alpha\beta}\, \tilde{W}^\beta + M_3\, \tilde{g}^\gamma\, \delta_{\gamma\delta}\, \tilde{g}^\delta + \text{h.c.}\Big) \\
& + m^2_{e,ij}\, (\tilde{e}^c_i)^*\, \tilde{e}^c_j + m^2_{L,ij}\, (\tilde{L}^\alpha_i)^*\, \delta_{\alpha\beta}\, \tilde{L}^\beta_j + m^2_{H_d}\, |H_d|^2 + m^2_{H_u}\, |H_u|^2 \\
& + m^2_{Q,ij}\, (\tilde{Q}^\alpha_i)^*\, \delta_{\alpha\beta}\, \tilde{Q}^\beta_j + m^2_{d,ij}\, (\tilde{d}^c_i)^*\, \tilde{d}^c_j + m^2_{u,ij}\, (\tilde{u}^c_i)^*\, \tilde{u}^c_j + \Big(B_\mu\, H^\alpha_u\, \epsilon_{\alpha\beta}\, H^\beta_d \\
& + T^{ij}_u\, \tilde{u}^c_i\, \tilde{Q}^\alpha_j\, \epsilon_{\alpha\beta}\, H^\beta_u - T^{ij}_d\, \tilde{d}^c_i\, \tilde{Q}^\alpha_j\, \epsilon_{\alpha\beta}\, H^\beta_d - T^{ij}_e\, \tilde{E}^C_i\, \tilde{L}^\alpha_j\, \epsilon_{\alpha\beta}\, H^\beta_d + \text{h.c.}\Big)\,,
\end{aligned}
\tag{2.36}
$$

where γ, δ are $SU(3)_c$ indices. The Majorana fermions $\tilde{B}, \tilde{W}, \tilde{g}$ are the gauginos associated with the hypercharge, $SU(2)_L$ and $SU(3)_c$ groups, respectively.

2.6.2 R-parity

The superpotential as defined in eq. (2.35) does not exhibit the most general form that is compatible with the symmetries of the theory. Instead, four more terms are, in principle, allowed, each inducing a vertex with an odd number of supersymmetric particles and breaking either baryon number (B) or lepton number (L). They read:

$$
W_{\not R} = \frac{1}{2}\lambda_{ijk}\hat{u}^c_i\hat{d}^c_j\hat{d}^c_k + \lambda'_{ijk}\hat{L}^\alpha_i\epsilon_{\alpha\beta}\hat{Q}^\beta_j\hat{d}^c_k + \frac{1}{2}\lambda''_{ijk}\hat{L}^\alpha_i\epsilon_{\alpha\beta}\hat{L}^\beta_j\hat{e}^c_k + \varepsilon_i\hat{L}^\alpha_i\epsilon_{\alpha\beta}\hat{H}^\beta_u \tag{2.37}
$$

If both L- and B-violating terms are simultaneously present, rapid proton decay is triggered; *e.g.*, the decay $p^+ \to \pi^0 e^+$ would be allowed through an s-channel squark when λ and λ' are non-zero and not extremely small. To prevent this disaster, a discrete symmetry is often introduced, the so-called R-parity, which connects the spin with the B and L quantum numbers [2]. It reads [47]:

$$
R = (-1)^{3(B-L)+2s}\,, \tag{2.38}
$$

where s is the spin of the respective field. As one can easily verify, this term forbids all vertices with an odd number of supersymmetric particles as those carry $R = -1$. Thus, each term in $W_{\not R}$ breaks R-parity so that proton decay is forbidden by demanding invariance

[2] see ref. [46] and refs. therein for an overview over R-parity violating supersymmetry.

under this symmetry. As a direct consequence, besides the stabilization of the proton, the lightest supersymmetric particle (LSP) is stable: the only possibility for the LSP to decay is into two lighter non-supersymmetric particles, which breaks R-parity as the corresponding vertex would feature $R = -1$. This is phenomenologically very interesting: if the LSP is electrically neutral, it is a candidate for dark matter which can, in some regions of the parameter space, contribute by the correct amount to the relic density observed in the universe. In the MSSM, the dark matter candidates are the gauginos (bino and wino) as well as the higgsinos, see ref. [27] for an overview over the different scenarios.

2.6.3 Mass spectrum of the model

We will now give a brief overview over the spectrum of the MSSM at the tree-level. This will be handy later as some properties even of extended SUSY models can be deduced from the simpler MSSM limit, and differences w.r.t. the MSSM are relevant for collider searches.

Tadpole equations and the Higgs sector

The electroweak symmetry $SU(2)_L \times U(1)_Y$ is broken down to the $U(1)_{em}$ as soon as the neutral components of the two Higgs doublets develop vevs. We hence split the complex neutral Higgs fields into a real and positive vev,[3] a real scalar as well as a real pseudoscalar field according to

$$H_u^0 = \frac{1}{\sqrt{2}}(v_u + \phi_u + i\sigma_u)\,, \qquad H_d^0 = \frac{1}{\sqrt{2}}(v_d + \phi_d + i\sigma_d)\,, \tag{2.39}$$

where the constraint $v_u^2 + v_d^2 = v^2$, v being the value of the Standard Model Higgs vev, is given by the electroweak gauge boson masses. For further reference we define the ratio of the vevs as

$$\tan\beta = \frac{v_u}{v_d}\,. \tag{2.40}$$

The conditions to find a minimum of the scalar potential V read

$$\frac{\partial V}{\partial \phi_i} = 0\,. \tag{2.41}$$

As these conditions correspond to the vanishing of Higgs tadpole diagrams, the minimization conditions are also commonly denoted tadpole equations. They read [4]

$$B_\mu = \frac{1}{2}\Big(m_{H_u}^2 - m_{H_d}^2 - M_Z^2\cos 2\beta\Big)\tan 2\beta\,, \tag{2.42}$$

$$|\mu|^2 = -\frac{1}{2}\Big(m_{H_u}^2 + m_{H_d}^2 + M_Z^2 - \frac{m_{H_u}^2 - m_{H_d}^2}{\cos 2\beta}\Big)\,, \tag{2.43}$$

where $M_Z^2 = \frac{1}{4}(g_1^2 + g_2^2)v^2$ is the tree-level Z mass. From the second equation one can deduce that $\tan\beta > 1$ if $m_{H_u}^2 < m_{H_d}^2$ by demanding that $|\mu|^2 + M_Z^2/2 > 0$. This hierarchy

[3] The vevs can always be made real and positive in the MSSM by suitable redefinitions of the Higgs fields.

[4] Here we also choose B_μ to be real which can be achieved by phase shifts in the Higgs fields.

of the soft SUSY-breaking masses is automatic as the top Yukawa contribution gives a negative contribution of [48]

$$\delta m_{H_u}^2 \simeq -\frac{3y_t^2}{4\pi^2} m_{\tilde{t}}^2 \log\left(\frac{\Lambda_{\cancel{SUSY}}}{m_{\tilde{t}}}\right) \tag{2.44}$$

in the RGE running from the scale of SUSY breaking $\Lambda_{\cancel{SUSY}}$ downwards, driving $m_{H_u}^2$ negative. Note that this implies that electroweak symmetry breaking does not have to be introduced by hand as it is the case in the Standard Model. Instead, it is generated radiatively as a *consequence* of supersymmetry breaking [49, 50]. The ratio $\tan\beta$ is furthermore constrained from below to $\tan\beta \gtrsim 1.2$ if one requires y_t to stay perturbative above the electroweak scale [26]. This is because the up-type (down-type) quark Yukawa couplings $Y_{u\,(d)}$ have to increase with decreasing (increasing) $\tan\beta$ in order to match the measured quark masses ($m_{u\,(d)} \propto Y_{u\,(d)}\, v_{u\,(d)}$).

In eq. (2.43) one can find a peculiarity: the SUSY-conserving superpotential parameter μ is connected to the SUSY-breaking sector through the values of $m_{H_{u/d}}$ and thus has to be of the same order of magnitude so that the relation holds. For $\tan\beta \gtrsim 5$, for instance, one has $-m_{H_u}^2 - |\mu|^2 \simeq M_Z^2/2$. This is somewhat unexpected as μ and the SUSY-breaking parameters originate from completely uncorrelated sectors. This issue is commonly known as the μ problem. In the case of heavy supersymmetric spectra, *i.e.* $m_{\text{soft}} \gg M_Z$, there is an additional issue as then some fine-tuning of the parameters is necessary in order to arrive at the required cancellation down to the electroweak scale M_Z, corresponding to a SUSY naturalness problem. While already inconvenient at the tree-level, the situation gets worse at the loop-level because of the large radiative corrections of the type of eq. (2.44) from the stops and also the gluinos. Consequently, for obtaining a "natural" setup, upper bounds on the stop and gluino mass can be set [51].

We turn to the mass spectrum of the Higgs bosons and first consider the CP-odd (pseudoscalar) Higgses. As in the Standard Model, one pseudoscalar boson becomes the longitudinal component of the Z boson. In the presence of two Higgs doublets, one physical state A^0 remains, with the mass

$$m_{A^0}^2 = \frac{2B_\mu}{\sin 2\beta}\,. \tag{2.45}$$

The CP-even Higgs masses then read in the basis (ϕ_d, ϕ_u):

$$m_{h^0}^2 = \begin{pmatrix} M_Z^2\cos^2\beta + m_{A^0}^2\sin^2\beta & -\frac{1}{2}(M_Z^2 + m_{A^0}^2)\sin 2\beta \\ -\frac{1}{2}(M_Z^2 + m_{A^0}^2)\sin 2\beta & M_Z^2\sin^2\beta + m_{A^0}^2\cos^2\beta \end{pmatrix}. \tag{2.46}$$

It turns out that $m_{h_1} < M_Z$ at tree-level, and only in the limit $\tan\beta \to \infty$, the Z mass is reached. Large $\tan\beta$ is therefore preferred and loop corrections have to account for the missing 35 GeV to explain the measured Higgs mass. For large $\tan\beta$, the lightest Higgs is mostly ϕ_u-like.

Apart from the neutral Higgs sector, there are also the two complex charged Higgs fields H_d^- and H_u^+. One mass eigenstate is the charged would-be Goldstone boson that becomes the longitudinal component of the massive W boson whereas the remaining

physical eigenstate $H^\pm$ has the mass

$$m_{H^\pm}^2 = \frac{g_2^2 v^2}{4} + m_{A^0}^2 \,. \tag{2.47}$$

Neutralinos and charginos

The higgsinos (with masses μ) and the $SU(2)_L \times U(1)_Y$ gauginos (with masses M_i) mix among each other after electroweak symmetry breaking and form four neutral Majorana states, the neutralinos $\tilde{\chi}_i^0$, and two complex Dirac fermions, the charginos $\tilde{\chi}_i^\pm$. The neutralino mass matrix reads in the basis $(\tilde{B}, \tilde{W}^3, \tilde{H}_d^0, \tilde{H}_u^0)$:

$$m_{\tilde{\chi}^0} = \begin{pmatrix} M_1 & 0 & -\frac{g_1 v_d}{2} & \frac{g_1 v_u}{2} \\ 0 & M_2 & \frac{g_2 v_d}{2} & -\frac{g_2 v_u}{2} \\ -\frac{g_1 v_d}{2} & \frac{g_2 v_d}{2} & 0 & -\mu \\ \frac{g_1 v_u}{2} & -\frac{g_2 v_u}{2} & -\mu & 0 \end{pmatrix} . \tag{2.48}$$

The chargino mass matrix in the basis $(\tilde{W}^-, \tilde{H}_d^-)$,$(\tilde{W}^+, \tilde{H}_u^+)$ is given by

$$m_{\tilde{\chi}^\pm} = \begin{pmatrix} M_2 & \frac{g_2 v_u}{\sqrt{2}} \\ \frac{g_2 v_d}{\sqrt{2}} & \mu \end{pmatrix} \tag{2.49}$$

and can be diagonalized by two unitary matrices U and V according to $m_{\tilde{\chi}^\pm}^{dia} = U^* m_{\tilde{\chi}^\pm} V^\dagger$.

Due of the unbroken $SU(3)_c$, the gluinos $\tilde{G}$ don't mix with other states and their mass is simply given by

$$m_{\tilde{g}} = |M_3| \,. \tag{2.50}$$

Sfermions

Each sfermion species consists of three complex scalar states per chirality, so that the charged slepton and squark masses can be expressed by 6×6 matrices while the sneutrinos only feature a 3×3 matrix due to the lack of right-handed neutrino superfields in the model. The masses of the latter read

$$m_{\tilde{\nu}}^2 = m_L^2 + \frac{1}{8}(g_1^2 + g_2^2)(v_d^2 - v_u^2)\mathbf{1} \,. \tag{2.51}$$

In addition to the soft SUSY-breaking masses and the D-terms, the charged sleptons also receive contributions from the F-terms. Their mass matrix reads in the basis $(\tilde{e}_L, \tilde{e}_R)$:

$$m_{\tilde{\ell}} = \begin{pmatrix} m_L^2 + \frac{v_d^2}{2} Y_e^\dagger Y_e + \frac{1}{8}(g_1^2 - g_2^2)(v_d^2 - v_u^2)\mathbf{1} & \frac{-v_u \mu Y_e^\dagger + v_d T_e^\dagger}{\sqrt{2}} \\ \frac{-v_u \mu^* Y_e + v_d T_e}{\sqrt{2}} & m_e^2 + \frac{v_d^2}{2} Y_e Y_e^\dagger - \frac{1}{4} g_1^2 (v_d^2 - v_u^2)\mathbf{1} \end{pmatrix} . \tag{2.52}$$

The squark mass matrices read in the bases $(\tilde{u}_L, \tilde{u}_R)$ and $(\tilde{d}_L, \tilde{d}_R)$, respectively:

$$m^2_{\tilde{u}} = \begin{pmatrix} m^2_Q + \frac{v_u^2}{2} Y_u^\dagger Y_u - \frac{1}{24}(g_1^2 - 3g_2^2)(v_d^2 - v_u^2)\mathbf{1} & \frac{-v_d \mu Y_u^\dagger + v_u T_u^\dagger}{\sqrt{2}} \\ \frac{-v_d \mu^* Y_u + v_u T_u}{\sqrt{2}} & m_u^2 + \frac{v_u^2}{2} Y_u Y_u^\dagger + \frac{1}{6} g_1^2 (v_d^2 - v_u^2) \end{pmatrix}, \tag{2.53}$$

$$m^2_{\tilde{d}} = \begin{pmatrix} m^2_Q + \frac{v_d^2}{2} Y_d^\dagger Y_d - \frac{1}{24}(g_1^2 + 3g_2^2)(v_d^2 - v_u^2)\mathbf{1} & \frac{-v_u \mu Y_d^\dagger + v_d T_d^\dagger}{\sqrt{2}} \\ \frac{-v_u \mu^* Y_d + v_d T_d}{\sqrt{2}} & m_d^2 + \frac{v_d^2}{2} Y_d Y_d^\dagger - \frac{1}{12} g_1^2 (v_d^2 - v_u^2) \end{pmatrix}. \tag{2.54}$$

2.6.4 The CMSSM

Counting in all soft SUSY-breaking parameters, the MSSM has over 100 free parameters. As a systematic study of this multi-dimensional parameter space is impossible, it is desirable to constrain the parameters to a smaller subset, which can be done by specifying the SUSY-breaking sector or setting simplified boundary conditions. A particularly widely-studied scenario, inspired by minimal supergravity [36], relates the SUSY-breaking masses to only three parameters at the GUT scale: it is assumed that there is a unified mass parameter for all scalars, one for all fermions and one for all trilinear couplings:

$$M_1 = M_2 = M_3 = M_{1/2}\,, \tag{2.55}$$

$$m_Q^2 = m_u^2 = m_d^2 = m_L^2 = m_e^2 = m_0^2 \mathbf{1}\,, \qquad m_{H_u}^2 = m_{H_d}^2 = m_0^2\,, \tag{2.56}$$

$$A_u = A_d = A_e = A_0\,, \text{ where } T_i = Y_i A_i\,. \tag{2.57}$$

The diagonal structure in the scalar soft masses and the proportionality of the trilinear couplings to the Yukawa couplings is assumed for convenience, in order to avoid the large flavour violating effects – *i.e.* to circumvent the SUSY flavour problem. Using those boundary conditions, all separate soft SUSY-breaking parameters can be evaluated at lower scales according to their RGE running, and the number of free parameters of the model reduces to five: $m_0\,,\ M_{1/2}\,,\ A_0\,,\ \tan\beta\,,\ \text{sign}\,(\mu)\,.$

This model setup is commonly called the constrained MSSM (CMSSM) [52], and is often used for setting benchmarks with specific features, *e.g.* with different neutralino dark matter scenarios. Analyses of LHC searches for squarks and gluinos often interpret the obtained cross-section limits in the $m_0 - M_{1/2}$ plane of the CMSSM, see, *e.g.*, ref. [53].

2.7 Beyond the MSSM: non-minimal supersymmetric models

The MSSM is a very popular model that includes many desirable features that the Standard Model lacks. Starting from a very simple principle, the extension of space-time symmetry to its most general non-trivial form, the unification of gauge couplings as well as the possibility of solving the hierarchy problem arise automatically. In addition, if R-parity is realized in nature, the neutralinos emerge as viable candidates for cold dark matter.

However, despite its virtues, LHC data so far tells us that supersymmetry is either rather heavy or hidden somehow. Although neither supersymmetry itself nor simple models

like the MSSM can be fully excluded by the LHC, the negative search results amplify some internal issues. Most of them have to do with the Higgs sector and the top squark: as evaluated in section 2.6.3, the Higgs mass within the MSSM can be at most as large as the Z mass – roughly 35 GeV have to be accounted for by loop corrections. As the top Yukawa coupling is the largest coupling to the Higgs, loops with tops and stops give the dominant contributions to these mass corrections. Those loop corrections vanish in the limit of exact SUSY and are logarithmically dependent on the SUSY-breaking parameters in the stop sector. Hence, if interpreted within the MSSM, the Higgs mass measurement tells us that the stop mass and/or the associated trilinear coupling T_u^{33} have to be large. This lays the foundation for the first serious doubts about the elegancy of supersymmetry: it was motivated as the solution to the hierarchy problem which eliminates the need for fine-tuning. However, the larger the stop masses, the less efficient is SUSY to ameliorate this issue, and in the end still some fine-tuning is required from the generic arguments provided in the motivation section. Moreover, also the SUSY naturalness problem gets more serious with a larger SUSY-breaking mass scale. SUSY in its minimal form is therefore already quite unnatural. This tension is relaxed in the framework of "natural supersymmetry" which assumes a heavy (= multi-TeV) supersymmetric spectrum except for the third-generation squarks, the gluinos and the higgsinos [54]. In this scenario, the fine-tuning associated with the SUSY naturalness problem is reduced and the loop corrections to the Higgs mass are driven by the left-right splitting in the stop sector induced by a large T_u^{33}. While increasing the naturalness, those scenarios are well compatible with LHC data: the stop production via a t-channel gluino exchange is suppressed because of the quark flavour content in the proton. In addition, the hadronic searches are less sensitive to third-generation squarks as the respective analyses suffer from larger uncertainties due to the difficulty to identify the top-quarks in the final states. Natural SUSY scenarios are, however, not compatible with the flavour-blind boundary conditions for the soft SUSY-breaking masses as is automatic in models with gauge mediation and assumed in the CMSSM and would thus require non-minimal SUSY-breaking mechanisms. More seriously, the large trilinear couplings required for achieving the correct Higgs mass tend to destabilize the vacuum and prefer charge- and colour-breaking minima [55, 56]. Although still very interesting for benchmarks and generic features, the MSSM hence loses popularity as a candidate for *the* theory beyond the Standard Model[5], and non-minimal supersymmetric realizations are considered more frequently. This non-minimality can be in the form of new particles and interactions, often inspired by additional global symmetries, or of an enlarged gauge symmetry (where the latter usually implies the former).

2.7.1 The NMSSM

A widely-studied example of the former is the next-to minimal supersymmetric standard model (NMSSM)[6] which introduces an extra gauge singlet S with a non-vanishing vev to the particle content. The extra scale-invariant superpotential terms read $W \supset \lambda \hat{S} \hat{H}_u^\alpha \epsilon_{\alpha\beta} \hat{H}_d^\beta + \frac{\kappa}{3} \hat{S}^3$, so that an effective μ-term $\mu_{\text{eff}} = \lambda \langle S \rangle$ is generated dynamically. In this course, the dimensionful couplings $W_{\text{dim}} = \mu H_u^\alpha \epsilon_{\alpha\beta} \hat{H}_d^\beta + \mu_S \hat{S}^2 + \xi_S \hat{S}$ can be forbidden by a discrete

[5] The latest global fit by the FITTINO collaboration already excludes the CMSSM at the 90 % confidence level [57].

[6] See refs. [58, 59] for recent reviews.

$\mathbb{Z}_3$ symmetry, leaving a scale-invariant superpotential and solving the μ problem. In addition, the tree-level Higgs mass is enhanced at the tree-level, relaxing the need for fine-tuning. The spontaneous breakdown of the $\mathbb{Z}_3$ symmetry by the vevs of S, H_u and H_d leads to a "domain wall" problem [60] which can, *e.g.*, be avoided by the introduction of non-renormalizable operators [61].

2.7.2 Models with Dirac gauginos

A further interesting possibility beyond the MSSM which nowadays gains increasing attention is the introduction of Dirac mass terms for the gauginos instead of Majorana masses, thus allowing for an additional $U(1)$ symmetry of the theory (the "$\mathcal{R}$-symmetry") as well as an $\mathcal{N} = 2$ supersymmetric Higgs and gauge sector. In order to form Dirac fermions, the gauginos have to pair up with new fermions in the adjoint representation of the respective gauge group. $\mathcal{R}$-symmetry forbids trilinear couplings, therefore alleviating the SUSY flavour problem also for non-flavour-blind SUSY-breaking mechanisms [62], yet without the need for large stop masses for explaining the measured Higgs mass [63, 64]. Because of the Dirac nature of the gluinos, they do not contribute to the RGEs, leading to an increased naturalness [65, 66]. In addition, the production cross sections at the LHC of (and thus the mass limits on) squarks get reduced [67] since the diagrams that require a chirality flip of the mediating gluino do not contribute. An unaesthetic property of this class of models is that the new superfields that have to be introduced to write the Dirac gaugino mass terms spoil the unification of gauge couplings so that awhile no conclusive high-scale models could be formulated. However, recently, this issue has been resolved with the development of the constrained minimal Dirac gaugino supersymmetric standard model [68] which manages to preserve this desirable feature by the introduction of intermediate vector-like fields charged under lepton number. Hence, a first phenomenological model with CMSSM-like boundary conditions for the soft SUSY-breaking parameters can be formulated which can serve, just like the CMSSM for MSSM studies, as a benchmark model for comprehensive studies of Dirac gaugino models. In ref. [69], we could identify regions in parameter space in which Dirac neutralino LSPs of higgsino or bino-singlino type have the right properties to play the role of cold dark matter while being consistent with direct detection measurements.

2.7.3 Neutrino mass models

So far the presented models only included the left-handed neutrinos, as is the case in the Standard Model. Simply writing down Majorana masses for those is not possible due to their belonging to $SU(2)_L$ doublets. Hence, the neutrinos are massless if no higher-dimensional operators or new particles are added by hand.[7] Adding the Weinberg operator [70] $\frac{1}{2}c_5|L_i^\alpha \epsilon_{\alpha\beta} H_u^\beta|^2$ is arguably the easiest possibility for achieving massive neutrinos. Being a dimension five operator, it is useful for an effective field theory description of neutrino masses.

If we do not want to allow non-renormalizable operators, the most obvious solution for achieving massive neutrinos is, of course, to add right-handed neutrino superfields $\hat{\nu}^c$ that are singlets under the gauge group to the particle content and write a Dirac Yukawa

[7] This is not true if R-parity is violated since in this case the neutrinos can get their masses via mixing with the neutralinos.

coupling $W_\nu = Y_\nu^{ij} \hat{L}_i^\alpha \epsilon_{\alpha\beta} \hat{H}_u^\beta \hat{\nu}_j^c$, leading to a Dirac mass $m_D = \frac{v_u}{\sqrt{2}} Y_\nu$. In this case, however, Y_ν has the inconvenient property that its largest entry has to be at least about six orders of magnitude smaller than the smallest (MS)SM coupling, the electron Yukawa, in order to comply with neutrino oscillation data – not to mention the required hierarchy between Y_ν and y_t. This large hierarchy seems to suggest that other mechanisms are at work that suppress the masses of left-handed neutrinos. Those scenarios are called seesaw mechanisms because of the way the first proposal works, namely by the interplay of two different scales where the heavier scale suppresses the mass of the lighter state, making it even lighter.

In this seesaw mechanism of type I [71–74], the right-handed neutrinos have a lepton-number-violating Majorana mass term M_R. The diagonalization of the ν mass matrix then leads to a mass of the light eigenstates of $m_\nu \simeq \frac{m_D^T m_D}{M_R}$. The ν mass suppression is therefore entirely due to the mass hierarchy between the two scales, and all eigenstates are Majorana particles. Integrating out ν_R eventually leads to the Weinberg operator defined above, where $c_5 = \frac{Y_\nu^T Y_\nu}{M_R}$. If Y_ν is of $\mathcal{O}(1)$, then M_R has to be of the order of the GUT scale, *i.e.* out of reach for the direct detection at collider experiments. Indications that this mechanism could be at work could at best be found indirectly by the confirmation that neutrinos are Majorana particles, *e.g.* by the measurement of neutrinoless double-β decay. If, in turn, one allows Y_ν to be small,[8] the right-handed neutrinos could as well be as light as a few hundred GeV. In chapter 3 we will make use of that and introduce a seesaw-I scenario in which M_R is generated dynamically by the TeV-scale vev of a scalar field.

The *inverse* seesaw mechanism [75], as the name suggests, relies on the reversed principle: a further singlet fields is introduced, and the light neutrino masses are explained by the *smallness* of their Majorana mass term which is naturally small as it violates lepton number. The resulting right-handed neutrino mass eigenstates are pseudo-Dirac particles. In chapter 4 as well as 5 we will present inverse seesaw realizations in more detail and explore possibilities to measure traces of such a mechanism, *e.g.* by detecting lepton-flavour-violating decays.

There exist many more mechanisms like the linear seesaw [76] and the seesaw mechanisms of type II [77,78] and III [79]. In the latter two mechanisms there is no need for right-handed neutrinos as the masses are generated via interactions with a scalar triplet under $SU(2)_L$ and a fermionic triplet, respectively.

2.7.4 Models with extended gauge groups

Already for a long time the idea is present that the Standard Model gauge group is not the definite symmetry of the theory but that it is in fact just a low-energy remnant of a larger group. In particular the hypercharge $U(1)_Y$ and the associated charges of the particles which do not possess any intuitive interpretation seem too random for an ultimate theory, and the possible gauge coupling unification in supersymmetric models suggests that there is a unified description of the gauge symmetries. The discovery that the SM gauge group and its particle content fit perfectly into an $SU(5)$ grand unified theory [18,80] has given an enormous boost to the field and strengthened the efforts to find the ultimate unified high-scale model. While minimal non-supersymmetric $SU(5)$ could be ruled out by the non-observation of the proton decay $p \to e^+\pi^0$ in the expected range [81][9],

[8] In this context, "small" means small w.r.t. y_t but still *of the order of other small Yukawa couplings*.
[9] and the prediction of an incorrect value for $\sin^2\theta_W$

supersymmetric models survive this constraint as they predict a larger unification scale compared to non-SUSY models and hence more strongly suppressed rates. However, minimal supersymmetric $SU(5)$ models predict observable rates of the the decay $p \to K^+\bar{\nu}$ by dimension five operators [82], so they could eventually be ruled out, too [83,84]. Although these constraints can be evaded in non-minimal supersymmetric $SU(5)$ models, also those face a number of problems, see the review in ref. [22]. Among those problems is that the $SU(5)$ GUT does not have the possibility to conveniently include all fermionic matter fields into a single irreducible representation – which one would expect from a unified theory. Instead, the ingredients for neutrino masses like right-handed neutrinos are the only matter fields that have to be added by hand.[10]

This is not the case in models with larger unified gauge groups like $SO(10)$ or E_6. Those models have a higher rank than $SU(5)$ and accordingly larger fundamental representations. One can easily convince oneself that the $SO(10)$ is a further GUT candidate because it contains the $SU(5)$: $SO(10) \to SU(5) \times U(1)$ [85]. A nice property of $SO(N)$ models is that they are automatically anomaly-free. This is not so in $SU(N)$ (except for $SU(2)$) models where one has to be careful with the choice of representations in order to find a vanishing anomaly coefficient [86]. Furthermore, in contrast to $SU(5)$, a very convenient consequence of the $SO(10)$ gauge group is that right-handed neutrinos are *required* in order to complete the matter content and to form a **16**-plet. In fact, while the gauge group we observe so far is left-chiral, $SO(10)$ models are originally left-right-symmetric. That can be seen by the decomposition [11]

$$\begin{aligned} SO(10) &\to SU(4)_C \times SU(2)_L \times SU(2)_R \\ &\to SU(3)_c \times SU(2)_L \times SU(2)_R \times U(1)_{B-L}\,, \end{aligned} \tag{2.58}$$

where $B - L$ is the difference between baryon and lepton number that we have already encountered in the definition of R-parity. Guided by the motivation that it is an intermediate breaking step of $SO(10)$, it is very interesting to work with this left-right-symmetric gauge group. While $B - L$ is an accidental symmetry in the Standard Model, it has to be introduced by hand in the MSSM, disguised as R-parity. In the left-right-symmetric context it becomes clear that those effects are just low-energy remnants of a local $B - L$ symmetry at higher scales. In the end, the conservation or violation of R-parity is determined by the exact mechanism that eventually breaks the left-right-symmetric stage $SU(2)_L \times SU(2)_R \times U(1)_{B-L}$ down to the left-chiral $SU(2)_L \times U(1)_Y$: if the fields responsible for the breakdown carry odd $B - L$ quantum numbers, also R-parity is violated. The opposite direction of this argument is not automatic, but one also has to take into account the minimization conditions of the scalar potential; in the next section we will investigate a model where $SU(2)_R \times U(1)_{B-L}$ is simultaneously broken by $SU(2)_R$ triplets with

[10] If neutrino masses are generated by a seesaw-II mechanism, in turn, the fermionic representations are complete as the needed triplets have to be accommodated in the Higgs representations.

[11] The first breaking step leads to Pati-Salam models [87]. Because of the unification of $SU(3)_c$ and $U(1)_{B-L}$ interactions into a single gauge group, those models predict compressed spectra if the Pati-Salam symmetry survives down to a scale not too far away from the TeV scale, see also ref. [88]. In particular after the null results of the LHC, those models gain relevance: if the mass difference between the coloured sparticles and the LSP is small, the corresponding decay products are soft and hence harder to detect. The LHC bounds are correspondingly weaker, allowing for lower SUSY scales and therefore a more natural theory.

$B - L = \pm 2$ and of which it was nevertheless believed that it must violate R-parity spontaneously by sneutrino vevs (which we shall see is not the case).

The choice of the Higgs sector is, of course, the part which distinguishes the different left-right supersymmetric models and to a large extent influences their phenomenology. The use of triplets is in this connection probably the most intuitive choice: because of the primal left-right-invariance, the right-handed fields appear in $SU(2)_R$ doublets, and in the presence of triplets, a gauge-invariant superpotential coupling of two right-handed lepton superfields to a $SU(2)_R$-breaking Higgs superfield is possible. This automatically results in a seesaw-I mechanism for neutrino masses, linking the seesaw-scale directly to the breaking scale of left-right symmetry.

This breaking scale can, in principle, lie anywhere in-between the TeV and the GUT scale. The former possibility is, of course, the much more interesting one as it is directly relevant for LHC physics. In supersymmetric manifestations, the particular advantage comes into play that the tree-level Higgs mass receives extra tree-level D-term contributions, ameliorating the fine-tuning issues discussed above. Clearly, those contributions decouple if left-right symmetry is unbroken only at high scales. There are, however, $SO(10)$ breaking chains in which $SU(2)_R$ is already broken at the high scale, but in which a local $U(1)_R$ symmetry is left over. The remaining $U(1)_R \times U(1)_{B-L}$ symmetry can then be kept unbroken down to energies as low as the TeV scale [89], bearing the same benefit in what concerns the Higgs mass, but of course a different phenomenology, most importantly in the gauge boson, the neutrino and the residual Higgs sector.

We will now go on with the exploration of a particular example of a minimal left-right supersymmetric model with triplet scalars at the TeV scale in which we will discuss and resolve open questions and consider the LHC phenomenology as well as constraints from vacuum stability. Afterwards we turn to a $U(1)_R \times U(1)_{B-L}$ model in which we especially focus on the Higgs sector and investigate whether the tree-level Higgs mass enhancement is enough to restore minimal gauge mediation as a relevant SUSY-breaking mechanism.

CHAPTER 3

LEFT-RIGHT SUPERSYMMETRY WITH TRIPLET SCALARS

3.1 The model

We work in a left-right supersymmetric model in which a seesaw mechanism for the generation of neutrino masses is automatically present. Therefore, Higgs triplets Δ in the adjoint representation of $SU(2)$ are introduced. For electroweak symmetry breaking as well as a successful fit to the CKM matrix, two copies of $SU(2)$ bidoublets Φ are needed. In addition, the presence of a singlet field S under all gauge groups is assumed which guarantees electroweak symmetry breaking in the supersymmetric limit. The superpotential reads

$$\begin{aligned} W =&(\hat{Q}_L\, y_1^Q)\cdot\hat{\Phi}_1\cdot\hat{Q}_R + (\hat{Q}_L\, y_2^Q)\cdot\hat{\Phi}_2\cdot\hat{Q}_R + (\hat{L}_L\, y_1^L)\cdot\hat{\Phi}_1\cdot\hat{L}_R + (\hat{L}_L\, y_2^L)\cdot\hat{\Phi}_2\cdot\hat{L}_R \\ &+ \left(\mu_1+\lambda_1\hat{S}\right)\hat{\Phi}_1\cdot\hat{\Phi}_1 + \left(\mu_2+\lambda_2\hat{S}\right)\hat{\Phi}_2\cdot\hat{\Phi}_2 + \left(\mu_{12}+\lambda_{12}\hat{S}\right)\hat{\Phi}_1\cdot\hat{\Phi}_2 \qquad (3.1)\\ &+ y_3^L\hat{L}_L\cdot\hat{\Delta}_{2L}\cdot\hat{L}_L + \left(\mu_L+\lambda_L\hat{S}\right)\hat{\Delta}_{1L}\cdot\hat{\Delta}_{2L} \\ &+ y_4^L\hat{L}_R\cdot\hat{\Delta}_{1R}\cdot\hat{L}_R + \left(\mu_R+\lambda_R\hat{S}\right)\hat{\Delta}_{1R}\cdot\hat{\Delta}_{2R} + \frac{1}{3}\lambda_S\hat{S}^3 + \mu_S\hat{S}^2 + \xi_S\hat{S}\,, \qquad (3.2)\end{aligned}$$

where the colour indices are suppressed and the Yukawa couplings $y_i^{L/Q}$ are 3×3 matrices in flavour space. The superfields with their respective quantum numbers are listed in table 3.1. The $SU(2)$-invariant products read

$$\hat{\Phi}_a\cdot\hat{\Phi}_b = (\hat{\Phi}_a)^j{}_i\,\epsilon_{jk}\,(\hat{\Phi}_b)^k{}_l\,\epsilon^{il}, \qquad (3.3)$$

$$\hat{\Delta}_a\cdot\hat{\Delta}_b = (\hat{\Delta}_a)^j{}_i\,\epsilon_{jk}\,(\hat{\Delta}_b)^k{}_l\,\epsilon^{il} = \mathrm{Tr}\left(\hat{\Delta}_a\hat{\Delta}_b\right), \qquad (3.4)$$

$$\hat{\Psi}_L\cdot\hat{\Phi}\cdot\hat{\Psi}_R = (\hat{\Psi}_L)^i\,\epsilon_{ij}\,\hat{\Phi}^j{}_k\,\epsilon^{lk}\,(\hat{\Psi}_R)_l\,, \qquad (3.5)$$

$$\hat{L}_L\cdot\hat{\Delta}\cdot\hat{L}_L = (\hat{L}_L)^i\epsilon_{ji}\,\hat{\Delta}^j{}_k\,(\hat{L}_L)^k\,, \qquad (3.6)$$

$$\hat{L}_R\cdot\hat{\Delta}\cdot\hat{L}_R = (\hat{L}_R)_i\,\hat{\Delta}^i{}_j\,\epsilon^{jk}\,(\hat{L}_R)_k\,, \qquad (3.7)$$

with the usual antisymmetric ϵ symbol, $\epsilon_{12} = -\epsilon_{21} = -\epsilon^{12} = \epsilon^{21} = 1$.

Superfield	Spin 0	Spin $\frac{1}{2}$	# Gen.	$SU(3)_c \times SU(2)_L \times SU(2)_R \times U(1)_{B-L}$
$\hat{Q}_L = (\hat{u}_L, \hat{d}_L)$	$\tilde{Q}_L$	Q_L	3	$(\mathbf{3}, \mathbf{2}, \mathbf{1}, \frac{1}{3})$
$\hat{Q}_R = (\hat{u}^c_R, \hat{d}^c_R)$	$\tilde{Q}_R$	Q_R	3	$(\overline{\mathbf{3}}, \mathbf{1}, \mathbf{2}^*, -\frac{1}{3})$
$\hat{L}_L = (\hat{\nu}_L, \hat{\ell}_L)$	$\tilde{L}_L$	L_L	3	$(\mathbf{1}, \mathbf{2}, \mathbf{1}, -1)$
$\hat{L}_R = (\hat{\nu}^c_R, \hat{\ell}^c_R)$	$\tilde{L}_R$	L_R	3	$(\mathbf{1}, \mathbf{1}, \mathbf{2}^*, 1)$
$\hat{\Phi}_i$	Φ_i	$\tilde{\Phi}_i$	2	$(\mathbf{1}, \mathbf{2}, \mathbf{2}^*, 0)$
$\hat{\Delta}_{1L}$	Δ_{1L}	$\tilde{\Delta}_{1L}$	1	$(\mathbf{1}, \mathbf{3}, \mathbf{1}, -2)$
$\hat{\Delta}_{2L}$	Δ_{2L}	$\tilde{\Delta}_{2L}$	1	$(\mathbf{1}, \mathbf{3}, \mathbf{1}, 2)$
$\hat{\Delta}_{1R}$	Δ_{1R}	$\tilde{\Delta}_{1R}$	1	$(\mathbf{1}, \mathbf{1}, \mathbf{3}, -2)$
$\hat{\Delta}_{2R}$	Δ_{2R}	$\tilde{\Delta}_{2R}$	1	$(\mathbf{1}, \mathbf{1}, \mathbf{3}, 2)$
$\hat{S}$	S	$\tilde{S}$	1	$(\mathbf{1}, \mathbf{1}, \mathbf{1}, 0)$

Table 3.1: Chiral superfields and their quantum numbers with respect to $SU(3)_c \times SU(2)_L \times SU(2)_R \times U(1)_{B-L}$. The $U(1)$ charges are normalized such that $Q_{em} = T^3_L + T^3_R + \frac{B-L}{2}$.

Because of the enlarged gauge symmetry with respect to the Standard Model group, the vector fields feature extra states. In the unbroken phase, the gauge boson sector contains the gluons, the neutral gauge singlet boson B associated with the $B - L$ Abelian group as well the $SU(2)_L$ and $SU(2)_R$ triplet vectors W^i_L and W^i_R. After the symmetry breaking steps described below, the latter three gauge eigenstates mix to the usual photon, Z and $W^\pm$ as well as new massive Z' and $W'^\pm$ states.

As soon as the electrically neutral components of the $SU(2)_R$-triplet scalars develop vevs, $SU(2)_R \times U(1)_{B-L}$ is spontaneously broken, leaving the residual hypercharge $U(1)_Y$. The necessary vacuum structure for that to happen is

$$\langle \Delta_{1R} \rangle = \left\langle \begin{pmatrix} \frac{\Delta^-_{1R}}{\sqrt{2}} & \Delta^0_{1R} \\ \Delta^{--}_{1R} & -\frac{\Delta^-_{1R}}{\sqrt{2}} \end{pmatrix} \right\rangle = \begin{pmatrix} 0 & \frac{v_{1R}}{\sqrt{2}} \\ 0 & 0 \end{pmatrix}, \quad \langle \Delta_{2R} \rangle = \left\langle \begin{pmatrix} \frac{\Delta^+_{2R}}{\sqrt{2}} & \Delta^{++}_{2R} \\ \Delta^0_{2R} & -\frac{\Delta^+_{2R}}{\sqrt{2}} \end{pmatrix} \right\rangle = \begin{pmatrix} 0 & 0 \\ \frac{v_{2R}}{\sqrt{2}} & 0 \end{pmatrix}. \tag{3.8}$$

A consequence of this vacuum structure is that the right-handed neutrinos, which lie in the L_R doublet, receive a Majorana mass $\sqrt{2}\, y^L_4 v_{1R}$ and are thus directly connected to the scale of $SU(2)_R$ breakdown. Since also the masses of the new gauge bosons W' and Z' are determined by the $SU(2)_R$ breaking scale, the above vevs have to lie at least at the TeV scale. Non-vanishing vevs for the Δ_{iL} scalars are also allowed and would, accordingly, lead to a Majorana mass for the left-handed neutrinos of $\sqrt{2}\, y^L_3 v_{2L}$. Consequently, in order to achieve massive right-handed neutrinos while the left-handed counterparts remain light, either v_{2L} has to be negligibly small or $y^L_4 \gg y^L_3$. The next breaking step $SU(2)_L \times U(1)_Y \to U(1)_{em}$ is due to vevs of the neutral bidoublet fields,

$$\langle \Phi_1 \rangle = \left\langle \begin{pmatrix} \Phi^0_1 & \Phi^+_1 \\ \Phi^-_1 & \Phi'^0_1 \end{pmatrix} \right\rangle = \begin{pmatrix} \frac{v_d}{\sqrt{2}} & 0 \\ 0 & \frac{v'_1}{\sqrt{2}} \end{pmatrix}, \quad \langle \Phi_2 \rangle = \left\langle \begin{pmatrix} \Phi'^0_2 & \Phi^+_2 \\ \Phi^-_2 & \Phi^0_2 \end{pmatrix} \right\rangle = \begin{pmatrix} \frac{v'_2}{\sqrt{2}} & 0 \\ 0 & \frac{v_u}{\sqrt{2}} \end{pmatrix}. \tag{3.9}$$

The primed vevs v'_i give rise to $W - W'$ as well as extra kaon mixing and we shall

neglect them henceforth [1]. In addition, we also allow a vev for the singlet field,

$$\langle S \rangle = \frac{v_S}{\sqrt{2}} \,. \tag{3.10}$$

We assume the hierarchy

$$v_S, v_{iR} \gg v_{u,d} \gg v_{iL} \approx v_i' \approx 0 \tag{3.11}$$

and define

$$v_R^2 = v_{1R}^2 + v_{2R}^2 \,, \qquad \tan\beta_R = \frac{v_{2R}}{v_{1R}} \,. \tag{3.12}$$

Similar to the NMSSM, we impose a discrete $\mathbb{Z}_3$ symmetry under which scalar fields transform as $\phi \to e^{\frac{2\pi i}{3}} \phi$ and which accordingly forbids all bilinear and linear terms in the superpotential, $\mu_i = \xi_S = 0$. As a consequence, all dimensionful parameters in the superpotential are dynamically generated by v_S and the couplings to the singlet field, so that, in this way, effective μ terms of

$$\mu^{\text{eff}} = \frac{\lambda_{12} v_S}{\sqrt{2}}, \qquad \mu_R^{\text{eff}} = \frac{\lambda_R v_S}{\sqrt{2}}, \qquad \mu_L^{\text{eff}} = \frac{\lambda_L v_S}{\sqrt{2}}, \qquad \mu_S^{\text{eff}} = \frac{\lambda_S v_S}{\sqrt{2}} \tag{3.13}$$

arise, hence solving the μ problem. In addition, we assume $\lambda_1 = \lambda_2 = 0$ analogously to refs. [93–96].

After the spontaneous symmetry breaking steps, the gauge eigenstates of the singlet, the bidoublets and the triplets as defined in table 3.1 will mix among each other according to their (broken and conserved) quantum numbers. The Higgs sector can thus be decomposed into irreducible sets of nine CP-even (h^0) and nine CP-odd neutral fields (A^0, two of which become the longitudinal part of the massive neutral gauge bosons after left-right- and electroweak symmetry breaking), eight singly-charged Higgs fields ($H^\pm$, two of which being the would-be Goldstone bosons of the charged gauge bosons) and four doubly-charged ones ($H^{\pm\pm}$). The fermionic counterparts include in addition to the higgsinos also the gauginos so that the neutralinos ($\tilde{\chi}^0$), the singly-charginos ($\tilde{\chi}^\pm$) and the doubly-charginos ($\tilde{\chi}^{\pm\pm}$) consist of twelve, six and two states, respectively.

3.1.1 Scalar potential and minimization conditions

For the derivation of the scalar potential we concentrate on the relevant parts for the following discussion, *i.e.* the $SU(2)_R$ triplets and their interactions. The parts of the superpotential that we have to take into account for this purpose are

$$W_\Delta = y_4^L \, \hat{L}_R^T \, \hat{\Delta}_{1R} \, \epsilon \, \hat{L}_R + \lambda_R \, \hat{S} \, \text{Tr}(\hat{\Delta}_{1R} \, \hat{\Delta}_{2R}) + \frac{1}{3} \lambda_S \, \hat{S}^3 \,, \tag{3.14}$$

where ϵ is treated as a 2×2 matrix. The corresponding tree-level scalar potential V_0 reads

$$V_0 = V_F + V_D + V_{\text{soft}} \,. \tag{3.15}$$

[1] The induced $W - W'$ mixing has been used by refs. [90, 91] to explain the recent excess in diboson events seen by ATLAS [92].

The separate parts read

$$V_F = \lambda_R^2 |S|^2 \left(\mathrm{Tr}(\Delta_{1R}^\dagger \Delta_{1R}) + \mathrm{Tr}(\Delta_{2R}^\dagger \Delta_{2R})\right) + \left|\lambda_R \,\mathrm{Tr}(\Delta_{1R}\Delta_{2R}) + \lambda_S S^2\right|^2 + y_4^L \lambda_R \left(S^* \tilde{L}_R^T \Delta_{2R}^\dagger \epsilon \tilde{L}_R + h.c.\right) + (y_4^L)^2 (\tilde{L}_R^\dagger \tilde{L}_R)^2 \,, \tag{3.16}$$

$$V_D = \frac{g_R^2}{2} \sum_{i=1}^{3} \left(\mathrm{Tr}(\Delta_{1R}^\dagger [\tau_i, \Delta_{1R}]) + \mathrm{Tr}(\Delta_{2R}^\dagger [\tau_i, \Delta_{2R}]) - \tilde{L}_R^\dagger \tau_i \tilde{L}_R\right)^2 + \frac{g_{BL}^2}{2}\left(\mathrm{Tr}(\Delta_{2R}^\dagger \Delta_{2R}) - \mathrm{Tr}(\Delta_{1R}^\dagger \Delta_{1R}) + \frac{1}{2}\tilde{L}_R^\dagger \tilde{L}_R\right), \tag{3.17}$$

$$V_{\text{soft}} = m_{\Delta_{1R}}^2 \mathrm{Tr}(\Delta_{1R}\Delta_{1R}^\dagger) + m_{\Delta_{2R}}^2 \mathrm{Tr}(\Delta_{2R}\Delta_{2R}^\dagger) + m_S^2 |S|^2 + m_{L_R}^2 \tilde{L}_R^\dagger \tilde{L}_R + \left(T_{\lambda_R} S \,\mathrm{Tr}(\Delta_{1R}\Delta_{2R}) + \frac{1}{3} T_{\lambda_S} S^3 + T_4^L \tilde{L}_R^T \Delta_{1R} \epsilon \tilde{L}_R + \text{h.c.}\right), \tag{3.18}$$

where $\tau_i = \frac{1}{2}\sigma_i$ and σ_i are the Pauli matrices. Inserting the vacuum expectation values of eqs. (3.8-3.10) and deriving w.r.t. the vevs yields the conditions for vacuum minimization

$$\frac{\partial V}{\partial v_S} = v_S\left(m_S^2 + \lambda_R\lambda_S v_{1R} v_{2R} + \frac{\lambda_R^2}{2}\left(v_{1R}^2 + v_{2R}^2\right)\right) + \lambda_S^2 v_S^3 + \frac{1}{\sqrt{2}}\left(v_{1R} v_{2R} T_{\lambda_R} + v_S^2 T_{\lambda_S}\right) = 0\,, \tag{3.19}$$

$$\frac{\partial V}{\partial v_{1R}} = v_{1R}\left(m_{\Delta_{1R}}^2 + \frac{g_{BL}^2}{2}\left(-v_{2R}^2 + v_{1R}^2\right) + \frac{g_R^2}{2}\left(v_{1R}^2 - v_{2R}^2\right)\right) + \frac{\lambda_R}{2} v_S^2 \left(\lambda_R v_{1R} + \lambda_S v_{2R}\right) + \frac{\lambda_R^2}{2} v_{1R} v_{2R}^2 + \frac{1}{\sqrt{2}} v_{2R} v_S T_{\lambda_R} = 0\,, \tag{3.20}$$

$$\frac{\partial V}{\partial v_{2R}} = v_{2R}\left(m_{\Delta_{2R}}^2 + \frac{g_{BL}^2}{2}\left(-v_{1R}^2 + v_{2R}^2\right) + \frac{g_R^2}{2}\left(-v_{1R}^2 + v_{2R}^2\right)\right) + \frac{\lambda_R}{2} v_S^2 \left(\lambda_R v_{2R} + \lambda_S v_{1R}\right) + \frac{\lambda_R^2}{2} v_{1R}^2 v_{2R} + \frac{1}{\sqrt{2}} v_{1R} v_S T_{\lambda_R} = 0\,, \tag{3.21}$$

and we refer to the appendix A for the complete tadpole equations with all possible terms.

As already observed in ref. [97], the vacuum configuration associated with these minimization conditions does not correspond to the global minimum of the scalar potential at tree level. Instead, the D-terms are minimized if the vevs are aligned along the τ_1 direction:

$$\langle \Delta_{1R}\rangle_{\text{CB}} = \begin{pmatrix} 0 & \frac{v_{1R}}{2} \\ \frac{v_{1R}}{2} & 0 \end{pmatrix}, \qquad \langle \Delta_{2R}\rangle_{\text{CB}} = \begin{pmatrix} 0 & \frac{v_{2R}}{2} \\ \frac{v_{2R}}{2} & 0 \end{pmatrix}, \tag{3.22}$$

leading to phenomenologically disastrous vevs for the Δ_{1R}^{--} and Δ_{2R}^{++} fields. Therefore the model favours, at the tree-level, a vacuum where electric charge is broken. Beyond that, it turns out that the desired vev structure doesn't even correspond to a true minimum of the scalar potential but merely to a saddle point, whereby the negative curvature is found in the field direction of the doubly charged scalars. We will address this issue in detail in section 3.2 where we discuss the tree-level $H^{\pm\pm}$ mass and show that the one-loop corrections are essential to understand the vacuum structure.

3.1.2 Some mass matrices

For the following discussion we present the relevant mass matrices in suitable approximations. For a complete account of all mass matrices exhibiting the full structure we refer to the appendix A.

Gauge bosons

The physical neutral gauge bosons are admixtures of the B and the electrically neutral components of the W_L and W_R triplets. Their mass matrix reads in the according basis (B, W_L^3, W_R^3):

$$m_{V^0}^2 = \begin{pmatrix} g_{BL}^2\, v_R^2 & 0 & -g_{BL}\, g_R\, v_R^2 \\ 0 & \frac{1}{4} g_L^2\, v^2 & -\frac{1}{4} g_L\, g_R\, v^2 \\ -g_{BL}\, g_R\, v_R^2 & -\frac{1}{4} g_L\, g_R\, v^2 & \frac{1}{4} g_R^2 (v^2 + 4 v_R^2) \end{pmatrix} . \tag{3.23}$$

The corresponding mixing matrix Z^Z rotates into the mass eigenbasis according to

$$\begin{pmatrix} B^\mu \\ W_{L,3}^\mu \\ W_{R,3}^\mu \end{pmatrix} = Z^Z \begin{pmatrix} \gamma^\mu \\ Z^\mu \\ Z'^\mu \end{pmatrix} \tag{3.24}$$

and can be parametrized, in the limit $v_R \gg v$, by two angles Θ_W, Θ'_W only:

$$Z^Z = \begin{pmatrix} \cos\Theta_W \cos\Theta'_W & -\cos\Theta'_W \sin\Theta_W & -\sin\Theta'_W \\ \sin\Theta_W & \cos\Theta_W & 0 \\ \cos\Theta_W \sin\Theta'_W & -\sin\Theta_W \sin\Theta'_W & \cos\Theta'_W \end{pmatrix} . \tag{3.25}$$

Neglecting all terms of $\mathcal{O}(v^2/v_R^2)$, the Z' mass is

$$M_{Z'} \simeq \sqrt{g_{BL}^2 + g_R^2}\, v_R^2 . \tag{3.26}$$

The charged gauge bosons consist of the combinations $W_{L/R}^\pm = \frac{1}{\sqrt{2}}(W_{L/R}^1 \mp i W_{L/R}^2)$. Those states do not mix among each other if v'_i vanishes, and the mass matrix reads in the basis (W_L^-, W_R^-):

$$m_{V^\pm}^2 = \begin{pmatrix} \frac{1}{4} g_L^2 v^2 & 0 \\ 0 & \frac{1}{4} g_R^2 (v^2 + 2 v_R^2) \end{pmatrix} , \tag{3.27}$$

so that $W = W_L$ and $W' = W_R$, and

$$M_{W'} = \frac{1}{2}\, g_R \sqrt{v^2 + 2 v_R^2} . \tag{3.28}$$

The relation $M_{Z'} > M_{W'}$ is a consequence of the $SU(2)_R \times U(1)_{B-L}$ breaking by $SU(2)_R$ triplets and is important for LHC physics. Should a Z' be found while W' searches yield bounds of $M_{W'} > M_{Z'}$, this breaking mechanism would be ruled out at once.

Neutralinos and charginos

As a consequence of $v_{iL}, v_i' \approx 0$, the scalar and fermionic Δ_{iL} and $\Phi_i'^0$ states each don't mix with the rest of the corresponding spectrum, making the mass matrices reducible. We will nevertheless include those states in the respective particle definitions.

The mass matrix for the neutralinos reads in the basis $\left(\tilde{W}_L^0, \tilde{W}_R^0, \tilde{B}, \tilde{\Phi}_2'^0, \tilde{\Phi}_2^0, \tilde{\Phi}_1^0, \tilde{\Phi}_1'^0, \tilde{\Delta}_{1L}^0, \tilde{\Delta}_{2R}^0, \tilde{\Delta}_{2L}^0, \tilde{\Delta}_{1R}^0, \tilde{S}\right)$:

$$m_{\tilde{\chi}^0} = \tag{3.29}$$

$$\begin{pmatrix}
M_{2L} & 0 & 0 & 0 & -\frac{g_L v_u}{2} & \frac{g_L v_d}{2} & 0 & 0 & 0 & 0 & 0 & 0 \\
0 & M_{2R} & 0 & 0 & \frac{g_R v_u}{2} & -\frac{g_R v_d}{2} & 0 & 0 & -g_R v_{2R} & 0 & g_R v_{1R} & 0 \\
0 & 0 & M_1 & 0 & 0 & 0 & 0 & 0 & g_{BL} v_{2R} & 0 & -g_{BL} v_{1R} & 0 \\
0 & 0 & 0 & 0 & 0 & 0 & -\mu^{\text{eff}} & 0 & 0 & 0 & 0 & 0 \\
-\frac{g_L v_u}{2} & \frac{g_R v_u}{2} & 0 & 0 & 0 & -\mu^{\text{eff}} & 0 & 0 & 0 & 0 & 0 & -\frac{\lambda_{12} v_d}{\sqrt{2}} \\
\frac{g_L v_d}{2} & -\frac{g_R v_d}{2} & 0 & 0 & -\mu^{\text{eff}} & 0 & 0 & 0 & 0 & 0 & 0 & -\frac{\lambda_{12} v_u}{\sqrt{2}} \\
0 & 0 & 0 & -\mu^{\text{eff}} & 0 & 0 & 0 & 0 & 0 & 0 & 0 & 0 \\
0 & 0 & 0 & 0 & 0 & 0 & 0 & 0 & 0 & \mu_L^{\text{eff}} & 0 & 0 \\
0 & -g_R v_{2R} & g_{BL} v_{2R} & 0 & 0 & 0 & 0 & 0 & 0 & 0 & \mu_R^{\text{eff}} & \frac{\lambda_R v_{1R}}{\sqrt{2}} \\
0 & 0 & 0 & 0 & 0 & 0 & 0 & \mu_L^{\text{eff}} & 0 & 0 & 0 & 0 \\
0 & g_R v_{1R} & -g_{BL} v_{1R} & 0 & 0 & 0 & 0 & 0 & \mu_R^{\text{eff}} & 0 & 0 & \frac{\lambda_R v_{2R}}{\sqrt{2}} \\
0 & 0 & 0 & 0 & -\frac{\lambda_{12} v_d}{\sqrt{2}} & -\frac{\lambda_{12} v_u}{\sqrt{2}} & 0 & 0 & \frac{\lambda_R v_{1R}}{\sqrt{2}} & 0 & \frac{\lambda_R v_{2R}}{\sqrt{2}} & 2\mu_S^{\text{eff}}
\end{pmatrix},$$

and is diagonalized by a unitary matrix U^0. $M_{2L/R}$ and M_1 are the soft SUSY-breaking gaugino masses of the $SU(2)_{L/R}$ and $U(1)_{B-L}$ gauge bosons.

The mass matrix of the singly-charginos is given in the bases $\left(\tilde{W}_L^+, \tilde{W}_R^+, \tilde{\Phi}_2^+, \tilde{\Phi}_1^+, \tilde{\Delta}_{2L}^+, \tilde{\Delta}_{2R}^+\right)$ and $\left(\tilde{W}_L^-, \tilde{W}_R^-, \tilde{\Phi}_2^-, \tilde{\Phi}_1^-, \tilde{\Delta}_{1L}^-, \tilde{\Delta}_{1R}^-\right)$ as:

$$m_{\tilde{\chi}^-} = \begin{pmatrix}
M_{2L} & 0 & 0 & \frac{1}{\sqrt{2}} g_L v_d & 0 & 0 \\
0 & M_{2R} & -\frac{1}{\sqrt{2}} g_R v_u & 0 & 0 & -g_R v_{1R} \\
\frac{1}{\sqrt{2}} g_L v_u & 0 & 0 & \mu^{\text{eff}} & 0 & 0 \\
0 & -\frac{1}{\sqrt{2}} g_R v_d & \mu^{\text{eff}} & 0 & 0 & 0 \\
0 & 0 & 0 & 0 & \mu_L^{\text{eff}} & 0 \\
0 & g_R v_{2R} & 0 & 0 & 0 & \mu_R^{\text{eff}}
\end{pmatrix}, \tag{3.30}$$

and is is diagonalized by U^+ and U^-

$$U^{+,*} m_{\tilde{\chi}^-} U^{-,\dagger} = m_{\tilde{\chi}^-}^{\text{diag}}. \tag{3.31}$$

As apparent from the neutralino and chargino mass matrices, the masses of four neutralinos and two charginos are given by $\sim \mu^{\text{eff}}$ whereby the $\tilde{\Phi}_{1,2}'^0$ states form an exact Dirac pair.

The doubly-charginos of the different $SU(2)$ sectors do not mix among each other so that the mass matrix is diagonal and the mass and gauge eigenstates coincide:

$$\tilde{\chi}_L^{--} = \tilde{\Delta}_{1L}^{--}, \qquad \tilde{\chi}_L^{++} = \tilde{\Delta}_{2L}^{++}, \qquad m_{\tilde{\chi}_L^{\pm\pm}} = \mu_L^{\text{eff}}, \tag{3.32}$$

$$\tilde{\chi}_R^{--} = \tilde{\Delta}_{1R}^{--}, \qquad \tilde{\chi}_R^{++} = \tilde{\Delta}_{2R}^{++}, \qquad m_{\tilde{\chi}_R^{\pm\pm}} = \mu_R^{\text{eff}}. \tag{3.33}$$

(S)neutrinos

The light neutrino masses are generated by a type-I seesaw mechanism due to the Majorana mass term for ν_R and the Dirac mass term from y_2^L after symmetry breaking. An additional type-II seesaw mechanism would only be at work with non-zero v_{2L}. In the basis (ν_L, ν_R^c), the neutrino mass matrix reads:

$$m_\nu = \begin{pmatrix} 0 & \frac{v_u}{\sqrt{2}} v_u (y_2^L)^T \\ \frac{v_u}{\sqrt{2}} v_u y_2^L & \sqrt{2}\, y_4^L\, v_{1R} \end{pmatrix} . \tag{3.34}$$

Assuming v_{1R} at the TeV scale, $y_2^L \ll y_4^L$ is needed for a successful explanation of the light neutrino masses. In particular, if y_4^L is of $\mathcal{O}(1)$, then $|y_2^L|_{ij} \lesssim \mathcal{O}(10^{-5})$ has to be satisfied. Accordingly, the heavy neutrino mass eigenstates are almost pure right-handed neutrinos with

$$m_{\nu_R} \simeq \sqrt{2}\, y_4^L\, v_{1R} . \tag{3.35}$$

The spin-zero superpartners of the right-handed neutrinos receive their mass by the soft SUSY-breaking masses $m_{L_R}^2$ as well as the appropriate D- and F-terms. The F-term coming from μ_R^{eff} thereby splits the right sneutrinos into scalar (S) and pseudoscalar (P) parts. Using $y_2^L \ll y_4^L$, the left-right mixing can be neglected and the resulting right sneutrino masses read

$$(m_{\tilde{\nu}_R}^{S/P})^2 \simeq m_{L_R}^2 + \frac{1}{4}(g_R^2 + g_{BL}^2)(v_{2R}^2 - v_{1R}^2)\, \mathbf{1} + y_4^L \left(2\, y_4^L\, v_{1R}^2 \pm (\lambda_R\, v_S\, v_{2R} + \sqrt{2}\, v_{1R}\, T_4^L) \right) , \tag{3.36}$$

In case of large $y_4^L\, \mu_R^{\text{eff}}$, the mass splitting can be substantial and even drive one eigenstate tachyonic. Therefore, a large soft SUSY-breaking mass is required for an increasing μ_R^{eff}.

Charged Higgses

Similar to the MSSM, the gauge eigenstate Φ_2^+ forms the would-be-Goldstone boson of the electroweak W boson together with Φ_1^-, whereas the W' would-be-Goldstone is a near maximal mixture of Δ_{1R}^- and Δ_{2R}^+ if we assume $\tan\beta_R \approx 1$. Hence there are six physical charged Higgs bosons. The mostly Φ_2^--like state is usually the lightest out of the six states. Its mass can be approximated by

$$m_{H_1^\pm}^2 \simeq \frac{g_R^2}{2}(v_{2R}^2 - v_{1R}^2) = g_R^2\, v_R^2\, \frac{\tan^2\beta_R - 1}{2(1 + \tan^2\beta_R)} , \tag{3.37}$$

whereas a small mixing with the $\Delta_{1R}^-/\Delta_{2R}^+$ state exists due to the off-diagonal D-terms to the mass matrix. The Δ_{1R}^- component within $H_1^\pm$ is roughly

$$\mathcal{R}_{H_1^-, \Delta_{1R}^-} \simeq \frac{v}{2\, v_R} . \tag{3.38}$$

This admixture is responsible for the coupling of the right-handed neutrinos to $H_1^\pm \ell^\mp$ which is proportional to $y_4^L \cdot \mathcal{R}_{H_1^-, \Delta_{1R}^-}$. We have checked that these approximate relations

agree with the full numerical values within 5 %. The full mass matrix, including the gauge fixing terms, is defined in the appendix A, eq. (A.217).

3.2 The $H^{\pm\pm}$ mass

The fact that the desired vacuum configuration does not reside in a true minimum at tree-level and that the scalar potential instead favours vevs for the doubly charged triplet scalars has serious implications for the $H^{\pm\pm}$ mass. We will discuss this issue in more detail here.

The $H^{\pm\pm}$ mass eigenstates consist of admixtures of the $\Delta^{--}_{1L,R}$ and $\Delta^{++}_{2L,R}$ fields to four $H^{\pm\pm}$ states. A mixing between the $SU(2)_L$- and the $SU(2)_R$-triplet states is only induced at loop level by the slepton trilinear couplings and turns out to be negligibly small so that we can safely neglect it in the following considerations. In the subsequent discussion, H^{--} always refers to the lightest eigenstate of the $\Delta^{--}_{1R} - \Delta^{++\,*}_{2R}$ admixture.

3.2.1 Tree level

The mass matrix of the doubly charged $SU(2)_R$ Higgs bosons reads in the basis $(\Delta^{--}_{1R},\ \Delta^{++\,*}_{2R})$: [2]

$$m^2 = \begin{pmatrix} D_{++} - \tan\beta_R F_{++} & F_{++} \\ F_{++} & -D_{++} - \cot\beta_R F_{++} \end{pmatrix} , \tag{3.39}$$

with

$$\begin{aligned} D_{++} &= \frac{g_R^2}{2}\left(v_d^2 - v_u^2 + 2(v_{2R}^2 - v_{1R}^2)\right) , \\ F_{++} &= \frac{\lambda_R^2}{2} v_{1R} v_{2R} + \frac{\lambda_R \lambda_S}{2} v_S^2 - \frac{\lambda_R \lambda_{12}}{2} v_d v_u + \frac{T_{\lambda_R}}{\sqrt{2}} v_S . \end{aligned}$$

The lightest eigenstate is massless and hence a pseudo-Goldstone boson in the limit of vanishing gauge coupling strength. The positive definiteness of m^2 can easily be checked by the trace and the determinant which both have to be positive for obtaining two positive eigenvalues. In the limit $v \to 0$, which is reasonable because of the imposed hierarchy $v_R \gg v$, it is an easy exercise to check that this is not possible: the lightest eigenvalue is always negative, apart from the case $\tan\beta_R = 1$ where it is zero. This case, however, corresponds to a saddle point of the potential and hence is of no relevance. That is to say, positive eigenvalues can only be achieved by the interplay of the vevs of the different, uncorrelated breaking steps. It has already been noted in ref. [98] that one only finds positive eigenvalues if

$$|v_u^2 - v_d^2| < 2|v_{2R}^2 - v_{1R}^2| \tag{3.40}$$

is fulfilled, independently from the other parameters in the mass matrix. However, because of the phenomenologically necessary hierarchy between v_R and v, eq. (3.40) is a very fine-tuned condition which requires $\tan\beta_R - 1 \ll 1$. This behaviour is depicted in figure 3.1

[2] In the appendix we define the full 4×4 mass matrix, see eq. (A.46).

where the lightest eigenvalue $m^2_{H^{\pm\pm}}$ of m^2 is shown. The upper curve in the left plot shows $m^2_{H^{\pm\pm}}$ as a function of $\tan\beta_R$ for the case that the vacuum exhibits the charge-breaking vev configuration of eq. (3.22): the eigenvalue is generically positive, corresponding to a positive curvature of the scalar potential in this direction. The desired configuration of eq. (3.8), however, features a negative curvature, represented by the negative squared mass values of the blue curve. Only in the region around $\tan\beta_R \approx 1$ this behaviour is interrupted by a tiny region with positive squared masses where the condition (3.40) holds. This region is augmented in the right plot. The cases $\tan\beta = 50$ (1) are shown, corresponding to large (vanishing) $|v_u^2 - v_d^2|$. Although the fraction of parameter space with large $\tan\beta$ and $\tan\beta_R$ very close to unity features positive eigenvalues of m^2, this possibility is rendered unphysical as well since one of the pseudoscalar Higgs bosons has a negative squared mass in this region [99].

This means that no phenomenologically feasible spectrum can be found at tree level, and that the desired vacuum configuration cannot be a minimum of the tree-level scalar potential but corresponds to a saddle point. A possibility to avoid these problems at tree level would be to introduce new terms to the scalar potential in the form of vevs for the right sneutrinos. These, however, violate R-parity, with all the associated inconveniences [97, 99].

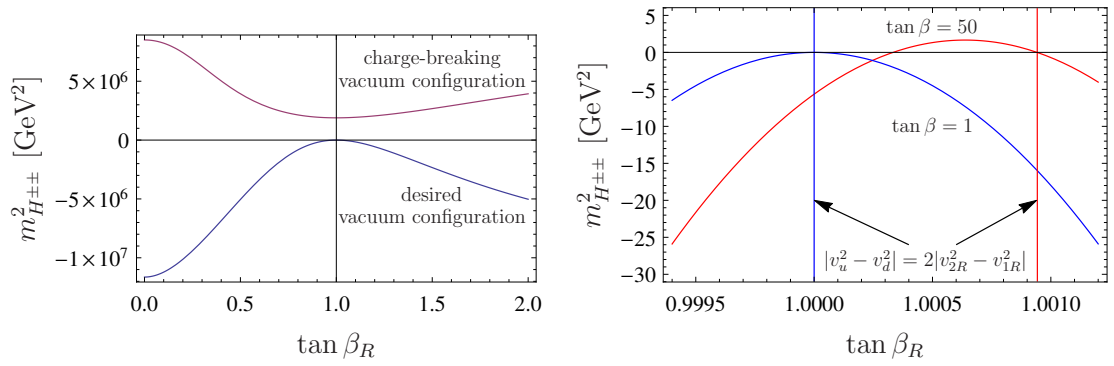

Figure 3.1: The lightest m^2 eigenvalues $m^2_{H^{\pm\pm}}$ as a function of $\tan\beta_R$. On the left figure the blue curve corresponds to the desired vacuum of eq. (3.8) and the purple line to the charge-breaking vacuum configuration of eq. (3.22). The parameters have been set to $v_R = 5.5$ TeV, $v_S = 10$ TeV, $\lambda_R = 0.5$, $\lambda_S = -0.5$, $\lambda_{12} = -0.02$, $T_{\lambda_R} = 0$, The right plot is a zoom into the left figure: we show the curve of the desired vacuum configuration for the cases $\tan\beta = 1$ and 50 in blue and red. The line which satisfies the condition $|v_u^2 - v_d^2| = 2|v_{2R}^2 - v_{1R}^2|$ is shown in red (blue) for the case $\tan\beta = 50$ (1).

3.2.2 Loop level

Although at the tree level, we find no possibility to construct a sensible model with R-parity conservation, it is not yet clear that the same argument holds in higher orders of perturbation theory. As has already been noted in the pioneering work by Coleman and Weinberg [100], radiative corrections can change the vacuum structure considerably, and hence also the adopted symmetry breaking or conservation. In left-right supersymmetric models, related considerations have been carried out [101], with the result that the one-loop

effective potential can change the saddle point discussed in the previous section to a charge-conserving minimum of the potential. These attempts suffer from the problem that the negative $m^2_{H^{\pm\pm}}$ will appear in the logarithms of the one-loop effective potential once the self-induced corrections are included. Simply disregarding the resulting imaginary parts of the one-loop potential is potentially dangerous since a complex potential indicates an unstable vacuum which eventually would decay [102]. We will return to considerations on the vacuum stability in section 3.4.

In more recent studies it was argued that the one-loop corrections induced by the Majorana neutrino Yukawa coupling y_4^L are sufficient to (i) render the $H^{\pm\pm}$ squared mass positive in the gaugeless limit [103], and to (ii) pull the desired minimum lower than the charge-breaking one, making it the global minimum [104]. In this case, $m^2_{L_R}$ is found to be required negative and, thus, large corrections from the gauginos to the slepton squared masses are necessary to avoid R-parity breaking. As those corrections grow with y_4^L, this means that it is very hard to achieve non-tachyonic sneutrinos because of the mass splitting induced by $y_4^L\,\mu_R^{\text{eff}}$, c.f. 3.36.

Here, we will perform a full Feynman-diagrammatic calculation which does not possess any of the flaws mentioned above: neither will we neglect any contributions or ignore the issue of imaginary logarithms, nor need negative values for $m^2_{L_R}$. For the numerical results we have implemented the model in the `Mathematica` package `SARAH` [105–110]. We have then used `SARAH` to generate source code for the spectrum generator `SPheno` [111, 112] which allows for a precise calculation of the mass spectrum at the one-loop level. The renormalization procedure is carried out in the $\overline{\text{DR}}$ scheme: first, the tadpole contributions are calculated with which the minimization equations are solved at one-loop. The solutions are inserted into the tree-level mass matrices to which the self energies are added and which are finally diagonalized. In the usual approach, the masses entering the loops are the tree-level values. Evidently, as argued above, this is a problem here due to the negative squared masses of the doubly charged Higgs bosons. Therefore, we modified the code in a way inspired by the on-shell scheme. Instead of inserting the tree-level masses into the loops, we use the loop-corrected ones in an iterative manner:

- 1^{st} iteration: $m^2_{[1]} = m^2(m^2_{[0]})$ using $m^2_{[0]} = |[m^2_{H^{\pm\pm}}]_{\text{tree-level}}|$
- $m^2_{[k]} = m^2(m^2_{[k-1]})$ until $\frac{|m_{[k]} - m_{[k-1]}|}{m_{[k]}} < \epsilon \ll 1$

We usually find convergence with $\epsilon = 10^{-4}$ after four iterations. Note that the starting point is in principle arbitrary, and we have verified that using other values such as $m_{[0]} = 0$ gives the same results. We want to remark that the above prescription breaks gauge invariance at the two-loop order. However, the associated effects are expected to be significantly smaller than the genuine two-loop contributions and are hence of no relevance here.

We now turn to the numerical results. As a first exercise we start by comparing our results to the analytical formula given in ref. [103]. For this purpose we have modified the code according to the approximations used there: (i) gaugeless limit ($g_i \to 0$), (ii) negligence of the electroweak vevs and (iii) inclusion of only the loop contributions stemming from one diagonal entry in y_4^L. As has been seen in the previous subsection 3.2.1, in this limit the lightest $H^{\pm\pm}$ eigenstate is a massless pseudo-Goldstone boson, implying that the loop corrections have to be finite [113]. In figure 3.2 we show the results for the squared $H^{\pm\pm}$ mass in these approximations as contour lines in various planes which display

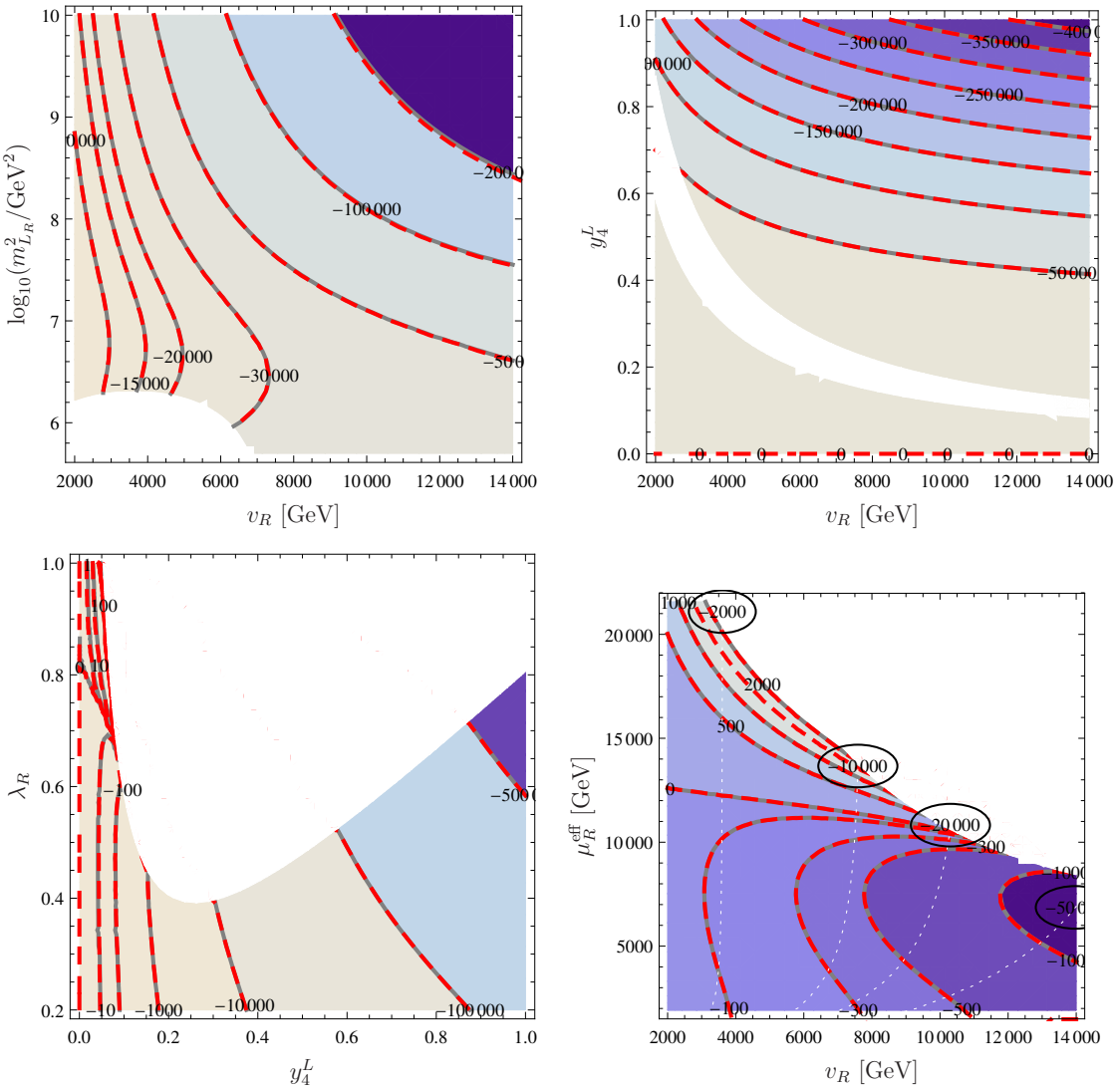

Figure 3.2: Comparison of our numerics with the analytical results obtained in ref. [103], using the same approximations. The grey contour lines depict the $H^{\pm\pm}$ squared mass values in GeV^2 obtained by the formulas of ref. [103] while the red dashed lines show the results using our modified code. The upper row shows the results in the $(v_R, \log_{10}(m^2_{L_R}/\text{GeV}^2))$ plane using $y_4^L = 0.4$ and in the (v_R, y_4^L) plane using $m^2_{L_R} = 2 \cdot 10^6$ GeV^2. The remaining relevant parameters have been fixed to $\lambda_R = 0.4, v_S = 10$ TeV. The lower row shows the $H^{\pm\pm}$ squared isomass lines in the (y_4^L, λ_R) plane on the left panel, using $v_R = 5.5$ TeV, $v_S = 10$ TeV and $m^2_{L_R} = 2 \cdot 10^6$ GeV^2. The right panel shows the $(v_R, \mu_R^{\text{eff}})$ plane with $m^2_{L_R} = 10^7$ $\text{GeV}^2, y_4^L = 0.1$. The white dashed lines show, for comparison, the $H^{\pm\pm}$ squared mass eigenvalues at the tree level without applying any approximations. In the white regions one sneutrino CP-eigenstate gets tachyonic in the gaugeless limit.

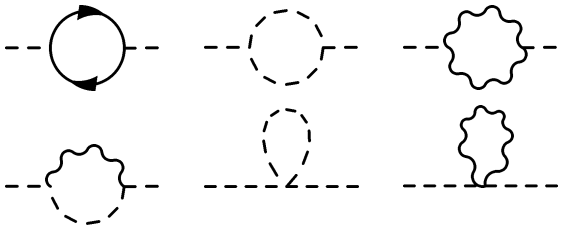

Figure 3.3: Generic one-loop diagrams contributing to the doubly-charged Higgs self-energy.

the most important dependencies. We observe excellent agreement between the grey contour lines and the red dashed ones, representing the analytical results and our numerical treatment, respectively. Therefore, we see our numerics confirmed. Interestingly, in most of the considered parameter regions these one-loop corrections contribute negatively to $m^2_{H^{\pm\pm}}$, *i.e.*, they are even *counterproductive* for achieving a viable spectrum. This is especially true for large y_L^4 and v_R. Only in regions with a large μ_R^{eff} parameter we find positive contributions, as seen in the lower row of figure 3.2. These positive values have to be compared with the actual tree-level eigenvalues which arise in the absence of any approximations (shown in white dashed contour lines). We find that very large values of μ_R^{eff} have to be paired with low values for v_R to achieve combined squared masses which are at least positive, see the upper left corner in the lower right image of figure 3.2. However, as those large μ_R^{eff} values decrease the mass of one of the $\tilde{\nu}_R$ CP eigenstates, one sneutrino easily gets tachyonic. This is what happens in the white regions in figure 3.2. For avoiding that, $m^2_{L_R}$ has to be large to compensate for this negative term. If one assumes that the soft mass terms of all sfermions are of approximately the same order of magnitude, it would be very unlikely in this case for the LHC to observe any of the squark or slepton states in direct production.

We stress again that the above discussion only includes the y_4^L-dependent corrections in the gaugeless limit, and we now move on to consider the full one-loop corrections. The generic Feynman diagrams which determine the $H^{\pm\pm}$ self energy are shown in figure 3.3. In addition, the one-loop corrections to the neutral triplet scalar tadpole diagrams contribute via the solutions to the tadpole equations. In figure 3.4 we present the analogue to the left upper image of figure 3.2, only with the full corrections turned on. Note that it is the actual masses which are shown, not the squared ones. It is striking that, although the tree-level mass as well as the previously considered partial corrections both point to tachyonic states, we find phenomenologically viable masses of several hundreds of GeV when we do the full calculation. The shape in $m^2_{L_R}$ is entirely due to the negatively contributing y_4^L-dependent corrections so that by reducing y_4^L (right panel) the dependence of $m^2_{L_R}$ is almost gone and the $H^{\pm\pm}$ masses increase notably. The white regions at low slepton soft masses are due to tachyonic sneutrinos as in the previous discussion, whereas the blank areas at large $m^2_{L_R}$ or v_R feature a tachyonic doubly-charged Higgs despite the large positive one-loop corrections to its mass.

Being comprised of transcendental equations, the analysis of the parametric dependence of the loop contributions is highly non-trivial. However, some conclusions can be drawn. For a first qualitative understanding we show in figure 3.5 the effect of gradually switching on different loop contributions to the tree-level squared mass which itself is represented by the grey solid line. As already discussed beforehand, the y_4^L-dependent loop contributions

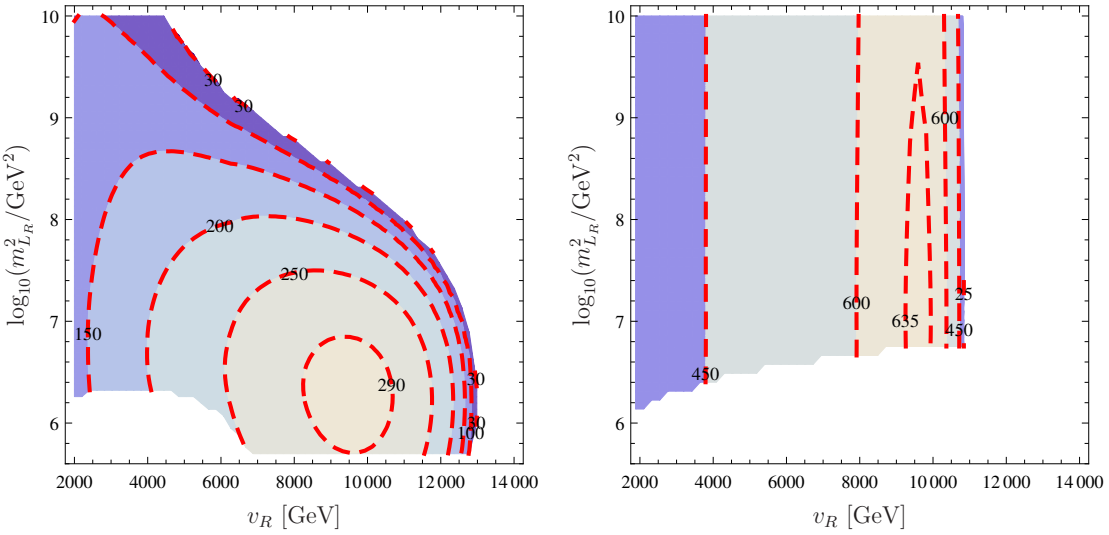

Figure 3.4: Mass of the lightest doubly-charged Higgs boson in GeV as evaluated from a complete one-loop calculation. The results are presented in $(v_R, \log_{10}(m^2_{L_R}/\mathrm{GeV}^2))$ planes for a scenario featuring the same setup as in the left panel of figure 3.2 (left), as well as for the case of a smaller $y_4^L = 0.1$ and a larger $\lambda_R = 0.9$ value (right).

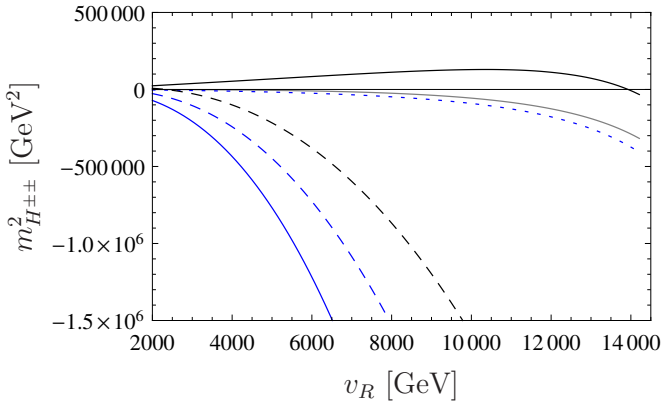

Figure 3.5: Dependence of $m_{H^{\pm\pm}}$ on v_R. Predictions are given at the tree level (grey solid) and after considering full (black solid) and partial (other curves) one-loop corrections. For the latter, we first include the sole y_4^L-dependent (s)lepton and (s)neutrino contributions (blue dotted) to the tree-level value, then add on top of them all diagrams featuring neutral gauge bosons as well as neutral and doubly-charged Higgs bosons (blue dashed). We next additionally include chargino contributions (blue solid) and further consider diagrams with neutralinos and doubly-charged higgsinos (black dashed). The full result finally also contains extra $W'^{\pm}/H^{\pm}$ contributions. The employed benchmark scenario is defined by $\lambda_R = 0.4$, $m^2_{L_R} = 2 \cdot 10^6$ GeV, $y_4^L = 0.25$ and features one generation of right-handed neutrinos.

from the (s)neutrinos and charged (s)leptons contribute negatively for large values of y_4^L and $m^2_{L_R}$. Understanding the remaining contributions that we have added for the first time in this kind of models requires a review of the relevant couplings between the $H^{\pm\pm}$ and the particles in the loop. The relevant couplings to charginos and neutralinos read

$$\begin{aligned}
\Gamma^L_{\tilde{\chi}_R^{++}\tilde{\chi}_j^0 H_k^{--}} &= -i\Big(\lambda_R U^{0,*}_{j,\tilde{S}} Z^{--}_{k,\Delta^{--}_{1R}} + \sqrt{2}\Big(g_{BL} U^{0,*}_{j,\tilde{B}} Z^{--}_{k,\Delta^{++,*}_{2R}} + g_R U^{0,*}_{j,\tilde{W}_{R,3}} Z^{--}_{k,\Delta^{++,*}_{2R}}\Big)\Big)\,, \\
\Gamma^R_{\tilde{\chi}_R^{++}\tilde{\chi}_j^0 H_k^{--}} &= -i\Big(\lambda_R U^{0}_{j,\tilde{S}} Z^{--}_{k,\Delta^{++,*}_{2R}} - \sqrt{2}\Big(g_{BL} U^{0}_{j,\tilde{B}} Z^{--}_{k,\Delta^{--}_{1R}} + g_R U^{0}_{j,\tilde{W}_{R,3}} Z^{--}_{k,\Delta^{--}_{1R}}\Big)\Big)\,, \\
\Gamma^L_{\tilde{\chi}_i^{+}\tilde{\chi}_j^{+} H_k^{--}} &= i\sqrt{2} g_R Z^{--}_{k,\Delta^{++,*}_{2R}} \Big(U^{+,*}_{i,\tilde{W}_R^+} U^{+,*}_{j,\tilde{\Delta}_R^+} + U^{+,*}_{i,\tilde{\Delta}_R^+} U^{+,*}_{j,\tilde{W}_R^+}\Big)\,, \\
\Gamma^R_{\tilde{\chi}_i^{+}\tilde{\chi}_j^{+} H_k^{--}} &= -i\sqrt{2} g_R Z^{--}_{k,\Delta^{--}_{1R}} \Big(U^{-}_{i,\tilde{W}_R^+} U^{-}_{j,\tilde{\Delta}_R^+} + U^{-}_{i,\tilde{\Delta}_R^+} U^{-}_{j,\tilde{W}_R^+}\Big)\,,
\end{aligned} \tag{3.41}$$

where we have parameterised the vertices as $\Gamma = \Gamma^L P_L + \Gamma^R P_R$. U^0, $U^\pm$ and Z^{--} are the mixing matrices of the neutralinos, charginos and doubly-charged Higgs bosons respectively, whose elements we name $U_{i,X}$ and $Z_{i,X}$. These matrix elements hence denote the X field component of the i^{th} mass eigenstate. The diagrams involving two charginos give a negative contribution to $m_{H^{\pm\pm}}$. Having naively expected a positive contribution, this sign can be understood from the large mixing between the gaugino and the singly-charged higgsino of the $SU(2)_R$ sector, see eq. (3.30). The respective diagonal contributions to the doubly-charged Higgs self energy are proportional to $(|\Gamma^L_{\tilde{\chi}_i^+\tilde{\chi}_j^+ H_k^{--}}|^2 + |\Gamma^R_{\tilde{\chi}_i^+\tilde{\chi}_j^+ H_k^{--}}|^2) m^2_{H^{\pm\pm}}$ whereas the off-diagonal contributions are proportional to $(\Gamma^L_{\tilde{\chi}_i^+\tilde{\chi}_j^+ H_k^{--}})(\Gamma^R_{\tilde{\chi}_i^+\tilde{\chi}_j^+ H_l^{--}})^* m_{\tilde{\chi}_i^+} m_{\tilde{\chi}_j^+}$. As the masses of the relevant charginos are proportional to v_R and the wino soft SUSY-breaking mass, they are in general much larger than $m_{H^{\pm\pm}}$. Hence, the contributions to the off-diagonal entries of the $H^{\pm\pm}$ mass matrix turn out to be much larger than those to the diagonal ones, yielding a negative contribution to $m_{H^{\pm\pm}}$ after diagonalization. The contribution from loop diagrams involving a neutralino and a doubly-charged higgsino, in turn, are positive. The difference w.r.t. the singly-chargino case depicted above stems from the singlino component of the neutralinos. In the respective entries of the mass matrix, the product $(\Gamma^{L/R}_{\tilde{\chi}_R^{++}\tilde{\chi}_j^0 H_k^{--}})(\Gamma^{L/R}_{\tilde{\chi}_R^{++}\tilde{\chi}_j^0 H_l^{--}})^*$ involves λ_R-dependent terms whose sign is different from the ones of the gauge contributions. These terms will dominate for large values of λ_R, and hence μ_R^{eff}. In addition, large μ_S^{eff} increases the singlino component of $\tilde{\chi}^0$ and therefore $U^0_{j,\tilde{S}}$.

Another important positive contribution comes from diagrams involving charged vector and Higgs bosons from the $SU(2)_R$ sector. The respective interactions read

$$\begin{aligned}
\Gamma_{H_j^{--}W'^{+}W'^{+}} &= -i\sqrt{2} g_R^2 \Big(v_{1R} Z^{--}_{j,\Delta^{--}_{1R}} + v_{2R} Z^{--}_{j,\Delta^{++}_{2R}}\Big)\,, \\
\Gamma_{H_j^{--}H_k^{+}W'^{+}} &= -i\Big(g_R Z^{-}_{k,\Delta^{-,*}_{1R}} Z^{--}_{j,\Delta^{--}_{1R}} + g_R Z^{-}_{k,\Delta^{+}_{2R}} Z^{--}_{j,\Delta^{++,*}_{2R}}\Big)\,, \\
\Gamma_{H_i^{--}H_j^{+}H_k^{+}} &= \frac{i}{\sqrt{2}} g_R^2 \Big(2\left(v_{2R} Z^{-}_{j,\Delta^{+}_{2R}} Z^{-}_{k,\Delta^{+}_{2R}} Z^{--}_{i,\Delta^{++,*}_{2R}} + v_{1R} Z^{-}_{j,\Delta^{-,*}_{1R}} Z^{-}_{k,\Delta^{-,*}_{1R}} Z^{--}_{i,\Delta^{--}_{1R}}\right) \\
&\quad - \left(Z^{-}_{j,\Delta^{+}_{2R}} Z^{-}_{k,\Delta^{-,*}_{1R}} + Z^{-}_{j,\Delta^{-,*}_{1R}} Z^{-}_{k,\Delta^{+}_{2R}}\right)\left(v_{2R} Z^{--}_{i,\Delta^{--}_{1R}} + v_{1R} Z^{--}_{i,\Delta^{++,*}_{2R}}\right)\Big)\,,
\end{aligned} \tag{3.42}$$

where we have omitted the momentum and metric dependence from the former two vertices

and neglected the electroweak vevs in the latter coupling. Being proportional to v_R, these contributions increase with the LR breaking scale.

In summary, the most important one-loop contributions to $m_{H^{\pm\pm}}$ are:

- negatively contributing: y_4^L-dependent loops ((s)neutrinos and charged (s)leptons) as well as $H^{\pm\pm}$ /$\{\gamma, Z, Z', h^0, A^0\}$ and $\tilde{\chi}^{\pm}$ loops,
- positively contributing: $\tilde{\chi}^{\pm\pm}/\tilde{\chi}^0$ and $W'^{\pm}/H^{\pm}$ loops.

Eventually, the tree-level contribution to $m_{H^{\pm\pm}}$, represented by the grey line in figure 3.5, grows too negative with increasing v_R and cannot be compensated anymore by the $\tilde{\chi}^{\pm\pm}/\tilde{\chi}^0$ and $W'^{\pm}/H^{\pm}$ loops so that $H^{\pm\pm}$ becomes tachyonic again for large enough v_R. This scale turns to be $v_R \simeq 14$ TeV for the example of figure 3.5.

We see from the shown examples that the use of incomplete one-loop considerations from the literature leads to the conclusion that a large parameter space is excluded due to tachyonic states. When applying a complete treatment, however, it turns out that a big portion of this parameter space is in fact viable. Fortunately, the predicted $H^{\pm\pm}$ masses turn out to be of the same order of magnitude as is currently probed at the LHC. Hence, they have to be confronted with the current limits set by the ATLAS and CMS collaborations [114,115]. Because of the Yukawa term $y_4^L \hat{L}_R \cdot \hat{\Delta}_{1R} \cdot \hat{L}_R$ in the superpotential, the decay products are two like-sign leptons, $H^{++} \to \ell^+\ell^+$, and the bounds vary depending on the flavour of the final state leptons. The lower bounds on the mass of a doubly-charged Higgs boson given in ref. [115] are 444 GeV, 459 GeV and 204 GeV for ee, $\mu\mu$ and $\tau\tau$ final states, respectively. However, it is assumed there that the the $H^{\pm\pm}$ originates from a $SU(2)_L$ triplet, the production cross sections of which being higher than for a $SU(2)_R$ triplet. In ref. [114], both cases are considered separately. While the bounds for $SU(2)_L$-gauged $H^{\pm\pm}$ states are generically tighter than the respective limits in [115], the bounds for $SU(2)_R$ triplet states are slightly looser: 374 GeV and 438 GeV for the final states of ee and $\mu\mu$ flavour, respectively. Bounds for a like-sign $\tau\tau$ pair are not provided.

3.3 Collider searches

The CMS and ATLAS collaborations are very actively searching for signals of extra gauge bosons. As shown earlier, in the setup under study, the W' is generically lighter and thus would show up first at a collider experiment. We will therefore concentrate on the interpretation of W' searches and evaluate the resulting constraints on the model's parameter space.

The W' can decay into a variety of final state particles. Apart from a pair of quarks, this comprises vector and Higgs bosons such as $W^{\pm}H^0$ or $H^{\mp}H^{\pm\pm}$. In addition, supersymmetric final states can appear as decay products, most prominently charginos and neutralinos, but also a pair of squarks or sleptons. Eventually, also the fermionic counterpart of the latter is possible: a charged lepton and a right-handed neutrino. While the final-state neutrino can in principle also be a light state (ν), its coupling to the W' is strongly suppressed by the small $\nu_L - \nu_R$ mixing angle so that, if kinematically accessible, the $\ell\,\nu_R$ channel is much more likely. Analyses looking for a charged lepton and missing energy, assuming a low-mass neutrino in the final state, hence do not apply to left-right symmetric models.

3.3.1 Hadronic W' searches

The easiest way to look for a W' is searching for deviations from the Standard Model in the quark-quark final state, whereas the differentiation between first- and second-generation quarks and third-generation quarks has to be done. The former case yields a simple dijet final state. In the latter case, the top quark decay products bW and the subsequent W decay have to be taken into account, so that the looked-for final state is two b-jets, a charged lepton and missing energy. While direct bounds on simplified left-right symmetric models have been derived in the corresponding analyses, it is not yet clear how these bounds translate to our model as the W' total width and consequently also the hadronic branching ratios depend on the complete set of open W' decays. We therefore revisit the corresponding most recent CMS search results [116, 117] in the context of our model. Here and in the following we will assume $g_R = g_L$.

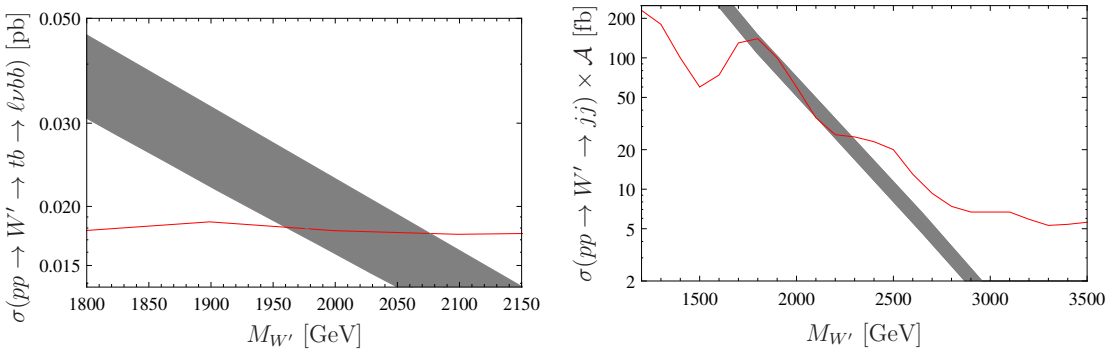

Figure 3.6: Bounds on the mass of the W' boson as obtained from the analysis of tb leptonic events ($\ell = e, \mu, \tau$) (left) and the CMS dijet search (right). The cross-sections for the model under study range within the grey bands, and the red lines represent the limits on the signal cross sections obtained from ref. [117] and ref. [116], respectively. The acceptance for the kinematic cuts as used in the dijet analysis is $\mathcal{A} \simeq 0.53$.

For a comparison of the given cross-section limits we used `SARAH` to produce `MadGraph` [118] code via the UFO [119] interface. The parton level results have been convoluted with with the parton density distribution set `CTEQ6L1` [120] and scaled to the next-to-leading order by multiplying with the appropriate K-factors of 1.23 and 1.2 for the processes $pp \to jj$ and $pp \to tb$, respectively.[3] In figure 3.6 we present the expected cross-sections which are compared to the tb (left image) and the dijet search limits (right). The grey bands correspond to the ranges in which the cross-section can vary in this model, depending on the spectrum: the upper edge of the curves corresponds to the case of a heavy supersymmetric spectrum in which case effectively only the W' decay channels into Standard Model particles or $\ell\,\nu_R$ are open, resulting in a comparatively small width. The lower edge corresponds to a light spectrum, in particular $\mu^{\text{eff}} = 150$ GeV, and an accordingly increased W' width. The broader the W' resonance, the more suppressed are the jj and tb branching fractions, which is the reason for the spread in the grey bands. The red lines each show the exclusion curves from CMS in the $\sigma - M_{W'}$ plane. In ref. [116], a lower limit on the mass of a W' stemming from a $SU(2)_R$ gauge symmetry of $2.05 - 2.1$ TeV is given which agrees with the upper edge of the grey band in the left panel of figure 3.6. In the case of a light spectrum,

[3] The numerical results have been cross-checked with output from `CalcHEP` [121].

in turn, the bounds are reduced to $M_{W'} \lesssim 1.95$ TeV. The CMS limit for dijet resonances depends a lot more on the specific spectrum. The reason for that is a small excess that has been observed at an invariant dijet mass around 1.8 TeV so that the bounds are weaker in its vicinity. Because of the spread of the grey bands according to the different possible W' widths, this has important consequences for setting bounds on our model: if the SUSY spectrum is light (lower edge of the grey band), the bounds of the jj search are not very constraining, and only masses up to 1.7 TeV can be excluded from this search. Hence, for these scenarios the tb bounds are relevant. If, in turn, the supersymmetric spectrum is heavy, then the dijet bounds are more constraining than the tb search. We deduce that

- light SUSY spectrum: $M_{W'} \gtrsim 1.95$ TeV and
- heavy SUSY spectrum: $M_{W'} \gtrsim 2.25$ TeV.

3.3.2 Combined W'-ν_R search

Apart from the hadronic searches, also combined analyses are performed which look for right-handed neutrinos that have been produced by a decaying W'. The limits obtained by these searches are typically interpreted in a simplified left-right-symmetric context where the Standard Model is extended by a W' and a ν_R, using $g_L = g_R$. Consequently, the assumptions are that (i) the W' has no other decay channels than a pair of quarks or a charged lepton and a right-handed neutrino and (ii) that the ν_R decays solely via an off-shell W' (denoted W'^* in the following). The considered production chain is

$$p\,p \to W' \to \ell\,\nu_R \to \ell\,\ell\,W'^* \to \ell\,\ell\,q_1\,\bar{q}_2\,, \tag{3.43}$$

and only leptons and quarks of the first two generations are considered. Assuming that the produced ν_R doesn't mix with the other neutrinos and is considerably heavier than the top quark leads to the assumption that the ν_R decays to a charged lepton plus first- or second-generation quarks in about two thirds of the cases. In the considered type of models, however, this assumption would be very premature [93, 95, 96, 122] as in general additional two-body decays are possible such as decays into a charged (neutral) slepton and a chargino (neutralino), and also into a charged lepton and a charged Higgs. The latter is often the case in the model under consideration because of the light mostly Φ_2^--like state with the non-negligible coupling to ν_R via the Δ_{1R} admixture, see eqs. (3.37-3.38). Via this mixture, the additional decay channel

$$\nu_R \to \ell^\mp H^\pm \tag{3.44}$$

is in general open, the charged Higgs subsequently decaying into tb. A further suppression of the $\nu_R \to \ell jj$ decay is present when the supersymmetric spectrum is light so that additional three-body decays of the form

$$\nu_R \to \ell\,W'^* \to \ell\,X\,Y\,, \qquad X\,Y \neq jj \tag{3.45}$$

are open. In particular the higgsino-like charginos and neutralinos whose mass is controlled by the size of μ^{eff} can reach large branching ratios. In figure 3.7 we show the branching ratios of right-handed neutrinos for the case that the lightest charged Higgs ranges between 200 and 300 GeV (left panel) as well as between 400 and 500 GeV (right panel) in mass. The

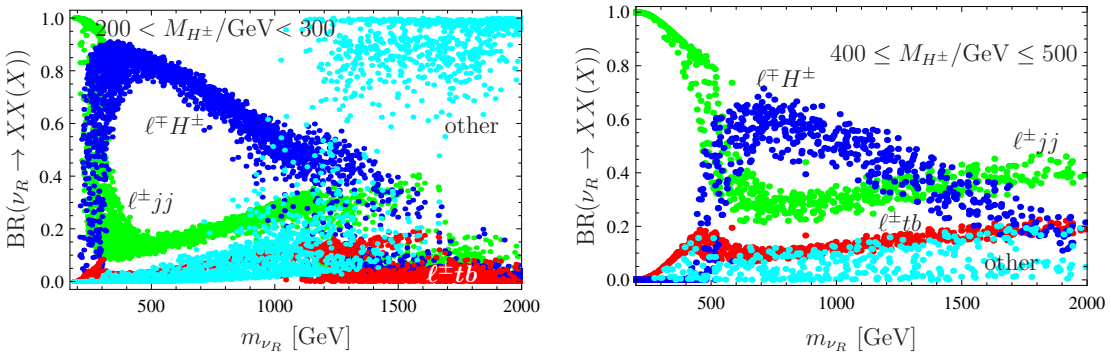

Figure 3.7: Branching ratios of the right-handed neutrino for a light spectrum, including a charged Higgs of mass 200 GeV $< M_{H^\pm} <$ 300 GeV (left) and for a heavier spectrum with 400 GeV $< M_{H^\pm} <$ 500 GeV (right). 'Other' refers to all other two- and three-body decays.

different regions can be easily identified. In the low ν_R mass region, the three-body decay via a virtual W' dominates, the final state being almost exclusively the ℓjj channel since the ℓtb channel has too little phase space available. For ν_R masses at the $H^\pm$ threshold, the associated two-body decay channel opens and the other channels are suppressed accordingly. The final state as used in the experimental analysis still amounts to around 10-40 % in this case. The magnitude of this branching ratio is mostly influenced by the mass ratio $m_{\nu_R}/M_{W'}$ because of the suppression of the W' propagator in the three-body decay. Accordingly, the heavier the decaying ν_R, the less suppressed the three-body decay, and consequently, ℓjj can become the dominant channel again. This is the case in the right figure at around $m_{\nu_R} \approx 1.5$ TeV. The other decay modes (cyan) are, in the lower mass regions of the right-handed neutrino, mostly three-body decays $\nu_R \to \ell^\mp \tilde{\chi}^\pm \tilde{\chi}^0$ via an intermediate W'. As soon as another two-body decay opens which isn't suppressed by a small mixing angle, it will dominate over the other decays. This is the case in the left figure where we have assumed a somewhat lighter spectrum than in the right panel, with accordingly lighter sleptons. Hence, as soon as this channel is kinematically allowed, the decays $\nu_R \to \tilde{\nu}\tilde{\chi}^0/\tilde{\ell}^\mp\tilde{\chi}^\pm$ amount to almost 100 % in branching ratio.

Evidently, the modified ν_R decays with respect to the simplified treatment change the interpretation of the experimental search results considerably, and a reanalysis in the framework of our model is in order. To this day, the most constraining bounds with this respect stem from the CMS collaboration, ref. [123], and the reported bounds on the W' mass range up to 3 TeV. In figures 3.8-3.9 we show the reinterpretation of this search in the $(M_{W'}, m_{\nu_R})$ plane for right-handed neutrinos of electron and muon flavour, respectively, using a suitable K-factor of 1.3 [124]. The area enclosed by the black line corresponds to the region which ref. [123] excludes for the kind of left-right models used there. The red dots correspond to parameter points of our model which are excluded because of the placed cross-section limits, whereas green points are allowed. In the low-mass region of the right-handed neutrinos, the analysis is not sensitive: the ν_R decay products are very collimated, and as the reconstruction in this analysis relies on high-p_T objects which are spacially well separated from one another, the signal drops rapidly for $m_{\nu_R}/M_{W'} \lesssim 0.1$ [123]. The overlap between red and green points in this area is quite significant and can be explained by the extra W' decay modes: in this low ν_R mass region, the $H^\pm$ is often too heavy for the

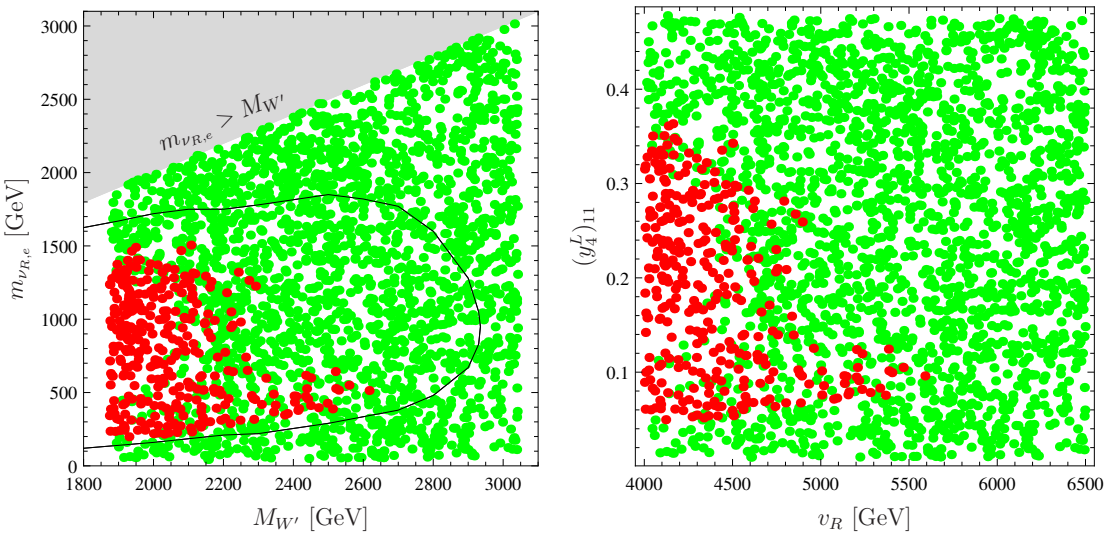

Figure 3.8: Random scan over the model parameters presented in the $(m_{\nu_{Re}}, M_{W'})$ plane (left) and $((y_L^4)_{11}, v_R)$ plane (right). Red (green) points are excluded (allowed) from the CMS search for W' and $\nu_{R,e}$ in the $eejj$ channel. The black curve in the left panel of the figure is taken from ref. [123] and contains the excluded region of the $W'/\nu_{R,e}$ combination when evaluated in the simplified model of ref. [123].

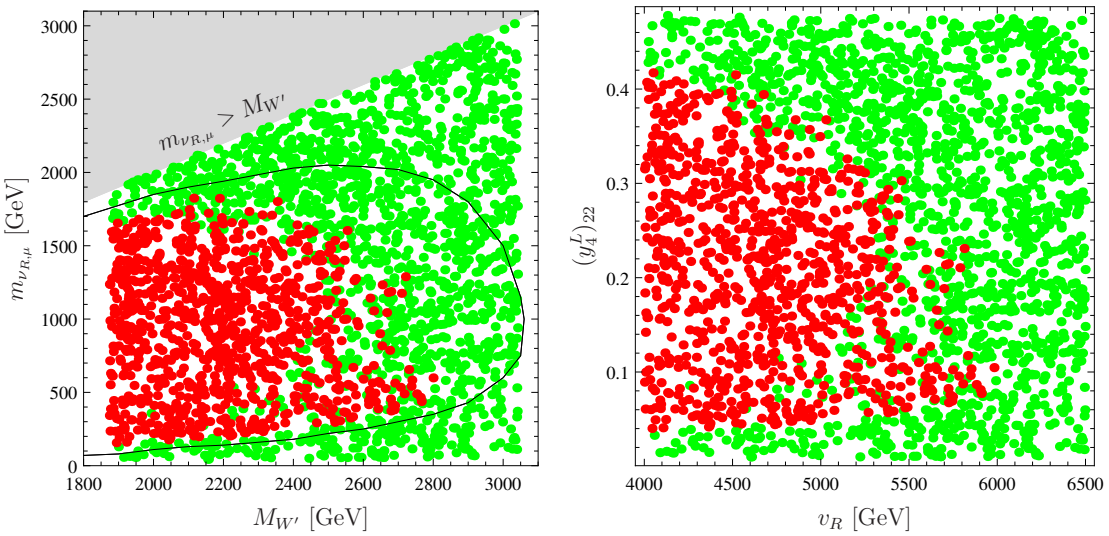

Figure 3.9: Same as in figure 3.8, for a right-handed neutrino of a muon flavour (of mass $m_{\nu_{R,\mu}}$).

ν_R to decay into. The assumptions of the simplified models thus apply for those parameter points where the W' decays dominantly into $q\bar{q}'$ or $\ell\nu_R$, *i.e.* those points exhibiting a heavy supersymmetric spectrum. Consequently, some of the points close to the border of the exclusion line are actually excluded. For those points whith a light supersymmetric spectrum, in turn, extra W' decays into higgsinos and other particles reduce the branching fraction into the searched-for final state. In this way, the $\ell\ell jj$ cross-section is reduced, leaving those points close to the black line still allowed.

In the region featuring large m_{ν_R}, in turn, all points which lie close to the black exclusion curve are still allowed. This is the combined effect of additional W' decays as well as the additional W'-mediated ν_R three-body decays and the open $\nu_R \to \ell^\mp H^\pm$ channel. The latter becomes more important in the bulk region where also $M_{W'}$ is large so that the three-body decays are further suppressed. As a result, no excluded points can be found in the vicinity of the exclusion curve in the high-$M_{W'}$ region but the W' bounds are reduced by up to 400 GeV and 700 GeV for the case of electron- and muon-flavoured neutrinos, respectively. In general, the bounds for the $\nu_{R,e}$ are less restrictive, and the effect of the open $\ell^\mp H^\pm$ channel is much more pronounced (see the notch at $m_{\nu_{R,e}} \gtrsim 500$ GeV in figure 3.8). This is because of the less stringent CMS cross-section bounds in ref. [123]. In fact, an excess with a local significance of $2.8\,\sigma$ has been observed in the $eejj$ channel for $1.8 < M_{W'}/\text{GeV} < 2.4$ whereas the muon channel agrees very well with the null hypothesis. In the experimental analysis it is stated that left-right symmetric models appear to fail to explain that excess, the main reason being that the estimated production cross section following eq. (3.43) is in general too large. However, this statement clearly does not hold when considering additional W' and ν_R decay channels which reduce the $eejj$ signal as in the scenarios discussed above, and in the following we shall see under which circumstances our model can fit this excess.

Note that our model in its described implementation can not explain the deficit of same-sign leptons within the final state (only one out of 14 potential signal events contains electrons of the same electric charge). Instead, as the neutrinos in our model are of Majorana type and we assume CP conservation in the lepton sector, one would expect the $e^\pm e^\mp jj$ and the $e^\pm e^\pm jj$ final states to be produced with the same rate. The more recent ATLAS analysis which only searches for same-sign lepton pairs and jets underpins this same-sign deficit as it does not see any excess in the data [125]. In the context of our model, this issue could *e.g.* be resolved by employing an inverse seesaw mechanism: in this way, the neutrinos would be pseudo-Dirac particles whereas the total rates addressed below are not affected [4]. Keeping that in mind, we will proceed with showing how in our model the necessary cross-sections are obtained.

As in the $\mu\mu jj$ channel no deviation from the background expectation has been observed, $\nu_{R,\mu}$ has to lie outside of the excluded mass range when compared to figure 3.9. We hence (conservatively) demand

$$m_{\nu_{R,\mu}} \lesssim 200 \text{ GeV} \qquad \text{or} \qquad m_{\nu_{R,\mu}} \gtrsim 1.8 \text{ TeV}\,, \tag{3.46}$$

[4] In ref. [126], a linear seesaw realization is presented which has the same effect of resolving this issue. An alternative explanation of the same-sign deficit in the context of left-right symmetry has been given in ref. [127]: in this analysis, the interference between two right-handed Majorana neutrinos with mixed flavour content and opposite CP parities is considered which can partially suppress same-sign lepton pairs.

or equivalently

$$(y_4^L)_{22} \lesssim 0.04 \qquad \text{or} \qquad (y_4^L)_{22} \gtrsim 0.36\,. \tag{3.47}$$

The ν_R of τ type remains unconstrained. For the following investigation we differentiate between three different ν_R mass hierarchies:

1. $m_{\nu_{R,e}} < m_{\nu_{R,\mu}} \approx m_{\nu_{R,\tau}}$,
2. $m_{\nu_{R,\mu}} \ll m_{\nu_{R,e}} < m_{\nu_{R,\tau}}$,
3. $m_{\nu_{R,\mu}} \approx m_{\nu_{R,\tau}} \ll m_{\nu_{R,e}}$.

The first hierarchy is in fact excluded if we apply an upper bound on the slepton soft mass parameter m_{L_R} of a few TeV: this scenario requires a rather large $(y_4^L)_{22}$ coupling which, as discussed before, decreases $m_{H^{\pm\pm}}$. This mass, in turn, is most constrained if $H^{\pm\pm}$ couples strongly to the muon flavour since in this case the most stringent bounds from $\mu^\pm\mu^\pm$ searches apply and hence it has to be heavier than ~ 400 GeV. For obtaining the sufficiently large one-loop corrections for this to happen, large μ_R^{eff} values are required which themselves enhance the splitting of the right sneutrino CP eigenstates. Eventually, for avoiding tachyonic sneutrinos, m_{L_R} has to be larger than ~ 3 TeV in this scenario, which we regard as undesirable. With the same line of argument we can also disregard the hierarchy $m_{\nu_{R,\tau}} \ll m_{\nu_{R,e}} < m_{\nu_{R,\mu}}$. As a consequence, only the cases in which $\nu_{R,\mu}$ is light are further considered. As we shall see in the following, both cases can in fact explain the observed excess, with both a light and a heavy supersymmetric spectrum.

Light supersymmetric spectrum

Let us consider a light supersymmetric spectrum now, in the sense that the higgsinos are light. In this case, the less stringent W' bound from the tb search applies, $M_{W'} \lesssim 1.95$ TeV. In figure 3.10 we present the signal cross sections using $\mu^{\text{eff}} = 150$ GeV and $m_{\nu_{R,e}} = M_{W'}/2$ for the cases of ν_R hierarchy 2 (black, solid) and 3 (black, dashed). The different values for μ_R^{eff} have no impact on the cross-section but were chosen in order to prevent a too small $m_{H^{\pm\pm}}$. The reason for the slight difference between both cases is the additional decay channel $\nu_{R,e} \to e^\pm \nu_{R,\tau} \tau^\mp$ for hierarchy 3. The observed (expected) cross-section limit is depicted by the red solid (dashed) line, and the green (yellow) band shows the expected limit $\pm 1\,\sigma$ ($2\,\sigma$). The blue line with the second largest cross-section depicts the case in which no additional ν_R decays are available but only the W'-mediated three-body decays $\nu_{R,e} \to eq\bar{q}'$. The difference between the neutrino hierarchies 2 and 3 in this case is very small so that only a single line is presented. The orange dashed line corresponds to the simplified left-right scenario as employed by ref. [123], in good agreement with the theoretical cross-section curve shown there.

As apparent from the figure, taking into account all decay modes of the W' is not enough for reducing the cross-section to the required value as this suppression only amounts to a factor of ~ 1.6. However, the combination with the additional ν_R decay modes, which result in a further suppression factor of 2.5, yields a cross-section which is of the right magnitude in order to explain the measured excess.

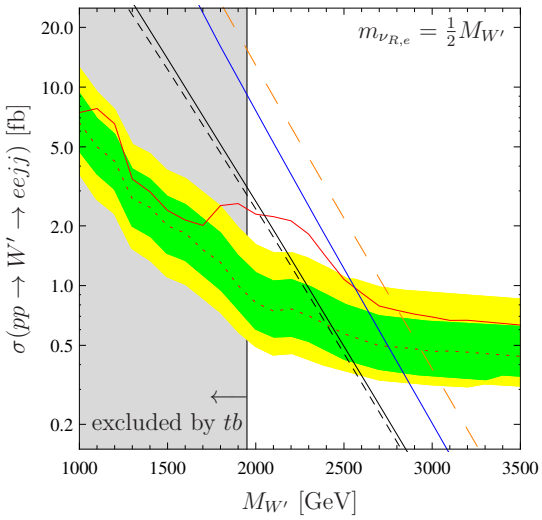

Figure 3.10: Expected cross section of the process $pp \to W' \to eejj$ at $\sqrt{s} = 8$ TeV using $\mu^{\text{eff}} = 150$ GeV, $\tan\beta_R = 1.02$ and $(y_4^L)_{11} \simeq 0.24$ which corresponds to $m_{\nu_{R,e}} = M_{W'}/2$. The black solid (dashed) line shows the case of ν_R hierarchy 2 (3) using $\mu_R^{\text{eff}} = 4$ (6) TeV. The blue line corresponds to the case in which the ν_R only decays into $\ell q\bar{q}'$. The orange dashed line represents the scenario of simplified left-right models where two-body ν_R decays as well as additional W' decays are absent. The grey area is excluded from the $W' \to tb$ searches in [117]. The red line shows the exclusion bound of ref. [123] and hence excludes all cross sections above the curve, while the red dotted line corresponds to the expected exclusion line using the background-only assumption. The green (yellow) band shows the expected exclusion $\pm 1\,\sigma$ $(2\,\sigma)$.

Heavy supersymmetric spectrum

The same consideration can be done if the higgsinos are heavy. In this case, the stronger W' bound from the dijet search applies and its mass has to be larger than ~ 2.25 TeV. Because of the smaller W' and ν_R width in this case, the $eejj$ cross-section is less reduced than for the case of light supersymmetry. We present in figure 3.11 the same situation as in figure 3.10 using $\mu^{\text{eff}} = 1.5$ TeV. Again we show the cases for neutrino mass hierarchy 2 (black lines) and 3 (blue) and see that hierarchy 3 features the smaller cross-sections when using the same value for $\tan\beta_R$. We present two different $\tan\beta_R$ values for the case of hierarchy 2. This is to show how the increase of $m_{H_1^\pm}$ with larger $\tan\beta_R$, c.f. eq. (3.37), reduces the phase space of the $\nu_R \to \ell^\mp H_1^\pm$ decay and consequently increases the $\ell\ell jj$ cross section. Eventually we find that despite the more stringent bounds on $M_{W'}$ and the relative factor of ~ 1.6 between these cross-sections and the ones in figure 3.10, also this scenario would still be compatible with the measured excess.

Consequences for the model

Taking the excess seriously, the necessary conditions for the fit to succeed have interesting consequences for the model. Of course, the most obvious consequence would be a W' of $\sim 2-2.3$ TeV which has to show up soon in the hadronic searches. This would immediately fix v_R. Secondly, if we take the same assumptions as above, in particular no flavour mixing within the ν_R sector, then $\nu_{R,\mu}$ has to be light, $m_{\nu_{R,\mu}} \lesssim 200$ GeV.

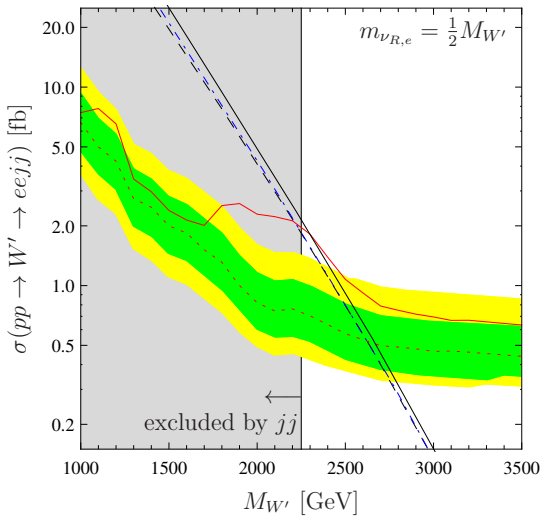

Figure 3.11: Cross-section of $pp \to W' \to eejj$ at $\sqrt{s} = 8$ TeV using μ^{eff} =1.5 TeV. The black solid (dashed) lines correspond to ν_R hierarchy 2 and $\tan\beta_R = 1.05$ (1.02) $\mu_R^{\text{eff}} = 6$ TeV (3.5 TeV), the parameters of blue dot-dashed line are $\tan\beta_R = 1.05$, $\mu_R^{\text{eff}} = 6$ TeV for hierarchy 3. The grey area is excluded from the dijet searches in ref. [116]. The rest of the figure is as in figure 3.10.

Interestingly, a near-future W' mass measurement can shed light on the underlying theory: should it be confirmed at 2 TeV, then an interpretation within our model will immediately demand a broad W' resonance, implying new particles of the order of a few hundred GeV as decay products, as are the higgsino-like charginos and neutralinos in the scenarios discussed above. A confirmation at 2.3 TeV, in turn, points to scenarios which lack such light additional decay final states.

Additional considerations on the $H^{\pm\pm}$ mass constrain the parameter space even further: for ν_R hierarchy 3, only a moderate largest y_4^L entry of ~ 0.24 is required for the case $m_{\nu_{R,e}} = M_{W'}/2$, so that $m_{H^{\pm\pm}}$ is not reduced by a large amount. However, as in this case $H^{\pm\pm}$ couples strongest to (and hence dominantly decays into) a pair of electrons, the respective LHC bounds already constrain its mass to be beyond 400 TeV. To achieve this, μ_R^{eff} has to be large ($\mu_R^{\text{eff}} \gtrsim 6$ TeV for $\tan\beta_R = 1.02$ and $M_{W'}$ around 2 TeV). As a consequence, in order to avoid a tachyonic sneutrino, $m_{L_R} \gtrsim 2.5$ TeV has to be satisfied so that the charged sleptons carry masses of the same order of magnitude. For hierarchy 2 these bounds are not as severe because in this case the dominant $H^{\pm\pm}$ decay mode is a τ pair, with the associated lower LHC bounds of roughly 200 GeV. Although the negative contributions from y_4^L to the one-loop $m_{H^{\pm\pm}}^2$ are larger than in the scenario (2), the conditions on μ_R^{eff} and also m_{L_R} are weaker in this case.

3.4 Vacuum stability

We have shown above that the tree-level saddle point of the charge-conserving vacuum can turn into a true minimum when considering the full one-loop corrections to the $H^{\pm\pm}$ mass. Of course, this merely means that it is one minimum among others, and at this stage we can not yet deduce a statement about the global minimum. In particular, it is not yet clear

if the desired vacuum configuration as in eq. (3.8) can feature a deeper minimum than the charge-breaking one of the tree-level potential, eq. (3.22), at all. Here we will analyse the stability of the desired vacuum for being able to provide statements about the valid parameter space from theory arguments, complementary to the experimental searches at the LHC.

We start by evaluating the one-loop effective potentials for the two most relevant vacua: the one exhibiting the desired symmetry breaking pattern and the charge-breaking one. In the following we denote the former as 'DSB' and the latter as 'CB'. The basic features can already be seen by the parts of the superpotential involving the $\hat{\Delta}_{iR}$, $\hat{L}_R$ and $\hat{S}$ superfields as in W_Δ of eq. (3.14) so that we work with the tree-level scalar potential as defined in eqs. (3.15-3.18). We calculate the soft Higgs masses $m^2_{\Delta_{1R}}$, $m^2_{\bar{\Delta}_{1R}}$ and m^2_S by solving the tadpole equations in the DSB case:

$$\frac{\partial V_0}{\partial X}\Big|_{\text{DSB}:\langle\Delta^0_{iR}\rangle=\frac{v_{iR}}{\sqrt{2}},\langle S\rangle=\frac{v_S}{\sqrt{2}}} = 0 \qquad \text{for} \qquad X = \{\Delta^0_{1R}, \Delta^0_{2R}, S\}\,. \tag{3.48}$$

Now V_{soft} is optimized for the DSB case. In order to account for this optimization in the CB case, the vevs v_{iR} have to be modified by a small amount, and we can relate the vevs of the CB vacuum to the corresponding DSB ones by

$$\langle\Delta^0_{1R}\rangle|_{\text{CB}} = \langle\Delta^{--}_{1R}\rangle|_{\text{CB}} = \alpha_1\frac{v_{1R}}{2} \qquad \text{and} \qquad \langle\Delta^0_{2R}\rangle|_{\text{CB}} = \langle\Delta^{++}_{2R}\rangle|_{\text{CB}} = \alpha_2\frac{v_{2R}}{2}\,, \tag{3.49}$$

and we therefore have to demand

$$\frac{\partial V_0|_{\text{CB}}}{\partial\alpha_i} = 0 \tag{3.50}$$

in order to find the global CB tree-level minimum. Those conditions result in α_i which are not equal to but close to unity. We proceed by calculating the masses of the scalar particles. As electromagnetism is not per se a good symmetry in this context, we split every complex scalar field X into its scalar and pseudoscalar components, $X = \frac{1}{\sqrt{2}}(v_X + \phi^S_X + i\phi^P_X)$. The non-zero vevs v_X are considered for the appropriate fields according to the CB and DSB vacuum configurations. The unphysical would-be-Goldstone bosons can be rotated out so that we end up with 15 real scalar fields, the mass matrix being calculated by

$$\left(M^2_S\right)^{\text{DSB/CB}}_{ij} = \frac{\partial^2 V_0}{\partial\phi_i\partial\phi_j}\Big|_{\text{DSB/CB}}\,. \tag{3.51}$$

The fermionic spectrum corresponding to W_Δ consists of the $SU(2)_R$ and $U(1)_{B-L}$ gauginos $\tilde{W}^i_R$ and $\tilde{B}$, the triplet higgsinos $\tilde{\Delta}_{iR}$ as well as the singlet fermion $\tilde{S}$ and the right-handed lepton doublet L_R. It can be evaluated from the Lagrangian terms

$$\mathcal{L}^{\text{fermions}}_{\text{mass}} = -\lambda_S\,S\,\tilde{S}\,\tilde{S} - \lambda_R\left(\tilde{S}\,\text{Tr}(\tilde{\Delta}_{1R}\,\Delta_{2R}) + \tilde{S}\,\text{Tr}(\Delta_{1R}\,\tilde{\Delta}_{2R}) + S\,\text{Tr}(\tilde{\Delta}_{1R}\,\tilde{\Delta}_{2R})\right) \tag{3.52}$$

$$-\frac{y^L_4}{2}\left(2L^T_R\,\Delta_{1R}\,\epsilon\,L_R + \tilde{L}^T_R\,\tilde{\Delta}_{1R}\,\epsilon\,L_R + L^T_R\,\tilde{\Delta}_{1R}\,\epsilon\,\tilde{L}_R\right) \tag{3.53}$$

$$-\sqrt{2}g_R\sum_{i=1}^{3}\tilde{W}_{R,i}\Big(\text{Tr}(\Delta^\dagger_{1R}[\tau_i,\tilde{\Delta}_{1R}]) + \text{Tr}(\Delta^\dagger_{2R}[\tau_i,\tilde{\Delta}_{2R}]) - \tilde{L}^\dagger_R\,\tau_i\,L_R\Big) \tag{3.54}$$

$$- \sqrt{2} g_{BL} \tilde{B} \Big(\mathrm{Tr}(\Delta_{2R}^\dagger \tilde{\Delta}_{2R}) - \mathrm{Tr}(\Delta_{1R}^\dagger \tilde{\Delta}_{1R}) + \frac{1}{2} \tilde{L}_R^\dagger \tau_i L_R \Big) \tag{3.55}$$

$$- \frac{1}{2} m_{\tilde{W}_R} \sum_{i=1}^{3} \tilde{W}_{R,i} \tilde{W}_{R,i} - \frac{1}{2} m_{\tilde{B}} \tilde{B} \tilde{B} + \text{h.c.}\,. \tag{3.56}$$

This results for example in lepton masses of

$$m_{\nu_R}|_{\text{DSB}} = \sqrt{2}\, v_{1R}\, y_4^L, \qquad m_{e_R}|_{\text{DSB}} = 0\,, \tag{3.57}$$

$$m_{\nu_R}|_{\text{CB}} = \alpha_1\, v_{1R}\, y_4^L, \qquad m_{e_R}|_{\text{CB}} = \alpha_1\, v_{1R}\, y_4^L\,. \tag{3.58}$$

The masses of the vector bosons W_R^i and B are obtained from the application of the covariant derivative to the Higgs fields $(D_\mu \phi)^\dagger (D^\mu \phi)$. The relevant non-derivative part of the corresponding Lagrangian reads

$$\begin{aligned} \mathcal{L}_{\text{mass}}^{\text{vector}} =& \mathrm{Tr}\Big((g_R \sum_{a=1}^{3} W_R^{\mu,a} [\Delta_{1R}^\dagger, \tau^a] - g_{BL} B^\mu \Delta_{1R}^\dagger)(g_R \sum_{b=1}^{3} W_{R,\mu}^b [\tau^b, \Delta_{1R}] - g_{BL} B_\mu \Delta_{1R}) \\ &+ (g_R \sum_{a=1}^{3} W_R^{\mu,a} [\Delta_{2R}^\dagger, \tau^a] + g_{BL} B^\mu \Delta_{2R}^\dagger)(g_R \sum_{b=1}^{3} W_{R,\mu}^b [\tau^b, \Delta_{2R}] + g_{BL} B_\mu \Delta_{2R}) \Big)\,. \end{aligned} \tag{3.59}$$

Three of the four mass eigenstates feature masses of $\mathcal{O}(v_R)$ whereas one eigenstate remains massless in each case. The latter is a consequence of the fact that a Higgs field in the adjoint representation of an $SU(N)$ cannot break the rank of this group. In the particular cases the massless bosons emerge from the following: in the DSB case the hypercharge $U(1)$ remains unbroken by the triplet scalar vevs. In the CB case, in turn, the vevs are aligned along τ_1 so that this generator remains unbroken due to $[\tau_1, \Delta_{iR}] = 0$ and W_R^1 turns out massless.

Having derived all masses for both symmetry breaking scenarios, we calculate the one-loop effective potential

$$V_{1L,\text{eff}} = V_0 + V_{CW}\,, \tag{3.60}$$

where V_{CW} is the Coleman-Weinberg potential [100] which reads, in the $\overline{\text{DR}}$ scheme and Landau gauge,

$$V_{CW} = \sum_n \frac{(-1)^{2s_n}(2s_n+1)}{64\pi^2} m_n^4 \Big(\log\Big(\frac{m_n^2}{Q^2}\Big) - \frac{3}{2} \Big)\,. \tag{3.61}$$

Here, n runs over all scalar fields, Weyl fermions and gauge bosons. The symbols s_n and m_n represent the spin and mass of the n^{th} field. Q is the renormalization scale which we fix to 1 TeV. We have checked that the features discussed below do not depend on the choice of Q by varying it up to $2\, v_R$.

In the following discussion we compare the depths of the minima of $V_{1L,\text{eff}}$ between the DSB and CB cases. Since the absolute depth of the minima is of no relevance, we are only

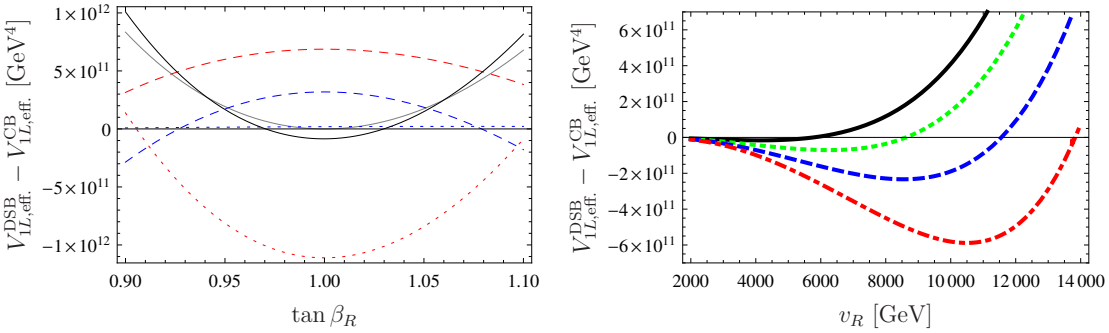

Figure 3.12: Results for $\Delta V = V^{\rm DSB}_{1L,\rm eff} - V^{\rm CB}_{1L,\rm eff}$ using the simplified approach with just the terms from W_Δ. For negative (positive) values of this difference, the DSB (CB) minimum is deeper. In the left panel we show this difference at the tree level (solid grey line) and at the one-loop level (solid black line) as a function of $\tan\beta_R$ for $v_R = 5.5$ TeV, $\lambda_R = 0.4$, $y_4^L = 0.25$, $m^2_{L_R} = 2 \cdot 10^6$ GeV^2 and $v_S = 10$ TeV. The additional lines represent the different contributions to ΔV: slepton and lepton fields (blue dotted line), Higgs fields (blue dashed line), gauginos/higgsinos (red dotted line) and vector bosons (red dashed line). In the right panel we depict the total difference for $\tan\beta_R = 1.02$ and $y_4^L = 0$ as well as $\lambda_R = 0.3$ (solid black line), 0.4 (green dotted line), 0.5 (blue dashed line) and 0.6 (red dot-dashed line).

interested in the difference of these values:

$$\Delta V = V^{\rm DSB}_{1L,\rm eff} - V^{\rm CB}_{1L,\rm eff}\,, \tag{3.62}$$

i.e. negative values imply that in this case the DSB vacuum at one-loop indeed features the lower minimum. In figure 3.12 we present ΔV as a function of $\tan\beta_R$ and v_R. In the left panel we show in addition to the total difference (black solid line) also the separate contributions to ΔV. Interestingly, we can confirm the suggestive statement of ref. [104] that the desired symmetry breaking variant can indeed turn out to result in a deeper minimum than the charge-breaking one once loop corrections are taken into account – with the difference that our findings motivate the inclusion the complete one-loop corrections as the sole y_4^L-dependent contributions from the (s)lepton sector are counterproductive with this respect. In the particular case depicted on the left panel of figure 3.12, the DSB case corresponds to the global minimum of the one-loop effective potential for $\tan\beta_R \in [0.97, 1.03]$. It is plainly seen that the DSB minimum can only be the deeper one because of the gaugino and higgsino contributions whereas the (s)lepton, Higgs and vector contributions usually add positively to ΔV. In section 3.2.2 it was argued that, besides the neutralino contributions, also the $W'^{\pm}/H^{\pm}$ loop contribute substantially to a positive $m^2_{H^{\pm\pm}}$ and hence to a one-loop DSB minimum. Note that this is not in contradiction with the statements made here since it is not the absolute contributions to $V^{\rm DSB}_{1L,\rm eff}$ that matter from a vacuum stability viewpoint but only the relative ones w.r.t. $V^{\rm CB}_{1L,\rm eff}$. The dependence of ΔV on v_R for different values of λ_R is shown in the right panel of figure 3.12. We observe that the DSB vacuum can only feature the deeper minimum up to a certain value of v_R which strongly depends on the other parameters like λ_R. This is similar to the $H^{\pm\pm}$ mass where the positive loop corrections from $\tilde{\chi}^0/\tilde{\chi}^{\pm\pm}$ are enhanced for larger λ_R.

In the above considerations we have shown that at one-loop, the desired symmetry breaking scenario can feature a deeper minimum than the vacuum structure corresponding

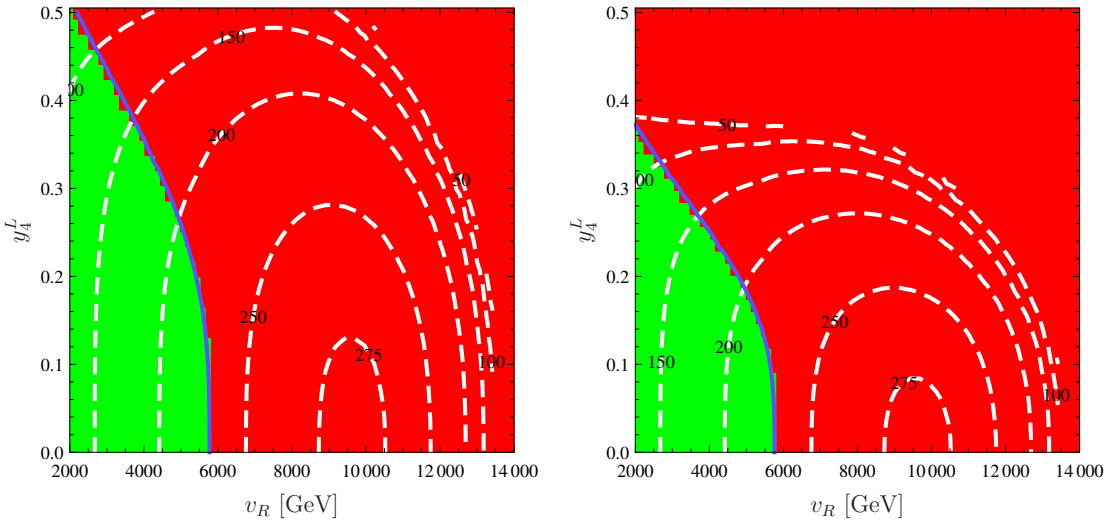

Figure 3.13: Analysis of the vacuum stability in the (v_R, y_4^L) plane using $\lambda_R = 0.3$, for one generation of right-handed neutrinos (left) and for three mass-degenerate ν_R states (right). The other fixed model parameters are $m^2_{L_R} = 2 \cdot 10^6$ GeV^2 and $v_S = 10$ TeV. The white contours indicate isomass lines for the doubly-charged Higgs boson in GeV as obtained with our full one-loop-corrected calculation. The green regions correspond to setups where the DSB vacuum configuration of eq. (3.8) is the global minimum of the scalar potential whereas in the red regions, the CB vacuum configuration consists of a deeper minimum. The blue line separates these cases using the results from the simplified analytical approach.

to the tree-level global minimum. For this analysis we have already known which ones the minima if interest were. In general, however, there are many more minima of the scalar potential with different vacuum structures which we have to take into account when asking for the global minimum and which we miss by only considering the two known ones. Therefore, we now turn to a numerical analysis of the vacuum structure of the full model, allowing for additional vevs. For this purpose we used `SARAH` to produce model files for `Vevacious` [128]. This is a programme that first evaluates all tree-level extrema of the scalar potential of a given model and continues by finding the nearby minima at the loop level via homotopy continuation, using the one-loop effective potential approach as done above. For checking if a given parameter point lives in a stable vacuum, one should, in principle, take into account all scalar fields and examine which ones develop a vev and which not. However, in models with as many scalars as in the present one, finding all possible minima in this multidimensional field space would require enormous amounts of CPU time well beyond a year for a single parameter point. Therefore, we restrict ourselves to allowing vevs for the most reasonable candidates only. In addition to the neutral Higgs scalars $\Phi^0_{1,2}$, $\Delta^0_{1R,2R}$ and S, we consider, as above, the possibility of non-zero vevs for Δ^{--}_{1R} and Δ^{++}_{2R} in order to account for the CB case. Moreover, we allow one generation of right sneutrinos $\tilde{\nu}_R$ to have a non-zero vev in order to cover the possibility of R-parity violating vacua. This is motivated by the fact that the tree-level saddle point of the CB vacuum can be turned into a minimum by allowing $\tilde{\nu}_R$ vevs.

It turns out that in regions where R-parity conserving spectra can be found at the one-loop level, the global minimum is always either

- of the DSB kind, *i.e.*
  $\langle \Phi_1^0 \rangle = v_d/\sqrt{2}\,,\ \langle \Phi_2^0 \rangle = v_u/\sqrt{2}\,,$
  $\langle \Delta_{1R}^0 \rangle = v_{1R}/\sqrt{2}\,,\ \langle \Delta_{1R}^{--} \rangle = 0\,,$
  $\langle \Delta_{2R}^0 \rangle = v_{2R}/\sqrt{2}\,,\ \langle \Delta_{2R}^{++} \rangle = 0\,,$
  $\langle S \rangle = v_S/\sqrt{2}\,,\ \langle \tilde{\nu}_R \rangle = 0\,,$

- or the CB kind, *i.e.*
  $\langle \Phi_1^0 \rangle = \langle \Phi_2^0 \rangle = 0\,,$
  $\langle \Delta_{1R}^0 \rangle = \langle \Delta_{1R}^{--} \rangle \simeq v_{1R}/2\,,$
  $\langle \Delta_{2R}^0 \rangle = \langle \Delta_{2R}^{++} \rangle \simeq v_{2R}/2\,,$
  $\langle S \rangle = v_S/\sqrt{2}\,,\ \langle \tilde{\nu}_R \rangle = 0\,.$

In figure 3.13 we show in the (v_R, y_4^L) plane the regions where the global minimum corresponds to the desired vacuum configuration (green) and where it corresponds to the charge-breaking scenario (red). The line that separates the DSB and CB cases due to $\Delta V = 0$ as obtained from the analytic approach used before is shown in blue. From the good agreement between both approaches we conclude that the simplified analytic approach can safely be used for a first understanding and an estimate of which of the known minima is deeper. The green-shaded parameter space of figure 3.13 is currently narrowed down from two sides by the LHC which sets lower limits on v_R (see section 3.3) as well as on $m_{H^{\pm\pm}}$ (see section 3.2). As for the y_4^L-dependent loop contributions to the $H^{\pm\pm}$ mass shown in figure 3.2, the region with the desired global minimum shrinks with growing Majorana neutrino Yukawa coupling and $SU(2)_R$ breaking scale, rendering these scenarios less likely. As each single ν_R contribution lifts the one-loop scalar potential, the net effect of including more than one non-zero y_4^L entry is that the region where a stable desired vacuum is possible gets reduced accordingly. This is seen in the right panel of figure 3.13 where we show for the otherwise same setup as in the left figure the case where all three right-handed neutrinos are degenerate in mass, *i.e.* $y_4^L \hat{=} (y_4^L)_{ii}$. As a matter of fact, the scenario on the left-hand side still contains parameter space that is not ruled out by LHC searches as long as the massive right-handed neutrino is of tau flavour. The scenario on the right panel, in contrast, is fully excluded because of the $H^{\pm\pm}$ searches as the decay $H^{\pm\pm} \to \ell^\pm \ell^\pm$ would be democratic in lepton flavour and the associated stronger bounds would apply.

While the parameter space in figure 3.13 is close to exclusion, this is not necessarily the case for other parameter regions. As has been shown in figure 3.12, larger λ_R values not only help raising the one-loop $H^{\pm\pm}$ mass but also pulling the DSB minimum below the charge-breaking analogue. In the left panel of figure 3.14 we show this effect in the (y_4^L, λ_R) plane. The figure on the right panel accordingly shows the analogue of figure 3.13 using $\lambda_R = 0.4$ instead of 0.3, featuring an accordingly larger region of allowed parameter space in the (v_R, y_4^L) plane. This increase in μ_R^{eff} comes with a prize, though. As discussed before, it enhances the F-term contribution to one of the sneutrinos and can consequently drive one of the CP-eigenstates tachyonic. The black curves in figure 3.14 enclose the regions in which that happens at the tree level. A natural consequence is R-parity violation in these parameter regions. Yet, similar to the $H^{\pm\pm}$ states which are tachyonic at the tree level, also the sneutrinos can be helped to a positive squared mass at the loop level which is the reason for small green strips beyond the black lines. Moving away from that frontier in parameter space, however, leads to larger negative squared masses at the tree level which

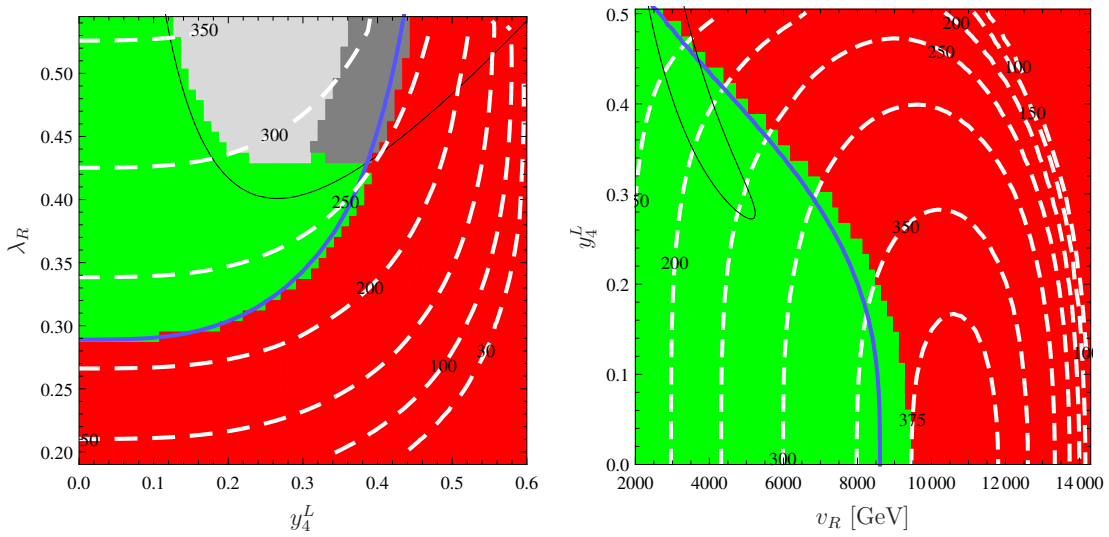

Figure 3.14: Analysis of the vacuum stability in the (y_4^L, λ_R) and the (v_R, y_4^L) plane. The parameters have been chosen as in the corresponding plots of figure 3.2 for one generation of right-handed neutrinos. The color code is as in figure 3.13. The blue line separates DSB and CB global minima as obtained from the simplified analytical approach. The additional black lines enclose regions where one sneutrino CP eigenstate gets tachyonic at the tree level due to the large negative F-term contributions. The grey areas indicate the parameter space in which the global minimum is found to violate R-parity, whereas the vacuum conserves electric charge in the lighter grey regions and in the darker grey regions it doesn't.

loop corrections cannot counteract. Hence, the $\tilde{\nu}_R$ field associated with the y_4^L entry has to aquire a vev in these areas, thereby breaking R-parity. This is the case in the grey regions in figure 3.14. A lighter grey shading indicates regions where R-parity is broken whereas the global minimum still conserves electric charge. However, although electroweak symmetry is also broken in this area, it does not happen at the correct scale since the electroweak vevs are of the order of one TeV. The darker grey shading, in turn, corresponds to scenarios where both, R-parity and electric charge invariance, are broken. Note that the R-parity violation here spoken of is solely an artefact of large negative F-term contributions to the sneutrino masses and could easily be avoided by a larger soft slepton mass $m^2_{L_R}$. In other words, in this case $\langle\tilde{\nu}_R\rangle \neq 0$ is necessary to acquire a minimum in the $\tilde{\nu}_R$ direction of the scalar potential. It is hence of completely different origin than the R-parity violation suggested in refs. [97, 99] which was thought necessary for a charge-conserving minimum at $\langle\Delta^{--}_{1R}\rangle = \langle\Delta^{++}_{2R}\rangle = 0$ – irrespective of the $\tilde{\nu}_R$ direction. In particular, as pointed out before, we did not find any R-parity violating global minima in regions where the tree-level squared masses of the sneutrinos are positive.

Finally, we remark that the parameter space in the red region of the figures does not necessarily have to be excluded because of a decaying vacuum. Instead, using a simple analysis of direct path tunneling at zero temperature, we found that in fact all points with a non-tachyonic $H^{\pm\pm}$ in the red region are metastable as the estimated tunneling time is many orders of magnitude larger than the age of the Universe. A more thorough investigation of this effect including the optimization of the tunneling path at $T \neq 0$ is beyond the time scale of this thesis. Investigations of this kind within the MSSM have

however shown that the consideration of additional non-zero vevs for other scalar fields such as squarks can prove a previously-thought metastable vacuum to be unstable [55, 56].

In conclusion, we have shown that the consistent calculation of one-loop mass corrections can not only ameliorate the situation of a tree-level tachyonic doubly-charged Higgs field but also increase the depth the corresponding vacuum beyond the dangerous charge-breaking one. Hence, other than concluded in early studies, the model under investigation is perfectly viable and in particular does not require R-parity violation to be kept alive. Fortunately, our study has shown that the regions of the parameter space which feature a large-enough $H^{\pm\pm}$ mass and at the same time a stable vacuum coincide with the scales currently under probe by the LHC, rendering this model highly testable.

CHAPTER 4

$SO(10)$ INSPIRED GMSB

We will now address the issue of the predicted Higgs mass in supersymmetry in the context of models with an extended gauge group. As briefly discussed before, in minimal supersymmetric models, the tree-level Higgs mass is constrained to be at most equal to the Z mass so that large loop corrections from stops are necessary to raise m_h to the measured value. This translates to the requirement that either the stop masses have to be in the multi-TeV range or that there is a large left-right splitting in the stop sector, incorporated in large stop trilinear couplings. The former is unattractive as then one of the main motivations for supersymmetry, namely it being the solution to the hierarchy problem, would be in a bad shape. The latter suffers from the problem that, for large ratios of the trilinear coupling to the average stop mass, the vacuum tends to grow unstable as a charge- and colour-breaking minimum featuring sfermion vevs emerges as the global minimum [55,56]. If the mechanism that breaks supersymmetry invariance works via gauge mediation, these trilinear couplings are tiny. Hence, the stop masses have to be very large which implies, in GMSB, large masses of the superpartners in general. Therefore, there is little hope for observing traces of such a model at the LHC and gauge mediation in its original form has been mostly disregarded recently. Instead, non-minimal realizations which include direct messenger-matter interactions have gained some popularity since they provide the possibility to generate large trilinear couplings [129–138].

In models exhibiting an extended gauge group such as the left-right-symmetric model discussed above, the condition $m_{h,tree} < M_Z$ does not apply anymore. The reason is that the Higgs fields are often also charged with respect to the new gauge symmetry so that extra D-terms add to the tree-level Higgs mass. In the following, we shall pursue the idea of minimal gauge mediated supersymmetry breaking in an explicit realization of a model with an extended gauge group and check to which extent these D-terms can loosen the lower bounds on the squark masses and which LHC phenomenology can be expected.

So far we have considered "true" left-right gauge symmetry at the TeV scale. A UV extension of these types of models is in general non-trivial as gauge coupling unification usually requires the addition of intermediate supermultiplets [139]. There are, however, classes of models in which a remnant left-right symmetry of $SU(3)_c \times SU(2)_L \times U(1)_R \times U(1)_{B-L}$ can remain unbroken down to the electroweak scale while retaining perturbative

gauge coupling unification at the GUT scale [88, 89]. Therefore we can assume that the left-right symmetric group gets broken down to the above group close to the GUT scale so that, starting from an $SO(10)$ GUT, the breaking works along the "minimal" left-right-symmetric chain:

$$\begin{aligned} SO(10) &\to SU(3)_c \times SU(2)_L \times SU(2)_R \times U(1)_{B-L} \\ &\to SU(3)_c \times SU(2)_L \times U(1)_R \times U(1)_{B-L} && \sim \text{GUT scale} \\ &\to SU(3)_c \times SU(2)_L \times U(1)_Y && \sim \text{TeV scale} \end{aligned} \tag{4.1}$$

As a consequence, the mass scale of supersymmetry breaking lies in the phase with broken $SU(2)_R$ but unbroken $U(1)_R \times U(1)_{B-L}$.

We will now start with presenting the central features of the model under consideration, define the messenger sector and derive the boundary conditions for the SUSY-breaking parameters before we go on with investigations of the Higgs properties and discuss different possibilities how a signal from this model could show up at the LHC.

4.1 Model definition

The matter sector as known from the MSSM is extended by three generations of a right-handed neutrino superfield $\hat{\nu}^c$ so that all matter fields can be accommodated in a complete **16**-plet under $SO(10)$ for each flavour. The Higgs sector has to be enlarged because of the need to break $U(1)_R \times U(1)_{B-L}$ down to the hypercharge group. This is achieved by two superfields $\hat{\chi}_R$ and $\hat{\bar{\chi}}_R$ bearing the opposite (same) $U(1)$ charges as $\hat{\nu}^c$. Because of these charge assignments, a seesaw of the inverse type is possible which requires the inclusion of an additional gauge singlet superfield $\hat{S}$. Note that the additional Higgs fields originate from $SU(2)_R$ doublets in the in the unbroken $SU(2)_L \times SU(2)_R \times U(1)_{B-L}$ phase close to the GUT scale, transforming as $(0, \mathbf{2}, \mp 1)$, and hence do not coincide with the additional Higgs sector from chapter 3 where $SU(2)_R$ triplets were used to break the symmetry and to implement a seesaw mechanism of type I. We will come back to this point and motivate the preference of this symmetry breaking and the corresponding seesaw mechanism over the previous one when discussing the tadpole equations in section 4.4.

The superpotential of the model reads

$$\begin{aligned} W =& Y_u^{ij}\, \hat{u}_i^c\, \hat{Q}_j^\alpha\, \epsilon_{\alpha\beta}\, \hat{H}_u - Y_d^{ij}\, \hat{d}_i^c\, \hat{Q}_j^\alpha\, \epsilon_{\alpha\beta}\, \hat{H}_d^\beta - Y_e^{ij}\, \hat{e}_i^c\, \hat{L}_j^\alpha\, \epsilon_{\alpha\beta}\, \hat{H}_d^\beta + \mu\, \hat{H}_u^\alpha\, \epsilon_{\alpha\beta}\, \hat{H}_d^\beta \\ &+ Y_\nu^{ij}\, \hat{\nu}_i^c\, \hat{L}_j^\alpha\, \epsilon_{\alpha\beta}\, \hat{H}_u^\beta + Y_S^{ij}\, \hat{\nu}_i^c\, \hat{S}_j\, \hat{\chi}_R - \mu_R\, \hat{\bar{\chi}}_R\, \hat{\chi}_R + \frac{1}{2}\mu_S^{ij}\, \hat{S}_i\, \hat{S}_j\,, \end{aligned} \tag{4.2}$$

which agrees with the one used in ref. [140].

It should be noted that the χ_R, $\bar{\chi}_R$ fields break R-parity spontaneously as soon as they develop a vev as they have $R = -1$ due to their $B - L$ quantum numbers. Moreover, gauge invariance would also allow terms like $\hat{\bar{\chi}}_R \hat{L} \hat{H}_u$ in the superpotential. Those would further contribute to this R-parity violation as soon as $\langle \bar{\chi}_R \rangle \neq 0$ and $\langle H_u^0 \rangle \neq 0$, respectively, hence mixing charged leptons with charginos as well as neutrinos with neutralinos. In order to avoid this, we introduce a discrete $\mathbb{Z}_2^M$ matter parity under which the Higgs superfields $\hat{H}_u, \hat{H}_d, \hat{\chi}_R, \hat{\bar{\chi}}_R$ are even and all other fields are odd. A discrete symmetry of that kind

has already been proposed in refs. [141, 142] for similar models. This parity is sufficient to forbid the dangerous terms leading to proton decay and to prevent the LSP from decaying, so that there is no need for the conventional R-parity. It is important to note that the contraints due to the discrete gauge symmetry anomalies are fulfilled [143, 144].

The soft SUSY-breaking Lagrange density is given by

$$-\mathcal{L}_{soft} = m_{ij}^2 \phi_i^* \phi_j + \Big(\frac{1}{2} M_{ab} \lambda_a \lambda_b + B_\mu \, H_u^\alpha \, \epsilon_{\alpha\beta} \, H_d^\beta - B_{\mu_R} \, \bar{\chi}_R \, \chi_R + B_{\mu_S} \, \tilde{S} \, \tilde{S} + T_S^{ij} \, \chi_R \, \tilde{\nu}_i^c \, \tilde{S}_j \\ - T_d^{ij} \, \tilde{d}_i^c \, \tilde{Q}_j^\alpha \, \epsilon_{\alpha\beta} \, H_d^\beta + T_u^{ij} \, \tilde{u}_i^c \, \tilde{Q}_j^\alpha \, \epsilon_{\alpha\beta} \, H_u^\beta \; - T_e^{ij} \, \tilde{e}_i^c \, \tilde{L}_j^\alpha \, \epsilon_{\alpha\beta} \, H_d^\beta + T_\nu^{ij} \, \tilde{\nu}_i^c \, \tilde{L}_j^\alpha \, \epsilon_{\alpha\beta} \, H_u^\beta + \text{h.c.} \Big) \,, \tag{4.3}$$

where we have used ϕ for all scalar particles, i and j being generation indices, and λ_a for the gaugino of gauge group a. Note that because of the two Abelian gauge groups and the resulting gauge kinetic mixing (see a discussion of that effect in the next section), also a mixed term $M_{R,B-L}\lambda_R\lambda_{B-L}$ is possible.

In table 4.1, we list the matter content of the model with the respective quantum numbers under the gauge groups. The $U(1)$ charges are normalized in such a way that, after the breaking $U(1)_R \times U(1)_{B-L} \to U(1)_Y$, the hypercharge operator reads

$$Y = T_R + T_{B-L} \,, \quad \text{where} \quad T_{B-L} \, \Phi = \frac{B-L}{2} \, \Phi \,. \tag{4.4}$$

After electroweak symmetry breaking, the electric charge is $Q_{em} = T_L^3 + Y$. For the UV completion and the respective relations at the GUT scale we use a different, GUT-compatible normalization of the charges under the Abelian groups. This results in the relation

$$Y_{GUT} = \sqrt{\frac{3}{5}} T_{R,GUT} + \sqrt{\frac{2}{5}} T_{B-L,GUT} \quad \text{where} \tag{4.5}$$

$$Y_{GUT} = \sqrt{\frac{3}{5}} Y \,, \quad \begin{pmatrix} T_{R,GUT} \\ T_{B-L,GUT} \end{pmatrix} = N \cdot \begin{pmatrix} T_R \\ T_{B-L} \end{pmatrix} \,, \quad \text{and} \quad N = \begin{pmatrix} 1 & 0 \\ 0 & \sqrt{\frac{3}{2}} \end{pmatrix} \,, \tag{4.6}$$

The vector of $U(1)$ gauge couplings $(g_R, g_{BL})^T$ is multiplied by N^{-1} so that the unification condition at the GUT-scale actually reads $g_3 = g_L = g_{R,GUT} = g_{BL,GUT}$.

4.2 Gauge kinetic mixing and the change of basis

Since the field-strength tensor of an Abelian group is gauge invariant by itself, the kinetic Lagrange density for this case can be written as

$$\mathcal{L}_{\text{kin}} = -\frac{1}{4} F_i^{\mu\nu} \chi_{ij} F_{j,\mu\nu} \,, \tag{4.7}$$

where χ is a symmetric $n \times n$ matrix, n being the number of $U(1)$ groups present. $F_{\mu\nu}$ is a vector that contains the field strength tensors, in our $U(1)_R \times U(1)_{B-L}$ theory it is $(F_{\mu\nu}^R, F_{\mu\nu}^{B-L})^T$. Hence, the mixing term $\mathcal{L}_{\text{kin, mix}} = -\frac{1}{2} F^{R,\mu\nu} \chi_{12} F_{\mu\nu}^{B-L}$ appears. Even if the two Abelian groups can be embedded orthogonally within an $SO(10)$ completion (which

Superfield	Spin 0	Spin $\frac{1}{2}$	# Gen.	$SU(3)_c \times SU(2)_L$	$U(1)_R \times U(1)_{B-L}$	$U(1)_Y \times U(1)_\chi$
$\hat{Q}$	$(\tilde{u}_L, \tilde{d}_L)$	(u_L, d_L)	3	$(\mathbf{3}, \mathbf{2})$	$(0, \frac{1}{3})$	$(\frac{1}{6}, \frac{1}{4})$
$\hat{d}^c$	$\tilde{d}^c_R$	d^c_R	3	$(\overline{\mathbf{3}}, \mathbf{1})$	$(\frac{1}{2}, -\frac{1}{3})$	$(\frac{1}{3}, -\frac{3}{4})$
$\hat{u}^c$	$\tilde{u}^c_R$	u^c_R	3	$(\overline{\mathbf{3}}, \mathbf{1})$	$(-\frac{1}{2}, -\frac{1}{3})$	$(-\frac{2}{3}, \frac{1}{4})$
$\hat{L}$	$(\tilde{\nu}_L, \tilde{e}_L)$	(ν_L, e_L)	3	$(\mathbf{1}, \mathbf{2})$	$(0, -1)$	$(-\frac{1}{2}, -\frac{3}{4})$
$\hat{e}^c$	$\tilde{e}^c_R$	e^c_R	3	$(\mathbf{1}, \mathbf{1})$	$(\frac{1}{2}, 1)$	$(1, \frac{1}{4})$
$\hat{\nu}^c$	$\tilde{\nu}^c_R$	ν^c_R	3	$(\mathbf{1}, \mathbf{1})$	$(-\frac{1}{2}, 1)$	$(0, \frac{5}{4})$
$\hat{S}$	$\tilde{S}$	S	3	$(\mathbf{1}, \mathbf{1})$	$(0, 0)$	$(0, 0)$
$\hat{H}_d$	(H^0_d, H^-_d)	$(\tilde{H}^0_d, \tilde{H}^-_d)$	1	$(\mathbf{1}, \mathbf{2})$	$(-\frac{1}{2}, 0)$	$(-\frac{1}{2}, \frac{1}{2})$
$\hat{H}_u$	(H^+_0, H^0_u)	$(\tilde{H}^+_0, \tilde{H}^0_u)$	1	$(\mathbf{1}, \mathbf{2})$	$(\frac{1}{2}, 0)$	$(\frac{1}{2}, -\frac{1}{2})$
$\hat{\chi}_R$	χ_R	$\tilde{\chi}_R$	1	$(\mathbf{1}, \mathbf{1})$	$(\frac{1}{2}, -1)$	$(0, -\frac{5}{4})$
$\hat{\bar{\chi}}_R$	$\bar{\chi}_R$	$\tilde{\bar{\chi}}_R$	1	$(\mathbf{1}, \mathbf{1})$	$(-\frac{1}{2}, 1)$	$(0, \frac{5}{4})$

Table 4.1: Chiral superfields and their quantum numbers with respect to $SU(3)_c \times SU(2)_L \times U(1)_R \times U(1)_{B-L}$. We also give the quantum numbers in the basis $SU(3)_c \times SU(2)_L \times U(1)_Y \times U(1)_\chi$ which will be defined in section 4.2.

means that one gets rid of χ_{12} at M_{GUT}), this term will arise with RGE running to the low scale as soon as some part of a formerly complete $SO(10)$ multiplet is being integrated out so that only an incomplete representation remains. This is true for the Higgs sector in our model. One can easily verify that by calculating the anomalous dimension

$$\gamma_{ab} = \frac{1}{16\pi^2} \mathrm{Tr}\left(Q_a Q_b\right) , \tag{4.8}$$

where a, b are the indices of the $U(1)$ gauge groups and the trace runs over all superfields with charge Q_a under $U(1)_a$. In the basis $(U(1)_R, U(1)_{B-L})$, it reads

$$\gamma = \frac{1}{16\pi^2} N \begin{pmatrix} \frac{15}{2} & -\frac{1}{2} \\ -\frac{1}{2} & \frac{9}{2} \end{pmatrix} N , \tag{4.9}$$

where N is the matrix that contains the GUT normalization as used in eq. (4.6). The non-zero off-diagonal elements are responsible for generating χ_{12} with RGE evolution.

For dealing with the gauge kinetic mixing we can either keep the χ_{12} term or apply the procedure introduced in ref. [145] where the mixing is shifted to the covariant derivative

$$D^\mu = \partial^\mu - i Q_l G_{lm} A^\mu_m \tag{4.10}$$

by re-defining the gauge fields as $A^\mu \to \chi^{1/2} A^\mu$. Here, A^μ is a vector containing the gauge fields, $A^\mu = (B^\mu_R, B^\mu_{B-L})^T$, and $Q = (T_R, T_{B-L})^T$ contains the charges. G is the formerly diagonal 2×2 gauge coupling matrix that now absorbs $\chi^{-1/2}$ in order to leave eq. (4.10) invariant,

$$G = \begin{pmatrix} g_R & g_{RBL} \\ g_{BLR} & g_{BL} \end{pmatrix} , \tag{4.11}$$

so that χ_{12} is traded for non-zero mixed gauge couplings g_{RBL} and g_{BLR}. The GUT

normalization

$$Q_{GUT} = NQ, \quad G_{GUT} = N^{-1}G\,. \tag{4.12}$$

leaves the product

$$Q^T G = (NQ)^T N^{-1} G = Q_{GUT}^T G_{GUT} \tag{4.13}$$

and hence also the covariant derivative invariant. At the GUT scale we demand that the off-diagonal couplings g_{BLR}, g_{RBL} vanish.

In order to simplify the comparison with known results from the MSSM, we now will rotate the basis $(U(1)_R, U_{B-L})$ in such a way that we recover the hypercharge as one orthogonal $U(1)$ direction. This freedom of choice of a basis exists because of the Abelian nature of the gauge groups. We name the other resulting orthogonal direction as χ according to the possible decomposition $SO(10) \to SU(5) \times U(1)_\chi$.

For a proper matching, we need to derive the charge and gauge coupling relations between the two different bases, $(U(1)_R, U(1)_{B-L})$ and $(U(1)_Y, U(1)_\chi)$. For that purpose we can perform two independent rotations on the charges and the gauge fields by inserting the orthonormal matrices O_1 and O_2 into the second term of eq. (4.10) :

$$iQ^T G A^\mu = i(NQ)^T N^{-1} G A^\mu \tag{4.14}$$

$$= i(NQ)^T O_1^T O_1 N^{-1} G O_2^T O_2 A^\mu = i(N'Q')^T N'^{-1} G' A'^\mu\,. \tag{4.15}$$

We now can identify $(Q'_{GUT})^T = (O_1 Q_{GUT})^T$ and hence $(N'Q')^T = (O_1 NQ)^T$ as well as $G'_{GUT} = N'^{-1}G' = O_1 G_{GUT} O_2^T = O_1 N^{-1} G O_2^T$ and $A'^\mu = O_2 A^\mu$. N' is the diagonal matrix that contains the GUT normalization of the rotated basis.

The rotations can be fixed by the phenomenological requirements that the new $U(1)_Y$ corresponds to the Standard Model hypercharge group. Therefore, O_1 can be determined by the requirement $Y = T_R + T_{B-L}$. In addition, the gauge boson B_Y related to the hypercharge must not have couplings to the χ charge which means that we have to find an upper-triangular form of the gauge coupling matrix:

$$G' = N' O_1 N^{-1} G O_2^T = \begin{pmatrix} g_Y & g_{Y\chi} \\ 0 & g_\chi \end{pmatrix} \tag{4.16}$$

This requirement determines O_2. We find that

$$Q' = \begin{pmatrix} Y \\ \chi \end{pmatrix} = \begin{pmatrix} T_R + T_{B-L} \\ \frac{3}{2} T_{B-L} - T_R \end{pmatrix}, \text{ with} \tag{4.17}$$

$$N' = \begin{pmatrix} \sqrt{\frac{3}{5}} & 0 \\ 0 & \sqrt{\frac{2}{5}} \end{pmatrix}, \tag{4.18}$$

$$\begin{aligned} g_Y &= \frac{g_{BL} g_R - g_{BLR} g_{RBL}}{\sqrt{(g_{BLR} - g_R)^2 + (g_{BL} - g_{RBL})^2}}\,, \\ g_\chi &= \frac{2}{5}\sqrt{(g_{BLR} - g_R)^2 + (g_{BL} - g_{RBL})^2}\,, \\ g_{Y\chi} &= \frac{2(g_{BL}^2 + g_{BLR}^2) + g_{BLR} g_R + g_{BL} g_{RBL} - 3(g_R^2 + g_{RBL}^2)}{5\sqrt{(g_{BLR} - g_R)^2 + (g_{BL} - g_{RBL})^2}}\,. \end{aligned} \tag{4.19}$$

As an aside, we see that the GUT-normalization N'_{11} for the hypercharge has exactly the same value as typically used in the MSSM. Applying the above definitions, one can verify that the unification condition

$$g_3 = g_L = g_{R,GUT} = g_{BL,GUT}\,, \qquad g_{RBL} = g_{BLR} = 0 \tag{4.20}$$

exactly translates to

$$g_3 = g_L = g_{Y,GUT} = g_{\chi,GUT}\,, \qquad g_{Y\chi} = 0\,. \tag{4.21}$$

The charges of the superfields under the new basis are listed in table 4.1. Note that they correspond to the $U(1)_\chi$ charges in ref. [146] up to a sign which we chose to absorb into the definitions of O_1 and O_2. Hence, the extra gauge boson Z' that we end up with corresponds to the Z_χ in ref. [146].

4.3 GMSB boundary conditions

As briefly discussed in section 2.5, gauge-mediated supersymmetry breaking works via so-called messenger superfields $\hat{\Phi}$ which are charged under the gauge group under consideration and coupled to the SUSY-breaking spurion field $\hat{X}$, hence transmitting supersymmetry breaking via loop-induced gauge interactions to the visible sector. We will assume for simplicity a single spurion field which couples universally to all messenger fields via a single coupling λ, described by the superpotential term

$$W_{GM} = \lambda\, \hat{X}\, \hat{\Phi}_i\, \hat{\bar{\Phi}}_i\,. \tag{4.22}$$

In the following we will get rid of λ by rescaling $\hat{X} \to \lambda \hat{X}$. We further assign a vev to both the scalar and the auxiliary component of $\hat{X}$,

$$\langle X \rangle = M + \theta^2 F\,, \tag{4.23}$$

so that the squared mass matrix of the scalar messenger fields reads

$$m^2_{\Phi_i, \bar{\Phi}_i} = \begin{pmatrix} M^2 & F \\ F & M^2 \end{pmatrix}\,. \tag{4.24}$$

Consequently, the scalar eigenstates have masses of $\sqrt{M^2 \pm F}$. The fermionic messenger components, however, only receive a mass of M. It is thus clear from the mass splitting of scalars and fermions within the same supermultiplet that supersymmetry is broken by the F-term vev of $\hat{X}$.

The requirement $|F| < |M|^2$ must hold for obtaining positive squared messenger masses, and we define the mass-dimension 1 and 0 quantities

$$\Lambda = \frac{F}{M}\,, \tag{4.25}$$

$$x = \frac{\Lambda}{M} < 1\,. \tag{4.26}$$

	$SU(3)_c \times SU(2)_L$	$U(1)_R \times U(1)_{B-L}$	$U(1)_Y \times U(1)_\chi$
$\hat{\Phi}_1$	$(\mathbf{1}, \mathbf{2})$	$(\frac{1}{2}, 0)$	$(\frac{1}{2}, -\frac{1}{2})$
$\hat{\bar{\Phi}}_1$	$(\mathbf{1}, \mathbf{2})$	$(-\frac{1}{2}, 0)$	$(-\frac{1}{2}, \frac{1}{2})$
$\hat{\Phi}_2$	$(\mathbf{3}, \mathbf{1})$	$(0, -\frac{2}{3})$	$(-\frac{1}{3}, -\frac{1}{2})$
$\hat{\bar{\Phi}}_2$	$(\bar{\mathbf{3}}, \mathbf{1})$	$(0, \frac{2}{3})$	$(\frac{1}{3}, \frac{1}{2})$

Table 4.2: Quantum numbers of the messenger fields in the respective bases.

In minimal GMSB scenarios within the MSSM, the representation of the messenger multiplets is usually assumed to be a $\mathbf{5} + \bar{\mathbf{5}}$ under $SU(5)$. This is because complete representations of the GUT group don't spoil gauge coupling unification, at whichever scale they may be introduced. For the same reason we introduce n generations of messenger multiplets which each form a complete $SO(10)$ representation. Below we will assume the messengers to form a **10**-plet which, under the decomposed gauge group under consideration, results in two $SU(2)_L$ doublets $\hat{\Phi}_1, \hat{\bar{\Phi}}_1$ and two $SU(3)_c$ triplets $\hat{\Phi}_2, \hat{\bar{\Phi}}_2$ with suitable charges under the additional Abelian gauge groups. We list these fields and their quantum numbers under both previously discussed $U(1)$ bases in table 4.2.

The soft SUSY-breaking masses are generated at the one- (two-) loop order for fermions (scalars) [44, 147–149] via diagrams of the kind of the ones in figure 2.1. We can then integrate out the messenger fields at M which we henceforth call the messenger scale. The boundary conditions for the soft masses at the messenger scale are well known in the literature (see, *e.g.*, [148]) if there is no kinetic mixing:

$$M_a = \frac{g_a^2}{16\pi^2} \Lambda \sum_i n_a(i)\, g(x_i)\,, \tag{4.27}$$

$$m_k^2 = 2\,\Lambda^2 \sum_a C_a(k) \frac{g_a^4}{(16\pi^2)^2} \sum_i n_a(i)\, f(x_i)\,, \tag{4.28}$$

where g_a denotes the GUT-normalized coupling of gauge group a and i runs over the messenger fields. $n_a(i)$ is the Dynkin index of the messenger i with respect to the gauge group a. We use a normalization where $\sum_i n_a(i) = 1$ for the **10** of $SO(10)$. $C_a(k)$ is the quadratic Casimir invariant of the scalar field k. It is $\frac{N^2-1}{2N}$ if k lies in the fundamental representation of $a \hat{=} SU(N)$ and equals the squared GUT-normalized charge $q^2_{X,GUT}$ if $a \hat{=} U(1)_X$. The functions $g(x_i)$ and $f(x_i)$ are approximately 1 for $x_i \lesssim 0.2$ [148], and since we use universal spurion-messenger couplings in our studies, we have $x_i = x$.

In eqs. (4.27-4.28) a sum over all messenger fields appears in the boundary conditions for the fermion masses and the scalar squared masses, respectively. This implies that the fermion soft masses depend, at the scale M, linearly on the number n of introduced messenger $SO(10)$ multiplets, whereas the scalar soft masses only go with $\sqrt{n}$. As a consequence, n influences the mass hierarchy, which will be of relevance in section 4.8 when we discuss the nature of the next-to-lightest supersymmetric particle.

For a consistent inclusion of gauge kinetic mixing we have to extend the eqs. (4.27-4.28). For this purpose we can use the substitution rules for multiple Abelian groups as derived

in ref. [145]. We arrive at

$$M_{A\neq Abelian} = \frac{g_A^2}{16\pi^2}\Lambda \sum_i n_A(i) g(x_i)\,, \tag{4.29}$$

$$M_{kl=Abelian} = \frac{1}{16\pi^2}\Lambda \Big(\sum_i g(x_i) G^T Q_i Q_i^T G \Big)_{kl}\,, \tag{4.30}$$

$$\begin{aligned} m_k^2 = \frac{2}{(16\pi^2)^2}\Lambda^2 \Big(& \sum_{A\neq Abelian} C_A(k) g_A^4 \sum_i f(x_i) n_A(i) \\ & + \sum_i f(x_i) (Q_k^T G G^T Q_i)^2 \Big)\,, \end{aligned} \tag{4.31}$$

where Q and G are as defined in the previous section. Note that eqs. (4.29-4.31) are invariant under the application or omission of a GUT normalization to the $U(1)$ couplings and charges.

The trilinear couplings are essentialy zero at the scale of gauge mediation and only pick up non-zero values via RGE running from M down to the renormalization scale. The same is true for the mass of the scalar gauge singlet S which does not couple to the messenger fields at the considered loop orders. However, through its coupling to χ_R and ν^c, it turns non-zero at the three-loop level, and we estimate this mass as

$$m_S^2 \simeq \frac{Y_S^2}{16\pi^2}\left(m_{\chi_R}^2 + m_{\nu^c}^2\right). \tag{4.32}$$

RGE effects usually drive this squared mass negative. In practice, however, it turns out that this is no problem since F-terms proportional to $M_{Z'}^2$ prevent the mass eigenstates from becoming tachyonic, see also the discussion of the sneutrino mass matrix in section 4.8.

4.4 Tadpole equations

We decompose the neutral scalar fields responsible for gauge symmetry breaking into their CP-even (odd) components ϕ_i (σ_i) and their vevs:

$$\begin{aligned} H_u &= \frac{1}{\sqrt{2}}(\phi_u + i\sigma_u + v_u), \quad H_d = \frac{1}{\sqrt{2}}(\phi_d + i\sigma_d + v_d), \\ \chi_R &= \frac{1}{\sqrt{2}}(\phi_R + i\sigma_R + v_{\chi_R}),\ \bar{\chi}_R = \frac{1}{\sqrt{2}}(\bar{\phi}_R + i\bar{\sigma}_R + v_{\bar{\chi}_R})\,. \end{aligned} \tag{4.33}$$

Beside the usual notation $v^2 = v_d^2 + v_u^2$ and $\tan\beta = v_u/v_d$ we re-define v_R and $\tan\beta_R$ as suitable for this model:

$$v_R^2 = v_{\chi_R}^2 + v_{\bar{\chi}_R}^2\,, \qquad \tan\beta_R = \frac{v_{\chi_R}}{v_{\bar{\chi}_R}}\,. \tag{4.34}$$

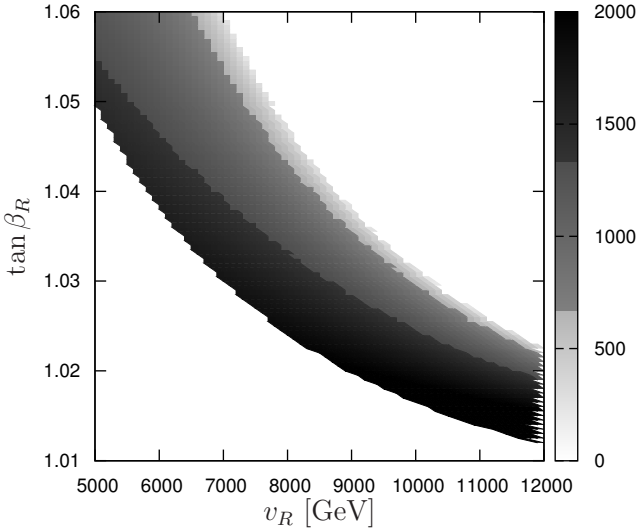

Figure 4.1: Allowed parameter space in the $v_R - \tan\beta_R$ plane. The plotted values correspond to $|\mu_R|$ which is calculated using the tadpole equations. The free parameters have been set to $n = 1,\ \Lambda = 5\cdot 10^5$ GeV, $M = 10^{11}$ GeV, $\tan\beta = 30,\ \mathrm{sign}(\mu_R) = -, Y_S = \mathrm{diag}(0.7, 0.6, 0.6),\ Y_\nu^{ii} = 0.01$.

We then use the minimization conditions for the scalar potential $\frac{\partial V}{\partial \phi_i} = 0$ to determine the parameters $|\mu|^2,\ |\mu_R|^2,\ B_\mu$, and B_{μ_R}:

$$B_\mu = \frac{t_\beta}{t_\beta^2 - 1}\Big(m_{H_d}^2 - m_{H_u}^2 + \frac{v^2}{4}c_{2\beta}(g_L^2 + g_Y^2 + (g_\chi - g_{Y\chi})^2) + \frac{5v_R^2}{8}c_{2\beta_R}g_\chi(g_\chi - g_{Y\chi})\Big)\,, \tag{4.35}$$

$$B_{\mu_R} = \frac{t_{\beta_R}}{t_{\beta_R}^2 - 1}\Big(m_{\bar\chi_R}^2 - m_{\chi_R}^2 - \frac{5v^2}{8}c_{2\beta}g_\chi(g_\chi - g_{Y\chi}) + \frac{25v_R^2}{16}c_{2\beta_R}g_\chi^2\Big)\,, \tag{4.36}$$

$$\begin{aligned}|\mu|^2 = \frac{1}{t_\beta^2 - 1}\Big(&m_{H_d}^2 - m_{H_u}^2 t_\beta^2 - \frac{v^2}{8}(g_L^2 + g_Y^2 + (g_\chi - g_{Y\chi})^2)(t_\beta^2 - 1)\\ &+ \frac{5v_R^2}{16}c_{2\beta_R}(1 + t_\beta^2)g_\chi(g_\chi - g_{Y\chi})\Big)\,,\end{aligned} \tag{4.37}$$

$$|\mu_R|^2 = \frac{1}{t_{\beta_R}^2 - 1}\Big(m_{\bar\chi_R}^2 - m_{\chi_R}^2 t_{\beta_R}^2 + \frac{5v^2}{16}c_{2\beta}(t_{\beta_R}^2 + 1)g_\chi(g_\chi - g_{Y\chi}) - \frac{25v_R^2}{32}(t_{\beta_R}^2 - 1)g_\chi^2\Big)\,, \tag{4.38}$$

where we have used the abbreviations $\{c_x, s_x, t_x\} = \{\cos x, \sin x, \tan x\}$. Let us examine eq. (4.38) in a bit more detail. The term proportional to v_R^2 will always contribute with a negative sign, whereas the v^2 term is negative (positive) for $\tan\beta_R > 1 (< 1)$. At the messenger scale, the soft masses of χ_R and $\bar\chi_R$ are equal and a splitting only takes place because of the different running from M downwards. The one-loop β functions read in the

limit of vanishing kinetic mixing

$$\beta^{(1)}_{m^2_{\bar{\chi}}} = -\frac{25}{2} g_\chi^2 |M_\chi|^2 + \frac{5}{2} g_\chi \sigma_\chi \,, \tag{4.39}$$

$$\beta^{(1)}_{m^2_{\chi}} = -\frac{25}{2} g_\chi^2 |M_\chi|^2 - \frac{5}{2} g_\chi \sigma_\chi + 2\mathrm{Tr}\Big((m^2_{\chi_R} + m^2_{\nu^c}) Y_S Y_S^\dagger + m_S^2 Y_S^\dagger Y_S + T_S^* T_S^T\Big) \,, \tag{4.40}$$

with

$$\begin{aligned} \sigma_\chi = \frac{g_\chi^2}{4}\Big(&5(m^2_{\bar{\chi}_R} - m^2_{\chi_R}) + 4(m^2_{H_d} - m^2_{H_u}) \\ &+ \mathrm{Tr}\big(m^2_{e^c} + 3m^2_u + 5m^2_{\nu^c} + 6(m^2_Q - m^2_L) - 9m^2_d\big)\Big) \,, \end{aligned} \tag{4.41}$$

which is zero at the messenger scale and remains zero at the level of one-loop RGEs. Therefore, the main splitting between $m^2_{\chi_R}$ and $m^2_{\bar{\chi}_R}$ is due to the impact of a non-zero Y_S, and at a scale below M we find $m^2_{\bar{\chi}_R} > m^2_{\chi_R}$. Compared to the boundary conditions from an mSUGRA-inspired scenario as in ref. [140], however, we find significantly less splitting. This is due to the shorter RGE running and the smallness of the trilinear couplings. From these arguments it is clear that only $\tan\beta_R = 1 + \epsilon$, with a small, positive ϵ will give a real solution to μ_R[1]. Apparently, it is much harder to get a solution to eq. (4.38) with a growing $U(1)_R \times U(1)_{B-L}$ breaking scale and hence there is an upper limit on $\tan\beta_R$ for a given value of v_R. This is exemplified in figure 4.1 where the values of $|\mu_R|$ are shown as contours depending on v_R and $\tan\beta_R$. The white space is where no physical spectrum exists: for large $\tan\beta_R$ because eq. (4.38) has no solution, and for low $\tan\beta_R$ because of tachyonic states.

We have also considered the case where neutrino masses are generated by a seesaw-I mechanism similar to [150, 151], in which case there is no need to introduce the singlet field S. That would imply that the χ_R fields would have to carry twice the $U(1)$ charges of the ν^c field in order to preserve gauge invariance so that Majorana masses for the right-handed neutrinos could be generated by the superpotential term $Y'_S\,\hat{\nu}^c\,\hat{\chi}_R\,\hat{\nu}^c$. These Higgs fields could originate from $SU(2)_R$ triplets in the unbroken left-right symmetric phase, as the Δ_{iR} fields used in chapter 3. However, we find that in this case it is even harder to obtain a reasonable splitting $m^2_{\bar{\chi}_R} - \tan^2\beta_R\, m^2_{\chi_R}$. The reason for that is the altered RGE running of the soft masses compared to the inverse seesaw scenario; in the case of seesaw-I, the larger gauge contributions prevent $m^2_{\chi_R}$ from becoming sufficiently small.

4.5 Neutrino masses

After electroweak symmetry breaking, the neutrino mass matrix reads in the basis (ν_L, ν_R^c, S):

$$m_\nu = \begin{pmatrix} 0 & \frac{1}{\sqrt{2}} v_u Y_\nu^T & 0 \\ \frac{1}{\sqrt{2}} v_u Y_\nu & 0 & \frac{1}{\sqrt{2}} v_{\chi_R} Y_S \\ 0 & \frac{1}{\sqrt{2}} v_{\chi_R} Y_S^T & \mu_S \end{pmatrix} . \tag{4.42}$$

[1] Note that $\epsilon = 0$ corresponds to a saddle point of the scalar potential and not to a minimum.

In the limit $\mu_S \ll \frac{1}{\sqrt{2}} v_u Y_\nu \ll \frac{1}{\sqrt{2}} v_{\chi_R} Y_S$, this mass matrix can be block-diagonalized, leading to an effective mass matrix for the light neutrinos ν of [75, 152]

$$M_{\text{light}} \simeq \frac{v_u^2}{v_{\chi_R}^2} Y_\nu^T (Y_S^T)^{-1} \mu_S Y_S^{-1} Y_\nu \,, \tag{4.43}$$

while being almost exclusively composed of ν_L states. The lightness of left-handed neutrino masses is hence achieved by $v_{\chi_R} \gg v_u$ as well as small μ_S and Y_ν. In addition to achieving a sufficient $m_{\bar{\chi}_R} - m_{\chi_R}$ splitting, large values for Y_S help suppressing the neutrino masses. While we can always find a basis in which Y_S is diagonal, it is apparent in eq. (4.43) that there is the possibility to fit the neutrino mixing angles by giving non-diagonal flavour structure to either Y_ν or μ_S, or a to combination of both.

Since $\mu_S, v_u Y_\nu \ll v_{\chi_R} Y_S$, the six heavy neutrino eigenstates ν_h form three quasi-Dirac pairs with masses

$$m_{\nu_h} \simeq \frac{1}{\sqrt{2}} v_{\chi_R} Y_S \,. \tag{4.44}$$

4.6 Higgs mass at tree-level

Let us turn to the Higgs sector of this model. One of the main motivations for this study was the question whether or not the measured Higgs mass can be accommodated without the need for multi-TeV stop masses or large trilinear couplings. Since the latter is not possible in models with minimal GMSB, the former must usually be the case (see, *e.g.*, [153–155]). In models with extended gauge symmetry, however, additional D-terms can help to raise the mass already at tree level. In our model, the mass matrix for the neutral scalar Higgs fields reads in the basis $(\phi_d, \phi_u, \bar{\phi}_R, \phi_R)$:

$$m_{h^0}^2 = \begin{pmatrix} m_{du}^2 & m_{duR}^2 \\ (m_{duR}^2)^T & m_{RR}^2 \end{pmatrix} \,, \tag{4.45}$$

where

$$\begin{aligned}
m_{du}^2 &= \frac{1}{4} \begin{pmatrix} \tilde{g}_\Sigma^2 v^2 \cos^2\beta + m_A^2 \sin^2\beta & -\frac{1}{2}\sin 2\beta (\tilde{g}_\Sigma^2 v^2 + 4 m_A^2) \\ -\frac{1}{2}\sin 2\beta (\tilde{g}_\Sigma^2 v^2 + 4 m_A^2) & \tilde{g}_\Sigma^2 v^2 \sin^2\beta + m_A^2 \cos\beta \end{pmatrix} \,, \\
m_{duR}^2 &= \frac{5}{8} \begin{pmatrix} \tilde{g}_\chi^2 v v_R \cos\beta \cos\beta_R & -\tilde{g}_\chi^2 v v_R \cos\beta \sin\beta_R \\ -\tilde{g}_\chi^2 v v_R \sin\beta \cos\beta_R & \tilde{g}_\chi^2 v v_R \sin\beta \sin\beta_R \end{pmatrix} \,, \\
m_{RR}^2 &= \begin{pmatrix} \frac{25}{16} g_\chi^2 v_R^2 \cos^2\beta_R + m_{A_R}^2 \sin^2\beta_R & -\frac{1}{32}\sin 2\beta_R (25 g_\chi^2 v_R^2 + 16 m_{A_R}^2) \\ -\frac{1}{32}\sin 2\beta_R (25 g_\chi^2 v_R^2 + 16 m_{A_R}^2) & \frac{25}{16} g_\chi^2 v_R^2 \sin^2\beta_R + m_{A_R}^2 \cos^2\beta_R \end{pmatrix} \,, \\
\tilde{g}_\Sigma^2 &= g_L^2 + g_Y^2 + (g_\chi - g_{Y\chi})^2, \quad \tilde{g}_\chi^2 = g_\chi (g_\chi - g_{Y\chi}) \,,
\end{aligned}$$

and $m_{A_{(R)}}^2 = 2B_{\mu_{(R)}} / \sin 2\beta_{(R)}$ are the tree-level squared masses of the pseudoscalar Higgs bosons. Applying some approximations ($\tan\beta_R \to 1, v_R \gg v$) and the decoupling limit ($\tan\beta \to \infty$), the upper bound for the eigenvalue associated with the lightest $SU(2)_L$

doublet Higgs can be found to be

$$m^2_{h,tree} \leq M_Z^2 + \frac{1}{4}(g_\chi - g_{Y\chi})^2 v^2 \,, \tag{4.46}$$

and we obtain typical values $g_\chi - g_{Y\chi} \simeq 0.27$. Hence, a tree-level enhancement of several GeV with respect to the MSSM upper limit is found for this model due to the extra D-terms. Note that, in the same limit, we also end up with a massless state for the $\phi_R/\bar{\phi}_R$ fields. In figure 4.2 we show the behaviour of the two lightest eigenvalues of eq. (4.45) with $\tan\beta_R$. With $\tan\beta_R > 1$, the former massless R-state gains mass and a mixing between the upper left and the lower right block of eq. (4.45) sets in. Because of that, $m_{h,tree}$ can even reach values well above 100 GeV at the cost of reduced resemblance to the pure $SU(2)_L$ doublet Higgs boson. This is depicted in the right panel of figure 4.2 where the doublet admixture $\mathcal{R}^2_{L_i} = |U_{i1}|^2 + |U_{i2}|^2$ is shown for the lightest and the next-to lightest Higgs. Similar to the solutions to the tadpole equations, values of $\tan\beta_R$ close to one are favoured for the desired feature of a tree-level enhancement while retaining a large doublet fraction. This also means that, in general, there is a second light Higgs state which we will henceforth call h_{χ_R}.

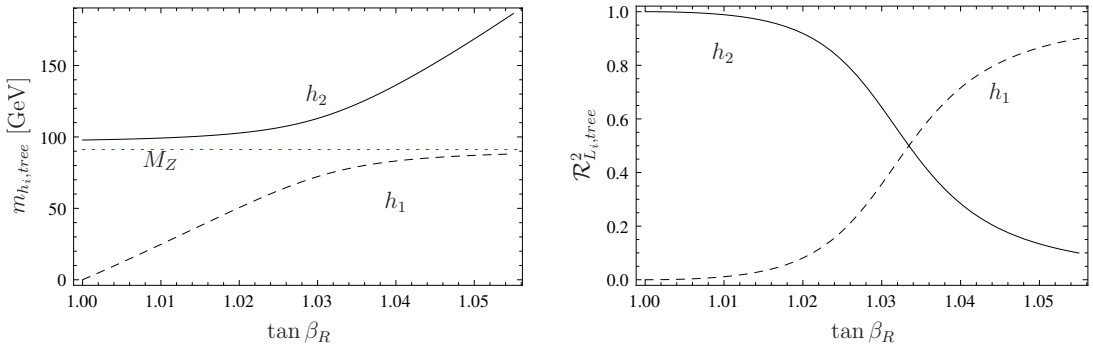

Figure 4.2: Tree-level dependence of the lightest Higgs masses (left) as well as the admixture of the $SU(2)_L$ doublet Higgses $\mathcal{R}^2_{L_i} = |U_{i1}|^2 + |U_{i2}|^2$ (right) on $\tan\beta_R$. The parameters have been chosen as in figure 4.1 and we have fixed $v_R = 7$ TeV. The horizontal small dashed (red) line shows the Z mass.

4.7 Numerical results

Having shown how the tree-level Higgs mass is enhanced by extra D-terms, we now have to add the loop-corrections in the framework of the discussed model. For this purpose we have extended the model implementation of ref. [140] in `SARAH` by up to four messenger **10**-plets as defined in table 4.2. The GMSB boundary conditions of eq. (4.31) are implemented at the messenger scale where the messenger fields themselves are being integrated out. We then use the `SPheno` source code generated by `SARAH` for a precise spectrum calculation which includes the full RGE running and at the two-loop order as well as the one-loop mass calculation. Furthermore, the known two-loop corrections to the MSSM Higgs masses [156–159] are included. As all soft SUSY-breaking masses and trilinear couplings

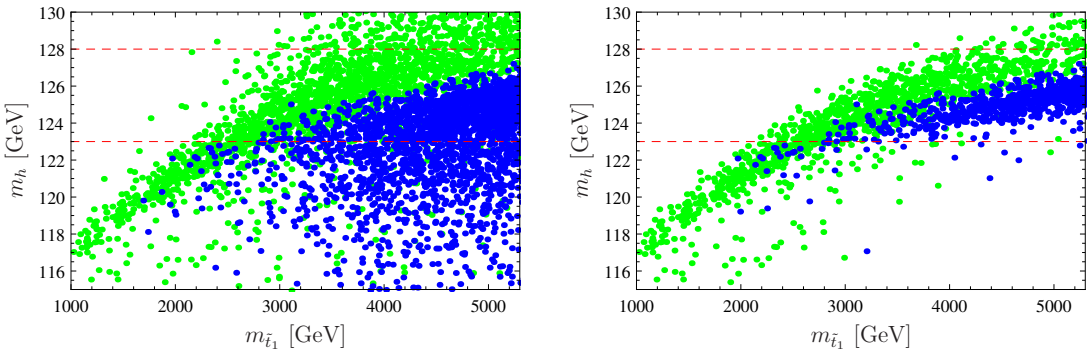

Figure 4.3: Mass of the doublet-like Higgs m_h vs. the mass of the lightest stop $m_{\tilde{t}_1}$ for the parameter scan defined in table 4.4, using one messenger **10**-plet. Only points with $R_{h\to\gamma\gamma} > 0.5$ (left) and 0.9 (right) were included. The blue dots represent parameter points where the lightest Higgs eigenstate is doublet-like, green dots points where h_{χ_R} is lighter.

are fixed by the boundary conditions at the messenger scale and $B_{\mu_{(R)}}$ as well as $|\mu_{(R)}|$ are determined by the solution of the tadpole equations, the remaining free parameters in our numerical setup are

$$n\,,\ \Lambda\,,\ M,\ \tan\beta\,,\ \tan\beta_R\,,\ \mathrm{sign}(\mu)\,,\ \mathrm{sign}(\mu_R)\,,\ v_R\,,\ Y_S\,,\ Y_\nu\,, \tag{4.47}$$

We furthermore fix μ_S by fitting neutrino data for a given Y_S and Y_ν. Since it does not affect the LHC phenomenology discussed in the following, we will, until further notice, assume that the neutrino mixing is explained by the inherent off-diagonal structure of μ_S and hence keep Y_S and Y_ν diagonal. Because of its smallness, μ_S is irrelevant for collider phenomenology and no flavour-violating LHC signals are expected in this scenario.[2]

To facilitate the discussion of the model properties, we have chosen a number of benchmark scenarios shown in table 4.3 which each possess certain distinct features that shall be of relevance in what follows.

4.7.1 Higgs physics

In order to determine the magnitude of the loop-corrected Higgs mass within our minimal GMSB scenario, we have performed a scan over a large portion of the parameter space of the model. The varied ranges are listed in table 4.4. Since Λ is roughly the mass scale of the soft SUSY-breaking masses, it is only varied in a narrow range which permits squark masses in the range of one or a few TeV.

In figure 4.3 we display the results of the scan and show the mass of the lightest doublet-like Higgs m_h vs. the mass of the lighter stop eigenstate for the case $n = 1$. We speak of an acceptable Higgs mass if it ranges within 123 GeV $< m_h <$ 128 GeV, due to the theoretical uncertainty of the Higgs mass calculation. It is distinguished between the case in which the doublet-like Higgs is the lightest eigenstate (blue points) and the case in which there is a lighter h_{χ_R} state (green points), whereas like in figure 4.2, the latter

[2] We will examine the consequences for lepton flavour violating observables in the case in which neutrino data is fitted by a non-trivial structure in Y_ν in chapter 5.

	BLRI	BLRII	BLRIII	BLRIV	BLRV	BLRVI
n	4			1	1	1
Λ [GeV]	$2.5 \cdot 10^5$			$5 \cdot 10^5$	$3.8 \cdot 10^5$	$5 \cdot 10^5$
M [GeV]	10^{11}			10^{10}	$9 \cdot 10^{11}$	10^{11}
$\tan\beta$	40			30	30	20
$\tan\beta_R$	1.04			1.03	1.05	1.02
$\mathrm{sign}(\mu_R)$	$-$			$+$	$-$	$+$
v_R [TeV]	7			7.5	6.7	12
Y_ν^{ii}	0.01			0.01	0.01	0.01
$\mathrm{diag}(Y_S)$	(.65,.65,.1)	(.65,.65,.3)	(.65,.65,.65)	(.6,.6,.6)	(.77,.73,.45)	(.7,.6,.6)
m_{h_1} [GeV]	70	92	125	70	108	98
$\mathcal{R}^2_{L,h_1}$	0.006	0.018	0.961	0.003	0.094	0.006
m_{h_2} [GeV]	126	127	156	124	124	124
$\mathcal{R}^2_{L,h_2}$	0.994	0.982	0.039	0.997	0.906	0.995
$M_{Z'}$ [TeV]	2.53			2.7	2.41	4.32
$m_{\nu_{h,1}}$ [GeV]	357	1070	2306	2277	1542	3633
$m_{\nu_{h,2}}$ [GeV]	2309	2308	2306	2278	2497	3633
$m_{\nu_{h,3}}$ [GeV]	2309	2308	2306	2278	2633	4238
$m_{\tilde{\nu}_1}$ [GeV]	334	909	1715	1728	1207	1863
$m_{\tilde{\nu}_2}$ [GeV]	1072	1546	1715	1757	1482	1879
$m_{\tilde{\nu}_3}$ [GeV]	2090	2048	1715	1759	1514	1879
$m_{\tilde{\tau}_1}$ [GeV]	906	906	905	867	764	1007
$m_{\tilde{\mu}_R}$ [GeV]	1166	1166	1165	976	877	1061
$m_{\tilde{e}_R}$ [GeV]	1167	1166	1166	976	877	1061
$m_{\tilde{\chi}_1^0}$ [GeV]	505	766	1156	575	453	589
$m_{\tilde{\chi}_2^0}$ [GeV]	1157	1157	1353	610	825	1043
$m_{\tilde{\chi}_1^\pm}$ [GeV]	2216	2216	2217	1113	883	1142
$m_{\tilde{\chi}_2^\pm}$ [GeV]	2591	2590	2588	1956	1600	2015
$m_{\tilde{g}}$ [GeV]	5460	5459	5456	3018	2423	3076
$m_{\tilde{t}_1}$ [GeV]	4209	4209	4206	2993	2231	2941

Table 4.3: Input parameters and mass spectrum of different representative parameter points. Note that the heavy neutrino mass eigenstates ν_h are quasi-Dirac states each so that the three listed masses correspond to six fermions.

case in general results in a heavier h state because of the enhanced tree-level contributions. Furthermore, we see that with stop masses around $m_{\tilde{t}_1} \approx 2$ TeV, the Higgs mass can already be of acceptable size if there is a substantial mixing between the doublet and the χ_R states. Filtering out points with a large χ_R admixture (which we have done here by requiring the decay rate into a photon pair not to be smaller than 90 % the SM rate), this lower "bound" on the stop mass increases by around one to two hundred GeV.

Compared to stop masses of 5 TeV and larger, which are needed in minimal GMSB scenarios within the MSSM [154], our model bears an improved naturalness with this respect. Nevertheless, also a stop with a mass around 2 TeV will be hard to detect at the LHC and a new collider might be required for a discovery.

Parameter	varied range
n	1 ... 4
Λ	$\frac{1}{\sqrt{n}}(10^5 \ldots 10^6)$ GeV
M	$(10^5 \ldots 10^{12})$ GeV
$\tan\beta$	1.5 ... 40
$\tan\beta_R$	1 ... 1.15
$\mathrm{sign}(\mu_R)$	± 1
v_R	(6.5 ... 10) TeV
Y_S^{ii}	0.01 ... 0.8
Y_ν^{ii}	10^{-5} ... 0.5

Table 4.4: Parameter ranges of the random scan. The sign of μ has aways been taken positive.

Apart from the mixing, the Higgs mass can also be enhanced by raising the messenger scale: with increasing M, the RGE running gets longer and with it the magnitude of the trilinear couplings increases. This is illustrated in figure 4.4 where we show on the left panel the dependence of the stop trilinear coupling T_u^{33} on the messenger scale for three benchmark scenarios and on the right panel the resulting Higgs mass. The sudden increase of m_h for BLRIII and BLRV (at $M \approx 10^{10}$ and 10^{11}, respectively) is due to a level crossing of h and h_{χ_R}.

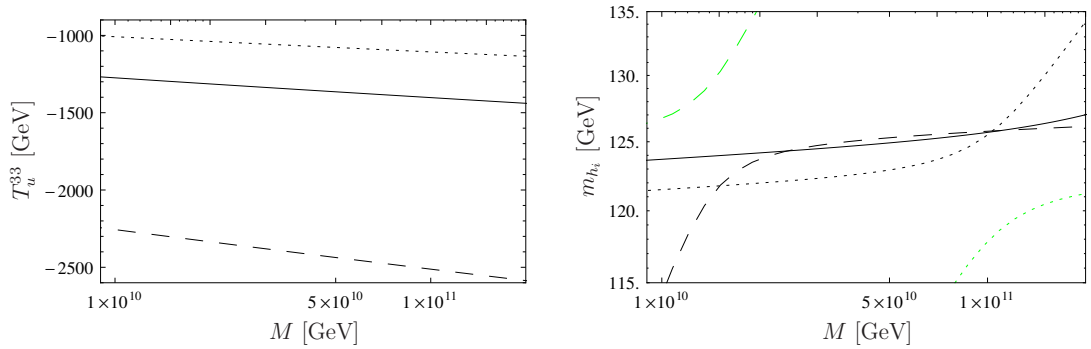

Figure 4.4: Stop trilinear coupling T_u^{33} and mass of the doublet-like Higgs as a function of M for BLRIII (black dashed line), BLRIV (black full line) and BLRV (black dotted line) (but for $\tan\beta_R = 1.03$). The associated light green lines correspond to the h_{χ_R} state of the respective parameter point.

We now turn to the Higgs branching ratio into a pair of photons which we have previously used to narrow down the number of parameter points in figure 4.3. We define the ratio $R_{h\to\gamma\gamma}$ by

$$R_{h\to\gamma\gamma} = \frac{[\sigma(pp\to h)\times BR(h\to\gamma\gamma)]_{BLR}}{[\sigma(pp\to h)\times BR(h\to\gamma\gamma)]_{SM}}\,. \tag{4.48}$$

The cross sections $pp \to h$ for the main production channels (gluon and vector boson fusion) are the same as in the Standard Model, up to the (effective) couplings of the Higgs boson

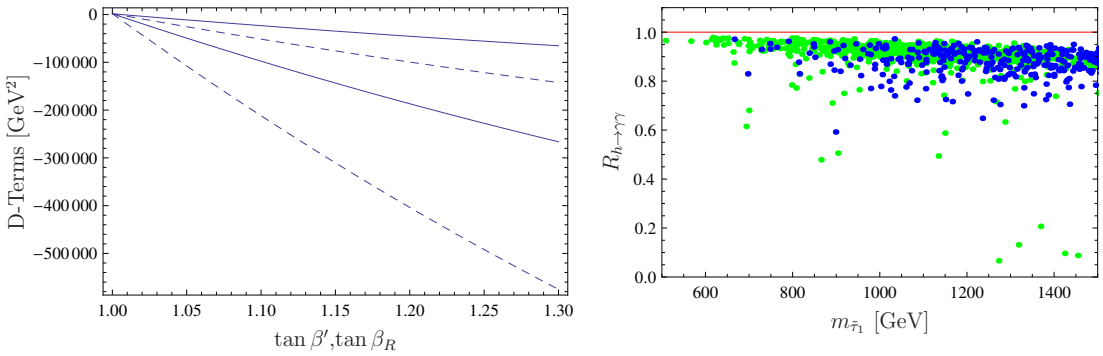

Figure 4.5: Left image: D-term contribution to the mass entries of the R-sleptons using $\tan\beta = 10$ as well as $M_{Z'} = 1.5, 3.0$ TeV and fixing the gauge couplings by the requirement of gauge coupling unification: $g_Y = 0.36$, $g_\chi^{Y\times\chi} = 0.29$, $g_{BL}^{Y\times BL} = 0.55$. The full (dashed) lines correspond to the $U(1)_Y \times U(1)_\chi$ ($U(1)_Y \times U(1)_{B-L}$) scenario. The right plot shows the rate of $h \to \gamma\gamma$ with respect to the Standard Model expectation vs. the lightest stau mass using $n = 4$. Only points with 123 GeV $< m_h <$ 128 GeV are included. The color coding of the parameter points is as in figure 4.3.

c_{hXX}^{BLR} to the initial states $X = g, W$. Consequently, we can write:

$$\sigma(XX \to h)_{BLR} = \sigma(XX \to h)_{SM} \left(\frac{c_{hXX}^{BLR}}{c_{hXX}^{SM}}\right)^2 .$$

Shortly after the discovery of the Higgs boson (essentially through the diphonon channel) [4, 5], there has been quite some excitement since both, ATLAS and CMS, reported an enhanced $h \to \gamma\gamma$ branching ratio with respect to the Standard Model expectations [160, 161]. With more statistics, however, this excess has largely vanished and the newest measurements are compatible with the SM rate [162, 163].

In many supersymmetric models, $R_{h\to\gamma\gamma}$ can have values above one due to a virtual light $\tilde{\tau}$ in the loop in addition to the Standard Model contributions from the W boson and the top quark. This is not so here: the largeness of $m_{\tilde{t}_1}$, which is required for the loop contributions to the Higgs to be large enough, also imposes a lower limit on Λ, and hence also on the slepton soft SUSY-breaking masses. Consequently, in our model, the lighter stau eigenstate is as heavy as 500 GeV or more. Although it has been shown that, even in models with large SUSY-breaking masses, the stau can be light enough to enhance $R_{h\to\gamma\gamma}$ (see, *e.g.*, ref. [164] in the context of a model exhibiting a $U(1)_Y \times U(1)_{B-L}$ gauge symmetry), we find that this is not the case here. In ref. [164], large D-term contributions are responsible for a suppression of the $\tilde{\tau}_1$ mass. This is different in our model: first, the D-terms itself are smaller for a given set of parameters. This is depicted in the left panel of figure 4.5 where we compare the D-terms between our model and the model used in ref. [164] for equivalent input values. Second, the ratio $\tan\beta_R$ (which enhances the D-terms) is more restricted to small values in our model due to the tadpole equation (4.38). The right plot of figure 4.5 presents the results for $R_{h\to\gamma\gamma}$ vs. the mass of the lightest stau for $n = 4$ and with the constraint that the Higgs mass is in the desired mass range. We find that our model actually prognosticates rates slightly smaller than the Standard Model prediction. Note that $R_{h\to\gamma\gamma} = 0.9$ is well compatible with the recent searches [162, 163] within $1\,\sigma$.

4.8 Dark matter and NLSP discussion

Because of the comparatively small scale at which SUSY gets broken, the gravitino is usually the LSP in models with gauge mediation. Its mass reads [44]:

$$m_{3/2} = \frac{F}{\sqrt{3}\, m_{Pl}}\,, \tag{4.49}$$

where m_{Pl} is the reduced Planck mass, so that $m_{3/2}$ is typically in the MeV range or above. All SUSY particles decay into it in a cosmologically short time [165–167]. The abundance of thermally produced gravitinos is under assumptions consistent with the standard thermal evolution of the early universe given by

$$\Omega_{3/2} h^2 = \frac{m_{3/2}}{\text{keV}} \frac{100}{g_\star}\,, \tag{4.50}$$

where $g_\star$ is the effective number of degrees of freedom at the time of gravitino decoupling. Even though for gravitino masses of $O(100\text{ GeV})$, the relic abundance would be in the correct range to agree with the observation, it is nontrivial to satisfy all relevant constraints, see the more detailed discussion in ref. [168]. A gravitino with a mass in the MeV range certainly results in a too large value for the relic density within the standard assumptions. These would, however, in general not apply if the reheating temperature was sufficiently low – which means that the gravitino might never have been in thermal equilibrium [169]. Because of these very model dependent statements we will not go into the dark matter description any further but concentrate on the phenomenology of the next-to-lightest supersymmetric particle (NLSP) instead. The latter is of particular interest in GMSB models since all heavier supersymmetric particles will first decay into the NLSP before this itself decays into the gravitino. As a result, all cascades at a collider experiment will (temporarily) end in Standard Model particles and the NLSP, as is the case for the LSP in models with gravity mediation. However, in contrast to the latter, the NLSP may also be a charged particle because of its eventual decay into the gravitino. The lifetime of the NLSP is generically proportional to F^2 [44] so that, in most of the parameter space under consideration, it is too long-lived to decay inside a collider detector, yet short-lived enough not to be in conflict with the bounds set by big bang nucleosynthesis.

In usual minimal GMSB secanarios, two candidates for the NLSP exist: the lightest neutralino and the lightest stau, each leading to phenomenologically very different possible signatures at a collider experiment. With an inverse seesaw mechanism at work, however, there is also the possibility of a $\tilde{S}$-like sneutrino to be the NLSP. This can be realized with a hierarchical structure in Y_S which makes one sneutrino eigenstate light. A neutralino can be the NLSP for little or no hierarchy in Y_S and messenger multiplicities $n \lesssim 2$, a stau for larger n. Alternatively, the $\tilde{\chi}_1^0$ can be lighter than the lightest stau for $n > 2$ if $|\mu_R|$ is small or if there is little left-right splitting in the slepton sector, meaning small $\tan\beta$. The reason for the dependence on n is the scaling of the soft SUSY-breaking masses at M. Recall that it is n for gauginos and $\sqrt{n}$ for scalars, so that the ratio of gaugino to sfermion masses at the messenger scale is proportional to $\sqrt{n}$. The impact of the Y_S hierarchy on the NLSP nature is already apparent in the spectra of the benchmark points BLRI-BLRIII which only differ in the Y_S^{33} entry, yet each choice features a different NLSP nature. This is further exemplified in figure 4.6 where we show the masses of the lightest neutralino,

sneutrino and stau eigenstates as a function of Y_S^{33}. While the charged slepton masses do not depend on the choice of Y_S, in particular the lightest sneutrino and neutralino eigenstates are very sensitive to this coupling. This will become clear in the subsequent discussion where the three different scenarios and their main differences to standard GMSB models are presented.

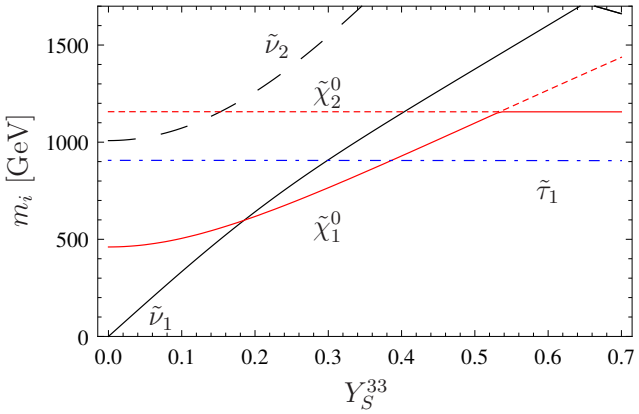

Figure 4.6: Masses of the lightest supersymmetric particles as a function of the [3,3] entry of Y_S, leaving the remaining parameters as in BLRI-BLRIII.

4.8.1 Neutralino NLSP

The neutralino sector consists, in addition to the usual higgsinos and gaguinos, of the R-higgsinos and the gaugino associated with the $U(1)_\chi$ gauge boson ($\tilde{B}_\chi$). The mass matrix reads in the basis $(\tilde{B}, \tilde{W}^3, \tilde{H}_d^0, \tilde{H}_u^0, \tilde{B}_\chi, \tilde{\bar{\chi}}_R, \tilde{\chi}_R)$:

$$M_{\tilde{\chi}^0} = \begin{pmatrix} M_1 & 0 & -\frac{g_Y v_d}{2} & \frac{g_Y v_u}{2} & \frac{M_{Y\chi}}{2} & 0 & 0 \\ 0 & M_2 & \frac{g_L v_d}{2} & -\frac{g_L v_u}{2} & 0 & 0 & 0 \\ -\frac{g_Y v_d}{2} & \frac{g_L v_d}{2} & 0 & -\mu & \frac{(g_\chi - g_{Y\chi})v_d}{2} & 0 & 0 \\ \frac{g_Y v_u}{2} & -\frac{g_L v_u}{2} & -\mu & 0 & -\frac{(g_\chi - g_{Y\chi})v_u}{2} & 0 & 0 \\ \frac{M_{Y\chi}}{2} & 0 & \frac{(g_\chi - g_{Y\chi})v_d}{2} & -\frac{(g_\chi - g_{Y\chi})v_u}{2} & M_\chi & \frac{5 g_\chi v_{\bar{\chi}_R}}{4} & -\frac{5 g_\chi v_{\chi_R}}{4} \\ 0 & 0 & 0 & 0 & \frac{5 g_\chi v_{\bar{\chi}_R}}{4} & 0 & -\mu_R \\ 0 & 0 & 0 & 0 & -\frac{5 g_\chi v_{\chi_R}}{4} & -\mu_R & 0 \end{pmatrix} . \tag{4.51}$$

In order to distinguish of which nature the lightest neutralino is, it is convenient to apply some approximations. In the limit of negligible mixing between the MSSM states and the new ones (the upper left 4×4 block and the lower right 3×3 block in the mass matrix) as well as $\tan\beta_R \to 1$, the three new neutralino states correspond to the mass eigenvalues

$$\mu_R\,, \quad \frac{1}{2}\left(M_\chi + \mu_R \pm \sqrt{\frac{1}{4} M_{Z'}^2 + M_\chi^2 - 2 M_\chi \mu_R + \mu_R^2} \right) , \tag{4.52}$$

where $M_{Z'}^2 \simeq \frac{25}{16} g_\chi^2 v_R^2$ in the considered limit. Because of the serious limitations from the tadpole equation (4.38), see also figure 4.1, we usually find $|\mu_R|, M_\chi \ll M'_Z$, so that the lightest state is governed by the value of μ_R. The two other states have masses around $M_{Z'}$ and can form a quasi-Dirac pair. The lightest state out of the upper left 4×4 block always turns out to be a bino since $M_1 < M_2, |\mu|$. Hence, the nature of a neutralino NLSP is mainly dictated by the relative sizes of $|\mu_R|$ and M_1, so we either find the MSSM-like bino ($M_1 < |\mu_R|$) or a maximally mixed $\tilde{\tilde{\chi}}_R - \tilde{\chi}_R$ state ($|\mu_R| < M_1$). Figure 4.7 shows the evolution of the neutralino masses as a function of μ_R in BLRIV. Here, the variation of μ_R was achieved by adjusting $\tan\beta_R$ within a suitable range. As the bino mass parameter is $M_1 \simeq 575$ GeV in this case, this is the very value for μ_R at which the NLSP nature changes from h_{χ_R}-like to bino-like.

Because of the dependence of the mass splitting $m^2_{\tilde{\chi}_R} - m^2_{\chi_R}$ on $Y_S^\dagger Y_S$, μ_R is sensitive to the particular Y_S entries. In figure 4.6, where Y_S^{33} has been varied, one can nicely see the associated evolution of the R-higgsino-like neutralino mass.

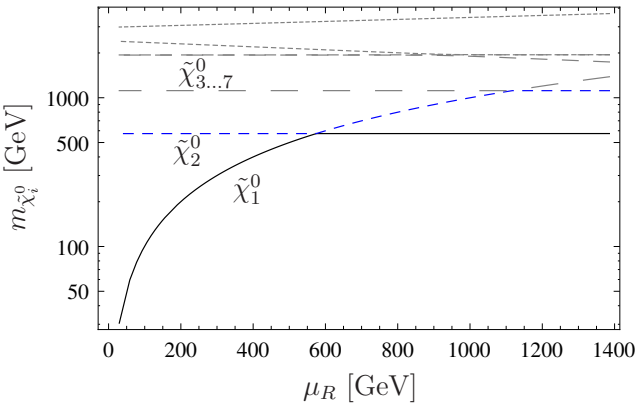

Figure 4.7: Masses of the different neutralino eigenstates as a function of μ_R. The ratio $\tan\beta_R$ has been adjusted within $1.02 < \tan\beta_R < 1.033$ in order to satisfy the tadpole equation (4.38). In other respects the parameters have been fixed to the values of BLRIV.

The signatures of the neutralino-NLSP scenario would be rather difficult to measure at the LHC. Because of the low messenger multiplicity which is usually required for a neutralino NLSP, the two lightest coloured states turn out to be the $\tilde{t}_1$ and the gluino, whereby the former has to be at least as heavy as 2 TeV to satisfy the Higgs mass constraints. Depending on whether the gluino turns out to be heavier or lighter than the lightest stop, it will dominantly decay either into $t\tilde{t}_1$ or a chargino/neutralino and a third-generation quark. Irrespective of the detailed decay chain, the final state will contain b jets and W bosons. The endpoint of such a cascade depends on the admixtures of the lightest and next-to-lightest neutralinos. As seen in the possible decays of the $\tilde{\chi}_2^0$ state in figure 4.8, additional final state particles could comprise Higgs bosons of the doublet and the $\tilde{\tilde{\chi}}_R/\tilde{\chi}_R$ type (for large (low) values of $|\mu_R|$, respectively). Interesting intermediate states could be light sneutrinos (not in the figure as they are too heavy for this choice of parameters) as well as charged sleptons. Those will eventually further decay into the lightest neutralino and a neutrino or a charged lepton, respectively. The different regions of dominant $\tilde{\chi}_2^0$ channels can easily be explained with the help of figure 4.7. Up to roughly $|\mu_R| \approx 670$ GeV,

the only kinematically accessible decay channels are $h_{\chi_R}\tilde{\chi}_1^0$ and $Z\tilde{\chi}_1^0$. The latter gets more important with decreasing mass diffenence $\tilde{\chi}_2^0 - \tilde{\chi}_1^0$ since h_{χ_R} is lighter than the Z at this benchmark point. At the small window centered around $|\mu_R| = 575$ GeV, $\tilde{\chi}_2^0 - \tilde{\chi}_1^0$ gets too small, so that only three-body decays via virtual Z or h_{χ_R} bosons are possible. As soon as the kinematical threshold is crossed, the decay into a charged slepton and and the corresponding lepton dominates. At very large values for $|\mu_R|$, the hierarchy $M_1 < M_2 < |\mu_R|$ emerges, so that the next-to-lightest neutralino is wino-like and the doublet-like Higgs gets to be a possible decay product.

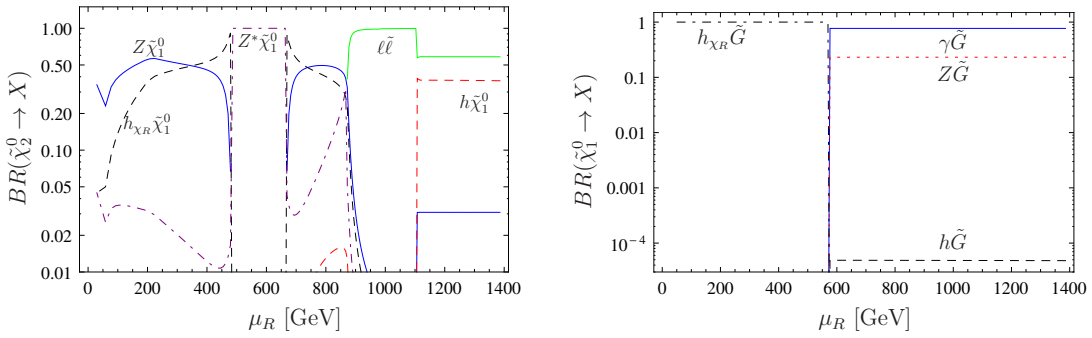

Figure 4.8: Branching ratios of the second lightest (left) as well as the lightest neutralino (right) as a function of μ_R using the same parameters as in figure 4.7.

The eventual decays of the NLSP, depicted in the right panel of figure 4.8, are heavily dependent on its nature: bino NLSPs decay, as in standard scenarios, into a gravitino and a neutral gauge boson. Only a small portion decays into the $h\,\tilde{G}$ final state. χ_R-like states, in turn, are not charged under the Standard Model gauge group and consequently decay, besides the gravitino, into a h_{χ_R}. Unfortunately, due to the long lifetime of the NLSP, such a decay will not happen inside a usual particle physics detector so that there is no hope of measuring such a process at the LHC.

4.8.2 Stau NLSP

The mass matrix of the sleptons reads in the basis $(\tilde{e}_L, \tilde{e}_R)$

$$m_{\tilde{l}}^2 = \begin{pmatrix} m_L^2 + \frac{1}{2}v^2 c_\beta^2 Y_e^\dagger Y_e + D_L & \frac{v}{\sqrt{2}}(T_e^\dagger c_\beta - \mu Y_e^\dagger s_\beta) \\ \frac{v}{\sqrt{2}}(T_e c_\beta - \mu^* Y_e s_\beta) & m_E^2 + \frac{1}{2}v^2 c_\beta^2 Y_e Y_e^\dagger + D_R \end{pmatrix}, \tag{4.53}$$

with the D-terms

$$\begin{aligned} D_L =& \frac{1}{32}\Big(2\big(-3g_\chi^2 + g_\chi g_{Y\chi} + 2(g_Y^2 - g_L^2 + g_{Y\chi}^2)\big)v^2 c_{2\beta} - 5g_\chi(3g_\chi + 2g_{Y\chi})v_R^2 c_{2\beta_R}\Big)\mathbf{1}\,, \\ D_R =& \frac{1}{32}\Big(2\big(g_\chi^2 + 3g_\chi g_{Y\chi} - 4(g_Y^2 + g_{Y\chi}^2)\big)v^2 c_{2\beta} + 5g_\chi(g_\chi + 4g_{Y\chi})v_R^2 c_{2\beta_R}\Big)\mathbf{1}\,. \end{aligned} \tag{4.54}$$

As remarked before, the stau can be the NLSP for $n \geq 3$ because of the suppression of the soft SUSY-breaking scalar masses of $\sqrt{n}$ with respect to the gaugino masses. Furthermore, large values for $\tan\beta$ help increasing the left-right splitting of the slepton states and thence reduce the mass of the lighter state. A further requirement is that the Y_S Yukawa coupling

should not inherit much hierarchy in the diagonal entries as otherwise a sneutrino or neutralino could nevertheless be lighter, see figure 4.6.

The gluino is the heaviest coloured particle here because of the large messenger multiplicity, rendering a discovery of this state at the LHC only possible for very high luminosities. The cascade decays anticipated in the stau NLSP scenario are different compared to the former case of a neutralino NLSP, in particular in the initial and the last decay step: first, the gluino will decay into all sorts of squarks instead of just the third-generation ones. The further decay of the squarks will eventually end in the lightest neutralino, implying the possibility of the alongside production of the h_{χ_R} scalar as above. The lightest neutralino itself then decays into a $\tau\tilde{\tau}_1$ final state. As the stau will decay outside of the detector, a typical event of this type would include, additionally to several jets and leptons, a charged track. As in particular the latter is a very promising signal, its phenomenology has been thoroughly studied, see, *e.g.*, refs. [170,171]. Explicit searches are currently being performed at the LHC, setting limits of roughly $m_{\tilde{\tau}} > 300$ GeV for long-lived staus within an MSSM scenario [172].

4.8.3 Sneutrino NLSP

In principle, one would have to split the sneutrinos into their CP-odd and CP-even eigenstates and regard these (pseudo-) scalar particles separately. However, the only source of CP-splitting is found in the F-terms induced by μ_S and the corresponding soft SUSY-breaking bilinear B_{μ_S} term. As the masses of the left-handed neutrinos within the inverse seesaw mechanism at work require μ_S to be small, this CP splitting is found to be negligibly small, so that we can safely work with complex scalar sneutrino fields in what follows. In the limit $\mu_S, B_{\mu_S} \to 0$, the sneutrino mass matrix reads in the basis $(\tilde{\nu}_L, \tilde{\nu}_R, \tilde{S})$:

$$M^2_{\tilde{\nu}} = \begin{pmatrix} m_L^2 + \frac{v^2 s_\beta^2}{2} Y_\nu^\dagger Y_\nu + D'_L & \frac{v}{\sqrt{2}}\left(T_\nu^\dagger s_\beta - \mu Y_\nu^\dagger c_\beta\right) & \frac{1}{2} v v_R Y_\nu^\dagger Y_S s_\beta s_{\beta_R} \\ \frac{v}{\sqrt{2}}\left(T_\nu s_\beta - \mu^* Y_\nu c_\beta\right) & m^2_{\nu^c} + \frac{v_R^2 s^2_{\beta_R}}{2} Y_S Y_S^\dagger + \frac{v^2 s_\beta^2}{2} Y_\nu Y_\nu^\dagger + D'_R & \frac{v_R}{\sqrt{2}}\left(T_S s_{\beta_R} - \mu_R^* Y_S c_{\beta_R}\right) \\ \frac{1}{2} v v_R Y_S^\dagger Y_\nu s_\beta s_{\beta_R} & \frac{v_R}{\sqrt{2}}\left(T_S^\dagger s_{\beta_R} - \mu_R Y_S^\dagger c_{\beta_R}\right) & m_S^2 + \frac{v_R^2 s^2_{\beta_R}}{2} Y_S^\dagger Y_S \end{pmatrix}, \tag{4.55}$$

with

$$\begin{aligned} D'_L =& \frac{1}{32}\Big(2\big(-3g_\chi^2 + g_\chi g_{Y\chi} + 2(g_L^2 + g_Y^2 + g_{Y\chi}^2)\big) v^2 c_{2\beta} - 5 g_\chi (3 g_\chi + 2 g_{Y\chi}) v_R^2 c_{2\beta_R}\Big)\mathbf{1}\,, \\ D'_R =& \frac{5 g_\chi}{32}\Big(2(g_\chi - g_{Y\chi}) v^2 c_{2\beta} + 5 g_\chi v_R^2 c_{2\beta_R}\Big)\mathbf{1}\,. \end{aligned} \tag{4.56}$$

The mixing between the left sneutrinos $\tilde{\nu}_L$ and the $\tilde{\nu}_R$ and $\tilde{S}$ states is small compared to the diagonal entries, so that we effectively end up with left sneutrinos as well as admixtures of singlet scalars and right sneutrinos. Although the soft SUSY-breaking singlet mass m_S^2 is driven negative by the RGEs, the much larger F-term $\frac{1}{2} v_R^2 s^2_{\beta_R} Y_S^\dagger Y_S$ prevents negative diagonal entries and hence tachyonic eigenstates. The entries mixing the $\tilde{\nu}_R$ and $\tilde{S}$ states

can reach the size of the diagonal entries for sufficiently large values of $|\mu_R|$. Therefore,

$$|\mu_R| \lesssim \sqrt{m_{\nu^c}^2 + v_R^2 Y_S^2/4} \tag{4.57}$$

must furthermore be fulfilled so that no tachyonic states occur. For this condition we have applied the approximations $\tan\beta_R \to 1$ and $D'_R, T_S \to 0$. Y_S is constrained from above by requiring that all couplings should stay perturbative up to the GUT scale whereas the product $|Y_S Y_S^\dagger|$ is constrained from below by requiring the correct symmetry breaking (see the discussion about generating $m_{\tilde{\chi}_R}^2 - m_{\chi_R}^2 \neq 0$ in section 4.4). Hence, we cannot have two or more light singlet-like sneutrinos as at least two diagonal Y_S entries should be large in order to have a large enough $|Y_S Y_S^\dagger|$. If, however, only one diagonal Y_S entry is small, *i.e.* $\lesssim 0.2$ while the other two are large, *i.e.* roughly 0.7, one generation of singlets is light enough for the NLSP to be a sneutrino of mainly singlet nature. The admixtures of the singlet and the $\tilde{\nu}_R$ of τ flavour within the lightest sneutrino state of figure 4.6 are depicted in figure 4.9. The sudden drop of the $\tilde{\nu}_{R,\tau}$ admixture at $Y_S^{33} \simeq 0.64$ is due to a level crossing of two sneutrino mass eigenstates.

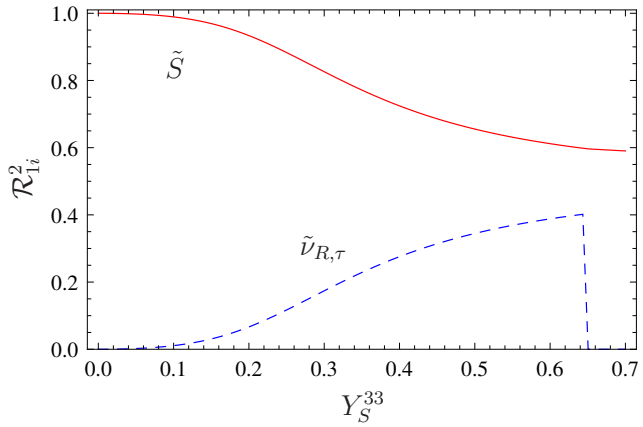

Figure 4.9: Relative admixtures of the singlet state $\tilde{S}$ and the right τ-sneutrino to the lightest sneutrino state as a function of the third diagonal Y_S entry while the remaining parameters are fixed to the values of the benchmark points BLRI, BLRIII and BLRIII, as in figure 4.6.

The smallness of the Y_S entry in case of the sneutrino NLSP also results in one rather light ν_h quasi-Dirac pair, see also the masses of BLRI in table 4.3. Nevertheless, these fermions are always heavier than the lightest sneutrino. This is due to the combined effect of the $\tilde{S} - \tilde{\nu}_R$ mixing and the negative m_S^2. Consequently, the sneutrino NLSP will always decay into a gravitino and a light neutrino. The next heavier supersymmetric state in the $\tilde{\nu}$-NLSP scenario is the R-higgsino-like neutralino. The reason for that is the small $|\mu_R|$ because of the condition (4.57) and the strong constraints from a small Y_S on μ_R via the tadpole equation (4.38). If kinematically allowed, this lightest neutralino will decay to the LSP and the corresponding heavy neutrino, yielding

$$\tilde{\chi}_1^0 \to \tilde{\nu}_1 \nu_{h_1} \to \nu \tilde{G} W^{(*)} \ell\,. \tag{4.58}$$

The W boson will be off-shell if $m_{\nu_{h_1}}$ turns out to be very small. Using the parameters

	BLRI	BLRII	BLRIII	BLRIV	BLRV	BLRVI
$M_{Z'}$ [TeV]	2.5			2.7	2.4	4.3
BR($d\bar{d}$)	0.45	0.49	0.52	0.52	0.52	0.48
BR($u\bar{u}$)	0.08	0.09	0.10	0.10	0.10	0.09
BR($\ell\bar{\ell}$)	0.17	0.18	0.20	0.20	0.20	0.18
BR($\nu\nu$)	0.15	0.16	0.17	0.17	0.17	0.16
BR(W^+W^-)	0.01	0.01	0.01	0.01	0.01	0.01
BR($\nu_h\nu_h$)	0.12	0.06	–	–	–	–
BR($h_1 Z$)	–	–	0.01	–	–	–
BR($h_2 Z$)	–	–	–	0.01	–	–
BR($\tilde{\ell}\tilde{\ell}^*$)	–	–	–	–	–	0.02
BR($\tilde{\nu}\tilde{\nu}$)	0.01	–	–	–	–	0.01
BR($\tilde{\chi}_i^0\tilde{\chi}_j^0$)	–	–	–	–	–	0.02
BR($\tilde{\chi}_2^+\tilde{\chi}_2^-$)	–	–	–	–	–	0.02

Table 4.5: Branching ratios of the Z' boson for the parameter points of table 4.3. Only branching ratios of 10^{-2} or larger are shown.

of figure 4.9, we find that the above neutralino decay will happen in almost 100 % of the cases for $|Y_S^{33}| \lesssim 0.07$, whereas it decays to a gravitino and a light neutrino with BR($\tilde{\chi}_1^0 \to \tilde{G}\nu$) $\simeq 1$ for larger values of $|Y_S^{33}|$. As the latter final state would be completely invisible at a collider experiment, this scenario couldn't be distinguished from the neutralino NLSP case in this model.

4.9 Z' phenomenology

We now turn to the Z' boson, its decays and the resulting phenomenology at the LHC. For a better orientation, we list the decay modes of the Z' and the corresponding branching ratios of the representative benchmark points of table 4.3 in table 4.5. Strikingly, decays into supersymmetric particles are hardly expected as long as the Z' is not heavier than around 4 TeV. This is a consequence of the very constraining GMSB boundary conditions and the required rather large scales for Λ. In variants of this or similar models which work via gravity mediation, it has been shown that supersymmetric Z' decays can lead to a rich LHC phenomenology, see, *e.g.*, [140, 151, 173, 174]. Here, for the parameter choices in BLRIII and BLRV, not even the sneutrinos and right-handed neutrinos are light enough for the Z' to decay into, so that only decay channels into SM particles are open. As $m_{\nu_h} \propto Y_S\, v_R$, only scenarios which feature small Y_S for one generation of singlets, and hence a large hierarchy in Y_S, exhibit a Z' decaying into heavy neutrinos. This is the case for BLRI-II. BLRVI features a Z' which is heavy enough for supersymmetric final states to occur.

The to date tightest bounds on the mass of a Z' boson stem from the search for dilepton resonances at a centre-of-mass energy of $\sqrt{s} = 8$ TeV by the ATLAS and CMS collaborations, refs. [175, 176]. The respective cross-section limits are of comparable size. As the ATLAS analysis distinguishes between different Z' models when deriving the cross-section limits and takes into account interference effects of the Z' with the Drell-Yan background, we

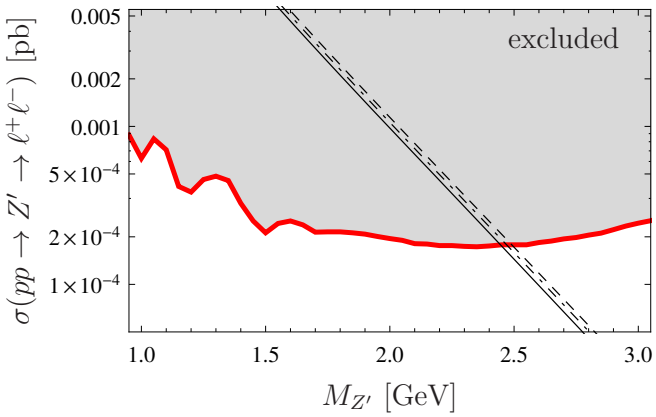

Figure 4.10: Cross section of the dilepton production via a Z' resonance at $\sqrt{s} = 8$ TeV for the benchmark points BLRI (solid line), BLRII (dot-dashed line) and BLRIII (dashed line). The red line shows the exclusion limit from ref. [175] as evaluated for the Z'_χ scenario.

will always refer to this analysis in the following and compare the predictions of our model to the bounds given in [175] for the scenario of a Z'_χ.

For an interpretation of the cross-section limits in the context of our model, we made use of the `SARAH` interface to `CalcHEP` which we used in version `3.4.2` [121], and calculated the production cross sections $\sigma(pp \to Z' \to \ell^+\ell^-)$ for the benchmark points of table 4.3. In figure 4.10, we present the results for BLRI-III. Naturally, the bound on BLRI is the less stringent one as the decays into the heavy neutrinos are most pronounced for this scenario and hence lead to a broadening of the Z' width. According to their smaller total width, the dilepton mode of the Z' bosons of BLRII and BLRIII is correspondingly larger, cf. table 4.5, leading to slightly tighter exclusion bounds. Nevertheless, as apart from the heavy neutrinos, no large non-SM decay channels are present, the limits do not vary much and we can place the bound $M_{Z'} > 2.5$ TeV, corresponding to $v_R > 6.9$ TeV, on our model. Therefore, BLRV with $M_{Z'} = 2.4$ TeV is already excluded.

For a Z' close to this mass, the supersymmetric decay modes are not accessible. While heavy Z' masses could nevertheless help in resonantly producing supersymmetric particles, there is little hope for a subsequent discovery of these high-mass sparticles, see the discussion of slepton production through a Z' resonance in ref. [151]. Therefore, the most promising possibility in which a Z' could tell about the underlying model is the decay mode into two heavy neutrinos. Those decay further into $W^\pm \ell^\mp$, $Z\,\nu$, or $h_i\,\nu$ $(i = 1, 2)$ with the branching ratios ~ 0.6, ~ 0.2 and ~ 0.2, respectively [140]. Naively, one would also expect the decay into sneutrinos to be sizeable in case of a sneutrino NLSP due to $m_{\tilde{\nu}_1} < m_{\nu_{h1}}$. However, the coupling to the Z' is suppressed because of the large $\tilde{S}$ portion and the rather moderate $\tilde{\nu}_R$ share in a light sneutrino state, see also figure 4.9. In principle, also the second-lightest sneutrino can be produced. However, as $\tilde{\nu}_2$ is the $\tilde{\nu}_R$-like sneutrino eigenstate, its mass is governed by the large SUSY-breaking mass parameter $m^2_{\nu^c}$, so that there is a kinematical suppression and we find only branching ratios of at most $O(0.01)$ for sneutrinos in the final state. In parts of the parameter space, the decay $\tilde{\nu}_2 \to \tilde{\nu}_1\, h_{\chi_R}$ is possible. Mostly, however,

it will undergo the decay

$$\tilde{\nu}_2 \to \nu_h \, \tilde{\chi}_1^0 \to \nu_h \, \nu_h \, \tilde{\nu}_1 \to \ell \, \ell \, W \, W + \not{E}_T \,, \tag{4.59}$$

where $\not{E}_T$ denotes the missing transverse energy due to the escaping sneutrino NLSP or its invisible decay products. The complete Z' decay chain would hence dominantly be

$$Z' \to \tilde{\nu}_2 \tilde{\nu}_2^* \to 4\ell \; 4W + \not{E}_T \,, \tag{4.60}$$

whereas also the other final states

$$\begin{aligned} &2\ell \; 2W \; 2Z + \not{E}_T \\ &2\ell \; 2W \; 2h + \not{E}_T \\ &4Z + \not{E}_T \\ &2Z \; 2h + \not{E}_T \\ &4h + \not{E}_T \end{aligned} \tag{4.61}$$

are feasible. The Z' decays into neutralinos are not expected to play an interesting role at the LHC. Despite the possibility of rather light $\tilde{\chi}_R / \tilde{\tilde{\chi}}_R$ states, the decays into these are suppressed: the $Z' - \tilde{\chi}_i^0 - \tilde{\chi}_j^0$ coupling is proportional to

$$g_\chi \left(2(Z_\chi^{i,3} Z_\chi^{j,3} - Z_\chi^{i,4} Z_\chi^{j,4}) + 5(Z_\chi^{i,6} Z_\chi^{j,6} - Z_\chi^{i,7} Z_\chi^{j,7}) \right) \,, \tag{4.62}$$

whereas the new higgsinos have admixtures of $Z_\chi^{1,6} \simeq Z_\chi^{1,7} \simeq \pm 1/\sqrt{2}$, Z_χ being the neutralino mixing matrix. The MSSM-like neutralinos and charginos which contain a large higgsino content can only be produced for large Z' masses with branching ratios of a few percent. In the scenario of BLRVI, the Z' production cross section is only of around 1 fb, requiring large statistics to study the final states.

In conclusion, while an enlarged gauge symmetry at the TeV scale can help softening the requirements for very large stop masses in scenarios with gauge mediation, the mass scale for supersymmetric particles is in general still too high for a detailed study of the model at the LHC. Therefore, the best hopes for discovery of parts of the model rest on the extra gauge boson.

CHAPTER 5

LEPTON FLAVOUR VIOLATION IN LOW-SCALE SEESAW MODELS

The models in the previous chapters each featured seesaw mechanisms which resulted in low-scale (*i.e.* significantly below the GUT scale) right-handed neutrinos, and we have explored the consequences for LHC physics while leaving out the low-energy phenomenology. This chapter is finally reserved for shedding some light on the particularly interesting lepton flavour violating processes which are expected to show enhanced rates in such low-scale seesaw mechanisms.

Other than in collider searches, the desirable possibility of the unambiguous identification of new particles is not given in low-energy experiments. Instead, in processes like rare decays or meson mixings, potential new heavy particles only enter as off-shell propagators, mostly in loops. This makes it much harder to identify the source of a possible discrepancy with respect to the SM predictions, and one has to compare different models in terms of their predictions for the effective operators which describe the process.

Nevertheless, in many cases the precise measurement of low-energy processes is sensitive to much higher mass scales than can be probed at current colliders as the background is comparatively much lower. Let us consider charged lepton flavour violation: in the Standard Model, the single lepton Yukawa coupling can be diagonalized while keeping all flavour eigenstates equal to the gauge eigenstates. Consequently, lepton flavour is conserved in the Standard Model. In the presence of right-handed neutrinos and the associated additional Yukawa coupling, this statement is not true anymore. Instead, analogous to the quark sector, one only has the freedom to choose a basis where one Yukawa coupling is diagonal, but not both – which means that, in general, lepton flavour *is* violated. This has finally been confirmed by the observation of neutrino oscillations [177] which implies, besides that neutrinos are massive, that the neutrino mass eigenstates are in fact different from the gauge eigenstates. Consequently, even though we can choose a basis where the charged lepton Yukawa coupling is diagonal, loop diagrams of the type of figure 5.1 with neutrinos and W bosons in the loop promote the flavour violation from the neutrino to the charged lepton sector. Accordingly, muons and tauons can, in principle, decay via processes like $\ell_\alpha \to \ell_\beta \gamma$ or $\ell_\alpha \to 3\,\ell_\beta$. In addition, in muon capture experiments, $\mu - e$

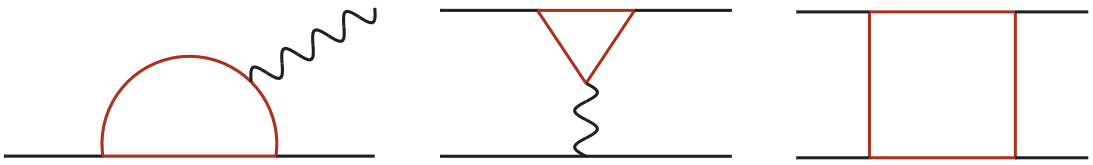

Figure 5.1: Examples for generic lepton flavour violating Feynman diagrams. In this illustration, the red propagators represent particles of all spins. Diagrams of the left type contribute to the radiative lepton decays $\ell_\alpha \to \ell_\beta \gamma$. The diagrams in the middle and at the right contribute to the leptonic three-body decays $\ell_\alpha \to \ell_\beta \ell_\gamma \ell_\delta$ as well as to $\mu - e$ conversion in nuclei.

conversion is imaginable, corresponding to the parton-level process $\mu\, q \to e\, q'$. However, in the SM extended by ν masses, those diagrams are suppressed by $(m_\nu/M_W)^4$, so that the respective cLFV branching rations are of the order of 10^{-50}. This is beyond the reach of any experiment we can imagine by now.

It is hence obvious that the measurement of any such process would be a plain sign of BSM physics. In fact, in many models of new physics, cLFV processes are potentially large. For instance, just considering the diagram with the supersymmetric analogue of the $\nu - W$ loop already makes clear that in SUSY there is no such huge suppression as in the SM since one expects chargino and sneutrino masses to be of the same order of magnitude. Consequently, the LFV rates could actually be accessible for current and/or future experiments.

The cLFV observable which is currently best constrained is $\mu \to e\,\gamma$. The MEG collaboration could set a lower limit of $\mathrm{BR}(\mu \to e\gamma) < 5.7 \cdot 10^{-13}$ [178] and in the future, the sensitivity will increase to $6 \cdot 10^{-14}$ [179]. This future sensitivity will be outplayed by experiments searching for $\mu \to 3\,e$ and $\mu - e$ conversion by the Mu3e and PRIME collaborations, respectively [180, 181]. In table 5.1 we summarize the current bounds as well as the expected future sensitivities for the various considered cLFV observables.

LFV Process	Present Bound	Future Sensitivity
$\mu \to e\gamma$	5.7×10^{-13} [178]	$6 \cdot 10^{-14}$ [179]
$\tau \to e\gamma$	$3.3 \cdot 10^{-8}$ [182]	$\sim 3 \cdot 10^{-9}$ [183]
$\tau \to \mu\gamma$	$4.4 \cdot 10^{-8}$ [182]	$\sim 3 \cdot 10^{-9}$ [183]
$\mu \to eee$	$1.0 \cdot 10^{-12}$ [184]	$\sim 10^{-16}$ [180]
$\tau \to \mu\mu\mu$	$2.1 \cdot 10^{-8}$ [185]	$\sim 10^{-9}$ [183]
$\tau^- \to e^-\mu^+\mu^-$	$2.7 \cdot 10^{-8}$ [185]	$\sim 10^{-9}$ [183]
$\tau^- \to \mu^- e^+ e^-$	$1.8 \cdot 10^{-8}$ [185]	$\sim 10^{-9}$ [183]
$\tau \to eee$	$2.7 \cdot 10^{-8}$ [185]	$\sim 10^{-9}$ [183]
$\mu^-, \mathrm{Ti} \to e^-, \mathrm{Ti}$	$4.3 \cdot 10^{-12}$ [186]	$\sim 10^{-18}$ [181]
$\mu^-, \mathrm{Au} \to e^-, \mathrm{Au}$	$7 \cdot 10^{-13}$ [187]	
$\mu^-, \mathrm{Al} \to e^-, \mathrm{Al}$		$10^{-15} - 10^{-18}$
$\mu^-, \mathrm{SiC} \to e^-, \mathrm{SiC}$		10^{-14} [188]

Table 5.1: Current experimental upper bounds and future sensitivities for lepton flavour violating radiative and three-body decays as well as conversion rates in the presence of nuclei.

Facing such bright prospects, it is interesting to see what theory tells us. As said

before, in case of a positive signal, it is not easy to determine of which origin the associated new physics is. However, with so many complementary experiments at operation, the combination of observations and non-observations can be illuminating. For instance, assuming the MSSM and employing a high-scale seesaw model, $\mu \to e\gamma$ will be orders of magnitude larger than $\mu \to 3e$ [189, 190]:[1]

$$\mathrm{BR}(\ell_\alpha \to 3\ell_\beta) \simeq \frac{\alpha}{3\pi}\left(\log\left(\frac{m^2_{\tilde{\ell}_\alpha}}{m^2_{\tilde{\ell}_\beta}}\right) - \frac{11}{4}\right)\mathrm{BR}(\ell_\alpha \to \ell_\beta\gamma)\,, \tag{5.1}$$

so the observation of a three-body decay combined with the (non-)observation of $\mu \to e\gamma$ could strongly (dis)favour said scenario. The simple relation between those observables can not be generalized to supersymmetric models featuring low-scale seesaw scenarios like the inverse seesaw. The reason is that, in addition to SUSY-scale right sneutrinos, also non-supersymmetric diagrams involving a W boson and a right-handed neutrino can be large [190–192], so that apart from the photonic penguins also other types of diagrams can contribute significantly. Recently there has been quite some discussion going on about the role of Z penguins in supersymmetric low-scale seesaw scenarios as enormous enhancements with respect to the γ penguins have been reported in refs. [193, 194]. In particular the fact that we made the same observation in association with the study of chapter 4, see ref. [168], motivated us to scrutinize (i) the origins of that effect [195], and subsequently (ii) the relative importance of all different contributions from the various types of diagrams to the cLFV observables which are listed in table 5.1 [196]. In the following, we will present the results of this investigation.

5.1 Mass spectrum of the model

We concentrate on the inverse seesaw mechanism based on the MSSM for which we add three generations of right-handed neutrino superfields $\hat{\nu}^c$ and three generations of singlets $\hat{X}$ to the MSSM field content. While the $\hat{\nu}^c$ fields have to carry a lepton number of -1, the singlets carry $L = +1$.[2] The corresponding superpotential reads

$$\begin{aligned} W =& Y_u^{ij}\,\hat{u}_i^c\,\hat{Q}_j^\alpha\,\epsilon_{\alpha\beta}\,\hat{H}_u^\beta - Y_d^{ij}\,\hat{d}_i^c\,\hat{Q}_j^\alpha\,\epsilon_{\alpha\beta}\,\hat{H}_d^\beta - Y_e^{ij}\,\hat{e}_i^c\,\hat{L}_j^\alpha\,\epsilon_{\alpha\beta}\,\hat{H}_d^\beta + \mu\,\hat{H}_u^\alpha\,\epsilon_{\alpha\beta}\,\hat{H}_d^\beta \\ &+ Y_\nu^{ij}\,\hat{\nu}_i^c\,\hat{L}_j^\alpha\,\epsilon_{\alpha\beta}\,\hat{H}_u^\beta + M_{R_{ij}}\,\hat{\nu}_i^c\,\hat{X}_j + \frac{1}{2}\mu_{X_{ij}}\,\hat{X}_i\,\hat{X}_j\,. \end{aligned} \tag{5.2}$$

While the M_R term is lepton number conserving and has no profound reason to be of a certain scale, μ_X violates L by two units. Hence, since lepton number is restored in the limit $\mu_X \to 0$, this parameter is expected to be naturally small, in the sense of 't Hooft [10].

[1] This can easily be estimated in this type of models as $\mu \to 3e$ is dominated by the γ penguin diagrams, so that the corresponding diagrams are related (compare the first and second diagram in figure 5.1).

[2] This is different to the assignments in chapter 4 where lepton number is part of a broken gauge group. Hence, there, the singlets S carry $L = 0$ while the Higgs fields charged under $B - L$ induce the inverse seesaw mechanism once they develop a vev.

The soft SUSY-breaking Lagrangian reads

$$-\mathcal{L}_{\text{soft}} = -\mathcal{L}_{\text{soft}}^{\text{MSSM}} + m^2_{\tilde{\nu}^c_{ij}} \tilde{\nu}^c_i \tilde{\nu}^{c*}_j + m^2_{X_{ij}} \tilde{X}^*_i \tilde{X}_j + (T^{ij}_\nu \tilde{\nu}^c_i \tilde{L}^\alpha_j \epsilon_{\alpha\beta} H^\beta_u + B^{ij}_{M_R} \tilde{\nu}^c_i \tilde{X}_j + \frac{1}{2} B^{ij}_{\mu_X} \tilde{X}_i \tilde{X}_j + m^2_{X\nu^c_{ij}} \tilde{X}^*_i \tilde{\nu}^c_j + \text{h.c.}) \,, \tag{5.3}$$

and $\mathcal{L}_{\text{soft}}^{\text{MSSM}}$ is defined in eq. (2.36). Also B_{μ_X} and $m^2_{X\nu_c}$ violate lepton number by two units and are therefore expected to be small.

The only difference in the mass spectrum of this model with respect to the MSSM is found in the (s)neutrino sector. In the following, we will discuss the corresponding mass matrices in some detail.

5.1.1 Fitting neutrino data within the inverse seesaw mechanism

The 9×9 neutrino mass matrix reads in the basis (ν_L, ν^c_R, X):

$$M_{\text{ISS}} = \begin{pmatrix} 0 & m_D^T & 0 \\ m_D & 0 & M_R \\ 0 & M_R^T & \mu_X \end{pmatrix} , \tag{5.4}$$

where we abbreviated $m_D = \frac{1}{\sqrt{2}} v_u Y_\nu$. Applying the replacement $M_R \to \frac{1}{\sqrt{2}} v_{\chi R} Y_S$ and $\mu_X \to \mu_S$, we arrive at the mass matrix of the $U(1)_R \times U(1)_{B-L}$ model of chapter 4, eq. (4.42). Hence, in the limit $\mu_X \ll m_D \ll M_R$, the effective mass matrix for the light neutrino eigenstates can be written in the same way as eq. (4.43):

$$M_{\text{light}} \simeq m_D^T (M_R^T)^{-1} \mu_X M_R^{-1} m_D \,. \tag{5.5}$$

Note that we can always work in a basis where M_R is diagonal. In that case, Y_ν and μ_X in general feature an off-diagonal structure.

We can now go on and fit the model parameters to the known neutrino data. For that purpose, we use M_R and μ_X as input and fix Y_ν using a parameterisation developed by Casas and Ibarra for the seesaw I [197], adapted to the inverse seesaw case [198, 199]:

$$Y_\nu = \frac{\sqrt{2}}{v_u} V^\dagger D_{\sqrt{X}} R D_{\sqrt{m_\nu}} U^\dagger_{\text{PMNS}} \,, \tag{5.6}$$

where $D_{\sqrt{m_\nu}} = \text{diag}(\sqrt{m_{\nu_i}})$, m_{ν_i} being the light neutrino masses, and $D_{\sqrt{X}} = \text{diag}(\sqrt{\hat{X}_i})$. $\hat{X}_i$ contains the eigenvalues of $X = M_R \, \mu_X^{-1} \, M_R^T$, and V is the matrix that diagonalizes X as $V X V^T = \hat{X}$.

The Pontecorvo-Maki-Nakagawa-Sakata (PMNS) matrix [200, 201] is the mixing matrix of the light neutrinos,

$$\begin{pmatrix} \nu_e \\ \nu_\mu \\ \nu_\tau \end{pmatrix} = U_{\text{PMNS}} \begin{pmatrix} \nu_1 \\ \nu_2 \\ \nu_3 \end{pmatrix} \tag{5.7}$$

and can be parameterised by three real angles $\theta_{12,23,13}$ and one Dirac CP phase δ_{CP}:

$$U_{\text{PMNS}} = \tag{5.8}$$
$$\begin{pmatrix} 1 & 0 & 0 \\ 0 & \cos\theta_{23} & \sin\theta_{23} \\ 0 & -\sin\theta_{23} & \cos\theta_{23} \end{pmatrix} \begin{pmatrix} \cos\theta_{13} & 0 & \sin\theta_{13}\, e^{-i\delta_{CP}} \\ 0 & 1 & 0 \\ -\sin\theta_{13}\, e^{i\delta_{CP}} & 0 & \cos\theta_{13} \end{pmatrix} \begin{pmatrix} \cos\theta_{12} & \sin\theta_{12} & 0 \\ -\sin\theta_{12} & \cos\theta_{12} & 0 \\ 0 & 0 & 1 \end{pmatrix}.$$

So far, the absolute mass scale of the neutrinos is not known since only squared mass differences can be extracted from neutrino oscillation experiments. Denoting the neutrino mass eigenstate of mostly electron flavour admixture as ν_1, the difference $\Delta m^2_{21} = m^2_{\nu_2} - m^2_{\nu_1}$ is known to a good precision, whereas the other mass difference can only be measured up to a sign. Therefore, it is not yet clear if the hierarchy $m_{\nu_1} < m_{\nu_2} < m_{\nu_3}$ (normal hierarchy) or $m_{\nu_3} < m_{\nu_1} < m_{\nu_2}$ (inverted hierarchy) is realized in nature. Consequently, while $\sin^2\theta_{12}$ can be determined unambiguously, the fits to θ_{13} and θ_{23} depend on the underlying neutrino mass hierarchy, and little is known about the CP phase.

R in eq. (5.6) is an arbitrary 3×3 complex orthogonal matrix which can be parameterised analogously to eq. (5.8) with the difference that all three angles $\theta^R_{12,23,13}$ can be complex.

Eventually, once M_R, μ_X and R are fixed, there is still freedom in choosing m_{ν_1}, the hierarchy and δ_{CP} for a successful fit of Y_ν. In the following, we will assume normal hierarchy together with $m_{\nu_1} = 10^{-4}$ eV and $\delta_{CP} = 0$ using the best-fit parameters as provided in ref. [202]

$$\begin{aligned} \Delta m^2_{21} &= 7.60 \cdot 10^{-5}\ \text{eV}^2\,, \qquad \Delta m^2_{31} = 2.48 \cdot 10^{-3}\ \text{eV}^2\,, \\ \sin^2\theta_{12} &= 0.323\,, \qquad \sin^2\theta_{23} = 0.467\,, \qquad \sin^2\theta_{13} = 0.0234\,, \end{aligned} \tag{5.9}$$

which are in good agreement with [203–205]. Fixing $M_R = \mathbf{1}\cdot 2$ TeV, $\mu_X = \mathbf{1}\cdot 10^{-5}$ GeV and $R = \mathbf{1}$ yields

$$Y_\nu = 10^{-2} \cdot \begin{pmatrix} 0.0956 & -0.0589 & 0.0348 \\ 0.616 & 0.594 & -0.687 \\ 0.404 & 1.78 & 1.91 \end{pmatrix}. \tag{5.10}$$

5.1.2 Sneutrino masses

The lepton number violating terms μ_X and B_{μ_X} induce a small mass splitting between the sneutrino CP eigenstates. To account for that, we split the complex sneutrino fields into their real and imaginary part according to $\tilde\nu_L = \frac{1}{\sqrt2}(\phi_L + i\sigma_L)$, $\tilde\nu_R = \frac{1}{\sqrt2}(\phi_R + i\sigma_R)$, $\tilde X = \frac{1}{\sqrt2}(\phi_X + i\sigma_X)$, so that the mass matrices of the scalar and pseudoscalar sneutrinos read in the basis (ϕ_L, ϕ_R, ϕ_X) and $(\sigma_L, \sigma_R, \sigma_X)$, respectively:

$$m^2_{\tilde\nu^{S/P}} = \tag{5.11}$$
$$\begin{pmatrix} m_L^2 + \frac12 v_u^2 Y_\nu^T Y_\nu^* + D_L & -\frac{1}{\sqrt2}\Big(v_d\mu Y_\nu^T - v_u T_\nu^\dagger\Big) & \frac{1}{\sqrt2} v_u \Re\Big(Y_\nu^T M_R^*\Big) \\ -\frac{1}{\sqrt2}\Big(v_d\mu Y_\nu^* - v_u T_\nu\Big) & m^2_{\tilde\nu^c} + M_R M_R^\dagger + \frac12 v_u^2 Y_\nu Y_\nu^\dagger & B_{M_R} \pm M_R\mu_X^* \\ \frac{1}{\sqrt2} v_u M_R^T Y_\nu^* & B_{M_R}^T \pm \mu_X M_R^\dagger & M_R^T M_R^* + m_X^2 + \mu_X\mu_X^* \pm B_{\mu_X} \end{pmatrix},$$

with

$$D_L = \frac{1}{8}(g_1^2 + g_2^2)(v_d^2 - v_u^2) = -m_Z^2 \cos^2\theta_W \cos 2\beta \, \mathbf{1} \,. \tag{5.12}$$

As one expects $|M_R \, \mu_X^*| \ll |B_{M_R}|$ and $|B_{\mu_X}| \ll |M_R|^2$, the CP-splitting has a negligible impact on the phenomenology of the model.

5.2 Lepton flavour violating decays

Because of the off-diagonal structure of Y_ν, it is obvious that lepton flavour violating processes can in general be introduced at the loop level. The experimentally most interesting observables are the radiative muon decay $\mu \to e\gamma$, three-body muon and tauon decays $\ell_\alpha \to \ell_\beta \ell_\gamma \ell_\gamma$ as well as coherent muon conversion in nuclei. In the appendix B, we define all relevant decay widths.

5.2.1 Numerical setup

For the numerical evaluation, we use the combination of `SARAH` and `SPheno` for the spectrum calculation, including the full RGE running at the two-loop level. For the calculation of the flavour observables, we use the `FlavorKit` package [206] as incorporated in `SARAH`. `FlavorKit` uses `FeynArts` and `FormCalc` [207–210] to calculate all one-loop amplitudes to any process relevant for flavour physics. Processes which are not yet predefined can be implemented via `PreSARAH` by providing the amplitude and the necessary `FeynArts` structure, see the manual for further information. In this manner, the `FlavorKit` repertoire has been extended to also include $\ell_\alpha^- \to \ell_\beta^- \ell_\beta^\pm \ell_\gamma^\mp$ in line with this project.

The tadpole equations are solved for $|\mu|$ and B_μ, the phase of μ being treated as a free parameter, as are M_R, B_{M_R} as well as μ_X and B_{μ_X}. We furthermore define as usual $\tan\beta = v_u/v_d$. The Standard Model masses and couplings are used as listed in table 5.2; the dimensionless parameters are evaluated up to the GUT scale (M_{GUT}, defined by the requirement $g_Y = g_L$) using the RGE equations provided by `SARAH`. At M_{GUT} we impose the CMSSM-like boundary conditions:

$$m_Q^2 = m_u^2 = m_d^2 = m_L^2 = m_e^2 = m_{\nu^c}^2 = m_X^2 = m_0^2 \mathbf{1} \,, \tag{5.13}$$

$$m_{H_u}^2 = m_{H_d}^2 = m_0^2 \,, \tag{5.14}$$

$$M_1 = M_2 = M_3 = M_{1/2} \,, \tag{5.15}$$

whereas the mixing soft parameter $m_{X\nu^c}$ is zero at M_{GUT} and is not induced by the RGEs. Additionally, it is assumed that, as usual, all soft SUSY-breaking trilinear couplings originate from a common A-term:

$$T_i = A_0 Y_i \,, \quad i = u, d, e, \nu \,. \tag{5.16}$$

These parameters are then evolved down to $Q_{\text{EWSB}} = \sqrt{\tilde{t}_1 \tilde{t}_2}$ where the mass spectrum is calculated at one loop. The lepton flavour violating processes, in turn, are calculated at M_Z. The effects of the RGE running of the operators down to the scale of the decaying particle can be taken into account to a good approximation by using $\alpha(0)$.

α_{em}^{-1}	127.92783	G_μ	$1.11639 \cdot 10^{-5}\text{GeV}^{-2}$
α_S	0.11720	M_Z	91.18760 GeV
$m_b(m_b)$	4.2 GeV	m_t	172.9 GeV
m_τ	1.777 GeV		

Table 5.2: Input values for the SM parameters taken at M_Z unless specified otherwise.

5.2.2 Results

m_0	1 TeV	$M_{1/2}$	1 TeV
A_0	-1.5 TeV	M_R	2 TeV
B_{μ_X}	$100\,\mu_X$	B_{M_R}	$100\,M_R$
$\tan\beta$	10	$\text{sign}(\mu)$	+

Table 5.3: Input values for the various parameters if not scanned over or stated otherwise. M_R and μ_X are taken proportional to the unit matrix.

We turn to the numerical results. In addition to M_R, we use diagonal μ_X and adapt Y_ν to fit neutrino data, and throughout the numerical evaluations we assume M_R to be degenerate, $M_R = M_R^{ii},\ i = 1...3$. Of particular interest is the dependence of the respective rates on the mass scale of the new particles. This scale is M_R for the right-handed neutrinos and M_{SUSY} for supersymmetric particles, and we define $M_{SUSY} = m_0 = M_{1/2} = -A_0$. If not scanned over or stated otherwise, we fix the model parameters according to table 5.3.

$\mu \to e\gamma$

In the majority of models, the most constraining LFV observable is the radiative muon decay $\mu \to e\gamma$. We shall see that this is also the case here, but that this situation can change with future experiments. In figure 5.2, we show the dependence of the decay rate on M_R and M_{SUSY} as well as for the case $M_R = M_{SUSY}$. In each scenario we present the complete decay rate as well as separately the contributions from the supersymmetric and the non-supersymmetric particles. The latter include, in addition to the SM fields, also the heavy neutrinos, the heavy neutral scalar and pseudoscalar as well as the charged Higgs boson. The latter is also the reason for the dip in the curve for the non-supersymmetric contributions: the major part of the non-SUSY amplitude is contributed by the $\nu - H^\pm$ and $\nu - W^\pm$ diagrams which add with a relative sign in $K_2^{L/R}$, so that a sign-flip occurs where both contributions cancel each other.[3] Note that $m_{H^\pm}$ is a function of the SUSY mass scale which means that the magnitudes of the non-SUSY diagrams actually also depend on M_{SUSY} in regions where the $\nu - H^\pm$ diagrams dominate. As apparent from the figures, the sign flip happens at $M_R > M_{SUSY}$, which is the reason why there is no such situation if $M_R = M_{SUSY}$ are varied together.

[3] This is in contrast to the known contributions to $b \to s\gamma$ where both types of diagrams with $t - W^\pm$ and $t - H^\pm$ in the loop interfere constructively. We have verified that we recover the $b \to s\gamma$ results when replacing the neutrino masses and Yukawa couplings with the top mass and coupling.

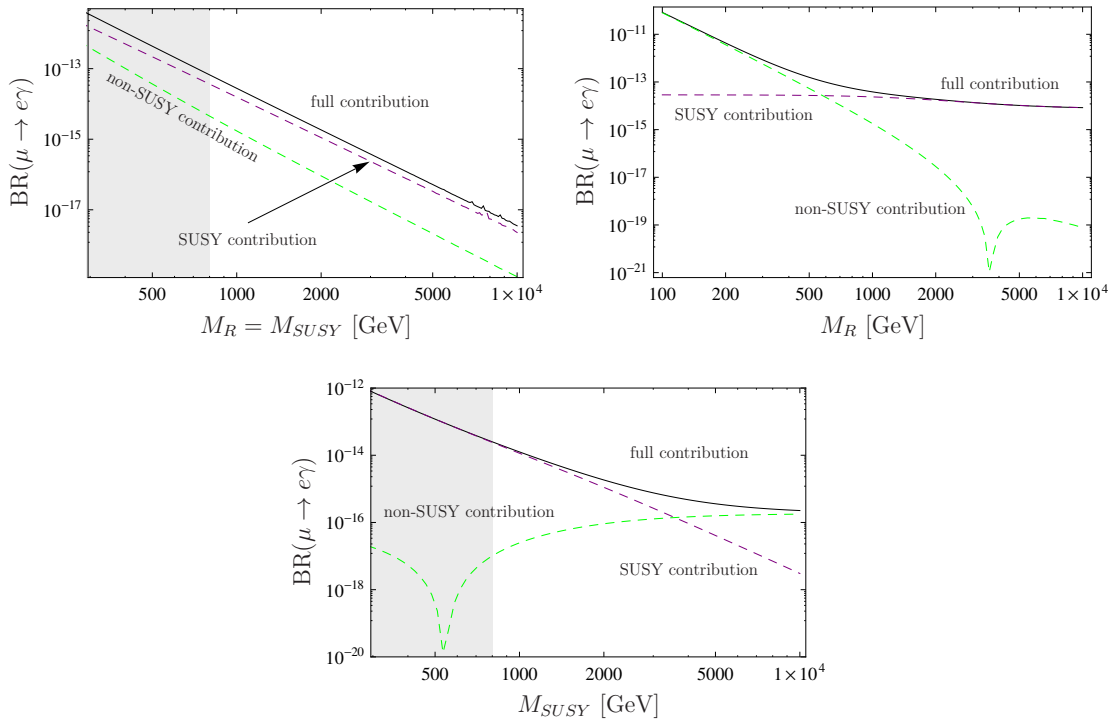

Figure 5.2: Branching ratio of the radiative decay $\mu \to e\,\gamma$ as a function of M_{SUSY} and M_R, the other parameters being given in the text. The grey shaded area roughly corresponds to the parameter space excluded currently by the LHC.

The dominating SUSY diagrams are the ones induced by the respective superpartners, the sneutrinos and charginos. We observe that, for the chosen parameter setup, the supersymmetric contributions dominate if the SUSY and ν_R mass scales coincide, $M = M_R = M_{SUSY}$, with the relative importance of the SUSY diagrams increasing with M.

The grey area here and in the following figures, indicating $M_{SUSY} < 0.8$ TeV, roughly corresponds to the recent LHC exclusions on the constrained SUSY parameter space which assume the CMSSM as the underlying model [53]. Although most of the model under consideration is similar to the CMSSM, the bounds cannot be translated one-to-one because of the enhanced (s)neutrino sector and the correspondingly different cascade decays, so that the shown bound may be regarded as conservative.

$\mu \to 3e$

A particularly promising observable because of the upcoming Mu3e experiment [180] is the three-body decay $\mu \to 3e$. In the same manner as in figure 5.2, we show in figure 5.3 the results for this observable as a function of M_R and M_{SUSY}. Before discussing the individual contributions to this decay, we will focus on the supersymmetric Z-penguin diagrams in a little more detail. Two conclusions can be drawn from the figures: these diagrams are (i) sub-dominant for each considered scenario and (ii) the respective operators decouple properly for large mediator scales, *i.e.* the amplitude decreases with increasing mass of the particles in the loop. Both observations, though sounding rather trivial, are in

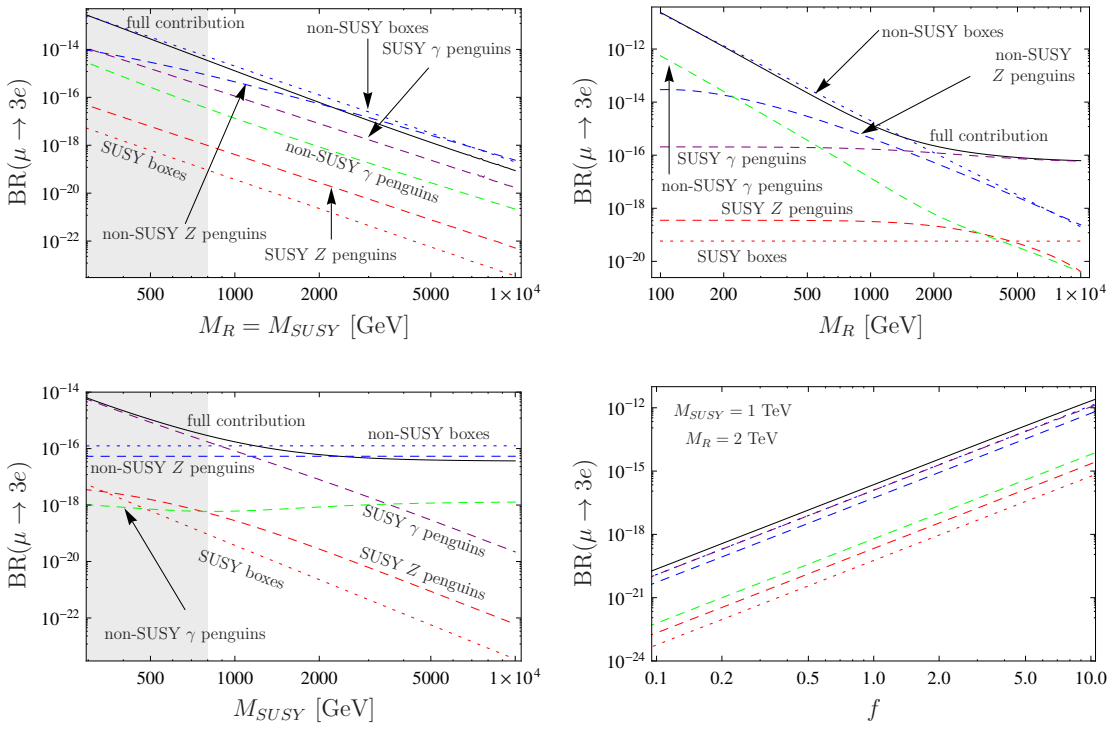

Figure 5.3: BR$(\mu \to 3\,e)$ as a function of M_{SUSY}, M_R and an overall scaling parameter f for Y_ν whereas $f = 1$ corresponds to the Yukawa matrix shown in eq. (5.10). The other parameters are given in table 5.3.

fact very interesting as previous studies reported otherwise for low-scale seesaw models, including the very model under consideration.

It has been first noted in ref. [193] that, using the amplitudes and loop functions of [189], the suppression of Z-mediated LFV diagrams (as it happens in the MSSM extended by a seesaw-I sector) does no longer happen in non-minimal scenarios such as models with inverse seesaw or R-parity violation. Instead, an enhancement of $(M_{SUSY}/M_Z)^4$ of supersymmetric Z-penguins with respect to supersymmetric photon penguins has been observed. A further study [194] confirmed these results and carved out the relevant part which leads to that effect within the supersymmetric inverse seesaw model. According to ref. [194], the effective $Z - \ell_i - \ell_j$ vertex as mediated by a charged higgsino and a right sneutrino can be written to first order as

$$\mathcal{F} = \frac{g}{8\cos\theta_W}\left(Y_\nu^\dagger Y_\nu\right)_{ij}(\cos^2\theta_W - \frac{1}{2})\,. \tag{5.17}$$

Since Y_ν is a generic complex matrix, the corresponding matrix element will be non-zero in general. Apparently, as eq. (5.17) does not depend on any mass scale, the contribution from this operator is non-decoupling, meaning that it will carry information from new physics – at whichever scale that may be. Consequently, it will dominate for large masses of loop particles, which is exactly the $(M_{SUSY}/M_Z)^4$ enhancement found in ref. [193]. Several other papers which made use of the same formulas have reported the Z-penguin

enhancement [140,194,211], including the publication associated with the study of chapter 4, ref. [168]. Moreover, this Z-penguin non-decoupling was one of the main motivations for the Mu3e experiment as it sets hopes to discover new physics even in case the associated energy scales are by far out of reach of the LHC. In fact, two out of the three explicit models discussed in the corresponding research proposal [180] rely on that effect.

However, as pointed out in ref. [195], those hopes are ill-founded. We could trace back the reported effect to a combination of an error in the loop amplitudes and an erroneous definition of the loop function C_{00} in the literature. Using the correct amplitude, the one-loop effective vertex of eq. (5.17) vanishes exactly and can only be non-zero by chargino- or left-right-sneutrino mixing.[4] Both mixings are suppressed roughly as v/M_{SUSY}, so that the amplitude decouples with M_{SUSY} as one would also have naively expected, and as is also clearly seen in figure 5.3. For a detailed investigation of that issue see appendix B.4. Based upon this finding, the authors of ref. [193] have revoked the reported Z-penguin enhancement in an erratum [212].

In figure 5.3, we observe that the non-supersymmetric diagrams dominate if $M_R = M_{SUSY}$. Interestingly, it is in fact the box diagrams which give the most important contributions if M_R is in the TeV region.[5] Note that this statement does not depend on the magnitude of Y_ν. This can be seen in the lower right panel of figure 5.3 where we scale Y_ν as $f\,Y_\nu$. The fact that all contributions scale in the same way can be spoiled if extra flavour violating entries in the soft SUSY-breaking parameters were present. For larger $M_{SUSY} = M_R$ or for $M_R < M_{SUSY}$, the interference between the non-SUSY boxes and Z-penguins becomes important: both types of diagrams contribute with a relative sign, so that the overall amplitude is suppressed by an order of magnitude in the region where both contributions cancel each other. This is *e.g.* the case for $M_{SUSY} = M_R \simeq 10$ TeV in the left upper plot in figure 5.3. With the chosen set of parameters, this region coincides with the values of branching ratios probed by future experiments, so that this interference has to be regarded when interpreting positive results or when setting bounds because of non-observations.

The non-supersymmetric γ penguins are in general at least an order of magnitude smaller than said diagrams. The sign-flip between the $\nu - H^\pm$ and the $\nu - W^\pm$ contributions to K_2, though present, is by far not as pronounced as in figure 5.2 where it led to a change of the overall sign, but can only be seen as a small kink. The reason is that for the off-shell photon, the monopole operators K_1 appear with a higher weight than the dipole contributions from K_2. See appendix B for a definition of these operators.

$\mu - e$ conversion in nuclei

The $\mu - e$ conversion rates behave similarly to the three-body decays as the difference only amounts to the exchange $ee \leftrightarrow qq$ in the corresponding diagrams. The main discrepancy to the $\mu \to 3e$ decay is seen in figure 5.4 in the very pronounced negative interference between the non-SUSY Z-penguins and boxes and the SUSY photon penguins, which is due to a relative sign between the SUSY γ penguins and the non-SUSY boxes. The rest of the figure shows no qualitative difference to the muonic three-body decay.

[4] Also the mass splitting of the sneutrinos into CP-even and CP-odd eigenstates can induce a non-zero $[ij]$ element; however, as explained earlier, this splitting is very small.

[5] Note that this finding is not new. It has first been observed by ref. [213] and confirmed by refs. [214–216].

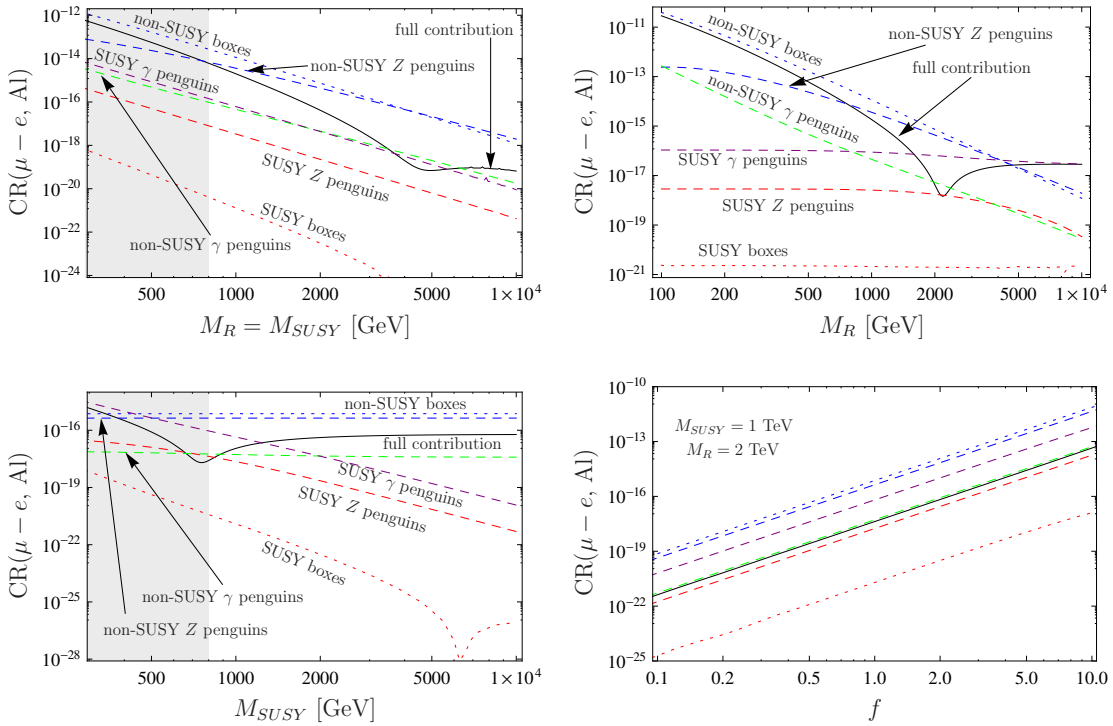

Figure 5.4: $\mu - e$ conversion on Al as a function of M_{SUSY} and M_R as well as the scaling parameter f for Y_ν.

The nuclei used for $\mu - e$ conversion experiments don't influence the generic behaviour of the conversion rate with $M_{R/SUSY}$. This is exemplified in figure 5.5 where we compare the absolute rates of the processes discussed so far, and show the $\mu - e$ conversion for the elements Al and Ti. Also apparent from this figure is that, with $\mu \to e\,\gamma$ bearing the strongest bounds up to date, this is the currently most constraining LFV process. In the future this situation will, however, change when muon capture experiments probe $\mu - e$ conversion down to rates of $\mathcal{O}(10^{-18})$. These experiments will in particular provide the best bounds to our model if $M_R \lesssim M_{SUSY}$.

τ decays

The different contributions from different types of diagrams to the flavour violating τ decays are analogous to the μ decays and, using the same texture of Y_ν, the total branching ratios are of the same order of magnitude as $\mu \to 3\,e$ for $\tau \to \mu\,\ell_i^+\ell_i^-$, $\ell_i = e, \mu$ and roughly two orders smaller for $\tau \to e\,\ell_i^+\ell_i^-$, see figure 5.6. The reason is the structure of $Y_\nu^\dagger Y_\nu$: the (2,3) and (1,2) entries using eq. (5.10) are larger than the (1,3) elements. In either case, the τ decay rates are too small to be observed in the near future. This statement, however, is specific to the assumptions made so far. Indeed, it is possible to find regions of the parameter space in which the τ observables are enhanced with respect to the μ decays because of a different Y_ν structure. This can already be the case if the generic matrix R as of eq. (5.6) exhibits a non-trivial structure and μ_X inherits a hierarchy in the diagonal

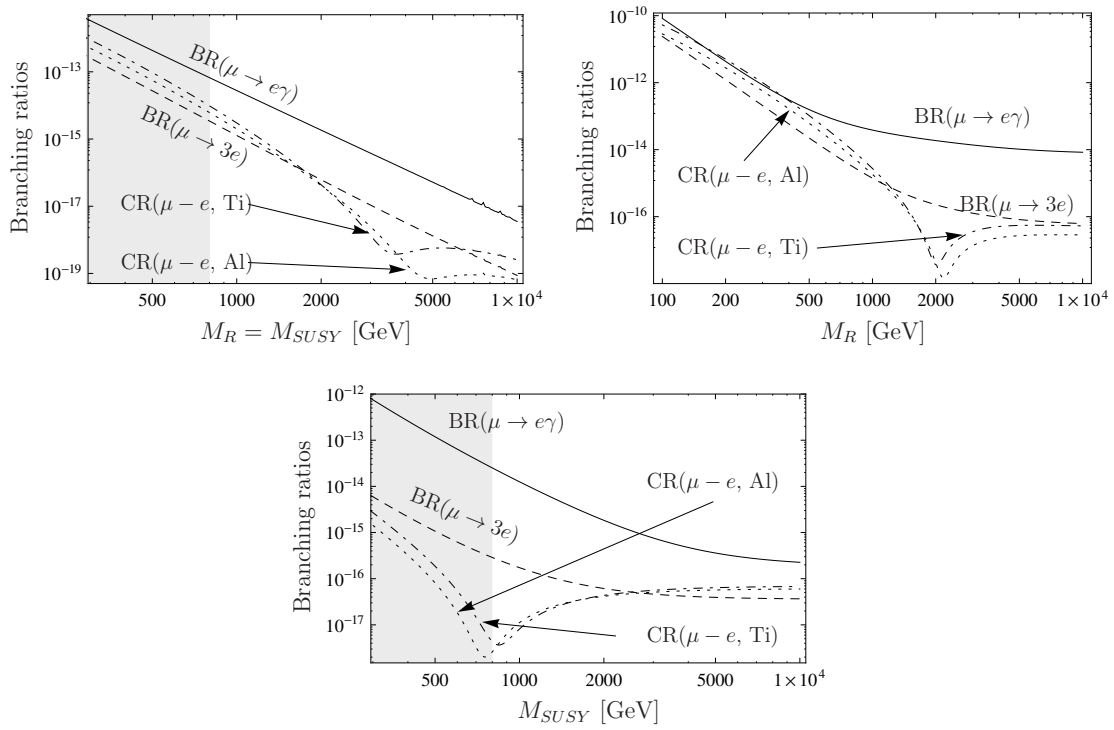

Figure 5.5: Comparison of the magnitudes of $\mathrm{BR}(\mu \to e\,\gamma)$, $\mathrm{BR}(\mu \to 3\,e)$, $\mu - e$ conversion on Ti and Al as functions of M_R and M_{SUSY}.

entries.

Those regions are of particular interest as the observation of more than one τ three-body decay channel could give insight into the underlying BSM physics which leads to the decay: for $M_{SUSY} < M_R$, the branching ratio is dominated by the SUSY γ penguins which prefer the decays into lighter particles since the corresponding final states have more phase space available. In case $M_R > M_{SUSY}$, in turn, the non-SUSY boxes usually give the dominant contribution. They favour the final state with three leptons of the same flavour: for the decay $\tau \to \mu\, e^+ e^-$, *e.g.*, most of the box diagrams require an an additional LFV vertex with respect to the $3\,\mu$ final state, so that $\mathrm{BR}(\tau^- \to \mu^- e^+ e^-) < \mathrm{BR}(\tau \to 3\,\mu)$. Hence, a measurement of both decays can give hints to the relative scales or even the existence of supersymmetric states or right-handed neutrinos. This behaviour is exemplified in the lower row of figure 5.6.

The remaining decays $\tau \to e\,\mu^- e^+$ and $\tau \to \mu\, e^- \mu^+$ are suppressed with respect to said processes since (i) the only possible contributing type of diagram is the boxes and (ii) at least one more lepton flavour violating vertex is required compared to the previous cases. Therefore, those decays are beyond hope of discovering in the near future.

We now turn to parameter regions which feature enhanced τ LFV decays, refraining from the previous assumptions that R is trivial and that μ_X is proportional to the unit matrix. Using the approach to fit Y_ν according to eq. (5.6) and keeping the other parameters fixed, a change of the overall μ_X prefactor obviously influences all LFV rates equally as it corresponds to an overall scaling of Y_ν as in the previous pictures. Implementing

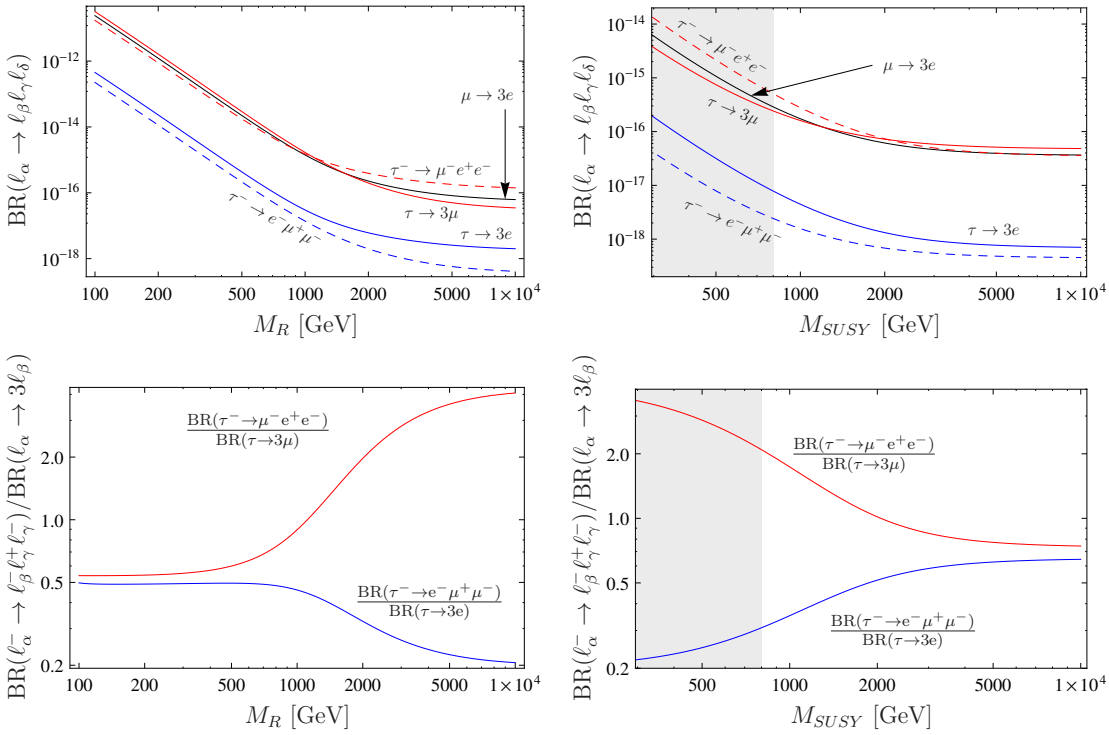

Figure 5.6: Branching ratios of the LFV τ decays as a function of M_R and M_{SUSY}. The lines in the upper row correspond to $\mathrm{BR}(\mu \to 3\,e)$ (black solid), $\mathrm{BR}(\tau \to 3e)$ (blue solid), $\mathrm{BR}(\tau \to 3\,\mu)$ (red solid), $\mathrm{BR}(\tau \to e\,\mu^+\mu^-)$ (blue dashed) and $\mathrm{BR}(\tau \to \mu\,e^+e^-)$ (red dashed). The lower row shows the ratios of the distinct decays $\tau \to \ell_i \ell_j^+ \ell_j^-$.

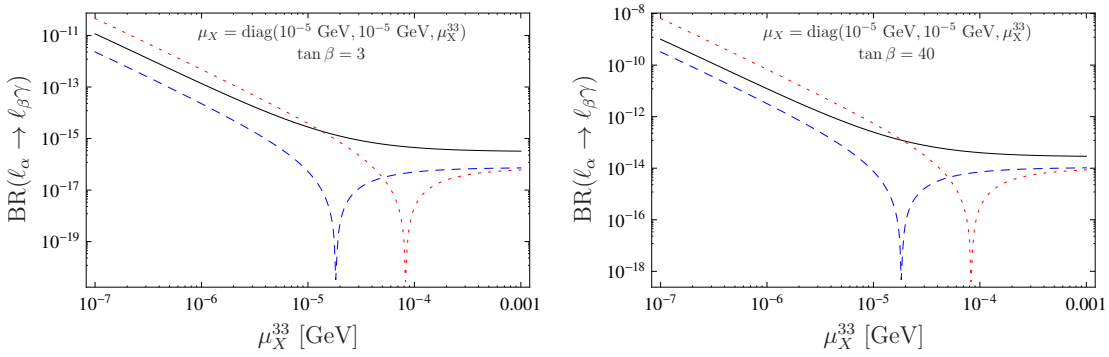

Figure 5.7: Dependence of $\ell_\alpha \to \ell_\beta \gamma$ on μ_X^{33} for $\tan\beta = 3$ (left) and $\tan\beta = 40$ (right). The lines correspond to $\mathrm{BR}(\mu \to e\,\gamma)$ (black), $\mathrm{BR}(\tau \to e\,\gamma)$ (blue dashed) and $\mathrm{BR}(\tau \to \mu\,\gamma)$ (red dotted).

a hierarchical structure while keeping μ_X diagonal, in turn, can influence the relative importance of τ and μ decays. This is illustrated in figure 5.7 where we show the radiative μ and τ decays as a function of the μ_X^{33} entry for two values of $\tan\beta$. Being dominated by the SUSY contribution, the branching ratios roughly scale like $\tan^2\beta$. In figure 5.8, we show how already one non-zero θ^R angle can lead to relative differences between the branching fractions of τ and μ decays for different hierarchies in μ_X.[6] Those differences are maximally enhanced if the amplitude of one observable undergoes a sign-flip. Hence, the best mechanism to enhance τ over μ LFV decays is finding parameter regions where the μ decays are suppressed for this reason. This is the case for certain values of θ_{23}^R, depending on the structure of μ_X. The behaviour of the radiative decays (upper row) compared to the three-body decays (lower row) with varying θ_{23}^R is the same.

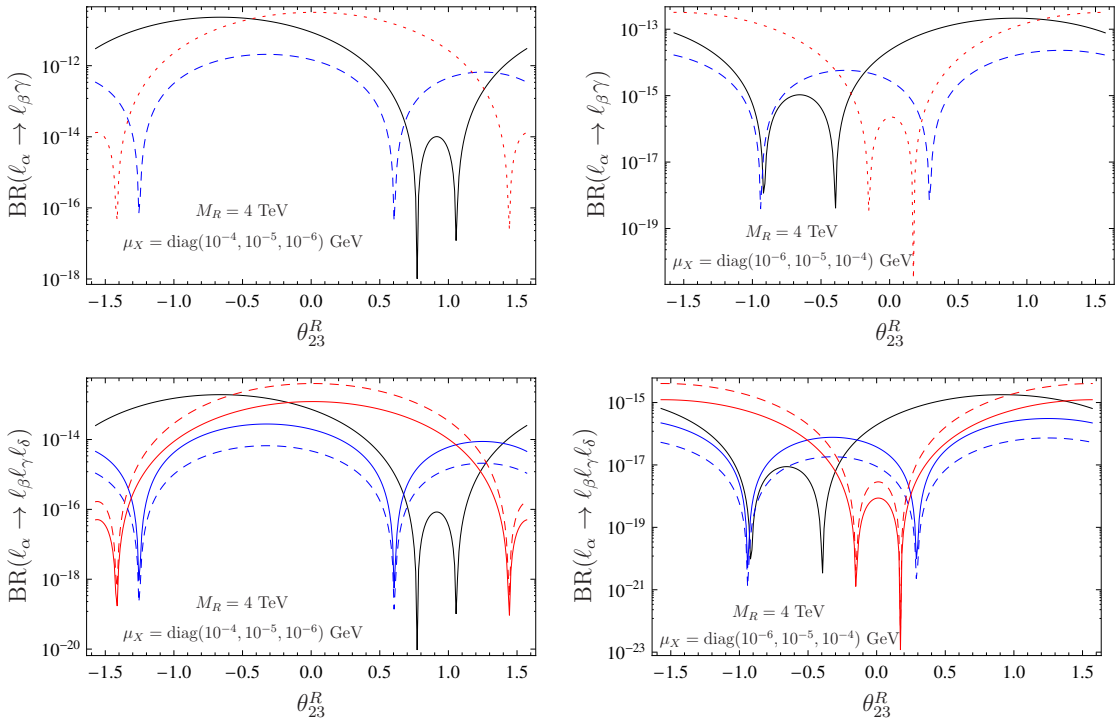

Figure 5.8: Dependence of $\ell_\alpha \to \ell_\beta\gamma$ (upper row) and $\ell_\alpha \to \ell_\beta\ell_\gamma\ell_\delta$ (lower row) on θ_{23}^R for two different μ_X hierarchies each, and $M_R = 4$ TeV. In the upper row, the lines correspond to $\mathrm{BR}(\mu \to e\,\gamma)$ (black solid), $\mathrm{BR}(\tau \to e\,\gamma)$ (blue dashed) and $\mathrm{BR}(\tau \to \mu\,\gamma)$ (red dotted). In the lower row, they correspond to the branching ratios of $\mu \to 3\,e$ (black solid), $\tau \to 3\,e$ (blue solid) and $\tau \to 3\,\mu$ (red solid), as well as $\tau \to e\,\mu^+\mu^-$ (blue dashed) and $\tau \to \mu\,e^+e^-$ (red dashed).

From these figures it is apparent that one can find small regions where τ decays might indeed be relevant for future experiments. We have exploited this fact in figure 5.9 where we show two special cases where most of the radiative and three-body decays are within reach of the future experiments. For those specific scenarios we have adapted θ_{23}^R such that the $\mu \to e\,\gamma$ amplitude is near a sign-flip and is hence suppressed with respect to $\tau \to \mu\,\gamma$. In that manner, the latter can still have a sizable branching ratio of $\mathcal{O}(10^8)$ which is within the reach of SuperB even when $\mu \to e\,\gamma$ is below its current bound. Interesting regions of

[6] Note that R has no impact if μ_X and M_R are proportional to the unit matrix.

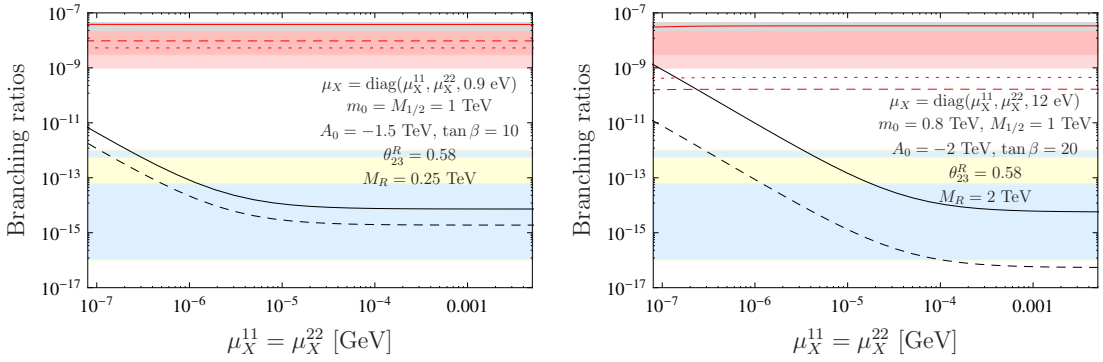

Figure 5.9: LFV μ- and τ-observables as a function of $\mu_X^{11} = \mu_X^{22}$ while keeping μ_X^{33} fixed. The underlying parameters are given in the plots. The lines correspond to $\mathrm{BR}(\tau \to \mu\,\gamma)$ (red, solid), $\mathrm{BR}(\tau \to 3\,\mu)$ (red, dashed), $\mathrm{BR}(\tau^- \to \mu^- e^+ e^-)$ (red, dotted), $\mathrm{BR}(\mu \to e\,\gamma)$ (black, solid) and $\mathrm{BR}(\mu \to 3\,e)$ (black, dashed). The light grey, red, yellow and blue bands show the expected future reach of the dedicated experiments to $\tau \to \mu\,\gamma$, $\tau \to 3\,\mu$, $\mu \to e\,\gamma$ and $\mu \to 3\,e$ as given in table 5.1.

this kind can be found for both cases, $M_R < M_{SUSY}$ (left panel) and $M_R > M_{SUSY}$ (right panel). Regarding the left plot, even the interesting ratio $\mathrm{BR}(\tau \to \mu\,e^+e^-)/\mathrm{BR}(\tau \to 3\,\mu)$ as discussed above is potentially accessible.

5.3 Lepton flavour violation in the $SO(10)$ inspired GMSB model

Considerations on lepton flavour violating decays have also been performed in the $U(1)_R \times U(1)_{B-L}$ model of chapter 4. By the time of the journal article, ref. [168], we had not yet corrected the LFV amplitudes as presented in section 5.2.2 and instead relied on the erroneous amplitudes of ref. [189]. Hence, the same observation as in refs. [193, 194] of a dominating Z penguin has been promoted, leading to the wrong conclusion that the Z-penguin diagrams in fact show a non-decoupling behaviour, scaling as $(M_{SUSY}/M_Z)^4$. While the results for the considered radiative decay $\mu \to e\,\gamma$ are unaffected, the findings for $\mu \to 3\,e$ and the $\mu - e$ conversion in nuclei as presented in figure 11 in ref. [168] are wrong. Therefore, we correct our findings as well as the plots of this figure in the following.

In chapter 4, the assumption was made that the complete flavour structure of the neutrino sector is encoded in μ_S. This will lead to undetectable rates for charged lepton flavour violating decays. Let us now assume that also in this model the neutrino mixing is present because of the non-diagonal form of Y_ν. In the following, we refrain from the Casas-Ibarra-like parameterisation used above in favour of a slight redefinition. This is done in order to compare the obtained results one-to-one with the ones reported in ref. [168]. Hence we use [218]

$$Y_\nu = f \begin{pmatrix} 0 & 0 & 0 \\ a & a(1 - \frac{\sin\theta_{13}}{\sqrt{2}}) & -a(1 + \frac{\sin\theta_{13}}{\sqrt{2}}) \\ \sqrt{2}\sin\theta_{13} & 1 & 1 \end{pmatrix},$$

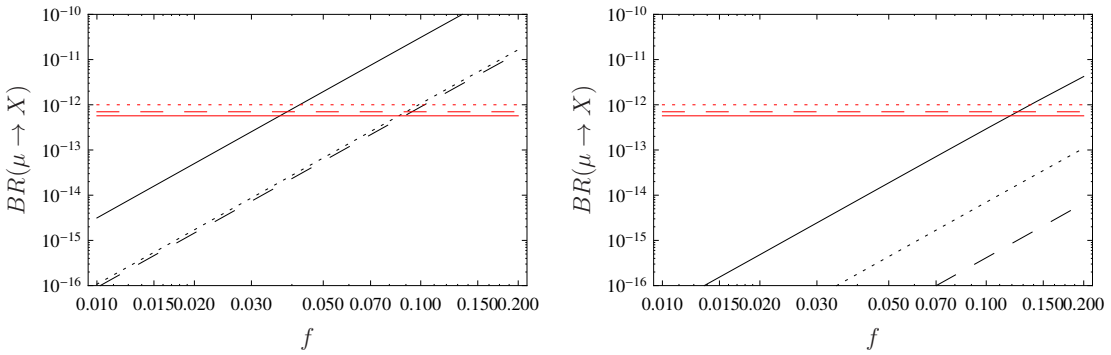

Figure 5.10: Flavour violating observables in the $U(1)_R \times U(1)_{B-L}$ model as a function of f as defined in eq. (5.18): $\mathrm{BR}(\mu \to e\,\gamma)$ (solid line), $\mathrm{BR}(\mu \to 3\,e)$ (dotted line) and $\mathrm{CR}(\mu \to e)$ in Au (dashed line) for the points BLRI (left) and BLRIII (right) defined in section 4.7, table 4.3 and using Y_ν to explain the neutrino data. The upper bounds ($\mathrm{BR}(\mu \to e\,\gamma) < 5.7 \cdot 10^{-13}$ [178]), $\mathrm{BR}(\mu \to 3\,e) < 1.0 \cdot 10^{-12}$ [217], $\mathrm{CR}(\mu - e) < 7.0 \cdot 10^{-13}$ [187]) are shown as a red horizontal line, respectively.

$$a = \left(\frac{\Delta m^2_\odot}{\Delta m^2_{\mathrm{Atm}}}\right)^{\frac{1}{4}} \approx 0.4\,, \tag{5.18}$$

where we assumed that the complete flavour structure of the neutrino sector is inherent in the neutrino Yukawa coupling Y_ν while Y_S and μ_S are diagonal. This parameterisation holds for a massless lightest neutrino eigenstate. The results for the lepton flavour violating rates of $\mu \to e\,\gamma$, $\mu \to 3\,e$ as well as the conversion rate of $\mu \to 3$ in gold nuclei are shown in figure 5.10 as a function of the scaling factor f within two benchmark scenarios as defined in table 4.3. Clearly, as is also the case for the inverse seesaw with elsewise MSSM particle content, the radiative $\mu \to e\gamma$ decay is the currently most constraining observable. The other processes, at most competing with each other in magnitude, are seen to be more than an order of magnitude smaller. This is in gross disagreement with the results for the exact same setup shown in ref. [168] where the conversion rate in nuclei was reported to be not only the most constraining process, but even around two orders of magnitude more pronounced than $\mu \to e\gamma$.

CHAPTER 6

SUMMARY

We studied the phenomenology of non-minimal supersymmetric models with or inspired by a left-right symmetric gauge group $SU(3)_c \times SU(2)_L \times SU(2)_R \times U(1)_{B-L}$. In the scenario which is most relevant for LHC physics, this gauge group gets broken at the TeV scale. Assuming the most economic version with $SU(2)_R$ triplets that break left-right symmetry by their vev, one is faced with the problem that a doubly-charged scalar gets tachyonic at the tree-level. Improving the approaches of previous studies which partially calculated its one-loop mass, we proposed an iterative method to calculate $m_{H^{\pm\pm}}$ which includes the full one-loop corrections. We demonstrated that our approach can reproduce the partial results from the literature and made clear that the full corrections are needed in order to get a realistic and reliable prediction. As a charged tachyonic particle goes hand in hand with a vacuum that breaks electromagnetic $U(1)_{em}$ invariance, we further performed a study of the vacuum stability at the one-loop order using the one-loop effective potential method. We found that low triplet vevs are favoured by vacuum stability arguments so that the current LHC run will be able to push this model close to exclusion in the case of absence of signals. So far, searches from the 8 TeV run of the LHC were able to constrain the mass of the predicted W' to $M_{W'} \gtrsim 2$ TeV. Particularly the lower edge of this bound is currently of interest because of excesses measured in the diboson and dilepton plus dijet channels. We demonstrated how in particular the latter measurement of $eejj$ events can be explained by the model under consideration. A confirmation of the excess would favour light supersymmetric states – especially charginos at a few hundred GeV – making the scenario very predictive.

We then turned to a related model where not the complete $SU(2)_R$ group but only the subgroup $U(1)_R$ survives down to the TeV scale. In this case, there is no TeV-scale W' but only a Z' to be expected. We implemented a minimal GMSB mechanism using messenger fields transforming as a **10** under $SO(10)$ while paying attention to the possible gauge kinetic mixing when deriving the boundary conditions for the SUSY-breaking parameters at the messenger scale. The tree-level Higgs mass can reach values up to $\sim$100 GeV in this model due to the presence of extra D-terms from the extended gauge sector. As a consequence, the stop masses can be as low as 2 TeV despite the smallness of the trilinear couplings, which are only generated by the RGE running from the messenger scale

downwards. This has to be seen opposed to the lower stop mass bound of 5 TeV in the MSSM context with minimal GMSB. Because of the weakly-coupled gravitino LSP, the next-to lightest SUSY particle is usually long-lived. While GMSB scenarios with MSSM particle content only feature either a neutralino or a stau NLSP, this model adds the possibility of a right sneutrino as NLSP. We investigated the different cases and specified the respective expectable cascade decays at a hadron collider. Finally we evaluated the lower bounds on the Z' and pointed out possibly interesting Z' decays.

In the last part of this thesis we moved away from LHC physics and studied lepton flavour violating low-energy observables. Those processes are enhanced in low-scale seesaw mechanisms with respect to high-scale scenarios because of the comparatively light right-handed neutrinos in the former case. Apart from the radiative decay $\ell_\alpha \to \ell_\beta \gamma$ we also considered the three-body decays $\ell_\alpha \to \ell_\beta \ell_\gamma \ell_\delta$ as well as $\mu - e$ conversion in nuclei, applying the supersymmetric inverse seesaw mechanism with CMSSM boundary conditions. We found that the non-supersymmetric Z-penguin and box contributions dominate over the supersymmetric ones in the latter two types of observables if $M_R \lesssim M_{SUSY}$, whereas negative interference between the respective diagrams can reduce the total rate by several orders of magnitude. As regards the radiative decays, the SUSY contributions dominate over the non-SUSY ones for $M_R \gtrsim M_{SUSY}/2$. Up to now, $\mu \to e\,\gamma$ gives the tightest constraints on this type of models. Comparing the prospects for future experiments, one finds that the three-body decay $\mu \to 3\,e$ will be most relevant in the medium term, whereas in the long run the $\mu - e$ conversion experiments will be able to set the tightest constraints. Finally, we considered cLFV τ decays and could demonstrate how the measurement of two different branching ratios like $\mathrm{BR}(\tau \to 3\,\mu)$ and $\mathrm{BR}(\tau \to \mu\, e^+ e^-)$ can give insight into the physics at work. This is because their relative size is sensitive to the types of diagrams that dominate; in particular, it is different in the case in which the $\nu - W$ box gives the dominant contribution as compared to the one in which the SUSY γ penguin dominates. It is further noteworthy that the increase of the respective scales M_R and M_{SUSY} results in the expected decoupling behaviour of the contributions of every type of diagram. This disproves previous claims of a non-decoupling behaviour of Z-penguins. Correspondingly, we also corrected the associated aspect in own published results from the study of the $U(1)_R \times U(1)_{B-L}$ model.

Appendices

APPENDIX A

MASS MATRICES IN LEFT-RIGHT SUPERSYMMETRY

A.1 Tree-level mass matrices and tadpole equations

Here we present the relevant tree-level mass matrices of the full model without approximations. In contrast to above, we include the other possible neutral and R-parity conserving vevs $\langle \Delta_{1L,2L} \rangle = v_{1L,2L}$ and $\langle H'^0_{1,2} \rangle = v'_{1,2}$. Moreover, we include the $SU(2)_L$ and $SU(2)_R$ Higgs fields which correspond to each other in the same multiplets even though in some cases the mass matrices turn out to be reducible, as is the case for the doubly-charged Higgses and their superpartners.

A.1.1 Tadpole equations

We split the neutral scalar fields into their CP-even and CP-odd parts as well as the vevs as follows:

$$S = \frac{1}{\sqrt{2}} v_S + \frac{1}{\sqrt{2}} \phi_S + i \frac{1}{\sqrt{2}} \sigma_S \,, \tag{A.1}$$

$$H_1^0 = \frac{1}{\sqrt{2}} v_d + \frac{1}{\sqrt{2}} \phi_{H_1^0} + i \frac{1}{\sqrt{2}} \sigma_{H_1^0} \,, \qquad H_2^0 = \frac{1}{\sqrt{2}} v_u + \frac{1}{\sqrt{2}} \phi_{H_2^0} + i \frac{1}{\sqrt{2}} \sigma_{H_2^0} \,, \tag{A.2}$$

$$\Delta_{1R}^0 = \frac{1}{\sqrt{2}} v_{1R} + \frac{1}{\sqrt{2}} \phi_{R_1^0} + i \frac{1}{\sqrt{2}} \sigma_{R_1^0} \,, \qquad \Delta_{2R}^0 = \frac{1}{\sqrt{2}} v_{2R} + \frac{1}{\sqrt{2}} \phi_{R_2^0} + i \frac{1}{\sqrt{2}} \sigma_{R_2^0} \,, \tag{A.3}$$

$$H_1'^0 = \frac{1}{\sqrt{2}} v'_1 + \frac{1}{\sqrt{2}} \phi_{H_1'^0} + i \frac{1}{\sqrt{2}} \sigma_{H_1'^0} \,, \qquad H_2'^0 = \frac{1}{\sqrt{2}} v'_2 + \frac{1}{\sqrt{2}} \phi_{H_2'^0} + i \frac{1}{\sqrt{2}} \sigma_{H_2'^0} \,, \tag{A.4}$$

$$\Delta_{1L}^0 = \frac{1}{\sqrt{2}} v_{1L} + \frac{1}{\sqrt{2}} \phi_{L_1^0} + i \frac{1}{\sqrt{2}} \sigma_{L_1^0} \,, \qquad \Delta_{2L}^0 = \frac{1}{\sqrt{2}} v_{2L} + \frac{1}{\sqrt{2}} \phi_{L_2^0} + i \frac{1}{\sqrt{2}} \sigma_{L_2^0} \,, \tag{A.5}$$

$$\tilde{\nu}_L = \frac{1}{\sqrt{2}} \phi_{\tilde{\nu}_L} + i \frac{1}{\sqrt{2}} \sigma_{\tilde{\nu}_L} \,, \qquad \tilde{\nu}_R^c = \frac{1}{\sqrt{2}} \phi_{\tilde{\nu}_R} + i \frac{1}{\sqrt{2}} \sigma_{\tilde{\nu}_R} \,. \tag{A.6}$$

With the soft SUSY-breaking mass terms $m_S^2,\ m_{\phi_{1,2}}^2,\ m_{\phi_1\phi_2}^2,\ m_{\Delta_{1R,2R,1L,2L}}$ the tadpole equations then read

$$\begin{aligned}
\frac{\partial V}{\partial \phi_S} &= \frac{1}{2}\Big(\Big(2\Big(\lambda_L\lambda_S v_{1L}v_{2L} + m_S^2\Big) + \lambda_L^2\Big(v_{1L}^2 + v_{2L}^2\Big) - 2\lambda_{12}\lambda_S\Big(v_1' v_2' + v_d v_u\Big) \\
&\quad + \lambda_{12}^2\Big(v_d^2 + {v_1'}^2 + v_u^2 + {v_2'}^2\Big) + \lambda_R\Big(2\lambda_S v_{1R}v_{2R} + \lambda_R\Big(v_{1R}^2 + v_{2R}^2\Big)\Big)\Big)v_S + 2\lambda_S^2 v_S^3 \\
&\quad + \sqrt{2}\Big(v_{1L}v_{2L}T_{\lambda_L} + v_{1R}v_{2R}T_{\lambda_R} - \Big(v_1' v_2' + v_d v_u\Big)T_{\lambda_{12}} + v_S^2 T_{\lambda_S}\Big)\Big) = 0\,, \qquad \text{(A.7)} \\
\frac{\partial V}{\partial \phi_{H_1^0}} &= +\frac{1}{8}v_d\Big(g_L^2\Big(2v_{1L}^2 - 2v_{2L}^2 - {v_1'}^2 - v_u^2 + v_d^2 + {v_2'}^2\Big) \\
&\quad + g_R^2\Big(-2v_{1R}^2 + 2v_{2R}^2 - {v_1'}^2 - v_u^2 + v_d^2 + {v_2'}^2\Big)\Big) \\
&\quad + \frac{1}{2}\Big(2\Big(m_{\phi_1}^2 v_d + m_{\phi_1\phi_2}^2 v_2'\Big) + \lambda_{12}^2\Big(v_1' v_u v_2' + v_d\Big(v_u^2 + v_S^2\Big)\Big) \\
&\quad + v_u\Big(-\lambda_{12}\Big(\lambda_L v_{1L}v_{2L} + \lambda_R v_{1R}v_{2R} + \lambda_S v_S^2\Big) - \sqrt{2}v_S T_{\lambda_{12}}\Big)\Big) = 0\,, \qquad \text{(A.8)} \\
\frac{\partial V}{\partial \phi_{H_2^0}} &= +\frac{1}{8}v_u\Big(g_L^2\Big(-2v_{1L}^2 + 2v_{2L}^2 - {v_2'}^2 - v_d^2 + {v_1'}^2 + v_u^2\Big) \\
&\quad + g_R^2\Big(2v_{1R}^2 - 2v_{2R}^2 - {v_2'}^2 - v_d^2 + {v_1'}^2 + v_u^2\Big)\Big) + \frac{1}{2}\Big(2\Big(m_{\phi_1\phi_2}^2 v_1' + m_{\phi_2}^2 v_u\Big) \\
&\quad + \lambda_{12}\Big(\Big(\lambda_{12}v_u - \lambda_S v_d\Big)v_S^2 + v_d\Big(\lambda_{12}\Big(v_1' v_2' + v_d v_u\Big) - \lambda_L v_{1L}v_{2L} - \lambda_R v_{1R}v_{2R}\Big)\Big) \\
&\quad - \sqrt{2}v_d v_S T_{\lambda_{12}}\Big) = 0\,, \qquad \text{(A.9)} \\
\frac{\partial V}{\partial \phi_{R_1^0}} &= +\frac{1}{4}v_{1R}\Big(2g_{BL}^2\Big(-v_{2L}^2 - v_{2R}^2 + v_{1L}^2 + v_{1R}^2\Big) \\
&\quad + g_R^2\Big(2v_{1R}^2 - 2v_{2R}^2 - {v_2'}^2 - v_d^2 + {v_1'}^2 + v_u^2\Big)\Big) \\
&\quad + \frac{1}{2}\Big(2m_{\Delta_{1R}}^2 v_{1R} + \lambda_R\Big(\Big(\lambda_R v_{1R} + \lambda_S v_{2R}\Big)v_S^2 \\
&\quad + v_{2R}\Big(-\lambda_{12}\Big(v_1' v_2' + v_d v_u\Big) + \lambda_L v_{1L}v_{2L} + \lambda_R v_{1R}v_{2R}\Big)\Big) + \sqrt{2}v_{2R}v_S T_{\lambda_R}\Big) = 0\,, \qquad \text{(A.10)} \\
\frac{\partial V}{\partial \phi_{R_2^0}} &= +\frac{1}{4}v_{2R}\Big(2g_{BL}^2\Big(-v_{1L}^2 - v_{1R}^2 + v_{2L}^2 + v_{2R}^2\Big) \\
&\quad + g_R^2\Big(-2v_{1R}^2 + 2v_{2R}^2 - {v_1'}^2 - v_u^2 + v_d^2 + {v_2'}^2\Big)\Big) \\
&\quad + \frac{1}{2}\Big(2m_{\Delta_{2R}}^2 v_{2R} + \lambda_R\Big(\Big(\lambda_R v_{2R} + \lambda_S v_{1R}\Big)v_S^2 \\
&\quad + v_{1R}\Big(-\lambda_{12}\Big(v_1' v_2' + v_d v_u\Big) + \lambda_L v_{1L}v_{2L} + \lambda_R v_{1R}v_{2R}\Big)\Big) + \sqrt{2}v_{1R}v_S T_{\lambda_R}\Big) = 0\,, \qquad \text{(A.11)} \\
\frac{\partial V}{\partial \phi_{H_1'^0}} &= +\frac{1}{8}v_1'\Big(g_L^2\Big(-2v_{1L}^2 + 2v_{2L}^2 - {v_2'}^2 - v_d^2 + {v_1'}^2 + v_u^2\Big) \\
&\quad + g_R^2\Big(2v_{1R}^2 - 2v_{2R}^2 - {v_2'}^2 - v_d^2 + {v_1'}^2 + v_u^2\Big)\Big)
\end{aligned}$$

$$
\begin{aligned}
&+\frac{1}{2}\Big(2\Big(m^2_{\phi_1}v'_1+m^2_{\phi_1\phi_2}v_u\Big)+\lambda_{12}\Big(\Big(\lambda_{12}v'_1-\lambda_S v'_2\Big)v_S^2\\
&+v'_2\Big(\lambda_{12}\Big(v'_1v'_2+v_dv_u\Big)-\lambda_L v_{1L}v_{2L}-\lambda_R v_{1R}v_{2R}\Big)\Big)-\sqrt{2}v'_2v_ST_{\lambda_{12}}\Big)=0\,, \qquad \text{(A.12)}\\
\frac{\partial V}{\partial\phi_{H_2'^0}}&=+\frac{1}{8}v'_2\Big(g_L^2\Big(2v_{1L}^2-2v_{2L}^2-{v'_1}^2-v_u^2+v_d^2+{v'_2}^2\Big)\\
&+g_R^2\Big(-2v_{1R}^2+2v_{2R}^2-{v'_1}^2-v_u^2+v_d^2+{v'_2}^2\Big)\Big)\\
&+\frac{1}{2}\Big(2\Big(m^2_{\phi_1\phi_2}v_d+m^2_{\phi_2}v'_2\Big)+\lambda_{12}^2\Big(v'_2\Big({v'_1}^2+v_S^2\Big)+v_dv'_1v_u\Big)\\
&+v'_1\Big(-\lambda_{12}\Big(\lambda_Lv_{1L}v_{2L}+\lambda_Rv_{1R}v_{2R}+\lambda_Sv_S^2\Big)-\sqrt{2}v_ST_{\lambda_{12}}\Big)\Big)=0\,, \qquad \text{(A.13)}\\
\frac{\partial V}{\partial\phi_{L_1^0}}&=+\frac{1}{4}v_{1L}\Big(2g_{BL}^2\Big(-v_{2L}^2-v_{2R}^2+v_{1L}^2+v_{1R}^2\Big)\\
&+g_L^2\Big(2v_{1L}^2-2v_{2L}^2-{v'_1}^2-v_u^2+v_d^2+{v'_2}^2\Big)\Big)\\
&+\frac{1}{2}\Big(2m^2_{\Delta_{1L}}v_{1L}+\lambda_L\Big(\Big(\lambda_Lv_{1L}+\lambda_Sv_{2L}\Big)v_S^2\\
&+v_{2L}\Big(-\lambda_{12}\Big(v'_1v'_2+v_dv_u\Big)+\lambda_Lv_{1L}v_{2L}+\lambda_Rv_{1R}v_{2R}\Big)\Big)+\sqrt{2}v_{2L}v_ST_{\lambda_L}\Big)=0\,, \qquad \text{(A.14)}\\
\frac{\partial V}{\partial\phi_{L_2^0}}&=+\frac{1}{4}v_{2L}\Big(2g_{BL}^2\Big(-v_{1L}^2-v_{1R}^2+v_{2L}^2+v_{2R}^2\Big)\\
&+g_L^2\Big(-2v_{1L}^2+2v_{2L}^2-{v'_2}^2-v_d^2+{v'_1}^2+v_u^2\Big)\Big)\\
&+\frac{1}{2}\Big(2m^2_{\Delta_{2L}}v_{2L}+\lambda_L\Big(\Big(\lambda_Lv_{2L}+\lambda_Sv_{1L}\Big)v_S^2\\
&+v_{1L}\Big(-\lambda_{12}\Big(v'_1v'_2+v_dv_u\Big)+\lambda_Lv_{1L}v_{2L}+\lambda_Rv_{1R}v_{2R}\Big)\Big)+\sqrt{2}v_{1L}v_ST_{\lambda_L}\Big)=0\,, \qquad \text{(A.15)}\\
\frac{\partial V}{\partial\phi_{\tilde{\nu}_{L}i}}&=0\,, \qquad \text{(A.16)}\\
\frac{\partial V}{\partial\phi_{\tilde{\nu}_{R}i}}&=0\,. \qquad \text{(A.17)}
\end{aligned}
$$

In our setup we chose to solve these equations for the soft SUSY-breaking parameters $\{m_S^2,\ m_{\phi_1^2},\ m^2_{\phi_2},\ m_{\Delta_{1R}^2},\ m^2_{\Delta_{2R}},\ m^2_{\phi_1\phi_2},\ T_{\lambda_{12}},\ m^2_{\Delta_{1L}},\ m^2_{\Delta_{2L}}\}$.

A.1.2 Mass matrices and rotations for the gauge bosons

Mass matrix for the neutral gauge bosons ($\gamma,\ Z,\ Z'$)

in the basis: $(B, W_{L,3}, W_{R,3})$

$$
m_{V^0}=\begin{pmatrix} g_{BL}^2(v_L^2+v_R^2) & -g_{BL}g_Lv_L^2 & -g_{BL}g_Rv_R^2\\ -g_{BL}g_Lv_L^2 & \frac{1}{4}g_L^2(v^2+v'^2+4v_L^2) & -\frac{1}{4}g_Lg_R(v^2+v'^2)\\ -g_{BL}g_Rv_R^2 & -\frac{1}{4}g_Lg_R(v^2+v'^2) & \frac{1}{4}g_R^2(v^2+v'^2+4v_R^2)\end{pmatrix}\,, \qquad \text{(A.18)}
$$

using $v^2 = v_u^2 + v_d^2,\ v'^2 = v_1'^2 + v_2'^2,\ v_L^2 = v_{1L}^2 + v_{2L}^2,\ v_R^2 = v_{1R}^2 + v_{2R}^2$, and Z^Z rotates into the mass eigenbasis:

$$\begin{pmatrix} B^\mu \\ W_{L,3}^\mu \\ W_{R,3}^\mu \end{pmatrix} = Z^Z \begin{pmatrix} \gamma^\mu \\ Z^\mu \\ Z'^\mu \end{pmatrix}, \tag{A.19}$$

where in the limit $v_R \gg v \gg v_L$, Z^Z can be parametrized by two angles Θ_W, Θ'_W only:

$$Z^Z = \begin{pmatrix} \cos\Theta_W \cos\Theta'_W & -\cos\Theta'_W \sin\Theta_W & -\sin\Theta'_W \\ \sin\Theta_W & \cos\Theta_W & 0 \\ \cos\Theta_W \sin\Theta'_W & -\sin\Theta_W \sin\Theta'_W & \cos\Theta'_W \end{pmatrix}. \tag{A.20}$$

Mass matrix for the charged gauge bosons ($W^\pm,\ W'^\pm$)

in the basis: (W_L^-, W_R^-)

$$m_{V^\pm} = \begin{pmatrix} \frac{1}{4}g_L^2(v^2 + v'^2 + 2v_L^2) & -\frac{1}{2}g_L g_R(v_1 v_1' + v_2 v_2') \\ -\frac{1}{2}g_L g_R(v_1 v_1' + v_2 v_2') & \frac{1}{4}g_R^2(v^2 + v'^2 + 2v_R^2) \end{pmatrix}. \tag{A.21}$$

This matrix is diagonalized by Z^W which we parametrize by one real angle

$$\begin{pmatrix} W_L^{-,\mu} \\ W_R^{-,\mu} \end{pmatrix} = \begin{pmatrix} \cos\phi_W & -\sin\phi_W \\ \sin\phi_W & \cos\phi_W \end{pmatrix} \begin{pmatrix} W^{-,\mu} \\ W'^{-,\mu} \end{pmatrix}. \tag{A.22}$$

A.1.3 Mass matrices and rotations for the scalars

Mass matrix for down-squarks ($\tilde{d}$)

in the basis: $\left(\tilde{d}_L, \tilde{d}_R\right)$:

$$m_{\tilde{d}}^2 = \tag{A.23}$$
$$\begin{pmatrix} m_{\tilde{d}_L \tilde{d}_L^*} & \frac{-\lambda_{12} v_S}{2}(v_1' y_2^Q + v_u y_1^Q)^\dagger + \frac{1}{\sqrt{2}}(v_2' T_2^Q + v_d T_1^Q)^\dagger \\ \frac{-\lambda_{12} v_S}{2}(v_1' y_2^Q + v_u y_1^Q) + \frac{1}{\sqrt{2}}(v_2' T_2^Q + v_d T_1^Q) & m_{\tilde{d}_R \tilde{d}_R^*} \end{pmatrix},$$

where

$$\begin{aligned} m_{\tilde{d}_L \tilde{d}_L^*} &= +\frac{1}{24}\mathbf{1}\Big(2g_{BL}^2\Big(-v_{1L}^2 - v_{1R}^2 + v_{2L}^2 + v_{2R}^2\Big) + 3g_L^2\Big(-2v_{1L}^2 + 2v_{2L}^2 - v_2'^2 - v_d^2 + v_1'^2 + v_u^2\Big)\Big) \\ &\quad + \frac{1}{2}\Big(2m_{Q_L}^2 + v_2'\Big(v_2' y_2^{Q\dagger} y_2^Q + v_d\Big(y_1^{Q\dagger} y_2^Q + y_2^{Q\dagger} y_1^Q\Big)\Big) + v_d^2 y_1^{Q\dagger} y_1^Q\Big), \end{aligned} \tag{A.24}$$

$$\begin{aligned} m_{\tilde{d}_R^c \tilde{d}_R^{c,*}} &= +\frac{1}{24}\mathbf{1}\Big(2g_{BL}^2\Big(-v_{2L}^2 - v_{2R}^2 + v_{1L}^2 + v_{1R}^2\Big) + 3g_R^2\Big(2v_{1R}^2 - 2v_{2R}^2 - v_2'^2 - v_d^2 + v_1'^2 + v_u^2\Big)\Big) \\ &\quad + \frac{1}{2}\Big(2m_{Q_R}^2 + v_2'\Big(v_2' y_2^Q y_2^{Q\dagger} + v_d\Big(y_1^Q y_2^{Q\dagger} + y_2^Q y_1^{Q\dagger}\Big)\Big) + v_d^2 y_1^Q y_1^{Q\dagger}\Big). \end{aligned} \tag{A.25}$$

This matrix is diagonalized by Z^D:

$$Z^D m_{\tilde{d}}^2 Z^{D,\dagger} = m_{dia,\tilde{d}}^2. \tag{A.26}$$

Mass matrix for up-squarks ($\tilde{u}$)

in the basis: $(\tilde{u}_{L,\alpha_1}, \tilde{u}_{R,\alpha_2})$:

$$m^2_{\tilde{u}} = \tag{A.27}$$

$$\begin{pmatrix} m_{\tilde{u}_L\tilde{u}_L^*} & \frac{-\lambda_{12}v_S}{2}(v_2' y_1^Q + v_d y_2^Q)^\dagger + \frac{1}{\sqrt{2}}(v_1' T_1^Q + v_u T_2^Q)^\dagger \\ \frac{-\lambda_{12}v_S}{2}(v_2' y_1^Q + v_d y_2^Q) + \frac{1}{\sqrt{2}}(v_1' T_1^Q + v_u T_2^Q) & m_{\tilde{u}_R\tilde{u}_R^*} \end{pmatrix}, \tag{A.28}$$

where

$$\begin{aligned} m_{\tilde{u}_L\tilde{u}_L^*} &= \frac{1}{24}\mathbf{1}\Big(2g_{BL}^2\Big(-v_{1L}^2 - v_{1R}^2 + v_{2L}^2 + v_{2R}^2\Big) + 3g_L^2\Big(2v_{1L}^2 - 2v_{2L}^2 - {v_1'}^2 - v_u^2 + v_d^2 + {v_2'}^2\Big)\Big) \\ &\quad + \frac{1}{2}\Big(2m_{Q_L}^2 + {v_1'}^2 y_1^{Q\dagger} y_1^Q + v_u\Big(v_1'\Big(y_1^{Q\dagger} y_2^Q + y_2^{Q\dagger} y_1^Q\Big) + v_u y_2^{Q\dagger} y_2^Q\Big)\Big), \end{aligned} \tag{A.29}$$

$$\begin{aligned} m_{\tilde{u}_R^c\tilde{u}_R^{c,*}} &= \frac{1}{24}\mathbf{1}\Big(2g_{BL}^2\Big(-v_{2L}^2 - v_{2R}^2 + v_{1L}^2 + v_{1R}^2\Big) + 3g_R^2\Big(-2v_{1R}^2 + 2v_{2R}^2 - {v_1'}^2 - v_u^2 + v_d^2 + {v_2'}^2\Big)\Big) \\ &\quad + \frac{1}{2}\Big(2m_{Q_R}^2 + {v_1'}^2 y_1^Q y_1^{Q\dagger} + v_u\Big(v_1'\Big(y_1^Q y_2^{Q\dagger} + y_2^Q y_1^{Q\dagger}\Big) + v_u y_2^Q y_2^{Q\dagger}\Big)\Big). \end{aligned} \tag{A.30}$$

This matrix is diagonalized by Z^U:

$$Z^U m_{\tilde{u}}^2 Z^{U,\dagger} = m_{dia,\tilde{u}}^2\,. \tag{A.31}$$

Mass matrix for charged sleptons ($\tilde{e}$)

in the basis: $(\tilde{e}_L, \tilde{e}_R)$:

$$m^2_{\tilde{e}} = \tag{A.32}$$

$$\begin{pmatrix} m_{\tilde{e}_L\tilde{e}_L^*} & \frac{-\lambda_{12}v_S}{2}(v_1' y_2^L + v_u y_1^L)^\dagger + \frac{1}{\sqrt{2}}(v_2' T_2^L + v_d T_1^L)^\dagger \\ \frac{-\lambda_{12}v_S}{2}(v_1' y_2^L + v_u y_1^L) + \frac{1}{\sqrt{2}}(v_2' T_2^L + v_d T_1^L) & m_{\tilde{e}_R^c\tilde{e}_R^{c,*}} \end{pmatrix},$$

where

$$\begin{aligned} m_{\tilde{e}_L\tilde{e}_L^*} &= +\frac{1}{8}\mathbf{1}\Big(2g_{BL}^2\Big(-v_{2L}^2 - v_{2R}^2 + v_{1L}^2 + v_{1R}^2\Big) + g_L^2\Big(-2v_{1L}^2 + 2v_{2L}^2 - {v_2'}^2 - v_d^2 + {v_1'}^2 + v_u^2\Big)\Big) \\ &\quad + \frac{1}{2}\Big(2m_{L_L}^2 + v_2'\Big(v_2' y_2^{L\dagger} y_2^L + v_d\Big(y_1^{L\dagger} y_2^L + y_2^{L\dagger} y_1^L\Big)\Big) + v_d^2 y_1^{L\dagger} y_1^L\Big), \end{aligned} \tag{A.33}$$

$$\begin{aligned} m_{\tilde{e}_R^c\tilde{e}_R^{c,*}} &= +\frac{1}{8}\mathbf{1}\Big(2g_{BL}^2\Big(-v_{1L}^2 - v_{1R}^2 + v_{2L}^2 + v_{2R}^2\Big) + g_R^2\Big(2v_{1R}^2 - 2v_{2R}^2 - {v_2'}^2 - v_d^2 + {v_1'}^2 + v_u^2\Big)\Big) \\ &\quad + \frac{1}{2}\Big(2m_{L_R}^2 + v_2'\Big(v_2' y_2^L y_2^{L\dagger} + v_d\Big(y_1^L y_2^{L\dagger} + y_2^L y_1^{L\dagger}\Big)\Big) + v_d^2 y_1^L y_1^{L\dagger}\Big). \end{aligned} \tag{A.34}$$

This matrix is diagonalized by Z^E:

$$Z^E m_{\tilde{e}}^2 Z^{E,\dagger} = m_{dia,\tilde{e}}^2\,. \tag{A.35}$$

Mass matrix for the CP-even sneutrinos ($\tilde{\nu}^S$)

in the basis: $(\phi_{\tilde{\nu}_L}, \phi_{\tilde{\nu}_R})\,, (\phi_{\tilde{\nu}_L}, \phi_{\tilde{\nu}_R})$:

$$m^2_{\tilde{\nu}^S} = \begin{pmatrix} m_{\phi_{\tilde{\nu}_L}\phi_{\tilde{\nu}_L}} & m^T_{\phi_{\tilde{\nu}_R}\phi_{\tilde{\nu}_L}} \\ m_{\phi_{\tilde{\nu}_L}\phi_{\tilde{\nu}_R}} & m_{\phi_{\tilde{\nu}_R}\phi_{\tilde{\nu}_R}} \end{pmatrix}, \tag{A.36}$$

where

$$\begin{aligned} m_{\phi_{\tilde{\nu}_L}\phi_{\tilde{\nu}_L}} &= \frac{1}{8}\mathbf{1}\Big(2g_{BL}^2\Big(-v_{2L}^2 - v_{2R}^2 + v_{1L}^2 + v_{1R}^2\Big) \\ &+ g_L^2\Big(2v_{1L}^2 - 2v_{2L}^2 - {v_1'}^2 - v_u^2 + v_d^2 + {v_2'}^2\Big)\Big) \\ &+ \frac{1}{4}\Big(4m_{L_L}^2 + 4\lambda_L v_{1L} v_S \Re\Big(y_3^L\Big) + 8v_{2L}^2\Re\Big(y_3^L y_3^{L*}\Big) + 2{v_1'}^2\Re\Big(y_1^{L,T} y_1^{L*}\Big) \\ &+ v_1' v_u\Big(2\Re\Big(y_1^{L,T} y_2^{L*}\Big) + 2\Re\Big(y_2^{L,T} y_1^{L*}\Big)\Big) + 2v_u^2\Re\Big(y_2^{L,T} y_2^{L*}\Big) + 4\sqrt{2}v_{2L}\Re\Big(T_3^L\Big)\Big), \end{aligned} \tag{A.37}$$

$$\begin{aligned} m_{\phi_{\tilde{\nu}_L}\phi_{\tilde{\nu}_R}} &= \frac{1}{4}\Big(-\lambda_{12} v_S\Big(2v_2'\Re\Big(y_1^L\Big) + 2v_d\Re\Big(y_2^L\Big)\Big) \\ &+ v_1'\Big(2\sqrt{2}\Re\Big(T_1^L\Big) + 4v_{1R}\Re\Big(y_4^L y_1^{L*}\Big) + 4v_{2L}\Re\Big(y_1^L y_3^{L*}\Big)\Big) \\ &+ v_u\Big(2\sqrt{2}\Re\Big(T_2^L\Big) + 4v_{1R}\Re\Big(y_4^L y_2^{L*}\Big) + 4v_{2L}\Re\Big(y_2^L y_3^{L*}\Big)\Big)\Big), \end{aligned} \tag{A.38}$$

$$\begin{aligned} m_{\phi_{\tilde{\nu}_R}\phi_{\tilde{\nu}_R}} &= +\frac{1}{8}\mathbf{1}\Big(2g_{BL}^2\Big(-v_{1L}^2 - v_{1R}^2 + v_{2L}^2 + v_{2R}^2\Big) \\ &+ g_R^2\Big(-2v_{1R}^2 + 2v_{2R}^2 - {v_1'}^2 - v_u^2 + v_d^2 + {v_2'}^2\Big)\Big) \\ &+ \frac{1}{4}\Big(4m_{L_R}^2 + 4\lambda_R v_{2R} v_S\Re\Big(y_4^L\Big) + 2{v_1'}^2\Re\Big(y_1^L y_1^{L\dagger}\Big) \\ &+ v_1' v_u\Big(2\Re\Big(y_1^L y_2^{L\dagger}\Big) + 2\Re\Big(y_2^L y_1^{L\dagger}\Big)\Big) \\ &+ 2v_u^2\Re\Big(y_2^L y_2^{L\dagger}\Big) + 8v_{1R}^2\Re\Big(y_4^L y_4^{L*}\Big) + 4\sqrt{2}v_{1R}\Re\Big(T_4^L\Big)\Big). \end{aligned} \tag{A.39}$$

Mass matrix for the CP-odd sneutrinos ($\tilde{\nu}^P$)

in the basis: $(\sigma_{\tilde{\nu}_L}, \sigma_{\tilde{\nu}_R})$:

$$m^2_{\tilde{\nu}^P} = \begin{pmatrix} m_{\sigma_{\tilde{\nu}_L}\sigma_{\tilde{\nu}_L}} & m^T_{\sigma_{\tilde{\nu}_R}\sigma_{\tilde{\nu}_L}} \\ m_{\sigma_{\tilde{\nu}_L}\sigma_{\tilde{\nu}_R}} & m_{\sigma_{\tilde{\nu}_R}\sigma_{\tilde{\nu}_R}} \end{pmatrix}, \tag{A.40}$$

where

$$\begin{aligned} m_{\sigma_{\tilde{\nu}_L}\sigma_{\tilde{\nu}_L}} &= +\frac{1}{8}\mathbf{1}\Big(2g_{BL}^2\Big(-v_{2L}^2 - v_{2R}^2 + v_{1L}^2 + v_{1R}^2\Big) \\ &+ g_L^2\Big(2v_{1L}^2 - 2v_{2L}^2 - {v_1'}^2 - v_u^2 + v_d^2 + {v_2'}^2\Big)\Big) \\ &+ \frac{1}{4}\Big(4m_{L_L}^2 - 4\lambda_L v_{1L} v_S\Re\Big(y_3^L\Big) + 8v_{2L}^2\Re\Big(y_3^L y_3^{L*}\Big) + 2{v_1'}^2\Re\Big(y_1^{L,T} y_1^{L*}\Big) \\ &+ v_1'\Big(2v_u\Re\Big(y_1^{L,T} y_2^{L*}\Big) + 2v_u\Re\Big(y_2^{L,T} y_1^{L*}\Big)\Big) + 2v_u^2\Re\Big(y_2^{L,T} y_2^{L*}\Big) - 4\sqrt{2}v_{2L}\Re\Big(T_3^L\Big)\Big), \end{aligned} \tag{A.41}$$

$$m_{\sigma_{\tilde{\nu}_L}\sigma_{\tilde{\nu}_R}} = \frac{1}{4}\Big(-\lambda_{12} v_S\Big(2v_2'\Re\Big(y_1^L\Big)$$

$$
\begin{aligned}
&+ 2v_d\Re\Big(y_2^L\Big)\Big) + v_1'\Big(2\sqrt{2}\Re\Big(T_1^L\Big) - 4v_{1R}\Re\Big(y_4^L y_1^{L*}\Big) - 4v_{2L}\Re\Big(y_1^L y_3^{L*}\Big)\Big)\\
&+ v_u\Big(2\sqrt{2}\Re\Big(T_2^L\Big) - 4v_{1R}\Re\Big(y_4^L y_2^{L*}\Big) - 4v_{2L}\Re\Big(y_2^L y_3^{L*}\Big)\Big)\Big)\,, \qquad \text{(A.42)}\\
m_{\sigma_{\tilde{\nu}_R}\sigma_{\tilde{\nu}_R}} &= +\frac{1}{8}\mathbf{1}\Big(2g_{BL}^2\Big(- v_{1L}^2 - v_{1R}^2 + v_{2L}^2 + v_{2R}^2\Big)\\
&+ g_R^2\Big(- 2v_{1R}^2 + 2v_{2R}^2 - {v_1'}^2 - v_u^2 + v_d^2 + {v_2'}^2\Big)\Big)\\
&+ \frac{1}{4}\Big(4m_{L_R}^2 - 4\lambda_R v_{2R} v_S\Re\Big(y_4^L\Big) + 2{v_1'}^2\Re\Big(y_1^L y_1^{L\dagger}\Big)\\
&+ v_1'\Big(2v_u\Re\Big(y_1^L y_2^{L\dagger}\Big) + 2v_u\Re\Big(y_2^L y_1^{L\dagger}\Big)\Big)\\
&+ 2v_u^2\Re\Big(y_2^L y_2^{L\dagger}\Big) + 8v_{1R}^2\Re\Big(y_4^L y_4^{L*}\Big) - 4\sqrt{2}v_{1R}\Re\Big(T_4^L\Big)\Big)\,. \qquad \text{(A.43)}
\end{aligned}
$$

In the limit applied in our study, i.e. $v'_{1,2}, v_{1L,2L} \to 0$, and additionally neglecting the Dirac-type Yukawa couplings $y^L_{1,2}$ and the corresponding trilinear couplings $T^L_{1,2}$, the matrix reduces to

$$
\begin{aligned}
m_{\phi_{\tilde{\nu}_L}\phi_{\tilde{\nu}_L}} &= m_{L_L}^2 + \mathbf{1}\frac{1}{8}\Big(2g_{BL}^2\Big(v_{1R}^2 - v_{2R}^2\Big) + g_L^2\Big(v_d^2 - v_u^2\Big)\Big)\,,\\
m_{\phi_{\tilde{\nu}_L}\phi_{\tilde{\nu}_R}} &= 0\,,\\
m_{\phi_{\tilde{\nu}_R}\phi_{\tilde{\nu}_R}} &= m_{L_R}^2 + 2v_{1R}^2\Re\Big(y_4^L y_4^{L*}\Big) + \mathbf{1}\frac{1}{8}\Big(2(g_{BL}^2 + g_R^2)\Big(v_{2R}^2 - v_{1R}^2\Big) + g_R^2\Big(v_d^2 - v_u^2\Big)\Big)\\
&\quad + \Big(\lambda_R v_{2R} v_S\Re\Big(y_4^L\Big) + \sqrt{2}v_{1R}\Re\Big(T_4^L\Big)\Big)\,. \qquad \text{(A.44)}
\end{aligned}
$$

and

$$
\begin{aligned}
m_{\sigma_{\tilde{\nu}_L}\sigma_{\tilde{\nu}_L}} &= m_{L_L}^2 + \mathbf{1}\frac{1}{8}\Big(2g_{BL}^2\Big(v_{1R}^2 - v_{2R}^2\Big) + g_L^2\Big(v_d^2 - v_u^2\Big)\Big)\,,\\
m_{\sigma_{\tilde{\nu}_L}\sigma_{\tilde{\nu}_R}} &= 0\,,\\
m_{\sigma_{\tilde{\nu}_R}\sigma_{\tilde{\nu}_R}} &= m_{L_R}^2 + 2v_{1R}^2\Re\Big(y_4^L y_4^{L*}\Big) + \mathbf{1}\frac{1}{8}\Big(2(g_{BL}^2 + g_R^2)\Big(v_{2R}^2 - v_{1R}^2\Big) + g_R^2\Big(v_d^2 - v_u^2\Big)\Big)\\
&\quad - \Big(\lambda_R v_{2R} v_S\Re\Big(y_4^L\Big) + \sqrt{2}v_{1R}\Re\Big(T_4^L\Big)\Big)\,. \qquad \text{(A.45)}
\end{aligned}
$$

Mass matrix for the doubly charged Higgs fields ($H^{\pm\pm}$)

in the basis:
$\Big(\Delta_{1R}^{--}, \Delta_{2R}^{++,*}, \Delta_{2L}^{--}, \Delta_{2L}^{++,*}\Big), \Big(\Delta_{1R}^{--,*}, \Delta_{2R}^{++}, \Delta_{2L}^{--,*}, \Delta_{2L}^{++}\Big)$:

$$
m_{H^{--}}^2 = \begin{pmatrix}
D_{--}^R - \frac{v_{2R}}{v_{1R}}F_{--}^R & F_{--}^R & 0 & 0\\
F_{--}^R & -D_{--}^R - \frac{v_{1R}}{v_{2R}}F_{--}^R & 0 & 0\\
0 & 0 & D_{--}^L - \frac{v_{2L}}{v_{1L}}F_{--}^L & F_{--}^L\\
0 & 0 & F_{--}^L & -D_{--}^L - \frac{v_{1L}}{v_{2L}}F_{--}^L
\end{pmatrix}, \qquad \text{(A.46)}
$$

where

$$D^R_{--} = \frac{g_R^2}{2}\left(v_d^2 + v_2'^2 - v_u^2 - v_1'^2 + 2(v_{2R}^2 - v_{1R}^2)\right)\,, \tag{A.47}$$

$$F^R_{--} = \frac{\lambda_R^2}{2}v_{1R}v_{2R} + \frac{\lambda_L\lambda_R}{2}v_{1L}v_{2L} + \frac{\lambda_R\lambda_S}{2}v_S^2 - \frac{\lambda_R\lambda_{12}}{2}(v_1'v_2' + v_uv_d) + \frac{T_{\lambda_R}}{\sqrt{2}}v_S\,, \tag{A.48}$$

$$D^L_{--} = \frac{g_L^2}{2}\left(v_u^2 + v_1'^2 - v_d^2 - v_2'^2 + 2(v_{2L}^2 - v_{1L}^2)\right)\,, \tag{A.49}$$

$$F^L_{--} = \frac{\lambda_L^2}{2}v_{1L}v_{2L} + \frac{\lambda_L\lambda_R}{2}v_{1R}v_{2R} + \frac{\lambda_L\lambda_S}{2}v_S^2 - \frac{\lambda_L\lambda_{12}}{2}(v_1'v_2' + v_uv_d) + \frac{T_{\lambda_L}}{\sqrt{2}}v_S\,. \tag{A.50}$$

Mass matrix for the Higgs bosons (h)

in the basis: $X = \left(\phi_{H_1^0}, \phi_{H_2^0}, \phi_{H_1'^0}, \phi_{H_2'^0}, \phi_{R_1^0}, \phi_{R_2^0}, \phi_S, \phi_{L_1^0}, \phi_{L_2^0}\right)$:
For reasons of brevity we show the mass matrix without having inserted the solutions to the tadpole equations. Because of the complexity of the system, the insertion of the solutions would lead to even more lengthy expressions.

We define the mass matrix as

$$(m_h^2)_{ij} = m_{X_iX_i}\,, \tag{A.51}$$

where

$$\begin{aligned} m_{\phi_{H_1^0}\phi_{H_1^0}} &= m_{\phi_1}^2 + \frac{1}{8}\Big(g_L^2\Big(2v_{1L}^2 - 2v_{2L}^2 + 3v_d^2 - v_1'^2 - v_u^2 + v_2'^2\Big) \\ &\quad + g_R^2\Big(-2v_{1R}^2 + 2v_{2R}^2 + 3v_d^2 - v_1'^2 - v_u^2 + v_2'^2\Big)\Big) + \frac{1}{2}\lambda_{12}^2\Big(v_u^2 + v_S^2\Big)\,, \end{aligned} \tag{A.52}$$

$$\begin{aligned} m_{\phi_{H_1^0}\phi_{H_2^0}} &= \frac{1}{2}\Big(\lambda_{12}\Big(\lambda_{12}\Big(2v_dv_u + v_1'v_2'\Big) - \lambda_Lv_{1L}v_{2L} - \lambda_Rv_{1R}v_{2R} - \lambda_Sv_S^2\Big) - \sqrt{2}v_ST_{\lambda_{12}}\Big) \\ &\quad - \frac{1}{4}\Big(g_L^2 + g_R^2\Big)v_dv_u\,, \end{aligned} \tag{A.53}$$

$$\begin{aligned} m_{\phi_{H_2^0}\phi_{H_2^0}} &= m_{\phi_2}^2 + \frac{1}{8}\Big(-g_L^2\Big(2v_{1L}^2 - 2v_{2L}^2 - 3v_u^2 - v_1'^2 + v_d^2 + v_2'^2\Big) \\ &\quad - g_R^2\Big(-2v_{1R}^2 + 2v_{2R}^2 - 3v_u^2 - v_1'^2 + v_d^2 + v_2'^2\Big)\Big) + \frac{1}{2}\lambda_{12}^2\Big(v_d^2 + v_S^2\Big)\,, \end{aligned} \tag{A.54}$$

$$m_{\phi_{H_1^0}\phi_{H_1'^0}} = \frac{1}{2}\lambda_{12}^2v_uv_2' - \frac{1}{4}\Big(g_L^2 + g_R^2\Big)v_dv_1'\,, \tag{A.55}$$

$$m_{\phi_{H_2^0}\phi_{H_1'^0}} = \frac{1}{2}\lambda_{12}^2v_dv_2' + \frac{1}{4}\Big(g_L^2 + g_R^2\Big)v_1'v_u + m_{\phi_1\phi_2}^2\,, \tag{A.56}$$

$$\begin{aligned} m_{\phi_{H_1'^0}\phi_{H_1'^0}} &= m_{\phi_1}^2 + \frac{1}{8}\Big(-g_L^2\Big(2v_{1L}^2 - 2v_{2L}^2 - 3v_1'^2 - v_u^2 + v_d^2 + v_2'^2\Big) \\ &\quad - g_R^2\Big(-2v_{1R}^2 + 2v_{2R}^2 - 3v_1'^2 - v_u^2 + v_d^2 + v_2'^2\Big)\Big) + \frac{1}{2}\lambda_{12}^2\Big(v_2'^2 + v_S^2\Big)\,, \end{aligned} \tag{A.57}$$

$$m_{\phi_{H_1^0}\phi_{H_2'^0}} = \frac{1}{2}\lambda_{12}^2v_1'v_u + \frac{1}{4}\Big(g_L^2 + g_R^2\Big)v_dv_2' + m_{\phi_1\phi_2}^2\,, \tag{A.58}$$

$$m_{\phi_{H_2^0}\phi_{H_2'^0}} = \frac{1}{2}\lambda_{12}^2v_dv_1' - \frac{1}{4}\Big(g_L^2 + g_R^2\Big)v_uv_2'\,, \tag{A.59}$$

$$\begin{aligned} m_{\phi_{H_1'^0}\phi_{H_2'^0}} &= \frac{1}{2}\Big(\lambda_{12}\Big(\lambda_{12}\Big(2v_1'v_2' + v_dv_u\Big) - \lambda_Lv_{1L}v_{2L} - \lambda_Rv_{1R}v_{2R} - \lambda_Sv_S^2\Big) - \sqrt{2}v_ST_{\lambda_{12}}\Big) \\ &\quad - \frac{1}{4}\Big(g_L^2 + g_R^2\Big)v_1'v_2'\,, \end{aligned} \tag{A.60}$$

$$m_{\phi_{H_2'^0}\phi_{H_2'^0}} = m_{\phi_2}^2 + \frac{1}{8}\Big(g_L^2\Big(2v_{1L}^2 - 2v_{2L}^2 + 3{v_2'}^2 - {v_1'}^2 - v_u^2 + v_d^2\Big) + g_R^2\Big(-2v_{1R}^2 + 2v_{2R}^2 + 3{v_2'}^2 - {v_1'}^2 - v_u^2 + v_d^2\Big)\Big) + \frac{1}{2}\lambda_{12}^2\Big({v_1'}^2 + v_S^2\Big), \tag{A.61}$$

$$m_{\phi_{H_1^0}\phi_{R_1^0}} = -\frac{1}{2}g_R^2 v_d v_{1R} - \frac{1}{2}\lambda_{12}\lambda_R v_u v_{2R}, \tag{A.62}$$

$$m_{\phi_{H_2^0}\phi_{R_1^0}} = \frac{1}{2}g_R^2 v_{1R} v_u - \frac{1}{2}\lambda_{12}\lambda_R v_d v_{2R}, \tag{A.63}$$

$$m_{\phi_{H_1'^0}\phi_{R_1^0}} = \frac{1}{2}g_R^2 v_1' v_{1R} - \frac{1}{2}\lambda_{12}\lambda_R v_2' v_{2R}, \tag{A.64}$$

$$m_{\phi_{H_2'^0}\phi_{R_1^0}} = -\frac{1}{2}g_R^2 v_{1R} v_2' - \frac{1}{2}\lambda_{12}\lambda_R v_1' v_{2R}, \tag{A.65}$$

$$m_{\phi_{R_1^0}\phi_{R_1^0}} = m_{\Delta_{1R}}^2 + \frac{1}{4}\Big(2g_{BL}^2\Big(3v_{1R}^2 - v_{2L}^2 - v_{2R}^2 + v_{1L}^2\Big) + g_R^2\Big(-2v_{2R}^2 + 6v_{1R}^2 - {v_2'}^2 - v_d^2 + {v_1'}^2 + v_u^2\Big)\Big) + \frac{1}{2}\lambda_R^2\Big(v_{2R}^2 + v_S^2\Big), \tag{A.66}$$

$$m_{\phi_{H_1^0}\phi_{R_2^0}} = \frac{1}{2}g_R^2 v_d v_{2R} - \frac{1}{2}\lambda_{12}\lambda_R v_{1R} v_u, \tag{A.67}$$

$$m_{\phi_{H_2^0}\phi_{R_2^0}} = -\frac{1}{2}g_R^2 v_u v_{2R} - \frac{1}{2}\lambda_{12}\lambda_R v_d v_{1R}, \tag{A.68}$$

$$m_{\phi_{H_1'^0}\phi_{R_2^0}} = -\frac{1}{2}g_R^2 v_1' v_{2R} - \frac{1}{2}\lambda_{12}\lambda_R v_{1R} v_2', \tag{A.69}$$

$$m_{\phi_{H_2'^0}\phi_{R_2^0}} = \frac{1}{2}g_R^2 v_2' v_{2R} - \frac{1}{2}\lambda_{12}\lambda_R v_1' v_{1R}, \tag{A.70}$$

$$m_{\phi_{R_1^0}\phi_{R_2^0}} = \frac{1}{2}\Big(\lambda_R\Big(2\lambda_R v_{1R} v_{2R} - \lambda_{12}\Big(v_1' v_2' + v_d v_u\Big) + \lambda_L v_{1L} v_{2L} + \lambda_S v_S^2\Big) + \sqrt{2}v_S T_{\lambda_R}\Big) - \Big(g_{BL}^2 + g_R^2\Big)v_{1R} v_{2R}, \tag{A.71}$$

$$m_{\phi_{R_2^0}\phi_{R_2^0}} = m_{\Delta_{2R}}^2 + \frac{1}{4}\Big(-2g_{BL}^2\Big(-3v_{2R}^2 - v_{2L}^2 + v_{1L}^2 + v_{1R}^2\Big) + g_R^2\Big(-2v_{1R}^2 + 6v_{2R}^2 - {v_1'}^2 - v_u^2 + v_d^2 + {v_2'}^2\Big)\Big) + \frac{1}{2}\lambda_R^2\Big(v_{1R}^2 + v_S^2\Big), \tag{A.72}$$

$$m_{\phi_{H_1^0}\phi_S} = -\frac{1}{\sqrt{2}}v_u T_{\lambda_{12}} + \lambda_{12}\Big(\lambda_{12}v_d - \lambda_S v_u\Big)v_S, \tag{A.73}$$

$$m_{\phi_{H_2^0}\phi_S} = -\frac{1}{\sqrt{2}}v_d T_{\lambda_{12}} + \lambda_{12}\Big(\lambda_{12}v_u - \lambda_S v_d\Big)v_S, \tag{A.74}$$

$$m_{\phi_{H_1'^0}\phi_S} = -\frac{1}{\sqrt{2}}v_2' T_{\lambda_{12}} + \lambda_{12}\Big(\lambda_{12}v_1' - \lambda_S v_2'\Big)v_S, \tag{A.75}$$

$$m_{\phi_{H_2'^0}\phi_S} = -\frac{1}{\sqrt{2}}v_1' T_{\lambda_{12}} + \lambda_{12}\Big(\lambda_{12}v_2' - \lambda_S v_1'\Big)v_S, \tag{A.76}$$

$$m_{\phi_{R_1^0}\phi_S} = \frac{1}{\sqrt{2}}v_{2R} T_{\lambda_R} + \lambda_R\Big(\lambda_R v_{1R} + \lambda_S v_{2R}\Big)v_S, \tag{A.77}$$

$$m_{\phi_{R_2^0}\phi_S} = \frac{1}{\sqrt{2}}v_{1R} T_{\lambda_R} + \lambda_R\Big(\lambda_R v_{2R} + \lambda_S v_{1R}\Big)v_S, \tag{A.78}$$

$$m_{\phi_S\phi_S} = m_S^2 + \frac{1}{2}\Big(\lambda_L^2\Big(v_{1L}^2 + v_{2L}^2\Big) + \lambda_{12}^2\Big(v_d^2 + {v_1'}^2 + v_u^2 + {v_2'}^2\Big) + \lambda_S\Big(-2\lambda_{12}\Big(v_1' v_2' + v_d v_u\Big) + 2\lambda_L v_{1L} v_{2L}\Big) + \lambda_R\Big(2\lambda_S v_{1R} v_{2R} + \lambda_R\Big(v_{1R}^2 + v_{2R}^2\Big)\Big) + 6\lambda_S^2 v_S^2 + 2\sqrt{2}v_S T_{\lambda_S}\Big), \tag{A.79}$$

$$m_{\phi_{H_1^0}\phi_{L_1^0}} = \frac{1}{2}g_L^2 v_d v_{1L} - \frac{1}{2}\lambda_{12}\lambda_L v_u v_{2L}, \tag{A.80}$$

$$m_{\phi_{H_2^0}\phi_{L_1^0}} = -\frac{1}{2}g_L^2 v_{1L} v_u - \frac{1}{2}\lambda_{12}\lambda_L v_d v_{2L}\,, \tag{A.81}$$

$$m_{\phi_{H_1'^0}\phi_{L_1^0}} = -\frac{1}{2}g_L^2 v_{1L} v_1' - \frac{1}{2}\lambda_{12}\lambda_L v_{2L} v_2'\,, \tag{A.82}$$

$$m_{\phi_{H_2'^0}\phi_{L_1^0}} = \frac{1}{2}g_L^2 v_{1L} v_2' - \frac{1}{2}\lambda_{12}\lambda_L v_1' v_{2L}\,, \tag{A.83}$$

$$m_{\phi_{R_1^0}\phi_{L_1^0}} = \frac{1}{2}\lambda_L\lambda_R v_{2L} v_{2R} + g_{BL}^2 v_{1L} v_{1R}\,, \tag{A.84}$$

$$m_{\phi_{R_2^0}\phi_{L_1^0}} = \frac{1}{2}\lambda_L\lambda_R v_{1R} v_{2L} - g_{BL}^2 v_{1L} v_{2R}\,, \tag{A.85}$$

$$m_{\phi_S\phi_{L_1^0}} = \frac{1}{\sqrt{2}} v_{2L} T_{\lambda_L} + \lambda_L\Big(\lambda_L v_{1L} + \lambda_S v_{2L}\Big) v_S\,, \tag{A.86}$$

$$\begin{aligned} m_{\phi_{L_1^0}\phi_{L_1^0}} &= m_{\Delta_{1L}}^2 + \frac{1}{4}\Big(2g_{BL}^2\Big(3v_{1L}^2 - v_{2L}^2 - v_{2R}^2 + v_{1R}^2\Big) \\ &\quad + g_L^2\Big(-2v_{2L}^2 + 6v_{1L}^2 - {v_1'}^2 - v_u^2 + v_d^2 + {v_2'}^2\Big)\Big) + \frac{1}{2}\lambda_L^2\Big(v_{2L}^2 + v_S^2\Big)\,, \end{aligned} \tag{A.87}$$

$$m_{\phi_{H_1^0}\phi_{L_2^0}} = -\frac{1}{2}g_L^2 v_d v_{2L} - \frac{1}{2}\lambda_{12}\lambda_L v_{1L} v_u\,, \tag{A.88}$$

$$m_{\phi_{H_2^0}\phi_{L_2^0}} = \frac{1}{2}g_L^2 v_u v_{2L} - \frac{1}{2}\lambda_{12}\lambda_L v_d v_{1L}\,, \tag{A.89}$$

$$m_{\phi_{H_1'^0}\phi_{L_2^0}} = \frac{1}{2}g_L^2 v_1' v_{2L} - \frac{1}{2}\lambda_{12}\lambda_L v_{1L} v_2'\,, \tag{A.90}$$

$$m_{\phi_{H_2'^0}\phi_{L_2^0}} = -\frac{1}{2}g_L^2 v_{2L} v_2' - \frac{1}{2}\lambda_{12}\lambda_L v_{1L} v_1'\,, \tag{A.91}$$

$$m_{\phi_{R_1^0}\phi_{L_2^0}} = \frac{1}{2}\lambda_L\lambda_R v_{1L} v_{2R} - g_{BL}^2 v_{1R} v_{2L}\,, \tag{A.92}$$

$$m_{\phi_{R_2^0}\phi_{L_2^0}} = \frac{1}{2}\lambda_L\lambda_R v_{1L} v_{1R} + g_{BL}^2 v_{2L} v_{2R}\,, \tag{A.93}$$

$$m_{\phi_S\phi_{L_2^0}} = \frac{1}{\sqrt{2}} v_{1L} T_{\lambda_L} + \lambda_L\Big(\lambda_L v_{2L} + \lambda_S v_{1L}\Big) v_S\,, \tag{A.94}$$

$$\begin{aligned} m_{\phi_{L_1^0}\phi_{L_2^0}} &= \frac{1}{2}\Big(\lambda_L\Big(2\lambda_L v_{1L} v_{2L} - \lambda_{12}\Big(v_1' v_2' + v_d v_u\Big) + \lambda_R v_{1R} v_{2R} + \lambda_S v_S^2\Big) + \sqrt{2} v_S T_{\lambda_L}\Big) \\ &\quad - \Big(g_{BL}^2 + g_L^2\Big) v_{1L} v_{2L}\,, \end{aligned} \tag{A.95}$$

$$\begin{aligned} m_{\phi_{L_2^0}\phi_{L_2^0}} &= m_{\Delta_{2L}}^2 + \frac{1}{4}\Big(-2g_{BL}^2\Big(-3v_{2L}^2 - v_{2R}^2 + v_{1L}^2 + v_{1R}^2\Big) \\ &\quad + g_L^2\Big(-2v_{1L}^2 + 6v_{2L}^2 - {v_2'}^2 - v_d^2 + {v_1'}^2 + v_u^2\Big)\Big) + \frac{1}{2}\lambda_L^2\Big(v_{1L}^2 + v_S^2\Big)\,. \end{aligned} \tag{A.96}$$

This matrix is diagonalized by Z^h:

$$Z^h m_h^2 Z^{h,\dagger} = m_{dia,h}^2\,. \tag{A.97}$$

Mass matrix for the pseudoscalar Higgs bosons (A^0)

in the basis: $X = \Big(\sigma_{H_1^0}, \sigma_{H_2^0}, \sigma_{H_1'^0}, \sigma_{H_2'^0}, \sigma_{R_1^0}, \sigma_{R_2^0}, \sigma_S, \sigma_{L_1^0}, \sigma_{L_2^0}\Big)$:

We define the mass matrix including the gauge fixing terms ξ as:

$$m_{A^0}^2 = m_{X_i X_j} + \xi_Z\, m_{X_i X_j}^{\xi,Z} + \xi_{Z'}\, m_{X_i X_j}^{\xi,Z'}\,, \tag{A.98}$$

where

$$m_{\sigma_{H_1^0}\sigma_{H_1^0}} = m_{\phi_1}^2 + \frac{1}{8}\Big(g_L^2\Big(2v_{1L}^2 - 2v_{2L}^2 - {v_1'}^2 - v_u^2 + v_d^2 + {v_2'}^2\Big) + g_R^2\Big(-2v_{1R}^2 + 2v_{2R}^2 - {v_1'}^2 - v_u^2 + v_d^2 + {v_2'}^2\Big)\Big) + \frac{1}{2}\lambda_{12}^2\Big(v_u^2 + v_S^2\Big), \tag{A.99}$$

$$m_{\sigma_{H_1^0}\sigma_{H_2^0}} = \frac{1}{2}\Big(\lambda_{12}\Big(-\lambda_{12}v_1'v_2' + \lambda_L v_{1L}v_{2L} + \lambda_R v_{1R}v_{2R} + \lambda_S v_S^2\Big) + \sqrt{2}v_S T_{\lambda_{12}}\Big), \tag{A.100}$$

$$m_{\sigma_{H_2^0}\sigma_{H_2^0}} = m_{\phi_2}^2 + \frac{1}{8}\Big(g_L^2\Big(-2v_{1L}^2 + 2v_{2L}^2 - {v_2'}^2 - v_d^2 + {v_1'}^2 + v_u^2\Big) + g_R^2\Big(2v_{1R}^2 - 2v_{2R}^2 - {v_2'}^2 - v_d^2 + {v_1'}^2 + v_u^2\Big)\Big) + \frac{1}{2}\lambda_{12}^2\Big(v_d^2 + v_S^2\Big), \tag{A.101}$$

$$m_{\sigma_{H_1^0}\sigma_{H_1'^0}} = \frac{1}{2}\lambda_{12}^2 v_u v_2', \tag{A.102}$$

$$m_{\sigma_{H_2^0}\sigma_{H_1'^0}} = \frac{1}{2}\lambda_{12}^2 v_d v_2' + m_{\phi_1\phi_2}^2, \tag{A.103}$$

$$m_{\sigma_{H_1'^0}\sigma_{H_1'^0}} = m_{\phi_1}^2 + \frac{1}{8}\Big(g_L^2\Big(-2v_{1L}^2 + 2v_{2L}^2 - {v_2'}^2 - v_d^2 + {v_1'}^2 + v_u^2\Big) + g_R^2\Big(2v_{1R}^2 - 2v_{2R}^2 - {v_2'}^2 - v_d^2 + {v_1'}^2 + v_u^2\Big)\Big) + \frac{1}{2}\lambda_{12}^2\Big({v_2'}^2 + v_S^2\Big), \tag{A.104}$$

$$m_{\sigma_{H_1^0}\sigma_{H_2'^0}} = \frac{1}{2}\lambda_{12}^2 v_1' v_u + m_{\phi_1\phi_2}^2, \tag{A.105}$$

$$m_{\sigma_{H_2^0}\sigma_{H_2'^0}} = \frac{1}{2}\lambda_{12}^2 v_d v_1', \tag{A.106}$$

$$m_{\sigma_{H_1'^0}\sigma_{H_2'^0}} = \frac{1}{2}\Big(\lambda_{12}\Big(-\lambda_{12}v_d v_u + \lambda_L v_{1L}v_{2L} + \lambda_R v_{1R}v_{2R} + \lambda_S v_S^2\Big) + \sqrt{2}v_S T_{\lambda_{12}}\Big), \tag{A.107}$$

$$m_{\sigma_{H_2'^0}\sigma_{H_2'^0}} = m_{\phi_2}^2 + \frac{1}{8}\Big(g_L^2\Big(2v_{1L}^2 - 2v_{2L}^2 - {v_1'}^2 - v_u^2 + v_d^2 + {v_2'}^2\Big) + g_R^2\Big(-2v_{1R}^2 + 2v_{2R}^2 - {v_1'}^2 - v_u^2 + v_d^2 + {v_2'}^2\Big)\Big) + \frac{1}{2}\lambda_{12}^2\Big({v_1'}^2 + v_S^2\Big), \tag{A.108}$$

$$m_{\sigma_{H_1^0}\sigma_{R_1^0}} = -\frac{1}{2}\lambda_{12}\lambda_R v_u v_{2R}, \tag{A.109}$$

$$m_{\sigma_{H_2^0}\sigma_{R_1^0}} = -\frac{1}{2}\lambda_{12}\lambda_R v_d v_{2R}, \tag{A.110}$$

$$m_{\sigma_{H_1'^0}\sigma_{R_1^0}} = -\frac{1}{2}\lambda_{12}\lambda_R v_2' v_{2R}, \tag{A.111}$$

$$m_{\sigma_{H_2'^0}\sigma_{R_1^0}} = -\frac{1}{2}\lambda_{12}\lambda_R v_1' v_{2R}, \tag{A.112}$$

$$m_{\sigma_{R_1^0}\sigma_{R_1^0}} = m_{\Delta_{1R}}^2 + \frac{1}{4}\Big(2g_{BL}^2\Big(-v_{2L}^2 - v_{2R}^2 + v_{1L}^2 + v_{1R}^2\Big) + g_R^2\Big(2v_{1R}^2 - 2v_{2R}^2 - {v_2'}^2 - v_d^2 + {v_1'}^2 + v_u^2\Big)\Big) + \frac{1}{2}\lambda_R^2\Big(v_{2R}^2 + v_S^2\Big), \tag{A.113}$$

$$m_{\sigma_{H_1^0}\sigma_{R_2^0}} = -\frac{1}{2}\lambda_{12}\lambda_R v_{1R} v_u, \tag{A.114}$$

$$m_{\sigma_{H_2^0}\sigma_{R_2^0}} = -\frac{1}{2}\lambda_{12}\lambda_R v_d v_{1R}, \tag{A.115}$$

$$m_{\sigma_{H_1'^0}\sigma_{R_2^0}} = -\frac{1}{2}\lambda_{12}\lambda_R v_{1R} v_2', \tag{A.116}$$

$$m_{\sigma_{H_2'^0}\sigma_{R_2^0}} = -\frac{1}{2}\lambda_{12}\lambda_R v_1' v_{1R}, \tag{A.117}$$

$$m_{\sigma_{R_1^0}\sigma_{R_2^0}} = \frac{1}{2}\Big(\lambda_R\Big(\lambda_{12}\Big(v_1'v_2' + v_d v_u\Big) - \lambda_L v_{1L}v_{2L} - \lambda_S v_S^2\Big) - \sqrt{2}v_S T_{\lambda_R}\Big), \tag{A.118}$$

$$m_{\sigma_{R_2^0}\sigma_{R_2^0}} = m^2_{\Delta_{2R}} + \frac{1}{4}\Big(2g^2_{BL}\Big(- v^2_{1L} - v^2_{1R} + v^2_{2L} + v^2_{2R}\Big) + g^2_R\Big(- 2v^2_{1R} + 2v^2_{2R} - {v'_1}^2 - v^2_u + v^2_d + {v'_2}^2\Big)\Big) + \frac{1}{2}\lambda^2_R\Big(v^2_{1R} + v^2_S\Big)\,, \tag{A.119}$$

$$m_{\sigma_{H_1^0}\sigma_S} = v_u\Big(\frac{1}{\sqrt{2}}T_{\lambda_{12}} - \lambda_{12}\lambda_S v_S\Big)\,, \tag{A.120}$$

$$m_{\sigma_{H_2^0}\sigma_S} = v_d\Big(\frac{1}{\sqrt{2}}T_{\lambda_{12}} - \lambda_{12}\lambda_S v_S\Big)\,, \tag{A.121}$$

$$m_{\sigma_{H_1'^0}\sigma_S} = v'_2\Big(\frac{1}{\sqrt{2}}T_{\lambda_{12}} - \lambda_{12}\lambda_S v_S\Big)\,, \tag{A.122}$$

$$m_{\sigma_{H_2'^0}\sigma_S} = v'_1\Big(\frac{1}{\sqrt{2}}T_{\lambda_{12}} - \lambda_{12}\lambda_S v_S\Big)\,, \tag{A.123}$$

$$m_{\sigma_{R_1^0}\sigma_S} = v_{2R}\Big(- \frac{1}{\sqrt{2}}T_{\lambda_R} + \lambda_R\lambda_S v_S\Big)\,, \tag{A.124}$$

$$m_{\sigma_{R_2^0}\sigma_S} = v_{1R}\Big(- \frac{1}{\sqrt{2}}T_{\lambda_R} + \lambda_R\lambda_S v_S\Big)\,, \tag{A.125}$$

$$m_{\sigma_S\sigma_S} = m^2_S + \frac{1}{2}\Big(\lambda^2_L\Big(v^2_{1L} + v^2_{2L}\Big) + \lambda^2_{12}\Big(v^2_d + {v'_1}^2 + v^2_u + {v'_2}^2\Big) + \lambda_S\Big(2\lambda_{12}\Big(v'_1v'_2 + v_dv_u\Big) - 2\lambda_L v_{1L}v_{2L}\Big) + \lambda_R\Big(- 2\lambda_S v_{1R}v_{2R} + \lambda_R\Big(v^2_{1R} + v^2_{2R}\Big)\Big) + 2\lambda^2_S v^2_S - 2\sqrt{2}v_S T_{\lambda_S}\Big)\,, \tag{A.126}$$

$$m_{\sigma_{H_1^0}\sigma_{L_1^0}} = -\frac{1}{2}\lambda_{12}\lambda_L v_u v_{2L}\,, \tag{A.127}$$

$$m_{\sigma_{H_2^0}\sigma_{L_1^0}} = -\frac{1}{2}\lambda_{12}\lambda_L v_d v_{2L}\,, \tag{A.128}$$

$$m_{\sigma_{H_1'^0}\sigma_{L_1^0}} = -\frac{1}{2}\lambda_{12}\lambda_L v_{2L}v'_2\,, \tag{A.129}$$

$$m_{\sigma_{H_2'^0}\sigma_{L_1^0}} = -\frac{1}{2}\lambda_{12}\lambda_L v'_1v_{2L}\,, \tag{A.130}$$

$$m_{\sigma_{R_1^0}\sigma_{L_1^0}} = \frac{1}{2}\lambda_L\lambda_R v_{2L}v_{2R}\,, \tag{A.131}$$

$$m_{\sigma_{R_2^0}\sigma_{L_1^0}} = \frac{1}{2}\lambda_L\lambda_R v_{1R}v_{2L}\,, \tag{A.132}$$

$$m_{\sigma_S\sigma_{L_1^0}} = v_{2L}\Big(- \frac{1}{\sqrt{2}}T_{\lambda_L} + \lambda_L\lambda_S v_S\Big)\,, \tag{A.133}$$

$$m_{\sigma_{L_1^0}\sigma_{L_1^0}} = m^2_{\Delta_{1L}} + \frac{1}{4}\Big(2g^2_{BL}\Big(- v^2_{2L} - v^2_{2R} + v^2_{1L} + v^2_{1R}\Big) + g^2_L\Big(2v^2_{1L} - 2v^2_{2L} - {v'_1}^2 - v^2_u + v^2_d + {v'_2}^2\Big)\Big) + \frac{1}{2}\lambda^2_L\Big(v^2_{2L} + v^2_S\Big)\,, \tag{A.134}$$

$$m_{\sigma_{H_1^0}\sigma_{L_2^0}} = -\frac{1}{2}\lambda_{12}\lambda_L v_{1L}v_u\,, \tag{A.135}$$

$$m_{\sigma_{H_2^0}\sigma_{L_2^0}} = -\frac{1}{2}\lambda_{12}\lambda_L v_d v_{1L}\,, \tag{A.136}$$

$$m_{\sigma_{H_1'^0}\sigma_{L_2^0}} = -\frac{1}{2}\lambda_{12}\lambda_L v_{1L}v'_2\,, \tag{A.137}$$

$$m_{\sigma_{H_2'^0}\sigma_{L_2^0}} = -\frac{1}{2}\lambda_{12}\lambda_L v_{1L}v'_1\,, \tag{A.138}$$

$$m_{\sigma_{R_1^0}\sigma_{L_2^0}} = \frac{1}{2}\lambda_L\lambda_R v_{1L}v_{2R}\,, \tag{A.139}$$

$$m_{\sigma_{R_2^0}\sigma_{L_2^0}} = \frac{1}{2}\lambda_L\lambda_R v_{1L}v_{1R}\,, \tag{A.140}$$

$$m_{\sigma_S \sigma_{L_2^0}} = v_{1L}\Big(-\frac{1}{\sqrt{2}} T_{\lambda_L} + \lambda_L \lambda_S v_S \Big), \tag{A.141}$$

$$m_{\sigma_{L_1^0}\sigma_{L_2^0}} = \frac{1}{2}\Big(\lambda_L\Big(\lambda_{12}\Big(v_1' v_2' + v_d v_u\Big) - \lambda_R v_{1R} v_{2R} - \lambda_S v_S^2\Big) - \sqrt{2} v_S T_{\lambda_L}\Big), \tag{A.142}$$

$$\begin{aligned} m_{\sigma_{L_2^0}\sigma_{L_2^0}} &= +m^2_{\Delta_{2L}} + \frac{1}{4}\Big(2 g_{BL}^2\Big(- v_{1L}^2 - v_{1R}^2 + v_{2L}^2 + v_{2R}^2\Big) \\ &\quad + g_L^2\Big(- 2v_{1L}^2 + 2v_{2L}^2 - {v_2'}^2 - v_d^2 + {v_1'}^2 + v_u^2\Big)\Big) + \frac{1}{2}\lambda_L^2\Big(v_{1L}^2 + v_S^2\Big). \end{aligned} \tag{A.143}$$

Gauge fixing contributions from ξ_Z:

$$m^{\xi,Z}_{\sigma_{H_1^0}\sigma_{H_1^0}} = \frac{1}{4} v_d^2 \Big(g_L \cos\Theta_W + g_R \sin\Theta_W \sin\Theta'_W\Big)^2, \tag{A.144}$$

$$m^{\xi,Z}_{\sigma_{H_1^0}\sigma_{H_2^0}} = -\frac{1}{4} v_d v_u \Big(g_L \cos\Theta_W + g_R \sin\Theta_W \sin\Theta'_W\Big)^2, \tag{A.145}$$

$$m^{\xi,Z}_{\sigma_{H_2^0}\sigma_{H_2^0}} = \frac{1}{4} v_u^2 \Big(g_L \cos\Theta_W + g_R \sin\Theta_W \sin\Theta'_W\Big)^2, \tag{A.146}$$

$$m^{\xi,Z}_{\sigma_{H_1^0}\sigma_{H_1'^0}} = -\frac{1}{4} v_d v_1' \Big(g_L \cos\Theta_W + g_R \sin\Theta_W \sin\Theta'_W\Big)^2, \tag{A.147}$$

$$m^{\xi,Z}_{\sigma_{H_2^0}\sigma_{H_1'^0}} = \frac{1}{4} v_1' v_u \Big(g_L \cos\Theta_W + g_R \sin\Theta_W \sin\Theta'_W\Big)^2, \tag{A.148}$$

$$m^{\xi,Z}_{\sigma_{H_1'^0}\sigma_{H_1'^0}} = \frac{1}{4} {v_1'}^2 \Big(g_L \cos\Theta_W + g_R \sin\Theta_W \sin\Theta'_W\Big)^2, \tag{A.149}$$

$$m^{\xi,Z}_{\sigma_{H_1^0}\sigma_{H_2'^0}} = \frac{1}{4} v_d v_2' \Big(g_L \cos\Theta_W + g_R \sin\Theta_W \sin\Theta'_W\Big)^2, \tag{A.150}$$

$$m^{\xi,Z}_{\sigma_{H_2^0}\sigma_{H_2'^0}} = -\frac{1}{4} v_u v_2' \Big(g_L \cos\Theta_W + g_R \sin\Theta_W \sin\Theta'_W\Big)^2, \tag{A.151}$$

$$m^{\xi,Z}_{\sigma_{H_1'^0}\sigma_{H_2'^0}} = -\frac{1}{4} v_1' v_2' \Big(g_L \cos\Theta_W + g_R \sin\Theta_W \sin\Theta'_W\Big)^2, \tag{A.152}$$

$$m^{\xi,Z}_{\sigma_{H_2'^0}\sigma_{H_2'^0}} = \frac{1}{4} {v_2'}^2 \Big(g_L \cos\Theta_W + g_R \sin\Theta_W \sin\Theta'_W\Big)^2, \tag{A.153}$$

$$m^{\xi,Z}_{\sigma_{H_1^0}\sigma_{R_1^0}} = \frac{1}{2} v_d v_{1R} \sin\Theta_W \Big(g_{BL} \cos\Theta'_W - g_R \sin\Theta'_W\Big)\Big(g_L \cos\Theta_W + g_R \sin\Theta_W \sin\Theta'_W\Big), \tag{A.154}$$

$$m^{\xi,Z}_{\sigma_{H_2^0}\sigma_{R_1^0}} = \frac{1}{2} v_{1R} v_u \sin\Theta_W \Big(- g_{BL} \cos\Theta'_W + g_R \sin\Theta'_W\Big)\Big(g_L \cos\Theta_W + g_R \sin\Theta_W \sin\Theta'_W\Big), \tag{A.155}$$

$$m^{\xi,Z}_{\sigma_{H_1'^0}\sigma_{R_1^0}} = \frac{1}{2} v_1' v_{1R} \sin\Theta_W \Big(- g_{BL} \cos\Theta'_W + g_R \sin\Theta'_W\Big)\Big(g_L \cos\Theta_W + g_R \sin\Theta_W \sin\Theta'_W\Big), \tag{A.156}$$

$$m^{\xi,Z}_{\sigma_{H_2'^0}\sigma_{R_1^0}} = \frac{1}{2} v_{1R} v_2' \sin\Theta_W \Big(g_{BL} \cos\Theta'_W - g_R \sin\Theta'_W\Big)\Big(g_L \cos\Theta_W + g_R \sin\Theta_W \sin\Theta'_W\Big), \tag{A.157}$$

$$m^{\xi,Z}_{\sigma_{R_1^0}\sigma_{R_1^0}} = v_{1R}^2 \sin\Theta_W^2 \Big(g_{BL} \cos\Theta'_W - g_R \sin\Theta'_W\Big)^2, \tag{A.158}$$

$$m^{\xi,Z}_{\sigma_{H_1^0}\sigma_{R_2^0}} = \frac{1}{2} v_d v_{2R} \sin\Theta_W \Big(- g_{BL} \cos\Theta'_W + g_R \sin\Theta'_W\Big)\Big(g_L \cos\Theta_W + g_R \sin\Theta_W \sin\Theta'_W\Big), \tag{A.159}$$

$$m^{\xi,Z}_{\sigma_{H_2^0}\sigma_{R_2^0}} = \frac{1}{2} v_u v_{2R} \sin\Theta_W \Big(g_{BL} \cos\Theta'_W - g_R \sin\Theta'_W\Big)\Big(g_L \cos\Theta_W + g_R \sin\Theta_W \sin\Theta'_W\Big), \tag{A.160}$$

$$m^{\xi,Z}_{\sigma_{H_1'^0}\sigma_{R_2^0}} = \frac{1}{2}v_1' v_{2R}\sin\Theta_W\Big(g_{BL}\cos\Theta'_W - g_R\sin\Theta'_W\Big)\Big(g_L\cos\Theta_W + g_R\sin\Theta_W\sin\Theta'_W\Big), \tag{A.161}$$

$$m^{\xi,Z}_{\sigma_{H_2'^0}\sigma_{R_2^0}} = \frac{1}{2}v_2' v_{2R}\sin\Theta_W\Big(-g_{BL}\cos\Theta'_W + g_R\sin\Theta'_W\Big)\Big(g_L\cos\Theta_W + g_R\sin\Theta_W\sin\Theta'_W\Big), \tag{A.162}$$

$$m^{\xi,Z}_{\sigma_{R_1^0}\sigma_{R_2^0}} = -v_{1R}v_{2R}\sin\Theta_W^2\Big(g_{BL}\cos\Theta'_W - g_R\sin\Theta'_W\Big)^2, \tag{A.163}$$

$$m^{\xi,Z}_{\sigma_{R_2^0}\sigma_{R_2^0}} = v_{2R}^2\sin\Theta_W^2\Big(g_{BL}\cos\Theta'_W - g_R\sin\Theta'_W\Big)^2, \tag{A.164}$$

$$m^{\xi,Z}_{\sigma_{H_1^0}\sigma_{L_1^0}} = \frac{1}{2}v_d v_{1L}\Big(g_{BL}\cos\Theta'_W\sin\Theta_W + g_L\cos\Theta_W\Big)\Big(g_L\cos\Theta_W + g_R\sin\Theta_W\sin\Theta'_W\Big), \tag{A.165}$$

$$m^{\xi,Z}_{\sigma_{H_2^0}\sigma_{L_1^0}} = -\frac{1}{2}v_{1L}v_u\Big(g_{BL}\cos\Theta'_W\sin\Theta_W + g_L\cos\Theta_W\Big)\Big(g_L\cos\Theta_W + g_R\sin\Theta_W\sin\Theta'_W\Big), \tag{A.166}$$

$$m^{\xi,Z}_{\sigma_{H_1'^0}\sigma_{L_1^0}} = -\frac{1}{2}v_{1L}v_1'\Big(g_{BL}\cos\Theta'_W\sin\Theta_W + g_L\cos\Theta_W\Big)\Big(g_L\cos\Theta_W + g_R\sin\Theta_W\sin\Theta'_W\Big), \tag{A.167}$$

$$m^{\xi,Z}_{\sigma_{H_2'^0}\sigma_{L_1^0}} = \frac{1}{2}v_{1L}v_2'\Big(g_{BL}\cos\Theta'_W\sin\Theta_W + g_L\cos\Theta_W\Big)\Big(g_L\cos\Theta_W + g_R\sin\Theta_W\sin\Theta'_W\Big), \tag{A.168}$$

$$m^{\xi,Z}_{\sigma_{R_1^0}\sigma_{L_1^0}} = v_{1L}v_{1R}\sin\Theta_W\Big(g_{BL}\cos\Theta'_W\sin\Theta_W + g_L\cos\Theta_W\Big)\Big(g_{BL}\cos\Theta'_W - g_R\sin\Theta'_W\Big), \tag{A.169}$$

$$m^{\xi,Z}_{\sigma_{R_2^0}\sigma_{L_1^0}} = -v_{1L}v_{2R}\sin\Theta_W\Big(g_{BL}\cos\Theta'_W\sin\Theta_W + g_L\cos\Theta_W\Big)\Big(g_{BL}\cos\Theta'_W - g_R\sin\Theta'_W\Big), \tag{A.170}$$

$$m^{\xi,Z}_{\sigma_{L_1^0}\sigma_{L_1^0}} = v_{1L}^2\Big(g_{BL}\cos\Theta'_W\sin\Theta_W + g_L\cos\Theta_W\Big)^2, \tag{A.171}$$

$$m^{\xi,Z}_{\sigma_{H_1^0}\sigma_{L_2^0}} = -\frac{1}{2}v_d v_{2L}\Big(g_{BL}\cos\Theta'_W\sin\Theta_W + g_L\cos\Theta_W\Big)\Big(g_L\cos\Theta_W + g_R\sin\Theta_W\sin\Theta'_W\Big), \tag{A.172}$$

$$m^{\xi,Z}_{\sigma_{H_2^0}\sigma_{L_2^0}} = \frac{1}{2}v_u v_{2L}\Big(g_{BL}\cos\Theta'_W\sin\Theta_W + g_L\cos\Theta_W\Big)\Big(g_L\cos\Theta_W + g_R\sin\Theta_W\sin\Theta'_W\Big), \tag{A.173}$$

$$m^{\xi,Z}_{\sigma_{H_1'^0}\sigma_{L_2^0}} = \frac{1}{2}v_1' v_{2L}\Big(g_{BL}\cos\Theta'_W\sin\Theta_W + g_L\cos\Theta_W\Big)\Big(g_L\cos\Theta_W + g_R\sin\Theta_W\sin\Theta'_W\Big), \tag{A.174}$$

$$m^{\xi,Z}_{\sigma_{H_2'^0}\sigma_{L_2^0}} = -\frac{1}{2}v_{2L}v_2'\Big(g_{BL}\cos\Theta'_W\sin\Theta_W + g_L\cos\Theta_W\Big)\Big(g_L\cos\Theta_W + g_R\sin\Theta_W\sin\Theta'_W\Big), \tag{A.175}$$

$$m^{\xi,Z}_{\sigma_{R_1^0}\sigma_{L_2^0}} = -v_{1R}v_{2L}\sin\Theta_W\Big(g_{BL}\cos\Theta'_W\sin\Theta_W + g_L\cos\Theta_W\Big)\Big(g_{BL}\cos\Theta'_W - g_R\sin\Theta'_W\Big), \tag{A.176}$$

$$m^{\xi,Z}_{\sigma_{R_2^0}\sigma_{L_2^0}} = v_{2L}v_{2R}\sin\Theta_W\Big(g_{BL}\cos\Theta'_W\sin\Theta_W + g_L\cos\Theta_W\Big)\Big(g_{BL}\cos\Theta'_W - g_R\sin\Theta'_W\Big), \tag{A.177}$$

$$m^{\xi,Z}_{\sigma_{L_1^0}\sigma_{L_2^0}} = -v_{1L}v_{2L}\Big(g_{BL}\cos\Theta'_W\sin\Theta_W + g_L\cos\Theta_W\Big)^2, \tag{A.178}$$

$$m^{\xi,Z}_{\sigma_{L_2^0}\sigma_{L_2^0}} = v_{2L}^2\Big(g_{BL}\cos\Theta'_W\sin\Theta_W + g_L\cos\Theta_W\Big)^2 . \tag{A.179}$$

Gauge fixing contributions from $\xi_{Z'}$:

$$m^{\xi,Z'}_{\sigma_{H_1^0}\sigma_{H_1^0}} = \frac{1}{4}g_R^2 v_d^2\cos\Theta'^2_W , \tag{A.180}$$

$$m^{\xi,Z'}_{\sigma_{H_1^0}\sigma_{H_2^0}} = -\frac{1}{4}g_R^2 v_d v_u\cos\Theta'^2_W , \tag{A.181}$$

$$m^{\xi,Z'}_{\sigma_{H_2^0}\sigma_{H_2^0}} = \frac{1}{4}g_R^2 v_u^2\cos\Theta'^2_W , \tag{A.182}$$

$$m^{\xi,Z'}_{\sigma_{H_1^0}\sigma_{H_1'^0}} = -\frac{1}{4}g_R^2 v_d v_1'\cos\Theta'^2_W , \tag{A.183}$$

$$m^{\xi,Z'}_{\sigma_{H_2^0}\sigma_{H_1'^0}} = \frac{1}{4}g_R^2 v_1' v_u\cos\Theta'^2_W , \tag{A.184}$$

$$m^{\xi,Z'}_{\sigma_{H_1'^0}\sigma_{H_1'^0}} = \frac{1}{4}g_R^2 {v_1'}^2\cos\Theta'^2_W , \tag{A.185}$$

$$m^{\xi,Z'}_{\sigma_{H_1^0}\sigma_{H_2'^0}} = \frac{1}{4}g_R^2 v_d v_2'\cos\Theta'^2_W , \tag{A.186}$$

$$m^{\xi,Z'}_{\sigma_{H_2^0}\sigma_{H_2'^0}} = -\frac{1}{4}g_R^2 v_u v_2'\cos\Theta'^2_W , \tag{A.187}$$

$$m^{\xi,Z'}_{\sigma_{H_1'^0}\sigma_{H_2'^0}} = -\frac{1}{4}g_R^2 v_1' v_2'\cos\Theta'^2_W , \tag{A.188}$$

$$m^{\xi,Z'}_{\sigma_{H_2'^0}\sigma_{H_2'^0}} = \frac{1}{4}g_R^2 {v_2'}^2\cos\Theta'^2_W , \tag{A.189}$$

$$m^{\xi,Z'}_{\sigma_{H_1^0}\sigma_{R_1^0}} = -\frac{1}{2}g_R v_d v_{1R}\cos\Theta'_W\Big(g_{BL}\sin\Theta'_W + g_R\cos\Theta'_W\Big) , \tag{A.190}$$

$$m^{\xi,Z'}_{\sigma_{H_2^0}\sigma_{R_1^0}} = \frac{1}{2}g_R v_{1R} v_u\cos\Theta'_W\Big(g_{BL}\sin\Theta'_W + g_R\cos\Theta'_W\Big) , \tag{A.191}$$

$$m^{\xi,Z'}_{\sigma_{H_1'^0}\sigma_{R_1^0}} = \frac{1}{2}g_R v_1' v_{1R}\cos\Theta'_W\Big(g_{BL}\sin\Theta'_W + g_R\cos\Theta'_W\Big) , \tag{A.192}$$

$$m^{\xi,Z'}_{\sigma_{H_2'^0}\sigma_{R_1^0}} = -\frac{1}{2}g_R v_{1R} v_2'\cos\Theta'_W\Big(g_{BL}\sin\Theta'_W + g_R\cos\Theta'_W\Big) , \tag{A.193}$$

$$m^{\xi,Z'}_{\sigma_{R_1^0}\sigma_{R_1^0}} = v_{1R}^2\Big(g_{BL}\sin\Theta'_W + g_R\cos\Theta'_W\Big)^2 , \tag{A.194}$$

$$m^{\xi,Z'}_{\sigma_{H_1^0}\sigma_{R_2^0}} = \frac{1}{2}g_R v_d v_{2R}\cos\Theta'_W\Big(g_{BL}\sin\Theta'_W + g_R\cos\Theta'_W\Big) , \tag{A.195}$$

$$m^{\xi,Z'}_{\sigma_{H_2^0}\sigma_{R_2^0}} = -\frac{1}{2}g_R v_u v_{2R}\cos\Theta'_W\Big(g_{BL}\sin\Theta'_W + g_R\cos\Theta'_W\Big) , \tag{A.196}$$

$$m^{\xi,Z'}_{\sigma_{H_1'^0}\sigma_{R_2^0}} = -\frac{1}{2}g_R v_1' v_{2R}\cos\Theta'_W\Big(g_{BL}\sin\Theta'_W + g_R\cos\Theta'_W\Big) , \tag{A.197}$$

$$m^{\xi,Z'}_{\sigma_{H_2'^0}\sigma_{R_2^0}} = \frac{1}{2}g_R v_2' v_{2R}\cos\Theta'_W\Big(g_{BL}\sin\Theta'_W + g_R\cos\Theta'_W\Big) , \tag{A.198}$$

$$m^{\xi,Z'}_{\sigma_{R_1^0}\sigma_{R_2^0}} = -v_{1R} v_{2R}\Big(g_{BL}\sin\Theta'_W + g_R\cos\Theta'_W\Big)^2 , \tag{A.199}$$

$$m^{\xi,Z'}_{\sigma_{R_2^0}\sigma_{R_2^0}} = v_{2R}^2\Big(g_{BL}\sin\Theta'_W + g_R\cos\Theta'_W\Big)^2 , \tag{A.200}$$

$$m^{\xi,Z'}_{\sigma_{H_1^0}\sigma_{L_1^0}} = -\frac{1}{2}g_{BL}g_R v_d v_{1L}\cos\Theta'_W\sin\Theta'_W , \tag{A.201}$$

$$m^{\xi,Z'}_{\sigma_{H_2^0}\sigma_{L_1^0}} = \frac{1}{2}g_{BL}g_R v_{1L} v_u\cos\Theta'_W\sin\Theta'_W , \tag{A.202}$$

$$m^{\xi,Z'}_{\sigma_{H_1'^0}\sigma_{L_1^0}} = \frac{1}{2} g_{BL} g_R v_{1L} v_1' \cos\Theta'_W \sin\Theta'_W \,, \tag{A.203}$$

$$m^{\xi,Z'}_{\sigma_{H_2'^0}\sigma_{L_1^0}} = -\frac{1}{2} g_{BL} g_R v_{1L} v_2' \cos\Theta'_W \sin\Theta'_W \,, \tag{A.204}$$

$$m^{\xi,Z'}_{\sigma_{R_1^0}\sigma_{L_1^0}} = g_{BL} v_{1L} v_{1R} \sin\Theta'_W \Big(g_{BL} \sin\Theta'_W + g_R \cos\Theta'_W \Big) \,, \tag{A.205}$$

$$m^{\xi,Z'}_{\sigma_{R_2^0}\sigma_{L_1^0}} = -g_{BL} v_{1L} v_{2R} \sin\Theta'_W \Big(g_{BL} \sin\Theta'_W + g_R \cos\Theta'_W \Big) \,, \tag{A.206}$$

$$m^{\xi,Z'}_{\sigma_{L_1^0}\sigma_{L_1^0}} = g_{BL}^2 v_{1L}^2 \sin\Theta'^2_W \,, \tag{A.207}$$

$$m^{\xi,Z'}_{\sigma_{H_1^0}\sigma_{L_2^0}} = \frac{1}{2} g_{BL} g_R v_d v_{2L} \cos\Theta'_W \sin\Theta'_W \,, \tag{A.208}$$

$$m^{\xi,Z'}_{\sigma_{H_2^0}\sigma_{L_2^0}} = -\frac{1}{2} g_{BL} g_R v_u v_{2L} \cos\Theta'_W \sin\Theta'_W \,, \tag{A.209}$$

$$m^{\xi,Z'}_{\sigma_{H_1'^0}\sigma_{L_2^0}} = -\frac{1}{2} g_{BL} g_R v_1' v_{2L} \cos\Theta'_W \sin\Theta'_W \,, \tag{A.210}$$

$$m^{\xi,Z'}_{\sigma_{H_2'^0}\sigma_{L_2^0}} = \frac{1}{2} g_{BL} g_R v_{2L} v_2' \cos\Theta'_W \sin\Theta'_W \,, \tag{A.211}$$

$$m^{\xi,Z'}_{\sigma_{R_1^0}\sigma_{L_2^0}} = -g_{BL} v_{1R} v_{2L} \sin\Theta'_W \Big(g_{BL} \sin\Theta'_W + g_R \cos\Theta'_W \Big) \,, \tag{A.212}$$

$$m^{\xi,Z'}_{\sigma_{R_2^0}\sigma_{L_2^0}} = g_{BL} v_{2L} v_{2R} \sin\Theta'_W \Big(g_{BL} \sin\Theta'_W + g_R \cos\Theta'_W \Big) \,, \tag{A.213}$$

$$m^{\xi,Z'}_{\sigma_{L_1^0}\sigma_{L_2^0}} = -g_{BL}^2 v_{1L} v_{2L} \sin\Theta'^2_W \,, \tag{A.214}$$

$$m^{\xi,Z'}_{\sigma_{L_2^0}\sigma_{L_2^0}} = g_{BL}^2 v_{2L}^2 \sin\Theta'^2_W \,. \tag{A.215}$$

The mass matrix is diagonalized by Z^{Ah}:

$$Z^{Ah} m^2_{A^0} Z^{Ah,\dagger} = m^2_{dia,A^0} \,. \tag{A.216}$$

Mass matrix for charged Higgs bosons ($H^\pm$)

in the basis: $X = \Big(H_1^-, H_1^{+,*}, H_2^-, H_2^{+,*}, \Delta_{1R}^-, \Delta_{2R}^{+,*}, \Delta_{1L}^-, \Delta_{2L}^{+,*} \Big)$,
$Y = \Big(H_1^{-,*}, H_1^+, H_2^{-,*}, H_2^+, \Delta_{1R}^{-,*}, \Delta_{2R}^+, \Delta_{1L}^{-,*}, \Delta_{2L}^+ \Big)$:

We define the mass matrix including the gauge fixing terms ξ as:

$$m^2_{H^-} = m_{X_i Y_j} + \xi_W \, m^{\xi,W}_{X_i Y_j} + \xi_{W'} \, m^{\xi,W'}_{X_i Y_j} \,, \tag{A.217}$$

where

$$\begin{aligned} m_{H_1^- H_1^{-,*}} = m^2_{\phi_1} + \frac{1}{8} \Big(& g_L^2 \Big(-2v_{1L}^2 + 2v_{2L}^2 - v_{2'}{}^2 + v_d^2 + v_{1'}{}^2 + v_u^2 \Big) \\ & + g_R^2 \Big(-2v_{1R}^2 + 2v_{2R}^2 - v_u^2 + v_d^2 + v_{1'}{}^2 + v_{2'}{}^2 \Big) \Big) + \frac{1}{2} \lambda_{12}^2 v_S^2 \,, \end{aligned} \tag{A.218}$$

$$m_{H_1^- H_1^+} = \frac{1}{4} \Big(g_L^2 + g_R^2 \Big) v_d v_1' \,, \tag{A.219}$$

$$\begin{aligned} m_{H_1^{+,*} H_1^+} = m^2_{\phi_1} + \frac{1}{8} \Big(& g_L^2 \Big(2v_{1L}^2 - 2v_{2L}^2 - v_u^2 + v_d^2 + v_{1'}{}^2 + v_{2'}{}^2 \Big) \\ & + g_R^2 \Big(2v_{1R}^2 - 2v_{2R}^2 - v_{2'}{}^2 + v_d^2 + v_{1'}{}^2 + v_u^2 \Big) \Big) + \frac{1}{2} \lambda_{12}^2 v_S^2 \,, \end{aligned} \tag{A.220}$$

$$m_{H_1^- H_2^{-,*}} = \frac{1}{4}\Big(g_L^2 v_d v_2' + g_R^2 v_1' v_u\Big) + m^2_{\phi_1\phi_2}\,, \tag{A.221}$$

$$m_{H_1^{+,*} H_2^{-,*}} = \frac{1}{2}\Big(\lambda_{12}\Big(-\lambda_{12}\Big(v_1' v_2' + v_d v_u\Big) + \lambda_L v_{1L} v_{2L} + \lambda_R v_{1R} v_{2R} + \lambda_S v_S^2\Big) + \sqrt{2} v_S T_{\lambda_{12}}\Big) + \frac{1}{4}\Big(g_L^2 v_1' v_2' + g_R^2 v_d v_u\Big)\,, \tag{A.222}$$

$$m_{H_2^- H_2^{-,*}} = m^2_{\phi_2} + \frac{1}{8}\Big(g_L^2\Big(-2v_{1L}^2 + 2v_{2L}^2 - v_d^2 + {v_{1'}}^2 + v_u^2 + {v_{2'}}^2\Big) + g_R^2\Big(-2v_{1R}^2 + 2v_{2R}^2 - {v_{1'}}^2 + v_d^2 + v_u^2 + {v_{2'}}^2\Big)\Big) + \frac{1}{2}\lambda_{12}^2 v_S^2\,, \tag{A.223}$$

$$m_{H_1^- H_2^+} = \frac{1}{2}\Big(\lambda_{12}\Big(-\lambda_{12}\Big(v_1' v_2' + v_d v_u\Big) + \lambda_L v_{1L} v_{2L} + \lambda_R v_{1R} v_{2R} + \lambda_S v_S^2\Big) + \sqrt{2} v_S T_{\lambda_{12}}\Big) + \frac{1}{4}\Big(g_L^2 v_d v_u + g_R^2 v_1' v_2'\Big)\,, \tag{A.224}$$

$$m_{H_1^{+,*} H_2^+} = \frac{1}{4}\Big(g_L^2 v_1' v_u + g_R^2 v_d v_2'\Big) + m^2_{\phi_1\phi_2}\,, \tag{A.225}$$

$$m_{H_2^- H_2^+} = \frac{1}{4}\Big(g_L^2 + g_R^2\Big) v_u v_2'\,, \tag{A.226}$$

$$m_{H_2^{+,*} H_2^+} = m^2_{\phi_2} + \frac{1}{8}\Big(g_L^2\Big(2v_{1L}^2 - 2v_{2L}^2 - {v_{1'}}^2 + v_d^2 + v_u^2 + {v_{2'}}^2\Big) + g_R^2\Big(2v_{1R}^2 - 2v_{2R}^2 - v_d^2 + {v_{1'}}^2 + v_u^2 + {v_{2'}}^2\Big)\Big) + \frac{1}{2}\lambda_{12}^2 v_S^2\,, \tag{A.227}$$

$$m_{H_1^- \Delta_{1R}^{-,*}} = \frac{1}{2}\frac{1}{\sqrt{2}} g_R^2 v_1' v_{1R}\,, \tag{A.228}$$

$$m_{H_1^{+,*} \Delta_{1R}^{-,*}} = \frac{1}{2}\frac{1}{\sqrt{2}} g_R^2 v_d v_{1R}\,, \tag{A.229}$$

$$m_{H_2^- \Delta_{1R}^{-,*}} = \frac{1}{2}\frac{1}{\sqrt{2}} g_R^2 v_{1R} v_u\,, \tag{A.230}$$

$$m_{H_2^{+,*} \Delta_{1R}^{-,*}} = \frac{1}{2}\frac{1}{\sqrt{2}} g_R^2 v_{1R} v_2'\,, \tag{A.231}$$

$$m_{\Delta_{1R}^- \Delta_{1R}^{-,*}} = \frac{1}{2}\Big(g_{BL}^2\Big(-v_{2L}^2 - v_{2R}^2 + v_{1L}^2 + v_{1R}^2\Big) + g_R^2 v_{1R}^2\Big) + \frac{1}{2}\lambda_R^2 v_S^2 + m^2_{\Delta_{1R}}\,, \tag{A.232}$$

$$m_{H_1^- \Delta_{2R}^+} = -\frac{1}{2}\frac{1}{\sqrt{2}} g_R^2 v_1' v_{2R}\,, \tag{A.233}$$

$$m_{H_1^{+,*} \Delta_{2R}^+} = -\frac{1}{2}\frac{1}{\sqrt{2}} g_R^2 v_d v_{2R}\,, \tag{A.234}$$

$$m_{H_2^- \Delta_{2R}^+} = -\frac{1}{2}\frac{1}{\sqrt{2}} g_R^2 v_u v_{2R}\,, \tag{A.235}$$

$$m_{H_2^{+,*} \Delta_{2R}^+} = -\frac{1}{2}\frac{1}{\sqrt{2}} g_R^2 v_2' v_{2R}\,, \tag{A.236}$$

$$m_{\Delta_{1R}^- \Delta_{2R}^+} = -\frac{1}{2} g_R^2 v_{1R} v_{2R} + \frac{1}{2}\Big(\lambda_R\Big(-\lambda_{12}\Big(v_1' v_2' + v_d v_u\Big) + \lambda_L v_{1L} v_{2L} + \lambda_R v_{1R} v_{2R} + \lambda_S v_S^2\Big) + \sqrt{2} v_S T_{\lambda_R}\Big)\,, \tag{A.237}$$

$$m_{\Delta_{2R}^{+,*} \Delta_{2R}^+} = \frac{1}{2}\Big(g_{BL}^2\Big(-v_{1L}^2 - v_{1R}^2 + v_{2L}^2 + v_{2R}^2\Big) + g_R^2 v_{2R}^2\Big) + \frac{1}{2}\lambda_R^2 v_S^2 + m^2_{\Delta_{2R}}\,, \tag{A.238}$$

$$m_{H_1^- \Delta_{1L}^{-,*}} = -\frac{1}{2}\frac{1}{\sqrt{2}} g_L^2 v_d v_{1L}\,, \tag{A.239}$$

$$m_{H_1^{+,*} \Delta_{1L}^{-,*}} = -\frac{1}{2}\frac{1}{\sqrt{2}} g_L^2 v_{1L} v_1'\,, \tag{A.240}$$

$$m_{H_2^- \Delta_{1L}^{-,*}} = -\frac{1}{2}\frac{1}{\sqrt{2}} g_L^2 v_{1L} v_2' \,, \tag{A.241}$$

$$m_{H_2^{+,*} \Delta_{1L}^{-,*}} = -\frac{1}{2}\frac{1}{\sqrt{2}} g_L^2 v_{1L} v_u \,, \tag{A.242}$$

$$m_{\Delta_{1L}^- \Delta_{1L}^{-,*}} = \frac{1}{2}\Big(g_{BL}^2\Big(- v_{2L}^2 - v_{2R}^2 + v_{1L}^2 + v_{1R}^2\Big) + g_L^2 v_{1L}^2\Big) + \frac{1}{2}\lambda_L^2 v_S^2 + m_{\Delta_{1L}}^2 \,, \tag{A.243}$$

$$m_{H_1^- \Delta_{2L}^+} = \frac{1}{2}\frac{1}{\sqrt{2}} g_L^2 v_d v_{2L} \,, \tag{A.244}$$

$$m_{H_1^{+,*} \Delta_{2L}^+} = \frac{1}{2}\frac{1}{\sqrt{2}} g_L^2 v_1' v_{2L} \,, \tag{A.245}$$

$$m_{H_2^- \Delta_{2L}^+} = \frac{1}{2}\frac{1}{\sqrt{2}} g_L^2 v_{2L} v_2' \,, \tag{A.246}$$

$$m_{H_2^{+,*} \Delta_{2L}^+} = \frac{1}{2}\frac{1}{\sqrt{2}} g_L^2 v_u v_{2L} \,, \tag{A.247}$$

$$\begin{aligned} m_{\Delta_{1L}^- \Delta_{2L}^+} = &-\frac{1}{2} g_L^2 v_{1L} v_{2L} + \frac{1}{2}\Big(\lambda_L\Big(- \lambda_{12}\Big(v_1' v_2' + v_d v_u\Big) \\ &+ \lambda_L v_{1L} v_{2L} + \lambda_R v_{1R} v_{2R} + \lambda_S v_S^2\Big) + \sqrt{2} v_S T_{\lambda_L}\Big) \,, \end{aligned} \tag{A.248}$$

$$m_{\Delta_{2L}^{+,*} \Delta_{2L}^+} = \frac{1}{2}\Big(g_{BL}^2\Big(- v_{1L}^2 - v_{1R}^2 + v_{2L}^2 + v_{2R}^2\Big) + g_L^2 v_{2L}^2\Big) + \frac{1}{2}\lambda_L^2 v_S^2 + m_{\Delta_{2L}}^2 \,. \tag{A.249}$$

Gauge fixing contributions from ξ_W:

$$m^{\xi,W}_{H_1^- H_1^{-,*}} = \frac{1}{4}\Big(g_L v_d \cos\phi_W - g_R v_1' \sin\phi_W\Big)^2 \,, \tag{A.250}$$

$$m^{\xi,W}_{H_1^- H_1^+} = \frac{1}{4}\Big(g_L v_1' \cos\phi_W - g_R v_d \sin\phi_W\Big)\Big(- g_L v_d \cos\phi_W + g_R v_1' \sin\phi_W\Big) \,, \tag{A.251}$$

$$m^{\xi,W}_{H_1^{+,*} H_1^+} = \frac{1}{4}\Big(g_L v_1' \cos\phi_W - g_R v_d \sin\phi_W\Big)^2 \,, \tag{A.252}$$

$$m^{\xi,W}_{H_1^- H_2^{-,*}} = \frac{1}{4}\Big(g_L v_d \cos\phi_W - g_R v_1' \sin\phi_W\Big)\Big(g_L v_2' \cos\phi_W - g_R v_u \sin\phi_W\Big) \,, \tag{A.253}$$

$$m^{\xi,W}_{H_1^{+,*} H_2^{-,*}} = -\frac{1}{4}\Big(g_L v_1' \cos\phi_W - g_R v_d \sin\phi_W\Big)\Big(g_L v_2' \cos\phi_W - g_R v_u \sin\phi_W\Big) \,, \tag{A.254}$$

$$m^{\xi,W}_{H_2^- H_2^{-,*}} = \frac{1}{4}\Big(g_L v_2' \cos\phi_W - g_R v_u \sin\phi_W\Big)^2 \,, \tag{A.255}$$

$$m^{\xi,W}_{H_1^- H_2^+} = -\frac{1}{4}\Big(g_L v_d \cos\phi_W - g_R v_1' \sin\phi_W\Big)\Big(g_L v_u \cos\phi_W - g_R v_2' \sin\phi_W\Big) \,, \tag{A.256}$$

$$m^{\xi,W}_{H_1^{+,*} H_2^+} = \frac{1}{4}\Big(g_L v_1' \cos\phi_W - g_R v_d \sin\phi_W\Big)\Big(g_L v_u \cos\phi_W - g_R v_2' \sin\phi_W\Big) \,, \tag{A.257}$$

$$m^{\xi,W}_{H_2^- H_2^+} = \frac{1}{4}\Big(g_L v_2' \cos\phi_W - g_R v_u \sin\phi_W\Big)\Big(- g_L v_u \cos\phi_W + g_R v_2' \sin\phi_W\Big) \,, \tag{A.258}$$

$$m^{\xi,W}_{H_2^{+,*} H_2^+} = \frac{1}{4}\Big(g_L v_u \cos\phi_W - g_R v_2' \sin\phi_W\Big)^2 \,, \tag{A.259}$$

$$m^{\xi,W}_{H_1^- \Delta_{1R}^{-,*}} = \frac{1}{2}\frac{1}{\sqrt{2}} g_R v_{1R} \sin\phi_W\Big(- g_L v_d \cos\phi_W + g_R v_1' \sin\phi_W\Big) \,, \tag{A.260}$$

$$m^{\xi,W}_{H_1^{+,*} \Delta_{1R}^{-,*}} = \frac{1}{2}\frac{1}{\sqrt{2}} g_R v_{1R} \sin\phi_W\Big(g_L v_1' \cos\phi_W - g_R v_d \sin\phi_W\Big) \,, \tag{A.261}$$

$$m^{\xi,W}_{H_2^- \Delta_{1R}^{-,*}} = \frac{1}{2}\frac{1}{\sqrt{2}} g_R v_{1R} \sin\phi_W\Big(- g_L v_2' \cos\phi_W + g_R v_u \sin\phi_W\Big) \,, \tag{A.262}$$

$$m^{\xi,W}_{H_2^{+,*} \Delta_{1R}^{-,*}} = \frac{1}{2}\frac{1}{\sqrt{2}} g_R v_{1R} \sin\phi_W\Big(g_L v_u \cos\phi_W - g_R v_2' \sin\phi_W\Big) \,, \tag{A.263}$$

$$m^{\xi,W}_{\Delta^-_{1R}\Delta^{-,*}_{1R}} = \frac{1}{2}g_R^2 v_{1R}^2 \sin\phi_W^2\,, \tag{A.264}$$

$$m^{\xi,W}_{H_1^-\Delta^+_{2R}} = \frac{1}{2}\frac{1}{\sqrt{2}}g_R v_{2R}\sin\phi_W\Big(-g_L v_d\cos\phi_W + g_R v_1'\sin\phi_W\Big)\,, \tag{A.265}$$

$$m^{\xi,W}_{H_1^{+,*}\Delta^+_{2R}} = \frac{1}{2}\frac{1}{\sqrt{2}}g_R v_{2R}\sin\phi_W\Big(g_L v_1'\cos\phi_W - g_R v_d\sin\phi_W\Big)\,, \tag{A.266}$$

$$m^{\xi,W}_{H_2^-\Delta^+_{2R}} = \frac{1}{2}\frac{1}{\sqrt{2}}g_R v_{2R}\sin\phi_W\Big(-g_L v_2'\cos\phi_W + g_R v_u\sin\phi_W\Big)\,, \tag{A.267}$$

$$m^{\xi,W}_{H_2^{+,*}\Delta^+_{2R}} = \frac{1}{2}\frac{1}{\sqrt{2}}g_R v_{2R}\sin\phi_W\Big(g_L v_u\cos\phi_W - g_R v_2'\sin\phi_W\Big)\,, \tag{A.268}$$

$$m^{\xi,W}_{\Delta^-_{1R}\Delta^+_{2R}} = \frac{1}{2}g_R^2 v_{1R}v_{2R}\sin\phi_W^2\,, \tag{A.269}$$

$$m^{\xi,W}_{\Delta^{+,*}_{2R}\Delta^+_{2R}} = \frac{1}{2}g_R^2 v_{2R}^2\sin\phi_W^2\,, \tag{A.270}$$

$$m^{\xi,W}_{H_1^-\Delta^{-,*}_{1L}} = \frac{1}{2}\frac{1}{\sqrt{2}}g_L v_{1L}\cos\phi_W\Big(-g_L v_d\cos\phi_W + g_R v_1'\sin\phi_W\Big)\,, \tag{A.271}$$

$$m^{\xi,W}_{H_1^{+,*}\Delta^{-,*}_{1L}} = \frac{1}{2}\frac{1}{\sqrt{2}}g_L v_{1L}\cos\phi_W\Big(g_L v_1'\cos\phi_W - g_R v_d\sin\phi_W\Big)\,, \tag{A.272}$$

$$m^{\xi,W}_{H_2^-\Delta^{-,*}_{1L}} = \frac{1}{2}\frac{1}{\sqrt{2}}g_L v_{1L}\cos\phi_W\Big(-g_L v_2'\cos\phi_W + g_R v_u\sin\phi_W\Big)\,, \tag{A.273}$$

$$m^{\xi,W}_{H_2^{+,*}\Delta^{-,*}_{1L}} = \frac{1}{2}\frac{1}{\sqrt{2}}g_L v_{1L}\cos\phi_W\Big(g_L v_u\cos\phi_W - g_R v_2'\sin\phi_W\Big)\,, \tag{A.274}$$

$$m^{\xi,W}_{\Delta^-_{1R}\Delta^{-,*}_{1L}} = \frac{1}{2}g_L g_R v_{1L}v_{1R}\cos\phi_W\sin\phi_W\,, \tag{A.275}$$

$$m^{\xi,W}_{\Delta^{+,*}_{2R}\Delta^{-,*}_{1L}} = \frac{1}{2}g_L g_R v_{1L}v_{2R}\cos\phi_W\sin\phi_W\,, \tag{A.276}$$

$$m^{\xi,W}_{\Delta^-_{1L}\Delta^{-,*}_{1L}} = \frac{1}{2}g_L^2 v_{1L}^2\cos\phi_W^2\,, \tag{A.277}$$

$$m^{\xi,W}_{H_1^-\Delta^+_{2L}} = \frac{1}{2}\frac{1}{\sqrt{2}}g_L v_{2L}\cos\phi_W\Big(-g_L v_d\cos\phi_W + g_R v_1'\sin\phi_W\Big)\,, \tag{A.278}$$

$$m^{\xi,W}_{H_1^{+,*}\Delta^+_{2L}} = \frac{1}{2}\frac{1}{\sqrt{2}}g_L v_{2L}\cos\phi_W\Big(g_L v_1'\cos\phi_W - g_R v_d\sin\phi_W\Big)\,, \tag{A.279}$$

$$m^{\xi,W}_{H_2^-\Delta^+_{2L}} = \frac{1}{2}\frac{1}{\sqrt{2}}g_L v_{2L}\cos\phi_W\Big(-g_L v_2'\cos\phi_W + g_R v_u\sin\phi_W\Big)\,, \tag{A.280}$$

$$m^{\xi,W}_{H_2^{+,*}\Delta^+_{2L}} = \frac{1}{2}\frac{1}{\sqrt{2}}g_L v_{2L}\cos\phi_W\Big(g_L v_u\cos\phi_W - g_R v_2'\sin\phi_W\Big)\,, \tag{A.281}$$

$$m^{\xi,W}_{\Delta^-_{1R}\Delta^+_{2L}} = \frac{1}{2}g_L g_R v_{1R}v_{2L}\cos\phi_W\sin\phi_W\,, \tag{A.282}$$

$$m^{\xi,W}_{\Delta^{+,*}_{2R}\Delta^+_{2L}} = \frac{1}{2}g_L g_R v_{2L}v_{2R}\cos\phi_W\sin\phi_W\,, \tag{A.283}$$

$$m^{\xi,W}_{\Delta^-_{1L}\Delta^+_{2L}} = \frac{1}{2}g_L^2 v_{1L}v_{2L}\cos\phi_W^2\,, \tag{A.284}$$

$$m^{\xi,W}_{\Delta^{+,*}_{2L}\Delta^+_{2L}} = \frac{1}{2}g_L^2 v_{2L}^2\cos\phi_W^2\,. \tag{A.285}$$

Gauge fixing contributions from $\xi_{W'}$:

$$m^{\xi,W'}_{H_1^-H_1^{-,*}} = \frac{1}{4}\Big(g_L v_d\sin\phi_W + g_R v_1'\cos\phi_W\Big)^2\,, \tag{A.286}$$

$$m^{\xi,W'}_{H_1^- H_1^+} = -\frac{1}{4}\Big(g_L v_d \sin\phi_W + g_R v_1' \cos\phi_W\Big)\Big(g_L v_1' \sin\phi_W + g_R v_d \cos\phi_W\Big)\,, \tag{A.287}$$

$$m^{\xi,W'}_{H_1^{+,*} H_1^+} = \frac{1}{4}\Big(g_L v_1' \sin\phi_W + g_R v_d \cos\phi_W\Big)^2\,, \tag{A.288}$$

$$m^{\xi,W'}_{H_1^- H_2^{-,*}} = \frac{1}{4}\Big(g_L v_d \sin\phi_W + g_R v_1' \cos\phi_W\Big)\Big(g_L v_2' \sin\phi_W + g_R v_u \cos\phi_W\Big)\,, \tag{A.289}$$

$$m^{\xi,W'}_{H_1^{+,*} H_2^{-,*}} = -\frac{1}{4}\Big(g_L v_1' \sin\phi_W + g_R v_d \cos\phi_W\Big)\Big(g_L v_2' \sin\phi_W + g_R v_u \cos\phi_W\Big)\,, \tag{A.290}$$

$$m^{\xi,W'}_{H_2^- H_2^{-,*}} = \frac{1}{4}\Big(g_L v_2' \sin\phi_W + g_R v_u \cos\phi_W\Big)^2\,, \tag{A.291}$$

$$m^{\xi,W'}_{H_1^- H_2^+} = -\frac{1}{4}\Big(g_L v_d \sin\phi_W + g_R v_1' \cos\phi_W\Big)\Big(g_L v_u \sin\phi_W + g_R v_2' \cos\phi_W\Big)\,, \tag{A.292}$$

$$m^{\xi,W'}_{H_1^{+,*} H_2^+} = \frac{1}{4}\Big(g_L v_1' \sin\phi_W + g_R v_d \cos\phi_W\Big)\Big(g_L v_u \sin\phi_W + g_R v_2' \cos\phi_W\Big)\,, \tag{A.293}$$

$$m^{\xi,W'}_{H_2^- H_2^+} = -\frac{1}{4}\Big(g_L v_u \sin\phi_W + g_R v_2' \cos\phi_W\Big)\Big(g_L v_2' \sin\phi_W + g_R v_u \cos\phi_W\Big)\,, \tag{A.294}$$

$$m^{\xi,W'}_{H_2^{+,*} H_2^+} = \frac{1}{4}\Big(g_L v_u \sin\phi_W + g_R v_2' \cos\phi_W\Big)^2\,, \tag{A.295}$$

$$m^{\xi,W'}_{H_1^- \Delta_{1R}^{-,*}} = \frac{1}{2}\frac{1}{\sqrt{2}} g_R v_{1R} \cos\phi_W \Big(g_L v_d \sin\phi_W + g_R v_1' \cos\phi_W\Big)\,, \tag{A.296}$$

$$m^{\xi,W'}_{H_1^{+,*} \Delta_{1R}^{-,*}} = -\frac{1}{2}\frac{1}{\sqrt{2}} g_R v_{1R} \cos\phi_W \Big(g_L v_1' \sin\phi_W + g_R v_d \cos\phi_W\Big)\,, \tag{A.297}$$

$$m^{\xi,W'}_{H_2^- \Delta_{1R}^{-,*}} = \frac{1}{2}\frac{1}{\sqrt{2}} g_R v_{1R} \cos\phi_W \Big(g_L v_2' \sin\phi_W + g_R v_u \cos\phi_W\Big)\,, \tag{A.298}$$

$$m^{\xi,W'}_{H_2^{+,*} \Delta_{1R}^{-,*}} = -\frac{1}{2}\frac{1}{\sqrt{2}} g_R v_{1R} \cos\phi_W \Big(g_L v_u \sin\phi_W + g_R v_2' \cos\phi_W\Big)\,, \tag{A.299}$$

$$m^{\xi,W'}_{\Delta_{1R}^- \Delta_{1R}^{-,*}} = \frac{1}{2} g_R^2 v_{1R}^2 \cos\phi_W^2\,, \tag{A.300}$$

$$m^{\xi,W'}_{H_1^- \Delta_{2R}^+} = \frac{1}{2}\frac{1}{\sqrt{2}} g_R v_{2R} \cos\phi_W \Big(g_L v_d \sin\phi_W + g_R v_1' \cos\phi_W\Big)\,, \tag{A.301}$$

$$m^{\xi,W'}_{H_1^{+,*} \Delta_{2R}^+} = -\frac{1}{2}\frac{1}{\sqrt{2}} g_R v_{2R} \cos\phi_W \Big(g_L v_1' \sin\phi_W + g_R v_d \cos\phi_W\Big)\,, \tag{A.302}$$

$$m^{\xi,W'}_{H_2^- \Delta_{2R}^+} = \frac{1}{2}\frac{1}{\sqrt{2}} g_R v_{2R} \cos\phi_W \Big(g_L v_2' \sin\phi_W + g_R v_u \cos\phi_W\Big)\,, \tag{A.303}$$

$$m^{\xi,W'}_{H_2^{+,*} \Delta_{2R}^+} = -\frac{1}{2}\frac{1}{\sqrt{2}} g_R v_{2R} \cos\phi_W \Big(g_L v_u \sin\phi_W + g_R v_2' \cos\phi_W\Big)\,, \tag{A.304}$$

$$m^{\xi,W'}_{\Delta_{1R}^- \Delta_{2R}^+} = \frac{1}{2} g_R^2 v_{1R} v_{2R} \cos\phi_W^2\,, \tag{A.305}$$

$$m^{\xi,W'}_{\Delta_{2R}^{+,*} \Delta_{2R}^+} = \frac{1}{2} g_R^2 v_{2R}^2 \cos\phi_W^2\,, \tag{A.306}$$

$$m^{\xi,W'}_{H_1^- \Delta_{1L}^{-,*}} = -\frac{1}{2}\frac{1}{\sqrt{2}} g_L v_{1L} \sin\phi_W \Big(g_L v_d \sin\phi_W + g_R v_1' \cos\phi_W\Big)\,, \tag{A.307}$$

$$m^{\xi,W'}_{H_1^{+,*} \Delta_{1L}^{-,*}} = \frac{1}{2}\frac{1}{\sqrt{2}} g_L v_{1L} \sin\phi_W \Big(g_L v_1' \sin\phi_W + g_R v_d \cos\phi_W\Big)\,, \tag{A.308}$$

$$m^{\xi,W'}_{H_2^- \Delta_{1L}^{-,*}} = -\frac{1}{2}\frac{1}{\sqrt{2}} g_L v_{1L} \sin\phi_W \Big(g_L v_2' \sin\phi_W + g_R v_u \cos\phi_W\Big)\,, \tag{A.309}$$

$$m^{\xi,W'}_{H_2^{+,*} \Delta_{1L}^{-,*}} = \frac{1}{2}\frac{1}{\sqrt{2}} g_L v_{1L} \sin\phi_W \Big(g_L v_u \sin\phi_W + g_R v_2' \cos\phi_W\Big)\,, \tag{A.310}$$

$$m^{\xi,W'}_{\Delta_{1R}^- \Delta_{1L}^{-,*}} = -\frac{1}{2} g_L g_R v_{1L} v_{1R} \cos\phi_W \sin\phi_W\,, \tag{A.311}$$

$$m^{\xi,W'}_{\Delta^{+,*}_{2R}\Delta^{-,*}_{1L}} = -\frac{1}{2}g_L g_R v_{1L} v_{2R}\cos\phi_W \sin\phi_W\,, \tag{A.312}$$

$$m^{\xi,W'}_{\Delta^{-}_{1L}\Delta^{-,*}_{1L}} = \frac{1}{2}g_L^2 v_{1L}^2 \sin\phi_W^2\,, \tag{A.313}$$

$$m^{\xi,W'}_{H_1^-\Delta^+_{2L}} = -\frac{1}{2}\frac{1}{\sqrt{2}}g_L v_{2L}\sin\phi_W\left(g_L v_d \sin\phi_W + g_R v_1' \cos\phi_W\right), \tag{A.314}$$

$$m^{\xi,W'}_{H_1^{+,*}\Delta^+_{2L}} = \frac{1}{2}\frac{1}{\sqrt{2}}g_L v_{2L}\sin\phi_W\left(g_L v_1' \sin\phi_W + g_R v_d \cos\phi_W\right), \tag{A.315}$$

$$m^{\xi,W'}_{H_2^-\Delta^+_{2L}} = -\frac{1}{2}\frac{1}{\sqrt{2}}g_L v_{2L}\sin\phi_W\left(g_L v_2' \sin\phi_W + g_R v_u \cos\phi_W\right), \tag{A.316}$$

$$m^{\xi,W'}_{H_2^{+,*}\Delta^+_{2L}} = \frac{1}{2}\frac{1}{\sqrt{2}}g_L v_{2L}\sin\phi_W\left(g_L v_u \sin\phi_W + g_R v_2' \cos\phi_W\right), \tag{A.317}$$

$$m^{\xi,W'}_{\Delta^-_{1R}\Delta^+_{2L}} = -\frac{1}{2}g_L g_R v_{1R} v_{2L}\cos\phi_W \sin\phi_W\,, \tag{A.318}$$

$$m^{\xi,W'}_{\Delta^{+,*}_{2R}\Delta^+_{2L}} = -\frac{1}{2}g_L g_R v_{2L} v_{2R}\cos\phi_W \sin\phi_W\,, \tag{A.319}$$

$$m^{\xi,W'}_{\Delta^-_{1L}\Delta^+_{2L}} = \frac{1}{2}g_L^2 v_{1L} v_{2L}\sin\phi_W^2\,, \tag{A.320}$$

$$m^{\xi,W'}_{\Delta^{+,*}_{2L}\Delta^+_{2L}} = \frac{1}{2}g_L^2 v_{2L}^2 \sin\phi_W^2\,. \tag{A.321}$$

In the case $v_1', v_2' \to 0$, the gauge fixing contributions reduce to

$$m^2(\xi_{W^-})\Big|_{v_1'=v_2'=0} = \tag{A.322}$$

$$\begin{pmatrix}
\frac{1}{4}g_L^2 v_d^2 & 0 & 0 & -\frac{1}{4}g_L^2 v_d v_u & 0 & 0 & -\frac{1}{2\sqrt{2}}g_L^2 v_d v_{1L} & -\frac{1}{2\sqrt{2}}g_L^2 v_d v_{2L} \\
0 & 0 & 0 & 0 & 0 & 0 & 0 & 0 \\
0 & 0 & 0 & 0 & 0 & 0 & 0 & 0 \\
-\frac{1}{4}g_L^2 v_d v_u & 0 & 0 & \frac{1}{4}g_L^2 v_u^2 & 0 & 0 & \frac{1}{2\sqrt{2}}g_L^2 v_{1L} v_u & \frac{1}{2\sqrt{2}}g_L^2 v_u v_{2L} \\
0 & 0 & 0 & 0 & 0 & 0 & 0 & 0 \\
0 & 0 & 0 & 0 & 0 & 0 & 0 & 0 \\
-\frac{1}{2\sqrt{2}}g_L^2 v_d v_{1L} & 0 & 0 & \frac{1}{2\sqrt{2}}g_L^2 v_{1L} v_u & 0 & 0 & \frac{1}{2}g_L^2 v_{1L}^2 & \frac{1}{2}g_L^2 v_{1L} v_{2L} \\
-\frac{1}{2\sqrt{2}}g_L^2 v_d v_{2L} & 0 & 0 & \frac{1}{2\sqrt{2}}g_L^2 v_u v_{2L} & 0 & 0 & \frac{1}{2}g_L^2 v_{1L} v_{2L} & \frac{1}{2}g_L^2 v_{2L}^2
\end{pmatrix},$$

$$m^2(\xi_{W'^-})\Big|_{v_1'=v_2'=0} = \tag{A.323}$$

$$\begin{pmatrix}
0 & 0 & 0 & 0 & 0 & 0 & 0 & 0 \\
0 & \frac{1}{4}g_R^2 v_d^2 & -\frac{1}{4}g_R^2 v_d v_u & 0 & -\frac{1}{2\sqrt{2}}g_R^2 v_d v_{1R} & -\frac{1}{2\sqrt{2}}g_R^2 v_d v_{2R} & 0 & 0 \\
0 & -\frac{1}{4}g_R^2 v_d v_u & \frac{1}{4}g_R^2 v_u^2 & 0 & \frac{1}{2\sqrt{2}}g_R^2 v_{1R} v_u & \frac{1}{2\sqrt{2}}g_R^2 v_u v_{2R} & 0 & 0 \\
0 & 0 & 0 & 0 & 0 & 0 & 0 & 0 \\
0 & -\frac{1}{2\sqrt{2}}g_R^2 v_d v_{1R} & \frac{1}{2\sqrt{2}}g_R^2 v_{1R} v_u & 0 & \frac{1}{2}g_R^2 v_{1R}^2 & \frac{1}{2}g_R^2 v_{1R} v_{2R} & 0 & 0 \\
0 & -\frac{1}{2\sqrt{2}}g_R^2 v_d v_{2R} & \frac{1}{2\sqrt{2}}g_R^2 v_u v_{2R} & 0 & \frac{1}{2}g_R^2 v_{1R} v_{2R} & \frac{1}{2}g_R^2 v_{2R}^2 & 0 & 0 \\
0 & 0 & 0 & 0 & 0 & 0 & 0 & 0 \\
0 & 0 & 0 & 0 & 0 & 0 & 0 & 0
\end{pmatrix}.$$

The mass matrix is diagonalized by Z^-:

$$Z^- m^2_{H^-} Z^{-,\dagger} = m^2_{dia,H^-} \,. \tag{A.324}$$

A.1.4 Mass matrices and rotations for the fermions

Mass matrix for the neutralinos ($\tilde{\chi}^0$)

in the basis: $\left(\tilde{W}^0_L, \tilde{W}^0_R, \tilde{B}, \tilde{H}'^0_2, \tilde{H}^0_2, \tilde{H}^0_1, \tilde{H}'^0_1, \tilde{\Delta}^0_{1L}, \tilde{\Delta}^0_{2R}, \tilde{\Delta}^0_{2L}, \tilde{\Delta}^0_{1R}, \tilde{S}\right)$:

$$m_{\tilde{\chi}^0} = \tag{A.325}$$

$$\begin{pmatrix}
M_{2L} & 0 & 0 & \frac{g_L v'_2}{2} & -\frac{g_L v_u}{2} & \frac{g_L v_d}{2} & -\frac{g_L v'_1}{2} & g_L v_{1L} & 0 & -g_L v_{2L} & 0 & 0 \\
0 & M_{2R} & 0 & -\frac{g_R v'_2}{2} & \frac{g_R v_u}{2} & -\frac{g_R v_d}{2} & \frac{g_R v'_1}{2} & 0 & -g_R v_{2R} & 0 & g_R v_{1R} & 0 \\
0 & 0 & M_1 & 0 & 0 & 0 & 0 & -g_{BL} v_{1L} & g_{BL} v_{2R} & g_{BL} v_{2L} & -g_{BL} v_{1R} & 0 \\
\frac{g_L v'_2}{2} & -\frac{g_R v'_2}{2} & 0 & 0 & 0 & 0 & -\frac{\lambda_{12} v_S}{\sqrt{2}} & 0 & 0 & 0 & 0 & -\frac{\lambda_{12} v'_1}{\sqrt{2}} \\
-\frac{g_L v_u}{2} & \frac{g_R v_u}{2} & 0 & 0 & 0 & -\frac{\lambda_{12} v_S}{\sqrt{2}} & 0 & 0 & 0 & 0 & 0 & -\frac{\lambda_{12} v_d}{\sqrt{2}} \\
\frac{g_L v_d}{2} & -\frac{g_R v_d}{2} & 0 & 0 & -\frac{\lambda_{12} v_S}{\sqrt{2}} & 0 & 0 & 0 & 0 & 0 & 0 & -\frac{\lambda_{12} v_u}{\sqrt{2}} \\
-\frac{g_L v'_1}{2} & \frac{g_R v'_1}{2} & 0 & -\frac{\lambda_{12} v_S}{\sqrt{2}} & 0 & 0 & 0 & 0 & 0 & 0 & 0 & -\frac{\lambda_{12} v'_2}{\sqrt{2}} \\
g_L v_{1L} & 0 & -g_{BL} v_{1L} & 0 & 0 & 0 & 0 & 0 & 0 & \frac{\lambda_L v_S}{\sqrt{2}} & 0 & \frac{\lambda_L v_{2L}}{\sqrt{2}} \\
0 & -g_R v_{2R} & g_{BL} v_{2R} & 0 & 0 & 0 & 0 & 0 & 0 & 0 & \frac{\lambda_R v_S}{\sqrt{2}} & \frac{\lambda_R v_{1R}}{\sqrt{2}} \\
-g_L v_{2L} & 0 & g_{BL} v_{2L} & 0 & 0 & 0 & 0 & \frac{\lambda_L v_S}{\sqrt{2}} & 0 & 0 & 0 & \frac{\lambda_L v_{1L}}{\sqrt{2}} \\
0 & g_R v_{1R} & -g_{BL} v_{1R} & 0 & 0 & 0 & 0 & 0 & \frac{\lambda_R v_S}{\sqrt{2}} & 0 & 0 & \frac{\lambda_R v_{2R}}{\sqrt{2}} \\
0 & 0 & 0 & -\frac{\lambda_{12} v'_1}{\sqrt{2}} & -\frac{\lambda_{12} v_d}{\sqrt{2}} & -\frac{\lambda_{12} v_u}{\sqrt{2}} & -\frac{\lambda_{12} v'_2}{\sqrt{2}} & \frac{\lambda_L v_{2L}}{\sqrt{2}} & \frac{\lambda_R v_{1R}}{\sqrt{2}} & \frac{\lambda_L v_{1L}}{\sqrt{2}} & \frac{\lambda_R v_{2R}}{\sqrt{2}} & \sqrt{2}\lambda_S v_S
\end{pmatrix} .$$

This matrix is diagonalized by Z^0:

$$Z^{0,*} m_{\tilde{\chi}^0} Z^{0,\dagger} = m^{dia}_{\tilde{\chi}^0} \,. \tag{A.326}$$

Mass matrix for the charginos, ($\tilde{\chi}^\pm$)

in the basis: $\left(\tilde{W}^+_L, \tilde{W}^+_R, \tilde{H}^+_2, \tilde{H}^+_1, \tilde{\Delta}^+_{2L}, \tilde{\Delta}^+_{2R}\right), \left(\tilde{W}^-_L, \tilde{W}^-_R, \tilde{H}^-_2, \tilde{H}^-_1, \tilde{\Delta}^-_{1L}, \tilde{\Delta}^-_{1R}\right)$

$$m_{\tilde{\chi}^-} = \begin{pmatrix}
M_{2L} & 0 & \frac{1}{\sqrt{2}} g_L v'_2 & \frac{1}{\sqrt{2}} g_L v_d & -g_L v_{1L} & 0 \\
0 & M_{2R} & -\frac{1}{\sqrt{2}} g_R v_u & -\frac{1}{\sqrt{2}} g_R v'_1 & 0 & -g_R v_{1R} \\
\frac{1}{\sqrt{2}} g_L v_u & -\frac{1}{\sqrt{2}} g_R v'_2 & 0 & \frac{1}{\sqrt{2}} \lambda_{12} v_S & 0 & 0 \\
\frac{1}{\sqrt{2}} g_L v'_1 & -\frac{1}{\sqrt{2}} g_R v_d & \frac{1}{\sqrt{2}} \lambda_{12} v_S & 0 & 0 & 0 \\
g_L v_{2L} & 0 & 0 & 0 & \frac{1}{\sqrt{2}} \lambda_L v_S & 0 \\
0 & g_R v_{2R} & 0 & 0 & 0 & \frac{1}{\sqrt{2}} \lambda_R v_S
\end{pmatrix} . \tag{A.327}$$

This matrix is diagonalized by U^+ and U^-

$$U^{+,*} m_{\tilde{\chi}^-} U^{-,\dagger} = m^{dia}_{\tilde{\chi}^-} \,. \tag{A.328}$$

Mass matrix for the doubly-charged higgsinos ($\tilde{\chi}^{\pm\pm}$)

in the basis: $\left(\tilde{\Delta}^{--}_{1L}, \tilde{\Delta}^{--}_{1R}\right), \left(\tilde{\Delta}^{++}_{2L}, \tilde{\Delta}^{++}_{2R}\right)$

$$m_{\tilde{\chi}^{--}} = \begin{pmatrix} \frac{1}{\sqrt{2}}\lambda_L v_S & 0 \\ 0 & \frac{1}{\sqrt{2}}\lambda_R v_S \end{pmatrix} . \tag{A.329}$$

Mass matrix for the neutrinos, (ν)

in the basis: $(\nu_L, \nu_R^c), (\nu_L, \nu_R^c)$

$$m_\nu = \begin{pmatrix} \sqrt{2}v_{2L}y_3^L & \frac{1}{\sqrt{2}}\left(v_1' y_1^{L,T} + v_u y_2^{L,T}\right) \\ \frac{1}{\sqrt{2}}\left(v_1' y_1^L + v_u y_2^L\right) & \sqrt{2}v_{1R}y_4^L \end{pmatrix} . \tag{A.330}$$

This matrix is diagonalized by U^V:

$$U^{V,*} m_\nu U^{V,\dagger} = m_\nu^{dia} . \tag{A.331}$$

Masses of the charged leptons (e), up- (u) and down-quarks (d)

They are obtained as follows

$$m_e = \frac{1}{\sqrt{2}}\left(v_2' y_2^{L,T} + v_d y_1^{L,T}\right) , \tag{A.332}$$

$$m_d = \frac{1}{\sqrt{2}}\left(v_2' y_2^{Q,T} + v_d y_1^{Q,T}\right) , \tag{A.333}$$

$$m_u = \frac{1}{\sqrt{2}}\left(v_1' y_1^{Q,T} + v_u y_2^{Q,T}\right) . \tag{A.334}$$

These matrices are diagonalized by $\{U_L^e, U_R^e\}$, $\{U_L^d, U_R^d\}$, and $\{U_L^u, U_R^u\}$, respectively:

$$U_L^{e,*} m_e U_R^{e,\dagger} = m_e^{dia} , \tag{A.335}$$

$$U_L^{d,*} m_d U_R^{d,\dagger} = m_d^{dia} , \tag{A.336}$$

$$U_L^{u,*} m_u U_R^{u,\dagger} = m_u^{dia} . \tag{A.337}$$

A.2 1-loop corrections to the mass of H^{--}

A.2.1 Self energy for the doubly charged Higgs bosons

$$\begin{aligned} &\Pi_{i,j}(p^2) = \\ &2\Big(-\frac{1}{2}r_{\rm MS} + B_0\Big(p^2, m_{W^-}^2, m_{W^-}^2\Big)\Big)\Gamma^*_{\check{H}_j^{++},W^-,W^-}\Gamma_{\check{H}_i^{++},W^-,W^-} \\ &+4\Big(-\frac{1}{2}r_{\rm MS} + B_0\Big(p^2, m_{W^-}^2, m_{W'^-}^2\Big)\Big)\Gamma^*_{\check{H}_j^{++},W'^-,W^-}\Gamma_{\check{H}_i^{++},W'^-,W^-} \\ &+2\Big(-\frac{1}{2}r_{\rm MS} + B_0\Big(p^2, m_{W'^-}^2, m_{W'^-}^2\Big)\Big)\Gamma^*_{\check{H}_j^{++},W'^-,W'^-}\Gamma_{\check{H}_i^{++},W'^-,W'^-} \end{aligned} \tag{A.338}$$

$$
\begin{aligned}
&- B_0\Big(p^2, m^2_{\eta_L^-}, m^2_{\eta_L^+}\Big)\Gamma_{\check{H}_i^{++},\bar{\eta}_L^+,\eta_L^-}\Gamma_{\check{H}_j^{--},\eta_L^+,\bar{\eta}_L^-} - B_0\Big(p^2, m^2_{\eta_R^-}, m^2_{\eta_L^+}\Big)\Gamma_{\check{H}_i^{++},\bar{\eta}_L^+,\eta_R^-}\Gamma_{\check{H}_j^{--},\eta_L^+,\bar{\eta}_R^-}\\
&- B_0\Big(p^2, m^2_{\eta_L^-}, m^2_{\eta_R^+}\Big)\Gamma_{\check{H}_i^{++},\bar{\eta}_R^+,\eta_L^-}\Gamma_{\check{H}_j^{--},\eta_R^+,\bar{\eta}_L^-}\\
&- B_0\Big(p^2, m^2_{\eta_R^-}, m^2_{\eta_R^+}\Big)\Gamma_{\check{H}_i^{++},\bar{\eta}_R^+,\eta_R^-}\Gamma_{\check{H}_j^{--},\eta_R^+,\bar{\eta}_R^-} + 4\Gamma_{\check{H}_i^{--},\check{H}_j^{++},W^+,W^-}\Big(-\frac{1}{2}r_{\rm MS}m^2_{W^-} + A_0\Big(m^2_{W^-}\Big)\Big)\\
&+ 4\Gamma_{\check{H}_i^{--},\check{H}_j^{++},W'^+,W'^-}\Big(-\frac{1}{2}r_{\rm MS}m^2_{W'^-} + A_0\Big(m^2_{W'^-}\Big)\Big) + 2\Gamma_{\check{H}_i^{--},\check{H}_j^{++},Z,Z}\Big(-\frac{1}{2}r_{\rm MS}m^2_{Z} + A_0\Big(m^2_{Z}\Big)\Big)\\
&+ 2\Gamma_{\check{H}_i^{--},\check{H}_j^{++},Z',Z'}\Big(-\frac{1}{2}r_{\rm MS}m^2_{Z'} + A_0\Big(m^2_{Z'}\Big)\Big)\\
&- 2\sum_{a=1}^{2} m_{\tilde{\chi}_a^-}\sum_{b=1}^{12} B_0\Big(p^2, m^2_{\tilde{\chi}_a^-}, m^2_{\tilde{\chi}_b^0}\Big)m_{\tilde{\chi}_b^0}\Big(\Gamma^{L*}_{\check{H}_j^{++},\tilde{\chi}_a^-,\tilde{\chi}_b^0}\Gamma^{R}_{\check{H}_i^{++},\tilde{\chi}_a^-,\tilde{\chi}_b^0} + \Gamma^{R*}_{\check{H}_j^{++},\tilde{\chi}_a^-,\tilde{\chi}_b^0}\Gamma^{L}_{\check{H}_i^{++},\tilde{\chi}_a^-,\tilde{\chi}_b^0}\Big)\\
&+ \sum_{a=1}^{2}\sum_{b=1}^{12} G_0\Big(p^2, m^2_{\tilde{\chi}_a^-}, m^2_{\tilde{\chi}_b^0}\Big)\Big(\Gamma^{L*}_{\check{H}_j^{++},\tilde{\chi}_a^-,\tilde{\chi}_b^0}\Gamma^{L}_{\check{H}_i^{++},\tilde{\chi}_a^-,\tilde{\chi}_b^0} + \Gamma^{R*}_{\check{H}_j^{++},\tilde{\chi}_a^-,\tilde{\chi}_b^0}\Gamma^{R}_{\check{H}_i^{++},\tilde{\chi}_a^-,\tilde{\chi}_b^0}\Big)\\
&- \sum_{a=1}^{3} m_{e_a}\sum_{b=1}^{3} B_0\Big(p^2, m^2_{e_a}, m^2_{e_b}\Big)m_{e_b}\Big(\Gamma^{L*}_{\check{H}_j^{++},e_a,e_b}\Gamma^{R}_{\check{H}_i^{++},e_a,e_b} + \Gamma^{R*}_{\check{H}_j^{++},e_a,e_b}\Gamma^{L}_{\check{H}_i^{++},e_a,e_b}\Big)\\
&+ \frac{1}{2}\sum_{a=1}^{3}\sum_{b=1}^{3} G_0\Big(p^2, m^2_{e_a}, m^2_{e_b}\Big)\Big(\Gamma^{L*}_{\check{H}_j^{++},e_a,e_b}\Gamma^{L}_{\check{H}_i^{++},e_a,e_b} + \Gamma^{R*}_{\check{H}_j^{++},e_a,e_b}\Gamma^{R}_{\check{H}_i^{++},e_a,e_b}\Big)\\
&- \sum_{a=1}^{4} A_0\Big(m^2_{H_a^{--}}\Big)\Gamma_{\check{H}_i^{--},\check{H}_j^{++},H_a^{++},H_a^{--}}\\
&+ \sum_{a=1}^{4}\sum_{b=1}^{9} B_0\Big(p^2, m^2_{H_a^{--}}, m^2_{A^0{}_b}\Big)\Gamma^{*}_{\check{H}_j^{++},H_a^{--},A^0{}_b}\Gamma_{\check{H}_i^{++},H_a^{--},A^0{}_b}\\
&+ \sum_{a=1}^{4}\sum_{b=1}^{9} B_0\Big(p^2, m^2_{H_a^{--}}, m^2_{h_b}\Big)\Gamma^{*}_{\check{H}_j^{++},H_a^{--},h_b}\Gamma_{\check{H}_i^{++},H_a^{--},h_b} - 3\sum_{a=1}^{6} A_0\Big(m^2_{\tilde{d}_a}\Big)\Gamma_{\check{H}_i^{--},\check{H}_j^{++},\tilde{d}_a^*,\tilde{d}_a}\\
&- \sum_{a=1}^{6} A_0\Big(m^2_{\tilde{e}_a}\Big)\Gamma_{\check{H}_i^{--},\check{H}_j^{++},\tilde{e}_a^*,\tilde{e}_a} - 3\sum_{a=1}^{6} A_0\Big(m^2_{\tilde{u}_a}\Big)\Gamma_{\check{H}_i^{--},\check{H}_j^{++},\tilde{u}_a^*,\tilde{u}_a}\\
&- \frac{1}{2}\sum_{a=1}^{6} A_0\Big(m^2_{\tilde{\nu}_a^P}\Big)\Gamma_{\check{H}_i^{--},\check{H}_j^{++},\tilde{\nu}_a^P,\tilde{\nu}_a^P} - \frac{1}{2}\sum_{a=1}^{6} A_0\Big(m^2_{\tilde{\nu}_a^S}\Big)\Gamma_{\check{H}_i^{--},\check{H}_j^{++},\tilde{\nu}_a^S,\tilde{\nu}_a^S}\\
&+ \frac{1}{2}\sum_{a=1}^{6}\sum_{b=1}^{6} B_0\Big(p^2, m^2_{\tilde{e}_a}, m^2_{\tilde{e}_b}\Big)\Gamma^{*}_{\check{H}_j^{++},\tilde{e}_a,\tilde{e}_b}\Gamma_{\check{H}_i^{++},\tilde{e}_a,\tilde{e}_b}\\
&- \sum_{a=1}^{6} m_{\tilde{\chi}_a^-}\sum_{b=1}^{6} B_0\Big(p^2, m^2_{\tilde{\chi}_a^-}, m^2_{\tilde{\chi}_b^-}\Big)m_{\tilde{\chi}_b^-}\Big(\Gamma^{L*}_{\check{H}_j^{++},\tilde{\chi}_a^-,\tilde{\chi}_b^-}\Gamma^{R}_{\check{H}_i^{++},\tilde{\chi}_a^-,\tilde{\chi}_b^-} + \Gamma^{R*}_{\check{H}_j^{++},\tilde{\chi}_a^-,\tilde{\chi}_b^-}\Gamma^{L}_{\check{H}_i^{++},\tilde{\chi}_a^-,\tilde{\chi}_b^-}\Big)\\
&+ \frac{1}{2}\sum_{a=1}^{6}\sum_{b=1}^{6} G_0\Big(p^2, m^2_{\tilde{\chi}_a^-}, m^2_{\tilde{\chi}_b^-}\Big)\Big(\Gamma^{L*}_{\check{H}_j^{++},\tilde{\chi}_a^-,\tilde{\chi}_b^-}\Gamma^{L}_{\check{H}_i^{++},\tilde{\chi}_a^-,\tilde{\chi}_b^-} + \Gamma^{R*}_{\check{H}_j^{++},\tilde{\chi}_a^-,\tilde{\chi}_b^-}\Gamma^{R}_{\check{H}_i^{++},\tilde{\chi}_a^-,\tilde{\chi}_b^-}\Big)\\
&- \sum_{a=1}^{8} A_0\Big(m^2_{H_a^-}\Big)\Gamma_{\check{H}_i^{--},\check{H}_j^{++},H_a^+,H_a^-} + \frac{1}{2}\sum_{a=1}^{8}\sum_{b=1}^{8} B_0\Big(p^2, m^2_{H_a^-}, m^2_{H_b^-}\Big)\Gamma^{*}_{\check{H}_j^{++},H_a^-,H_b^-}\Gamma_{\check{H}_i^{++},H_a^-,H_b^-}\\
&- \frac{1}{2}\sum_{a=1}^{9} A_0\Big(m^2_{A^0{}_a}\Big)\Gamma_{\check{H}_i^{--},\check{H}_j^{++},A^0{}_a,A^0{}_a} - \frac{1}{2}\sum_{a=1}^{9} A_0\Big(m^2_{h_a}\Big)\Gamma_{\check{H}_i^{--},\check{H}_j^{++},h_a,h_a}\\
&+ \sum_{b=1}^{4}\Gamma^{*}_{\check{H}_j^{++},\gamma,H_b^{--}}\Gamma_{\check{H}_i^{++},\gamma,H_b^{--}}F_0\Big(p^2, m^2_{H_b^{--}}, 0\Big) + \sum_{b=1}^{4}\Gamma^{*}_{\check{H}_j^{++},Z,H_b^{--}}\Gamma_{\check{H}_i^{++},Z,H_b^{--}}F_0\Big(p^2, m^2_{H_b^{--}}, m^2_{Z}\Big)
\end{aligned}
$$

$$+\sum_{b=1}^{4}\Gamma^{*}_{\check{H}_j^{++},Z',H_b^{--}}\Gamma_{\check{H}_i^{++},Z',H_b^{--}}F_0\Big(p^2,m^2_{H_b^{--}},m^2_{Z'}\Big)$$
$$+\sum_{b=1}^{8}\Gamma^{*}_{\check{H}_j^{++},W^-,H_b^{-}}\Gamma_{\check{H}_i^{++},W^-,H_b^{-}}F_0\Big(p^2,m^2_{H_b^{-}},m^2_{W^-}\Big)$$
$$+\sum_{b=1}^{8}\Gamma^{*}_{\check{H}_j^{++},W'^-,H_b^{-}}\Gamma_{\check{H}_i^{++},W'^-,H_b^{-}}F_0\Big(p^2,m^2_{H_b^{-}},m^2_{W'^-}\Big)\,.$$

where Γ_{ijk} denotes the vertex factor between the particles i,j,k. A "ˇ" on a particle index in a vertex means that this particle is to be taken in the gauge eigenstate, *i.e.* its mixing matrix occurring in the vertex has to be replaced by the unit matrix, which is due to the fact that the self energy defined above denotes the 1-loop corrections to the mass matrix and not to the already diagonalized mass eigenvalues. The parameter $r_{\rm MS}$ depends on the regularization scheme and is zero for $\overline{\rm DR}$ and 1 for dimensional regularization. Since we work in a supersymmetric model we apply the $\overline{\rm DR}$ scheme.

A.2.2 1-loop corrections to the tadpoles

$$\begin{aligned}
\delta t_h^{(1)} = &\qquad\qquad\qquad\qquad\qquad\qquad\qquad\qquad\qquad\qquad\qquad \text{(A.339)}\\
&A_0\Big(m^2_{\eta_L^-}\Big)\Gamma_{\check{h}_i,\bar{\eta}_L^-,\eta_L^-}+A_0\Big(m^2_{\eta_L^+}\Big)\Gamma_{\check{h}_i,\bar{\eta}_L^+,\eta_L^+}+A_0\Big(m^2_{\eta_R^-}\Big)\Gamma_{\check{h}_i,\bar{\eta}_R^-,\eta_R^-}\\
&+A_0\Big(m^2_{\eta_R^+}\Big)\Gamma_{\check{h}_i,\bar{\eta}_R^+,\eta_R^+}+A_0\Big(m^2_{\eta^Z}\Big)\Gamma_{\check{h}_i,\bar{\eta}^Z,\eta^Z}+A_0\Big(m^2_{\eta^{Z'}}\Big)\Gamma_{\check{h}_i,\bar{\eta}^{Z'},\eta^{Z'}}\\
&+4\Gamma_{\check{h}_i,W^+,W^-}\Big(-\frac{1}{2}r_{\rm MS}m^2_{W^-}+A_0\Big(m^2_{W^-}\Big)\Big)+4\Gamma_{\check{h}_i,W'^+,W'^-}\Big(-\frac{1}{2}r_{\rm MS}m^2_{W'^-}+A_0\Big(m^2_{W'^-}\Big)\Big)\\
&+2\Gamma_{\check{h}_i,Z,Z}\Big(-\frac{1}{2}r_{\rm MS}m^2_{Z}+A_0\Big(m^2_{Z}\Big)\Big)+2\Gamma_{\check{h}_i,Z',Z'}\Big(-\frac{1}{2}r_{\rm MS}m^2_{Z'}+A_0\Big(m^2_{Z'}\Big)\Big)\\
&+2\sum_{a=1}^{2}A_0\Big(m^2_{\tilde{\chi}_a^{--}}\Big)m_{\tilde{\chi}_a^{--}}\Big(\Gamma^L_{\check{h}_i,\bar{\tilde{\chi}}_a^{--},\tilde{\chi}_a^{--}}+\Gamma^R_{\check{h}_i,\bar{\tilde{\chi}}_a^{--},\tilde{\chi}_a^{--}}\Big)\\
&+6\sum_{a=1}^{3}A_0\Big(m^2_{d_a}\Big)m_{d_a}\Big(\Gamma^L_{\check{h}_i,\bar{d}_a,d_a}+\Gamma^R_{\check{h}_i,\bar{d}_a,d_a}\Big)+2\sum_{a=1}^{3}A_0\Big(m^2_{e_a}\Big)m_{e_a}\Big(\Gamma^L_{\check{h}_i,\bar{e}_a,e_a}+\Gamma^R_{\check{h}_i,\bar{e}_a,e_a}\Big)\\
&+6\sum_{a=1}^{3}A_0\Big(m^2_{u_a}\Big)m_{u_a}\Big(\Gamma^L_{\check{h}_i,\bar{u}_a,u_a}+\Gamma^R_{\check{h}_i,\bar{u}_a,u_a}\Big)-\sum_{a=1}^{4}A_0\Big(m^2_{H_a^{--}}\Big)\Gamma_{\check{h}_i,H_a^{++},H_a^{--}}\\
&-3\sum_{a=1}^{6}A_0\Big(m^2_{\tilde{d}_a}\Big)\Gamma_{\check{h}_i,\tilde{d}_a^*,\tilde{d}_a}-\sum_{a=1}^{6}A_0\Big(m^2_{\tilde{e}_a}\Big)\Gamma_{\check{h}_i,\tilde{e}_a^*,\tilde{e}_a}-3\sum_{a=1}^{6}A_0\Big(m^2_{\tilde{u}_a}\Big)\Gamma_{\check{h}_i,\tilde{u}_a^*,\tilde{u}_a}\\
&-\frac{1}{2}\sum_{a=1}^{6}A_0\Big(m^2_{\tilde{\nu}_a^P}\Big)\Gamma_{\check{h}_i,\tilde{\nu}_a^P,\tilde{\nu}_a^P}-\frac{1}{2}\sum_{a=1}^{6}A_0\Big(m^2_{\tilde{\nu}_a^S}\Big)\Gamma_{\check{h}_i,\tilde{\nu}_a^S,\tilde{\nu}_a^S}\\
&+2\sum_{a=1}^{6}A_0\Big(m^2_{\tilde{\chi}_a^-}\Big)m_{\tilde{\chi}_a^-}\Big(\Gamma^L_{\check{h}_i,\bar{\tilde{\chi}}_a^-,\tilde{\chi}_a^-}+\Gamma^R_{\check{h}_i,\bar{\tilde{\chi}}_a^-,\tilde{\chi}_a^-}\Big)+\sum_{a=1}^{6}A_0\Big(m^2_{\nu_a}\Big)m_{\nu_a}\Big(\Gamma^L_{\check{h}_i,\nu_a,\nu_a}+\Gamma^R_{\check{h}_i,\nu_a,\nu_a}\Big)\\
&-\sum_{a=1}^{8}A_0\Big(m^2_{H_a^-}\Big)\Gamma_{\check{h}_i,H_a^+,H_a^-}-\frac{1}{2}\sum_{a=1}^{9}A_0\Big(m^2_{A^0{}_a}\Big)\Gamma_{\check{h}_i,A^0{}_a,A^0{}_a}-\frac{1}{2}\sum_{a=1}^{9}A_0\Big(m^2_{h_a}\Big)\Gamma_{\check{h}_i,h_a,h_a}\\
&+\sum_{a=1}^{12}A_0\Big(m^2_{\tilde{\chi}_a^0}\Big)m_{\tilde{\chi}_a^0}\Big(\Gamma^L_{\check{h}_i,\tilde{\chi}_a^0,\tilde{\chi}_a^0}+\Gamma^R_{\check{h}_i,\tilde{\chi}_a^0,\tilde{\chi}_a^0}\Big)\,,
\end{aligned}$$

$$\delta t^{(1)}_{\tilde{\nu}^S} = 0\,. \tag{A.340}$$

APPENDIX B

LOW ENERGY OBSERVABLES

The effective Lagrangian for the lepton flavour violating low energy observables $\ell_\alpha \to \ell_\beta\gamma$, $\ell_\alpha \to \ell_\beta\ell_\gamma\ell_\delta$ as well as $\mu - e$ conversion in nuclei can be written as

$$\mathcal{L}_{\text{LFV}} = \mathcal{L}_{\ell\ell\gamma} + \mathcal{L}_{4\ell} + \mathcal{L}_{2\ell 2d} + \mathcal{L}_{2\ell 2u}\,, \tag{B.1}$$

with

$$\mathcal{L}_{\ell\ell\gamma} = e\,\bar{\ell}_\beta\left[\gamma^\mu\left(K_1^L P_L + K_1^R P_R\right) + im_{\ell_\alpha}\sigma^{\mu\nu}q_\nu\left(K_2^L P_L + K_2^R P_R\right)\right]\ell_\alpha A_\mu + \text{h.c.} \tag{B.2}$$

$$\mathcal{L}_{4\ell} = \sum_{\substack{I=S,V,T\\X,Y=L,R}} A_{XY}^I\,\bar{\ell}_\beta\Gamma_I P_X\ell_\alpha\bar{\ell}_\delta\Gamma_I P_Y\ell_\gamma + \text{h.c.} \tag{B.3}$$

$$\mathcal{L}_{2\ell 2d} = \sum_{\substack{I=S,V,T\\X,Y=L,R}} B_{XY}^I\,\bar{\ell}_\beta\Gamma_I P_X\ell_\alpha\bar{d}_\gamma\Gamma_I P_Y d_\gamma + \text{h.c.} \tag{B.4}$$

$$\mathcal{L}_{2\ell 2u} = \mathcal{L}_{2\ell 2d}|_{d\to u,\,B\to C}\,. \tag{B.5}$$

Let us specify the conventions used above. In the first equation defining the $\ell_\alpha \to \ell_\beta\gamma$ interaction Lagrangian, e is the electric charge, A_μ the photon field and q its 4-momentum. $P_{L/R} = \frac{1}{2}(1 \mp \gamma_5)$ are the chirality projectors while the scalar, vector and tensor operators Γ_I read $\Gamma_S = 1$, $\Gamma_V = \gamma_\mu$ and $\Gamma_T = \sigma_{\mu\nu}$. The form factors K_i^X, A_{XY}^I and B_{XY}^I (C_{XY}^I) correspond to the effective vertices of the $\ell_\alpha \to \ell_\beta\gamma$, $\ell_\alpha \to \ell_\beta\ell_\gamma\ell_\delta$ and $\ell_\alpha d_\gamma \to \ell_\beta d_\gamma$ ($\ell_\alpha u_\gamma \to \ell_\beta u_\gamma$) interactions. For simplicity, their indices have been suppressed.

The decay widths/conversion rates of these processes in terms of the lepton masses and the form factors are defined in the following and we refer to ref. [196] for a complete account of all contributing Feynman diagrams as well the corresponding form factors.

B.1 Radiative decay: $\ell_\alpha \to \ell_\beta\gamma$

The width of the radiative decay $\ell_\alpha \to \ell_\beta\gamma$ takes the simple form [219]

$$\Gamma\left(\ell_\alpha \to \ell_\beta\gamma\right) = \frac{\alpha_{\rm em} m_{\ell_\alpha}^5}{4}\left(|K_2^L|^2 + |K_2^R|^2\right) , \tag{B.6}$$

with $K_2^{L,R}$ as defined in eq. (B.2) and the fine structure constant $\alpha_{\rm em} = e^2/(4\pi)$. Note that the monopole contribution coming from $K_1^{L,R}$ vanishes for on-shell photons and only contributes to photon-mediated three-body decays, see below.

B.2 Three-body decays

B.2.1 Same-flavour final state: $\ell_\alpha^- \to \ell_\beta^-\ell_\beta^-\ell_\beta^+$

We now consider the tree-body decays $\mu \to 3e$, $\tau \to 3e$ or $\tau \to 3\mu$. Defining the external momenta as $\ell_\alpha^-(p) \to \ell_\beta^-(p_1)\,\ell_\beta^-(p_2)\,\ell_\beta^+(p_3)$, the decay width is given by

$$\begin{aligned}
\Gamma\left(\ell_\alpha \to 3\,\ell_\beta\right) \;=\; & \frac{m_{\ell_\alpha}^5}{512\pi^3}\left[e^4\left(\left|K_2^L\right|^2 + \left|K_2^R\right|^2\right)\left(\frac{16}{3}\log\frac{m_{\ell_\alpha}}{m_{\ell_\beta}} - \frac{22}{3}\right)\right. \\
+ \; & \frac{1}{24}\left(\left|A_{LL}^S\right|^2 + \left|A_{RR}^S\right|^2\right) + \frac{1}{12}\left(\left|A_{LR}^S\right|^2 + \left|A_{RL}^S\right|^2\right) \\
+ \; & \frac{2}{3}\left(\left|\hat{A}_{LL}^V\right|^2 + \left|\hat{A}_{RR}^V\right|^2\right) + \frac{1}{3}\left(\left|\hat{A}_{LR}^V\right|^2 + \left|\hat{A}_{RL}^V\right|^2\right) + 6\left(\left|A_{LL}^T\right|^2 + \left|A_{RR}^T\right|^2\right) \\
+ \; & \frac{e^2}{3}\left(K_2^L A_{RL}^{S*} + K_2^R A_{LR}^{S*} + c.c.\right) - \frac{2e^2}{3}\left(K_2^L \hat{A}_{RL}^{V*} + K_2^R \hat{A}_{LR}^{V*} + c.c.\right) \\
- \; & \frac{4e^2}{3}\left(K_2^L \hat{A}_{RR}^{V*} + K_2^R \hat{A}_{LL}^{V*} + c.c.\right) \\
- \; & \left.\frac{1}{2}\left(A_{LL}^S A_{LL}^{T*} + A_{RR}^S A_{RR}^{T*} + c.c.\right) - \frac{1}{6}\left(A_{LR}^S \hat{A}_{LR}^{V*} + A_{RL}^S \hat{A}_{RL}^{V*} + c.c.\right)\right] ,
\end{aligned} \tag{B.7}$$

where the mass of the final state leptons has been neglected but for the prefactors multiplying $K_2^{L,R}$. The photonic monopole form factors have been absorbed in the definition of the vectorial operators $\hat{A}^V$:

$$\hat{A}_{XY}^V = A_{XY}^V + e^2 K_1^X \qquad (X, Y = L, R) . \tag{B.8}$$

Note that eq. (B.7) agrees with ref. [216] and, although the form of eq. (B.7) differs from the corresponding formula given in ref. [189], both are in agreement. The reason for that is that the scalar form factors A_{LR}^S and A_{RL}^S as in eq. (B.7) have been absorbed in the corresponding vector form factors A_{LR}^V and A_{RL}^V in [189] by means of a Fierz transformation [220].

B.2.2 Final state of differing flavour: $\ell_\alpha^- \to \ell_\beta^- \ell_\gamma^- \ell_\gamma^+$

We next consider the three-body decay $\ell_\alpha^-(p) \to \ell_\beta^-(p_1)\,\ell_\gamma^-(p_2)\,\ell_\gamma^+(p_3)$ with $\beta \neq \gamma$. The decay width is given by

$$\begin{aligned}\Gamma\left(\ell_\alpha^- \to \ell_\beta^-\ell_\gamma^-\ell_\gamma^+\right) &= \frac{m_{\ell_\alpha}^5}{512\pi^3}\left[e^4\left(\left|K_2^L\right|^2+\left|K_2^R\right|^2\right)\left(\frac{16}{3}\log\frac{m_{\ell_\alpha}}{m_{\ell_\gamma}}-8\right)\right. \\ &+ \frac{1}{12}\left(\left|A_{LL}^S\right|^2+\left|A_{RR}^S\right|^2\right)+\frac{1}{12}\left(\left|A_{LR}^S\right|^2+\left|A_{RL}^S\right|^2\right) \\ &+ \frac{1}{3}\left(\left|\hat{A}_{LL}^V\right|^2+\left|\hat{A}_{RR}^V\right|^2\right)+\frac{1}{3}\left(\left|\hat{A}_{LR}^V\right|^2+\left|\hat{A}_{RL}^V\right|^2\right)+4\left(\left|A_{LL}^T\right|^2+\left|A_{RR}^T\right|^2\right) \\ &- \left.\frac{2e^2}{3}\left(K_2^L\hat{A}_{RL}^{V*}+K_2^R\hat{A}_{LR}^{V*}+K_2^L\hat{A}_{RR}^{V*}+K_2^R\hat{A}_{LL}^{V*}+c.c.\right)\right],\end{aligned} \tag{B.9}$$

where we have used the same definitions and approximations as in eq. (B.7). Finally, also eq. (B.9) is in perfect agreement with the expressions given in ref. [216].

B.2.3 Final state of differing flavour: $\ell_\alpha^- \to \ell_\beta^+ \ell_\gamma^- \ell_\gamma^-$

The decay width of the process $\ell_\alpha^-(p) \to \ell_\beta^+(p_1)\,\ell_\gamma^-(p_2)\,\ell_\gamma^-(p_3)$, $\beta \neq \gamma$, is given by

$$\begin{aligned}\Gamma\left(\ell_\alpha^- \to \ell_\beta^+\ell_\gamma^-\ell_\gamma^-\right) &= \frac{m_{\ell_\alpha}^5}{512\pi^3}\left[\frac{1}{24}\left(\left|A_{LL}^S\right|^2+\left|A_{RR}^S\right|^2\right)+\frac{1}{12}\left(\left|A_{LR}^S\right|^2+\left|A_{RL}^S\right|^2\right)\right. \\ &+ \frac{2}{3}\left(\left|\hat{A}_{LL}^V\right|^2+\left|\hat{A}_{RR}^V\right|^2\right)+\frac{1}{3}\left(\left|\hat{A}_{LR}^V\right|^2+\left|\hat{A}_{RL}^V\right|^2\right)+6\left(\left|A_{LL}^T\right|^2+\left|A_{RR}^T\right|^2\right) \\ &- \left.\frac{1}{2}\left(A_{LL}^S A_{LL}^{T*}+A_{RR}^S A_{RR}^{T*}+c.c.\right)-\frac{1}{6}\left(A_{LR}^S\hat{A}_{LR}^{V*}+A_{RL}^S\hat{A}_{RL}^{V*}+c.c.\right)\right],\end{aligned} \tag{B.10}$$

using the same conventions as in eq. (B.7). This process does not receive any contribution from penguin diagrams but only from boxes.

B.3 Coherent $\mu - e$ conversion in nuclei

For the discussion of $\mu-e$ conversion in nuclei we follow the conventions and approximations described in Ref. [221, 222][1] The conversion rate, relative to the the muon capture rate, is given by

$$\begin{aligned}\mathrm{CR}(\mu-e,\mathrm{Nucleus}) &= \frac{p_e\,E_e\,m_\mu^3\,G_F^2\,\alpha_{\mathrm{em}}^3\,Z_{\mathrm{eff}}^4\,F_p^2}{8\,\pi^2\,Z} \\ &\times\left\{\left|(Z+N)\left(g_{LV}^{(0)}+g_{LS}^{(0)}\right)+(Z-N)\left(g_{LV}^{(1)}+g_{LS}^{(1)}\right)\right|^2+\right.\end{aligned}$$

[1] See also [223–225] for detailed works regarding the effective Lagrangian at the nucleon level, [214, 226] for a calculation including the effects of the atomic electric field and [227] for recent improvements on the hadronic uncertainties.

$$\left|(Z+N)\left(g_{RV}^{(0)}+g_{RS}^{(0)}\right)+(Z-N)\left(g_{RV}^{(1)}+g_{RS}^{(1)}\right)\right|^2\Bigg\}\frac{1}{\Gamma_{\rm capt}}\,, \tag{B.11}$$

Z and N being the number of protons and neutrons in the nucleus and $Z_{\rm eff}$ the effective atomic charge [228]. G_F is the usual Fermi constant, F_p the nuclear matrix element and $\Gamma_{\rm capt}$ the total muon capture rate. E_e and p_e (which is $\simeq m_\mu$ in our numerical evaluation) denote the electron momentum and energy and m_μ the muon mass. The coupling parameters $g_{XK}^{(0)}$ and $g_{XK}^{(1)}$ (with $X=L,R$ and $K=S,V$) can be written in terms of effective couplings at the quark level as

$$\begin{aligned} g_{XK}^{(0)} &= \frac{1}{2}\sum_{q=u,d,s}\left(g_{XK(q)}G_K^{(q,p)}+g_{XK(q)}G_K^{(q,n)}\right)\,,\\ g_{XK}^{(1)} &= \frac{1}{2}\sum_{q=u,d,s}\left(g_{XK(q)}G_K^{(q,p)}-g_{XK(q)}G_K^{(q,n)}\right)\,. \end{aligned} \tag{B.12}$$

Only the scalar (S) and vector (V) couplings contribute to coherent $\mu-e$ conversion in nuclei [221], and the only sizeable contributions are expected from the up, down and strange quarks. The numerical values of the relevant G_K factors are [221, 229]

$$\begin{aligned} G_V^{(u,p)} &= G_V^{(d,n)} = 2\,; \quad G_V^{(d,p)} = G_V^{(u,n)} = 1\,;\\ G_S^{(u,p)} &= G_S^{(d,n)} = 5.1\,; \quad G_S^{(d,p)} = G_S^{(u,n)} = 4.3\,;\\ G_S^{(s,p)} &= G_S^{(s,n)} = 2.5\,. \end{aligned} \tag{B.13}$$

Finally, the $g_{XK(q)}$ coefficients can be written in terms of the form factors in eqs. (B.2-B.5) as

$$g_{LV(q)} = \frac{\sqrt{2}}{G_F}\left[e^2Q_q\left(K_1^L-K_2^R\right)-\frac{1}{2}\left(C_{\ell\ell qq}^{VLL}+C_{\ell\ell qq}^{VLR}\right)\right] \tag{B.14}$$

$$g_{RV(q)} = g_{LV(q)}\big|_{L\to R} \tag{B.15}$$

$$g_{LS(q)} = -\frac{\sqrt{2}}{G_F}\frac{1}{2}\left(C_{\ell\ell qq}^{SLL}+C_{\ell\ell qq}^{SLR}\right) \tag{B.16}$$

$$g_{RS(q)} = g_{LS(q)}\big|_{L\to R}\,, \tag{B.17}$$

Q_q being the electric charge ($Q_d=-1/3$, $Q_u=2/3$), and $C_{\ell\ell qq}^{IXK}=B_{XY}^K\,(C_{XY}^K)$ for d-quarks (u-quarks), with $X=L,R$ and $K=S,V$.

B.4 Decoupling of the Z penguin contributions

Here we discuss in more detail the circumstances and errors that led to the reported non-decoupling of lepton flavour violating Z-penguin diagrams. The results of this section have been published in ref. [195].

It is common to parameterise loop-induced flavour violating couplings in terms of effective vertices. The processes we are interested in here feature effective couplings

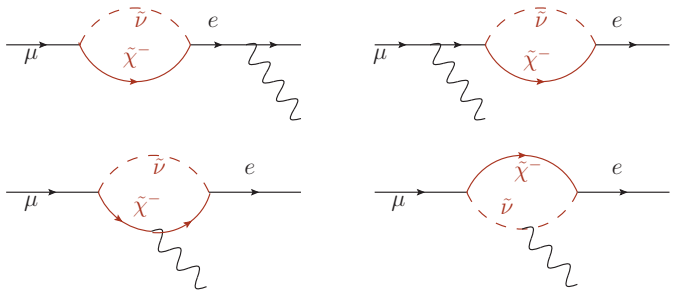

Figure B.1: Chargino-sneutrino loops contributing to the effective $\mu - e - Z$ coupling.

$\ell_i - \ell_j - Z$ which can be written as

$$\bar{\ell}_j \gamma_\mu \big(F_L P_L + F_R P_R\big) \ell_i Z^\mu \,. \tag{B.18}$$

Here, $P_{L/R}$ are the usual left/right projection operators, and $F_{L,R}$ are the form factors which contain the different loop-induced contributions to this vertex. $F_{L,R}$ contribute to the three-body decays $\ell_j \to \ell_i \ell_k^+ \ell_k^-$ [189], $\mu - e$ conversion in nuclei [222] as well as τ mesonic LFV decays [230].

In ref. [189], the contributions from supersymmetric loops containing charginos and sneutrinos as shown in figure B.1 were calculated as

$$\begin{aligned} &F_L^{(c)}|_{\text{AH}} = \\ &-\frac{1}{16\pi^2}\Big(C_{iBX}^R C_{jAX}^{R*}\big(2E_{BA}^{R(c)} C_{24}(m^2_{\tilde{\nu}_X}, m^2_{\tilde{\chi}_A^-}, m^2_{\tilde{\chi}_B^-}) - E_{BA}^{L(c)} m_{\tilde{\chi}_A^-} m_{\tilde{\chi}_B^-} C_0(m^2_{\tilde{\nu}_X}, m^2_{\tilde{\chi}_A^-}, m^2_{\tilde{\chi}_B^-})\big) \\ &+ C_{iAX}^R C_{jAY}^{R*}\big(2Q^{\tilde{\nu}}_{XY} C_{24}(m^2_{\tilde{\chi}_A^-}, m^2_{\tilde{\nu}_X}, m^2_{\tilde{\nu}_Y})\big) + C_{iAX}^R C_{jAX}^{R*} Z_L^{(\ell)} B_1(m^2_{\tilde{\chi}_A^-}, m^2_{\tilde{\nu}_X})\Big)\,, \end{aligned} \tag{B.19}$$

where C_{iAX}^R, $E_{BA}^{R(c),L(c)}$, $Q^{\tilde{\nu}}_{XY}$ and $Z_L^{(\ell)}$ denote the $\tilde{\chi}_A - \ell_i - \tilde{\nu}_X$, $\tilde{\chi}^A - \tilde{\chi}^B - Z$, $\tilde{\nu}_X - \tilde{\nu}_Y - Z$ and $\ell - \ell - Z$ couplings, respectively. C_0 and B_1 are well-known Passarino-Veltman loop functions evaluated in the limit of vanishing external momenta. Combining the definitions provided in [189] and [231], C_{24} is given by

$$4\, C_{24}(m_0^2, m_1^2, m_2^2) = B_0(m_1^2, m_2^2) + m_0^2 C_0(m_0^2, m_1^2, m_2^2)\,. \tag{B.20}$$

For the detailed definitions see section B.4.1 or ref. [189]. The form factor F_R can be neglected to a good approximation as all contributions thereto require a chirality flip and are hence proportional to the Yukawa couplings of the charged leptons.

It has been first observed in ref. [193] that $F_L^{(c)}|_{\text{AH}}$ contains non-decoupling terms for certain types of supersymmetric models, in particular for models featuring an inverse seesaw mechanism or R-parity violation. As those terms cannot depend on the chargino mixing angle ϕ_χ, one can concentrate on the leading parts $F^{(c,0)}$ in the expansion in ϕ_χ; while doing so, we split the form factor into the wino and higgsino contributions $\mathcal{F}_L^{\tilde{W}(0)}$ and $\mathcal{F}_L^{\tilde{H}(0)}$:

$$F^{(c,0)} = -\frac{1}{16\pi^2}\left(\mathcal{F}_L^{\tilde{W}(0)} + \mathcal{F}_L^{\tilde{H}(0)}\right)\,. \tag{B.21}$$

In ref. [194], the origin of the terms leading to the non-decoupling effect were identified for the MSSM extended by an inverse seesaw mechanism, as is used in chapter 5. In particular, it has been found that the leading-order higgsino contribution contains a term which only depends on the gauge and Yukawa couplings:

$$\mathcal{F}_L^{\tilde{H}(0)} = \frac{g}{8\cos\theta_W}\left(Y_\nu^\dagger Y_\nu\right)_{ij}(\cos^2\theta_W - \frac{1}{2})\,. \tag{B.22}$$

As $Y_\nu^\dagger Y_\nu$ is in general non-diagonal, this coupling induces an effective $\ell_i - \ell_j - Z$ vertex which stays constant, irrespective of the mass scale of the virtual particles in the loop, *i.e.* that doesn't decouple.

Motivated by this puzzling finding we re-computed the underlying form factor and found a slightly different result:

$$\begin{aligned} F_L^{(c)} = -\frac{1}{16\pi^2}\Big(&C_{iBX}^R C_{jAX}^{R*}\big(E_{BA}^{R(c)}\big[B_0(m^2_{\tilde{\chi}_A^-}, m^2_{\tilde{\chi}_B^-}) - 2C_{00}(m^2_{\tilde{\nu}_X}, m^2_{\tilde{\chi}_A^-}, m^2_{\tilde{\chi}_B^-}) \\ &+ m^2_{\tilde{\nu}_X} C_0(m^2_{\tilde{\nu}_X}, m^2_{\tilde{\chi}_A^-}, m^2_{\tilde{\chi}_B^-})\big] - E_{BA}^{L(c)} m_{\tilde{\chi}_A^-} m_{\tilde{\chi}_B^-} C_0(m^2_{\tilde{\nu}_X}, m^2_{\tilde{\chi}_A^-}, m^2_{\tilde{\chi}_B^-})\big) \\ &+ C_{iAX}^R C_{jAY}^{R*}\big(2Q^{\tilde{\nu}}_{XY} C_{00}(m^2_{\tilde{\chi}_A^-}, m^2_{\tilde{\nu}_X}, m^2_{\tilde{\nu}_Y})\big) + C_{iAX}^R C_{jAX}^{R*} Z_L^{(\ell)} B_1(m^2_{\tilde{\chi}_A^-}, m^2_{\tilde{\nu}_X})\Big)\,. \end{aligned} \tag{B.23}$$

Using the analytical relation between the loop functions B_0, C_0 and C_{00}

$$D\,C_{00}(m_0^2, m_1^2, m_2^2) = B_0(m_1^2, m_2^2) + m_0^2 C_0(m_0^2, m_1^2, m_2^2)\,, \tag{B.24}$$

we can now compare our result to eq. (B.19). In the above, $D = 4 - 2\,\varepsilon$ as commonly used in dimensional regularization/reduction, and $D\,C_{00} = 4\,C_{00} - \frac{1}{2}$ because of a $\frac{1}{4\,\varepsilon}$ singularity within C_{00}. Using eq. (B.24) together with (B.20), we can identify $C_{24} = C_{00} - \frac{1}{8}$.

We find that our result would agree with eq. (B.19) if we made the mistake of neglecting ε when applying D to C_{00} so that $D\,C_{00} \to 4\,C_{00}$ and if we in addition identified C_{24} with C_{00}. It is hence clear that the differences between our form factor and the one of [189] are two constant terms which originate from the handling of $1/\varepsilon$ singularities as well as a wrong definition of C_{24}. In the following it is shown how using the correct form factor disproves the non-decoupling claims by an explicit re-evaluation of eq. (B.22) as well as the analytical results of ref. [193].

To do so, we first extract the parts of $F_L^{(c)}$ proportional to $Y_\nu^\dagger Y_\nu$, corresponding to a projection on the higgsinos in the loop. We find

$$\mathcal{F}_L^{\tilde{H}} = -\frac{1}{4}\sum_{P,S} Y^*_{\nu,ai} Y_{\nu,bj} V_{B2} V^*_{A2}\left(\mathcal{A}^{\text{wave}}_{abAB} + \mathcal{A}^{\chi}_{abAB} + \mathcal{A}^{\nu}_{abAB}\right), \tag{B.25}$$

$$\begin{aligned} \mathcal{A}^{\text{wave}}_{abAB} =& -Z^{P/S*}_{X,3+a} Z^{P/S*}_{X,3+b}\delta_{BA}\left(g_2\cos\theta_W - g_1\sin\theta_W\right) B_1(m^2_{\tilde{\chi}_A^-}, m^2_{\tilde{\nu}_X})\,, \\ \mathcal{A}^{\chi}_{abAB} =& Z^{P/S*}_{X,3+a} Z^{P/S*}_{X,3+b}\Big[\Big(2g_2\cos\theta_W V^*_{B1} V_{A1} + V^*_{B2} V_{A2}\left(g_2\cos\theta_W - g_1\sin\theta_W\right)\Big)\times \\ &\Big(2C_{00}(m^2_{\tilde{\nu}_X}, m^2_{\tilde{\chi}_A^-}, m^2_{\tilde{\chi}_B^-}) - B_0(m^2_{\tilde{\chi}_A^-}, m^2_{\tilde{\chi}_B^-}) - m^2_{\tilde{\nu}_X} C_0(m^2_{\tilde{\nu}_X}, m^2_{\tilde{\chi}_A^-}, m^2_{\tilde{\chi}_B^-})\Big) + \\ &\Big(\left(2g_2\cos\theta_W U^*_{A1} U_{B1} + U^*_{A2} U_{B2}(g_2\cos\theta_W - g_1\sin\theta_W)\right) m_{\tilde{\chi}_A} m_{\tilde{\chi}_B} C_0(m^2_{\tilde{\nu}_X}, m^2_{\tilde{\chi}_A^-}, m^2_{\tilde{\chi}_B^-})\Big]\,, \\ \mathcal{A}^{\nu}_{abAB} =& \left(g_2\cos\theta_W + g_1\sin\theta_W\right)\delta_{BA} Z^{P/S*}_{Xc} Z^{S/P*}_{Yc} Z^{P/S*}_{X,3+a} Z^{S/P*}_{Y,3+b} 2C_{00}(m^2_{\tilde{\chi}_A^-}, m^2_{\tilde{\nu}_X}, m^2_{\tilde{\nu}_Y})\,. \end{aligned}$$

Here, we have distinguished between the CP-even and CP-odd sneutrino eigenstates $\tilde{\nu}^S$ and $\tilde{\nu}^P$ because of the mass splitting induced by the lepton number violating terms μ_X and B_{μ_X}, see eq. (5.11). $Z^{S/P}$ are the sneutrino mixing matrices, and $m_{\tilde{\nu}_k}$ corresponds to the respective CP-state, with the index k covering all mass eigenstates. U and V are the unitary matrices diagonalizing the chargino mass matrix; $k1$ and $k2$ project on the wino and higgsino component of $\tilde{\chi}_k^\pm$, respectively. Sums over repeated indices are implicitly understood and $a, b, c = 1, \ldots, 3$. In the limit of $U, V \to \mathbf{1}$, *i.e.* of no chargino mixing, eq. (B.25) reduces to

$$\begin{aligned}
\mathcal{F}_L^{\tilde{H}(0)} &= -\frac{1}{4}\sum_{P,S} Y^*_{\nu,ai} Y_{\nu,bj} \big(g_2 \cos\theta_W - g_1 \sin\theta_W\big) \mathcal{A}^{\text{sum}}_{ab}\,, \qquad \text{(B.26)}\\
\mathcal{A}^{\text{sum}}_{ab} &= Z^{P/S*}_{X,3+a} Z^{P/S*}_{X,3+b} \Big(- B_1(m^2_{\tilde{\chi}_2^-}, m^2_{\tilde{\nu}_X}) + (m^2_{\tilde{\chi}_2^-} - m^2_{\tilde{\nu}_X}) C_0(m^2_{\tilde{\nu}_X}, m^2_{\tilde{\chi}_2^-}, m^2_{\tilde{\chi}_2^-}) \\
&\quad + 2C_{00}(m^2_{\tilde{\nu}_X}, m^2_{\tilde{\chi}_2^-}, m^2_{\tilde{\chi}_2^-}) - B_0(m^2_{\tilde{\chi}_2^-}, m^2_{\tilde{\chi}_2^-}) \Big) \\
&\quad + 2 Z^{P/S*}_{Xc} Z^{S/P*}_{Yc} Z^{P/S*}_{X,3+a} Z^{S/P*}_{Y,3+b} C_{00}(m^2_{\tilde{\chi}_2^-}, m^2_{\tilde{\nu}_X}, m^2_{\tilde{\nu}_Y})\,.
\end{aligned}$$

In the limit of no left-right mixing in the sneutrino sector, this expression further simplifies to

$$\begin{aligned}
\mathcal{A}^{\text{sum}}_{ab} &= Z^{P/S*}_{X,3+a} Z^{P/S*}_{X,3+b} \Big(- B_1(m^2_{\tilde{\chi}_2^-}, m^2_{\tilde{\nu}_X}) + (m^2_{\tilde{\chi}_2^-} - m^2_{\tilde{\nu}_X}) C_0(m^2_{\tilde{\nu}_X}, m^2_{\tilde{\chi}_2^-}, m^2_{\tilde{\chi}_2^-}) \\
&\quad + 2C_{00}(m^2_{\tilde{\nu}_X}, m^2_{\tilde{\chi}_2^-}, m^2_{\tilde{\chi}_2^-}) - B_0(m^2_{\tilde{\chi}_2^-}, m^2_{\tilde{\chi}_2^-}) \Big) \qquad \text{(B.27)}\\
&= Z^{P/S*}_{X,3+a} Z^{P/S*}_{X,3+b} \Big(- B_1(m^2_{\tilde{\chi}_2^-}, m^2_{\tilde{\nu}_X}) + m^2_{\tilde{\chi}_2^-} C_0(m^2_{\tilde{\nu}_X}, m^2_{\tilde{\chi}_2^-}, m^2_{\tilde{\chi}_2^-}) \\
&\quad - 2C_{00}(m^2_{\tilde{\nu}_X}, m^2_{\tilde{\chi}_2^-}, m^2_{\tilde{\chi}_2^-}) + \frac{1}{2} \Big)\,. \qquad \text{(B.28)}\\
&= 0\,.
\end{aligned}$$

One can easily confirm that $\mathcal{A}^{\text{sum}}_{ab}$ vanishes when explicitly inserting the analytic forms of the loop functions given in section B.4.1. The step from eq. (B.27) to eq. (B.28) has been done for a better comparison with the results from ref. [194], using eq. (B.24). The difference of a mass-independent constant term of $\frac{1}{4}$ leads to the disappearance of the reported non-decoupling contribution (B.22).[2]

For completeness, we now also provide the results for the pure wino contribution. In [193, 194] it was reported that the off-diagonal (*i.e.* flavour-changing) parts of $\mathcal{F}_L^{\tilde{W}(0)}$ vanish in the MSSM limit (*i.e.* no sneutrino left-right mixing and no mass splitting of the CP eigenstates) because of the unitarity of the sneutrino mixing matrix while the diagonal parts remain finite. Defining

$$\mathcal{F}_L^{\tilde{W}(0)} = -\frac{1}{4}\sum_{P,S} g_2^2 \big(g_2 \cos\theta_W Y_1 + g_1 \sin\theta_W Y_2\big)\,, \qquad \text{(B.29)}$$

they found $Y_1 \to \text{diag}(-\frac{3}{4})$ and $Y_2 \to \text{diag}(-\frac{1}{4})$. Using the correct equations, however, we

[2] The additional different overall factor of $\frac{1}{2}$ between the above equation and the result in ref. [194] can be traced back to the part where $Z^{P/S*}_{X,3+a} Z^{P/S*}_{X,3+b} = \delta_{ba}$ which was erroneously taken to be $\frac{1}{2}\delta_{ba}$ in ref. [194].

arrive at

$$\begin{aligned} Y_1 =& Z_{Xi}^{P/S*} Z_{Xj}^{P/S*} \Big(- B_1(m^2_{\tilde{\chi}_1^-}, m^2_{\tilde{\nu}_X}) + 2(m^2_{\tilde{\chi}_1^-} - m^2_{\tilde{\nu}_X}) C_0(m^2_{\tilde{\nu}_X}, m^2_{\tilde{\chi}_1^-}, m^2_{\tilde{\chi}_1^-}) \\ &+ 4C_{00}(m^2_{\tilde{\nu}_X}, m^2_{\tilde{\chi}_1^-}, m^2_{\tilde{\chi}_1^-}) - 2B_0(m^2_{\tilde{\chi}_1^-}, m^2_{\tilde{\chi}_1^-}) \Big) \qquad \text{(B.30)} \\ &+ 2Z_{Xc}^{P/S*} Z_{Yc}^{S/P*} Z_{Xi}^{P/S*} Z_{Yj}^{S/P*} C_{00}(m^2_{\tilde{\chi}_1^-}, m^2_{\tilde{\nu}_X}, m^2_{\tilde{\nu}_Y}) \,, \qquad \text{(B.31)} \\ Y_2 =& Z_{Xi}^{P/S*} Z_{Xj}^{P/S*} B_1(m^2_{\tilde{\chi}_1^-}, m^2_{\tilde{\nu}_X}) + 2Z_{Xc}^{P/S*} Z_{Yc}^{S/P*} Z_{Xi}^{P/S*} Z_{Yj}^{S/P*} C_{00}(m^2_{\tilde{\chi}_1^-}, m^2_{\tilde{\nu}_X}, m^2_{\tilde{\nu}_Y}) \,. \end{aligned}$$

Both contributions vanish exactly in the MSSM limit because of an exact cancellation of the different loop functions, *i.e.* also the diagonal entries vanish and $Y_1 = Y_2 = 0$. Although the conclusion for LFV amplitudes is the same, the cancellation of the off-diagonal wino contributions happens due to a different reason. Compared to [193, 194], Y_1 differs by a constant term originating from the handling of the $1/\varepsilon$ singularities whereas Y_2 vanishes because of correct the usage of C_{00} instead of the ill-defined C_{24}.

Departing from the limits of no chargino mixing or no sneutrino left-right mixing of course re-introduces off-diagonal terms for both, wino and higgsino amplitudes. Because of the sole origin in the particle mixing, those amplitudes drop with the mass of the loop particles, hence decoupling with the SUSY mass scale. This is beautifully seen in the numerical examples for $\mu \to 3\,e$ and $\mu - e$ conversion in figures 5.3-5.4.

B.4.1 Relevant vertices and loop functions

The vertices relevant for the derivations above read for the supersymmetric inverse seesaw model:

$$C^R_{iAX(P)} = \Gamma^R_{\bar{e}_i \tilde{\chi}_A^- \tilde{\nu}_X^P} = -\frac{i}{\sqrt{2}} \Big(g_2 Z^{P,*}_{Xi} V_{A1} - \sum_{a=1}^{3} Y^*_{\nu,ai} Z^{P,*}_{X3+a} V_{A2} \Big) \,, \qquad \text{(B.32)}$$

$$C^R_{iAX(S)} = \Gamma^R_{\bar{e}_i \tilde{\chi}_A^- \tilde{\nu}_X^S} = -\frac{1}{\sqrt{2}} \Big(g_2 Z^{S,*}_{Xi} V_{A1} - \sum_{a=1}^{3} Y^*_{\nu,ai} Z^{S,*}_{X3+a} V_{A2} \Big) \,, \qquad \text{(B.33)}$$

$$E^{L(c)}_{BA} = \Gamma^L_{\tilde{\chi}_B^+ \tilde{\chi}_A^- Z_\mu} = \frac{1}{2} \Big(2g_2 U^*_{A1} \cos\theta_W U_{B1} + U^*_{A2} \Big(- g_1 \sin\theta_W + g_2 \cos\theta_W \Big) U_{B2} \Big) \,, \qquad \text{(B.34)}$$

$$E^{R(c)}_{BA} = \Gamma^R_{\tilde{\chi}_B^+ \tilde{\chi}_A^- Z_\mu} = \frac{1}{2} \Big(2g_2 V^*_{B1} \cos\theta_W V_{A1} + V^*_{B2} \Big(- g_1 \sin\theta_W + g_2 \cos\theta_W \Big) V_{A2} \Big) \,, \qquad \text{(B.35)}$$

$$Q^{\tilde{\nu}}_{XY} = \Gamma_{\tilde{\nu}_X^P \tilde{\nu}_Y^S Z_\mu} = -\frac{i}{2} \Big(g_1 \sin\theta_W + g_2 \cos\theta_W \Big) \sum_{a=1}^{3} Z^{P,*}_{Xa} Z^{S,*}_{Ya} \,, \qquad \text{(B.36)}$$

$$Z^{(\ell)}_L = \Gamma^L_{\bar{e}_i e_i Z_\mu} = \frac{1}{2} \Big(- g_1 \sin\theta_W + g_2 \cos\theta_W \Big) \,. \qquad \text{(B.37)}$$

The loop functions needed for the above discussion read in the limit of vanishing external momenta:

$$B_0(m_1^2, m_2^2) = -\log\left(\frac{m_2^2}{Q^2}\right) + \frac{1}{m_2^2 - m_1^2} \left[m_2^2 - m_1^2 + m_1^2 \log\left(\frac{m_1^2}{m_2^2}\right) \right] , \qquad \text{(B.38)}$$

$$B_1(m_1^2, m_2^2) = -\frac{1}{2} + \frac{1}{2}\log\left(\frac{m_2^2}{Q^2}\right) - \frac{1}{4(m_1^2 - m_2^2)^2}\Big[m_1^4 - m_2^4 + 2m_1^4 \log\left(\frac{m_2^2}{m_1^2}\right)\Big], \tag{B.39}$$

$$C_0(m_1^2, m_2^2, m_3^2) = \frac{1}{(m_1^2 - m_2^2)(m_3^2 - m_1^2)(m_2^2 - m_3^2)} \times \Big[m_2^2(m_3^2 - m_1^2)\log\left(\frac{m_2^2}{m_1^2}\right) + m_3^2(m_1^2 - m_2^2)\log\left(\frac{m_3^2}{m_1^2}\right)\Big], \tag{B.40}$$

$$C_{00}(m_1^2, m_2^2, m_3^2) = \frac{1}{8(m_1^2 - m_2^2)(m_1^2 - m_3^2)(m_2^2 - m_3^2)} \times \Big[(m_3^2 - m_1^2)\left((m_1^2 - m_2^2)(2\log\left(\frac{m_1^2}{Q^2}\right) - 3)(m_2^2 - m_3^2) - 2m_2^4 \log\left(\frac{m_2^2}{m_1^2}\right)\right) + 2m_3^4(m_2^2 - m_1^2)\log\left(\frac{m_3^2}{m_1^2}\right)\Big]. \tag{B.41}$$

LIST OF FIGURES

LIST OF TABLES

REFERENCES

[1] L. Evans and P. Bryant, *LHC Machine*, *JINST* **3** (2008) S08001.

[2] F. Englert and R. Brout, *Broken Symmetry and the Mass of Gauge Vector Mesons*, *Phys. Rev. Lett.* **13** (1964) 321–323.

[3] P. W. Higgs, *Broken Symmetries and the Masses of Gauge Bosons*, *Phys. Rev. Lett.* **13** (1964) 508–509.

[4] **ATLAS** Collaboration, G. Aad et al., *Combined search for the Standard Model Higgs boson using up to 4.9 fb^{-1} of pp collision data at $\sqrt{s} = 7$ TeV with the ATLAS detector at the LHC*, *Phys.Lett.* **B710** (2012) 49–66, [arXiv:1202.1408].

[5] **CMS** Collaboration, S. Chatrchyan et al., *Combined results of searches for the standard model Higgs boson in pp collisions at $\sqrt{s} = 7$ TeV*, *Phys.Lett.* **B710** (2012) 26–48, [arXiv:1202.1488].

[6] **ATLAS** Collaboration, *Exotics Public Results*, *twiki.cern.ch/AtlasPublic/ExoticsPublicResults*.

[7] **CMS** Collaboration, *Exotica Public Physics Results*, *twiki.cern.ch/CMSPublic/PhysicsResultsEXO*.

[8] J. Wess and B. Zumino, *Supergauge Transformations in Four-Dimensions*, *Nucl. Phys.* **B70** (1974) 39–50.

[9] J. Wess and B. Zumino, *A Lagrangian Model Invariant Under Supergauge Transformations*, *Phys.Lett.* **B49** (1974) 52.

[10] G. 't Hooft, *Naturalness, chiral symmetry, and spontaneous chiral symmetry breaking*, *NATO Adv.Study Inst.Ser.B Phys.* **59** (1980) 135.

[11] W. A. Bardeen, *On naturalness in the standard model*, 1995.

[12] G. Marques Tavares, M. Schmaltz, and W. Skiba, *Higgs mass naturalness and scale invariance in the UV*, *Phys.Rev.* **D89** (2014), no. 1 015009, [arXiv:1308.0025].

[13] G. Panico and A. Wulzer, *The Composite Nambu-Goldstone Higgs*, arXiv:1506.01961.

[14] M. Schmaltz and D. Tucker-Smith, *Little Higgs review*, *Ann.Rev.Nucl.Part.Sci.* **55** (2005) 229–270, [hep-ph/0502182].

[15] N. Arkani-Hamed, S. Dimopoulos, and G. R. Dvali, *The Hierarchy problem and new dimensions at a millimeter*, *Phys. Lett.* **B429** (1998) 263–272, [hep-ph/9803315].

[16] L. Randall and R. Sundrum, *A Large mass hierarchy from a small extra dimension*, *Phys. Rev. Lett.* **83** (1999) 3370–3373, [hep-ph/9905221].

[17] R. Barbieri and G. F. Giudice, *Upper Bounds on Supersymmetric Particle Masses*, *Nucl. Phys.* **B306** (1988) 63.

[18] H. Georgi, H. R. Quinn, and S. Weinberg, *Hierarchy of Interactions in Unified Gauge Theories*, *Phys. Rev. Lett.* **33** (1974) 451–454.

[19] P. Langacker and M.-x. Luo, *Implications of precision electroweak experiments for M_t, ρ_0, $\sin^2\theta_W$ and grand unification*, *Phys. Rev.* **D44** (1991) 817–822.

[20] U. Amaldi, W. de Boer, and H. Furstenau, *Comparison of grand unified theories with electroweak and strong coupling constants measured at LEP*, *Phys. Lett.* **B260** (1991) 447–455.

[21] J. R. Ellis, S. Kelley, and D. V. Nanopoulos, *Probing the desert using gauge coupling unification*, *Phys. Lett.* **B260** (1991) 131–137.

[22] R. N. Mohapatra, *Supersymmetric grand unification: An Update*, in *Particle physics. Proceedings, Summer School, Trieste, Italy, June 21-July 9, 1999*, pp. 336–394, 1999. hep-ph/9911272.

[23] J. R. Ellis, J. S. Hagelin, D. V. Nanopoulos, K. A. Olive, and M. Srednicki, *Supersymmetric Relics from the Big Bang*, *Nucl. Phys.* **B238** (1984) 453–476.

[24] S. Coleman and J. Mandula, *All possible symmetries of the s matrix*, *Phys. Rev.* **159** (Jul, 1967) 1251–1256.

[25] R. Haag, J. T. Lopuszanski, and M. Sohnius, *All Possible Generators of Supersymmetries of the S- Matrix*, *Nucl.Phys.* **B88** (1975) 257.

[26] S. P. Martin, *A Supersymmetry primer*, hep-ph/9709356. [Adv. Ser. Direct. High Energy Phys.18,1(1998)].

[27] M. Drees, R. Godbole, and P. Roy, *Theory and phenomenology of sparticles: An account of four-dimensional N=1 supersymmetry in high energy physics*. World Scientific, 2004.

[28] A. Salam and J. A. Strathdee, *Supergauge Transformations*, *Nucl. Phys.* **B76** (1974) 477–482.

[29] J. Wess and B. Zumino, *Supergauge Invariant Extension of Quantum Electrodynamics*, *Nucl. Phys.* **B78** (1974) 1.

[30] P. Fayet and J. Iliopoulos, *Spontaneously Broken Supergauge Symmetries and Goldstone Spinors*, *Phys. Lett.* **B51** (1974) 461–464.

[31] P. Fayet, *Supergauge Invariant Extension of the Higgs Mechanism and a Model for the electron and Its Neutrino*, *Nucl. Phys.* **B90** (1975) 104–124.

[32] L. O'Raifeartaigh, *Spontaneous Symmetry Breaking for Chiral Scalar Superfields*, *Nucl. Phys.* **B96** (1975) 331.

[33] D. Shih, *Spontaneous R-symmetry breaking in O'Raifeartaigh models*, *JHEP* **02** (2008) 091, [hep-th/0703196].

[34] S. Ferrara, L. Girardello, and F. Palumbo, *A General Mass Formula in Broken Supersymmetry*, *Phys. Rev.* **D20** (1979) 403.

[35] M. A. Luty, *2004 TASI lectures on supersymmetry breaking*, in *Physics in D >= 4. Proceedings, Theoretical Advanced Study Institute in elementary particle physics, TASI 2004, Boulder, USA, June 6-July 2, 2004*, pp. 495–582, 2005. hep-th/0509029.

[36] H. P. Nilles, *Supersymmetry, Supergravity and Particle Physics*, *Phys.Rept.* **110** (1984) 1–162.

[37] A. H. Chamseddine, R. L. Arnowitt, and P. Nath, *Locally Supersymmetric Grand Unification*, *Phys. Rev. Lett.* **49** (1982) 970.

[38] M. Dine and W. Fischler, *A Phenomenological Model of Particle Physics Based on Supersymmetry*, *Phys. Lett.* **B110** (1982) 227.

[39] C. R. Nappi and B. A. Ovrut, *Supersymmetric Extension of the SU(3) x SU(2) x U(1) Model*, *Phys. Lett.* **B113** (1982) 175.

[40] L. Alvarez-Gaume, M. Claudson, and M. B. Wise, *Low-Energy Supersymmetry*, *Nucl. Phys.* **B207** (1982) 96.

[41] M. Dine and A. E. Nelson, *Dynamical supersymmetry breaking at low-energies*, *Phys. Rev.* **D48** (1993) 1277–1287, [hep-ph/9303230].

[42] M. Dine, A. E. Nelson, and Y. Shirman, *Low-energy dynamical supersymmetry breaking simplified*, *Phys. Rev.* **D51** (1995) 1362–1370, [hep-ph/9408384].

[43] M. Dine, A. E. Nelson, Y. Nir, and Y. Shirman, *New tools for low-energy dynamical supersymmetry breaking*, *Phys. Rev.* **D53** (1996) 2658–2669, [hep-ph/9507378].

[44] G. Giudice and R. Rattazzi, *Theories with gauge mediated supersymmetry breaking*, *Phys.Rept.* **322** (1999) 419–499, [hep-ph/9801271].

[45] H. E. Haber and G. L. Kane, *The Search for Supersymmetry: Probing Physics Beyond the Standard Model*, *Phys. Rept.* **117** (1985) 75–263.

[46] H. K. Dreiner, *An Introduction to explicit R-parity violation*, hep-ph/9707435. [Adv. Ser. Direct. High Energy Phys.21,565(2010)].

[47] G. R. Farrar and P. Fayet, *Phenomenology of the Production, Decay, and Detection of New Hadronic States Associated with Supersymmetry*, *Phys. Lett.* **B76** (1978) 575–579.

[48] R. Kitano and Y. Nomura, *A Solution to the supersymmetric fine-tuning problem within the MSSM*, *Phys. Lett.* **B631** (2005) 58–67, [hep-ph/0509039].

[49] L. E. Ibanez and G. G. Ross, *SU(2)-L x U(1) Symmetry Breaking as a Radiative Effect of Supersymmetry Breaking in Guts*, *Phys. Lett.* **B110** (1982) 215–220.

[50] H. P. Nilles, M. Srednicki, and D. Wyler, *Weak Interaction Breakdown Induced by Supergravity*, *Phys. Lett.* **B120** (1983) 346.

[51] K. Kowalska and E. M. Sessolo, *Natural MSSM after the LHC 8 TeV run*, *Phys. Rev.* **D88** (2013), no. 7 075001, [arXiv:1307.5790].

[52] G. L. Kane, C. F. Kolda, L. Roszkowski, and J. D. Wells, *Study of constrained minimal supersymmetry*, *Phys. Rev.* **D49** (1994) 6173–6210, [hep-ph/9312272].

[53] **ATLAS** Collaboration, G. Aad et al., *Summary of the searches for squarks and gluinos using $\sqrt{s} = 8$ TeV pp collisions with the ATLAS experiment at the LHC*, arXiv:1507.05525.

[54] M. Papucci, J. T. Ruderman, and A. Weiler, *Natural SUSY Endures*, *JHEP* **09** (2012) 035, [arXiv:1110.6926].

[55] J. Camargo-Molina, B. O'Leary, W. Porod, and F. Staub, *Stability of the CMSSM against sfermion VEVs*, *JHEP* **1312** (2013) 103, [arXiv:1309.7212].

[56] J. Camargo-Molina, B. Garbrecht, B. O'Leary, W. Porod, and F. Staub, *Constraining the Natural MSSM through tunneling to color-breaking vacua at zero and non-zero temperature*, *Phys.Lett.* **B737** (2014) 156–161, [arXiv:1405.7376].

[57] P. Bechtle et al., *Killing the cMSSM softly*, arXiv:1508.05951.

[58] U. Ellwanger, C. Hugonie, and A. M. Teixeira, *The Next-to-Minimal Supersymmetric Standard Model*, *Phys. Rept.* **496** (2010) 1–77, [arXiv:0910.1785].

[59] M. Maniatis, *The Next-to-Minimal Supersymmetric extension of the Standard Model reviewed*, *Int. J. Mod. Phys.* **A25** (2010) 3505–3602, [arXiv:0906.0777].

[60] A. Vilenkin, *Cosmic Strings and Domain Walls*, *Phys. Rept.* **121** (1985) 263–315.

[61] C. Panagiotakopoulos and K. Tamvakis, *Stabilized NMSSM without domain walls*, *Phys. Lett.* **B446** (1999) 224–227, [hep-ph/9809475].

[62] G. D. Kribs, E. Poppitz, and N. Weiner, *Flavor in supersymmetry with an extended R-symmetry*, *Phys. Rev.* **D78** (2008) 055010, [arXiv:0712.2039].

[63] P. Diessner, J. Kalinowski, W. Kotlarski, and D. Stockinger, *Higgs boson mass and electroweak observables in the MRSSM*, *JHEP* **12** (2014) 124, [arXiv:1410.4791].

[64] K. Benakli, M. D. Goodsell, and F. Staub, *Dirac Gauginos and the 125 GeV Higgs*, *JHEP* **06** (2013) 073, [arXiv:1211.0552].

[65] P. J. Fox, A. E. Nelson, and N. Weiner, *Dirac gaugino masses and supersoft supersymmetry breaking*, *JHEP* **08** (2002) 035, [hep-ph/0206096].

[66] A. Arvanitaki, M. Baryakhtar, X. Huang, K. van Tilburg, and G. Villadoro, *The Last Vestiges of Naturalness*, *JHEP* **03** (2014) 022, [arXiv:1309.3568].

[67] G. D. Kribs and A. Martin, *Supersoft Supersymmetry is Super-Safe*, *Phys. Rev.* **D85** (2012) 115014, [arXiv:1203.4821].

[68] K. Benakli, M. Goodsell, F. Staub, and W. Porod, *Constrained minimal Dirac gaugino supersymmetric standard model*, *Phys. Rev.* **D90** (2014), no. 4 045017, [arXiv:1403.5122].

[69] M. D. Goodsell, M. E. Krauss, T. Muller, W. Porod, and F. Staub, *Dark matter scenarios in a constrained model with Dirac gauginos*, *JHEP* **10** (2015) 132, [arXiv:1507.01010].

[70] S. Weinberg, *Baryon and Lepton Nonconserving Processes*, *Phys. Rev. Lett.* **43** (1979) 1566–1570.

[71] P. Minkowski, $\mu \to e\gamma$ *at a Rate of One Out of* 10^9 *Muon Decays?*, *Phys. Lett.* **B67** (1977) 421–428.

[72] M. Gell-Mann, P. Ramond, and R. Slansky, *Complex Spinors and Unified Theories*, *Conf. Proc.* **C790927** (1979) 315–321, [arXiv:1306.4669].

[73] T. Yanagida, *HORIZONTAL SYMMETRY AND MASSES OF NEUTRINOS*, *Conf.Proc.* **C7902131** (1979) 95.

[74] R. N. Mohapatra and G. Senjanovic, *Neutrino Mass and Spontaneous Parity Violation*, *Phys. Rev. Lett.* **44** (1980) 912.

[75] R. Mohapatra and J. Valle, *Neutrino Mass and Baryon Number Nonconservation in Superstring Models*, *Phys.Rev.* **D34** (1986) 1642.

[76] E. K. Akhmedov, M. Lindner, E. Schnapka, and J. W. F. Valle, *Dynamical left-right symmetry breaking*, *Phys. Rev.* **D53** (1996) 2752–2780, [hep-ph/9509255].

[77] J. Schechter and J. W. F. Valle, *Neutrino Masses in SU(2) x U(1) Theories*, *Phys. Rev.* **D22** (1980) 2227.

[78] T. P. Cheng and L.-F. Li, *Neutrino Masses, Mixings and Oscillations in SU(2) x U(1) Models of Electroweak Interactions*, *Phys. Rev.* **D22** (1980) 2860.

[79] R. Foot, H. Lew, X. G. He, and G. C. Joshi, *Seesaw Neutrino Masses Induced by a Triplet of Leptons*, *Z. Phys.* **C44** (1989) 441.

[80] H. Georgi and S. L. Glashow, *Unity of All Elementary Particle Forces*, *Phys. Rev. Lett.* **32** (1974) 438–441.

[81] **Kamiokande-II** Collaboration, K. S. Hirata et al., *Experimental Limits on Nucleon Lifetime for Lepton + Meson Decay Modes*, *Phys. Lett.* **B220** (1989) 308.

[82] J. R. Ellis, D. V. Nanopoulos, and S. Rudaz, *GUTs 3: SUSY GUTs 2*, *Nucl. Phys.* **B202** (1982) 43.

[83] **Super-Kamiokande** Collaboration, Y. Hayato et al., *Search for proton decay through p —> anti-neutrino K+ in a large water Cherenkov detector*, *Phys. Rev. Lett.* **83** (1999) 1529–1533, [hep-ex/9904020].

[84] H. Murayama and A. Pierce, *Not even decoupling can save minimal supersymmetric SU(5)*, *Phys. Rev.* **D65** (2002) 055009, [hep-ph/0108104].

[85] R. Slansky, *Group Theory for Unified Model Building*, *Phys. Rept.* **79** (1981) 1–128.

[86] M. Srednicki, *Quantum field theory*. Cambridge University Press, 2007.

[87] J. C. Pati and A. Salam, *Lepton Number as the Fourth Color*, *Phys.Rev.* **D10** (1974) 275–289.

[88] V. De Romeri, M. Hirsch, and M. Malinsky, *Soft masses in SUSY SO(10) GUTs with low intermediate scales*, *Phys.Rev.* **D84** (2011) 053012, [arXiv:1107.3412].

[89] M. Malinsky, J. Romao, and J. Valle, *Novel supersymmetric SO(10) seesaw mechanism*, *Phys.Rev.Lett.* **95** (2005) 161801, [hep-ph/0506296].

[90] J. Brehmer, J. Hewett, J. Kopp, T. Rizzo, and J. Tattersall, *Symmetry Restored in Dibosons at the LHC?*, arXiv:1507.00013.

[91] B. A. Dobrescu and Z. Liu, *Heavy Higgs bosons and the 2 TeV W' boson*, arXiv:1507.01923.

[92] **ATLAS** Collaboration, G. Aad et al., *Search for high-mass diboson resonances with boson-tagged jets in proton-proton collisions at $\sqrt{s}$ = 8 TeV with the ATLAS detector*, arXiv:1506.00962.

[93] G. Brooijmans, R. Contino, B. Fuks, F. Moortgat, P. Richardson, et al., *Les Houches 2013: Physics at TeV Colliders: New Physics Working Group Report*, arXiv:1405.1617.

[94] A. Alloul, M. Frank, B. Fuks, and M. Rausch de Traubenberg, *Chargino and neutralino production at the Large Hadron Collider in left-right supersymmetric models*, *JHEP* **1310** (2013) 033, [arXiv:1307.5073].

[95] L. Basso, B. Fuks, M. E. Krauss, and W. Porod, *Doubly-charged Higgs and vacuum stability in left-right supersymmetry*, *JHEP* **07** (2015) 147, [arXiv:1503.08211].

[96] M. E. Krauss and W. Porod, *Is the CMS eejj excess a hint for light supersymmetry?*, *Phys.Rev.* **D92** (2015) 055019, [arXiv:1507.04349].

[97] R. Kuchimanchi and R. Mohapatra, *No parity violation without R-parity violation*, *Phys.Rev.* **D48** (1993) 4352–4360, [hep-ph/9306290].

[98] Z. Chacko and R. Mohapatra, *Supersymmetric left-right model and light doubly charged Higgs bosons and Higgsinos*, *Phys.Rev.* **D58** (1998) 015003, [hep-ph/9712359].

[99] K. Huitu and J. Maalampi, *The Higgs sector of a supersymmetric left-right model*, *Phys.Lett.* **B344** (1995) 217–224, [hep-ph/9410342].

[100] S. R. Coleman and E. J. Weinberg, *Radiative Corrections as the Origin of Spontaneous Symmetry Breaking*, *Phys.Rev.* **D7** (1973) 1888–1910.

[101] M. Cvetic and J. C. Pati, $N = 1$ *Supergravity Within the Minimal Left-right Symmetric Model*, *Phys.Lett.* **B135** (1984) 57.

[102] E. J. Weinberg and A.-q. Wu, *UNDERSTANDING COMPLEX PERTURBATIVE EFFECTIVE POTENTIALS*, *Phys.Rev.* **D36** (1987) 2474.

[103] K. Babu and A. Patra, *Higgs Boson Spectra in Supersymmetric Left-Right Models*, arXiv:1412.8714.

[104] K. Babu and R. N. Mohapatra, *Minimal Supersymmetric Left-Right Model*, *Phys.Lett.* **B668** (2008) 404–409, [arXiv:0807.0481].

[105] F. Staub, *SARAH*, arXiv:0806.0538.

[106] F. Staub, *From Superpotential to Model Files for FeynArts and CalcHep/CompHep*, *Comput.Phys.Commun.* **181** (2010) 1077–1086, [arXiv:0909.2863].

[107] F. Staub, *Automatic Calculation of supersymmetric Renormalization Group Equations and Self Energies*, *Comput.Phys.Commun.* **182** (2011) 808–833, [arXiv:1002.0840].

[108] F. Staub, *SARAH 3.2: Dirac Gauginos, UFO output, and more*, *Computer Physics Communications* **184** (2013) pp. 1792–1809, [arXiv:1207.0906].

[109] F. Staub, *SARAH 4: A tool for (not only SUSY) model builders*, *Comput.Phys.Commun.* **185** (2014) 1773–1790, [arXiv:1309.7223].

[110] F. Staub, *Exploring new models in all detail with SARAH*, arXiv:1503.04200.

[111] W. Porod, *SPheno, a program for calculating supersymmetric spectra, SUSY particle decays and SUSY particle production at e+ e- colliders*, *Comput.Phys.Commun.* **153** (2003) 275–315, [hep-ph/0301101].

[112] W. Porod and F. Staub, *SPheno 3.1: Extensions including flavour, CP-phases and models beyond the MSSM*, *Comput.Phys.Commun.* **183** (2012) 2458–2469, [arXiv:1104.1573].

[113] S. Weinberg, *Perturbative Calculations of Symmetry Breaking*, *Phys. Rev.* **D7** (1973) 2887–2910.

[114] **ATLAS** Collaboration, G. Aad et al., *Search for anomalous production of prompt same-sign lepton pairs and pair-produced doubly charged Higgs bosons with* $\sqrt{s} = 8$ *TeV pp collisions using the ATLAS detector*, *JHEP* **1503** (2015) 041, [arXiv:1412.0237].

[115] **CMS Collaboration** Collaboration, S. Chatrchyan et al., *A search for a doubly-charged Higgs boson in pp collisions at* $\sqrt{s} = 7$ *TeV*, *Eur.Phys.J.* **C72** (2012) 2189, [arXiv:1207.2666].

[116] **CMS** Collaboration, V. Khachatryan et al., *Search for resonances and quantum black holes using dijet mass spectra in proton-proton collisions at* $\sqrt{s}$*=8 TeV*, arXiv:1501.04198.

[117] **CMS** Collaboration, S. Chatrchyan et al., *Search for W' → tb decays in the lepton + jets final state in pp collisions at* $\sqrt{s} = 8$ *TeV*, *JHEP* **1405** (2014) 108, [arXiv:1402.2176].

[118] J. Alwall, R. Frederix, S. Frixione, V. Hirschi, F. Maltoni, et al., *The automated computation of tree-level and next-to-leading order differential cross sections, and their matching to parton shower simulations*, *JHEP* **1407** (2014) 079, [arXiv:1405.0301].

[119] C. Degrande, C. Duhr, B. Fuks, D. Grellscheid, O. Mattelaer, et al., *UFO - The Universal FeynRules Output*, *Comput.Phys.Commun.* **183** (2012) 1201–1214, [arXiv:1108.2040].

[120] J. Pumplin, D. Stump, J. Huston, H. Lai, P. M. Nadolsky, et al., *New generation of parton distributions with uncertainties from global QCD analysis*, *JHEP* **0207** (2002) 012, [hep-ph/0201195].

[121] A. Belyaev, N. D. Christensen, and A. Pukhov, *CalcHEP 3.4 for collider physics within and beyond the Standard Model*, *Comput.Phys.Commun.* **184** (2013) 1729–1769, [arXiv:1207.6082].

[122] S. Bar-Shalom, G. Eilam, T. Han, and A. Soni, *Charged Higgs Boson Effects in the Production and Decay of a Heavy Majorana Neutrino at the CERN LHC*, *Phys.Rev.* **D77** (2008) 115019, [arXiv:0803.2835].

[123] **CMS** Collaboration, V. Khachatryan et al., *Search for heavy neutrinos and* W *bosons with right-handed couplings in proton-proton collisions at* $\sqrt{s} = 8$ *TeV*, *Eur.Phys.J.* **C74** (2014), no. 11 3149, [arXiv:1407.3683].

[124] CMS-Collaboration, *Search for a heavy neutrino and right-handed W of the left-right symmetric model in pp collisions at 8 TeV*, CMS-PAS-EXO-12-017.

[125] **ATLAS** Collaboration, G. Aad et al., *Search for heavy Majorana neutrinos with the ATLAS detector in pp collisions at* $\sqrt{s} = 8$ *TeV*, *JHEP* **07** (2015) 162, [arXiv:1506.06020].

[126] F. F. Deppisch, L. Graf, S. Kulkarni, S. Patra, W. Rodejohann, N. Sahu, and U. Sarkar, *Reconciling the 2 TeV Excesses at the LHC in a Linear Seesaw Left-Right Model*, arXiv:1508.05940.

[127] J. Gluza and T. Jelinski, *Heavy neutrinos and the pp → lljj CMS data*, *Phys. Lett.* **B748** (2015) 125–131, [arXiv:1504.05568].

[128] J. Camargo-Molina, B. O'Leary, W. Porod, and F. Staub, **Vevacious***: A Tool For Finding The Global Minima Of One-Loop Effective Potentials With Many Scalars*, *Eur.Phys.J.* **C73** (2013), no. 10 2588, [arXiv:1307.1477].

[129] Y. Shadmi and P. Z. Szabo, *Flavored Gauge-Mediation*, *JHEP* **1206** (2012) 124, [arXiv:1103.0292].

[130] J. L. Evans, M. Ibe, and T. T. Yanagida, *Relatively Heavy Higgs Boson in More Generic Gauge Mediation*, *Phys.Lett.* **B705** (2011) 342–348, [arXiv:1107.3006].

[131] J. L. Evans, M. Ibe, S. Shirai, and T. T. Yanagida, *A 125GeV Higgs Boson and Muon g-2 in More Generic Gauge Mediation*, *Phys.Rev.* **D85** (2012) 095004, [arXiv:1201.2611].

[132] A. Albaid and K. Babu, *Higgs boson of mass 125 GeV in GMSB models with messenger-matter mixing*, *Phys.Rev.* **D88** (2013) 055007, [arXiv:1207.1014].

[133] M. Abdullah, I. Galon, Y. Shadmi, and Y. Shirman, *Flavored Gauge Mediation, A Heavy Higgs, and Supersymmetric Alignment*, *JHEP* **1306** (2013) 057, [arXiv:1209.4904].

[134] N. Craig, S. Knapen, D. Shih, and Y. Zhao, *A Complete Model of Low-Scale Gauge Mediation*, *JHEP* **1303** (2013) 154, [arXiv:1206.4086].

[135] J. A. Evans and D. Shih, *Surveying Extended GMSB Models with m_h=125 GeV*, *JHEP* **1308** (2013) 093, [arXiv:1303.0228].

[136] I. Donkin and A. K. Knochel, *NMSSM with Lopsided Gauge Mediation*, arXiv:1205.5515.

[137] P. Byakti and T. S. Ray, *Burgeoning the Higgs mass to 125 GeV through messenger-matter interactions in GMSB models*, *JHEP* **1305** (2013) 055, [arXiv:1301.7605].

[138] P. Grajek, A. Mariotti, and D. Redigolo, *Phenomenology of General Gauge Mediation in light of a 125 GeV Higgs*, *JHEP* **1307** (2013) 109, [arXiv:1303.0870].

[139] S. K. Majee, M. K. Parida, A. Raychaudhuri, and U. Sarkar, *Low intermediate scales for leptogenesis in SUSY SO(10) GUTs*, *Phys.Rev.* **D75** (2007) 075003, [hep-ph/0701109].

[140] M. Hirsch, W. Porod, L. Reichert, and F. Staub, *Phenomenology of the minimal supersymmetric $U(1)_{B-L} \times U(1)_R$ extension of the standard model*, *Phys.Rev.* **D86** (2012) 093018, [arXiv:1206.3516].

[141] P. B. Dev and R. Mohapatra, *TeV Scale Inverse Seesaw in SO(10) and Leptonic Non-Unitarity Effects*, *Phys.Rev.* **D81** (2010) 013001, [arXiv:0910.3924].

[142] P. Bhupal Dev and R. Mohapatra, *Electroweak Symmetry Breaking and Proton Decay in SO(10) SUSY-GUT with TeV W(R)*, *Phys.Rev.* **D82** (2010) 035014, [arXiv:1003.6102].

[143] L. E. Ibanez and G. G. Ross, *Discrete gauge symmetry anomalies*, *Phys.Lett.* **B260** (1991) 291–295.

[144] H. K. Dreiner, C. Luhn, and M. Thormeier, *What is the discrete gauge symmetry of the MSSM?*, *Phys.Rev.* **D73** (2006) 075007, [hep-ph/0512163].

[145] R. M. Fonseca, M. Malinsky, W. Porod, and F. Staub, *Running soft parameters in SUSY models with multiple U(1) gauge factors*, *Nucl.Phys.* **B854** (2012) 28–53, [arXiv:1107.2670].

[146] J. Erler, P. Langacker, S. Munir, and E. Rojas, *Z' Bosons at Colliders: a Bayesian Viewpoint*, *JHEP* **1111** (2011) 076, [arXiv:1103.2659].

[147] G. Giudice and R. Rattazzi, *Extracting supersymmetry breaking effects from wave function renormalization*, *Nucl.Phys.* **B511** (1998) 25–44, [hep-ph/9706540].

[148] S. P. Martin, *Generalized messengers of supersymmetry breaking and the sparticle mass spectrum*, *Phys.Rev.* **D55** (1997) 3177–3187, [hep-ph/9608224].

[149] N. Arkani-Hamed, G. F. Giudice, M. A. Luty, and R. Rattazzi, *Supersymmetry breaking loops from analytic continuation into superspace*, *Phys.Rev.* **D58** (1998) 115005, [hep-ph/9803290].

[150] B. O'Leary, W. Porod, and F. Staub, *Mass spectrum of the minimal SUSY B-L model*, *JHEP* **1205** (2012) 042, [arXiv:1112.4600].

[151] M. E. Krauss, B. O'Leary, W. Porod, and F. Staub, *Implications of gauge kinetic mixing on Z' and slepton production at the LHC*, *Phys.Rev.* **D86** (2012) 055017, [arXiv:1206.3513].

[152] M. Gonzalez-Garcia and J. Valle, *Fast Decaying Neutrinos and Observable Flavor Violation in a New Class of Majoron Models*, *Phys.Lett.* **B216** (1989) 360.

[153] P. Draper, P. Meade, M. Reece, and D. Shih, *Implications of a 125 GeV Higgs for the MSSM and Low-Scale SUSY Breaking*, *Phys.Rev.* **D85** (2012) 095007, [arXiv:1112.3068].

[154] M. A. Ajaib, I. Gogoladze, F. Nasir, and Q. Shafi, *Revisiting mGMSB in Light of a 125 GeV Higgs*, *Phys.Lett.* **B713** (2012) 462–468, [arXiv:1204.2856].

[155] F. Brummer, S. Kraml, and S. Kulkarni, *Anatomy of maximal stop mixing in the MSSM*, *JHEP* **1208** (2012) 089, [arXiv:1204.5977].

[156] A. Dedes, G. Degrassi, and P. Slavich, *On the two loop Yukawa corrections to the MSSM Higgs boson masses at large tan beta*, *Nucl.Phys.* **B672** (2003) 144–162, [hep-ph/0305127].

[157] A. Brignole, G. Degrassi, P. Slavich, and F. Zwirner, *On the two loop sbottom corrections to the neutral Higgs boson masses in the MSSM*, *Nucl.Phys.* **B643** (2002) 79–92, [hep-ph/0206101].

[158] A. Brignole, G. Degrassi, P. Slavich, and F. Zwirner, *On the O(alpha(t)**2) two loop corrections to the neutral Higgs boson masses in the MSSM*, *Nucl.Phys.* **B631** (2002) 195–218, [hep-ph/0112177].

[159] G. Degrassi, P. Slavich, and F. Zwirner, *On the neutral Higgs boson masses in the MSSM for arbitrary stop mixing*, *Nucl.Phys.* **B611** (2001) 403–422, [hep-ph/0105096].

[160] **ATLAS Collaboration** Collaboration, G. Aad et al., *Observation of a new particle in the search for the Standard Model Higgs boson with the ATLAS detector at the LHC*, *Phys.Lett.* **B716** (2012) 1–29, [arXiv:1207.7214].

[161] **CMS Collaboration** Collaboration, S. Chatrchyan et al., *Observation of a new boson at a mass of 125 GeV with the CMS experiment at the LHC*, *Phys.Lett.* **B716** (2012) 30–61, [arXiv:1207.7235].

[162] **ATLAS** Collaboration, G. Aad et al., *Measurement of Higgs boson production in the diphoton decay channel in pp collisions at center-of-mass energies of 7 and 8 TeV with the ATLAS detector*, *Phys.Rev.* **D90** (2014), no. 11 112015, [arXiv:1408.7084].

[163] **CMS** Collaboration, V. Khachatryan et al., *Observation of the diphoton decay of the Higgs boson and measurement of its properties*, *Eur.Phys.J.* **C74** (2014), no. 10 3076, [arXiv:1407.0558].

[164] L. Basso and F. Staub, *Enhancing $h \to \gamma\gamma$ with staus in SUSY models with extended gauge sector*, *Phys.Rev.* **D87** (2013), no. 1 015011, [arXiv:1210.7946].

[165] S. Dimopoulos, G. Giudice, and A. Pomarol, *Dark matter in theories of gauge mediated supersymmetry breaking*, *Phys.Lett.* **B389** (1996) 37–42, [hep-ph/9607225].

[166] M. Fujii and T. Yanagida, *Baryogenesis and gravitino dark matter in gauge mediated supersymmetry breaking models*, *Phys.Rev.* **D66** (2002) 123515, [hep-ph/0207339].

[167] K. Jedamzik, M. Lemoine, and G. Moultaka, *Gravitino dark matter in gauge mediated supersymmetry breaking*, *Phys.Rev.* **D73** (2006) 043514, [hep-ph/0506129].

[168] M. E. Krauss, W. Porod, and F. Staub, *SO(10) inspired gauge-mediated supersymmetry breaking*, *Phys.Rev.* **D88** (2013), no. 1 015014, [arXiv:1304.0769].

[169] K. Choi, K. Hwang, H. B. Kim, and T. Lee, *Cosmological gravitino production in gauge mediated supersymmetry breaking models*, *Phys.Lett.* **B467** (1999) 211–217, [hep-ph/9902291].

[170] J. L. Feng and T. Moroi, *Tevatron signatures of longlived charged sleptons in gauge mediated supersymmetry breaking models*, *Phys.Rev.* **D58** (1998) 035001, [hep-ph/9712499].

[171] M. Drees and X. Tata, *Signals for heavy exotics at hadron colliders and supercolliders*, *Phys.Lett.* **B252** (1990) 695–702.

[172] **ATLAS** Collaboration, *A search for heavy long-lived sleptons using 16 fb^{-1} of pp collisions at $\sqrt{s} = 8$ TeV with the ATLAS detector*, .

[173] T. Gherghetta, T. A. Kaeding, and G. L. Kane, *Supersymmetric contributions to the decay of an extra Z boson*, *Phys.Rev.* **D57** (1998) 3178–3181, [hep-ph/9701343].

[174] C.-F. Chang, K. Cheung, and T.-C. Yuan, *Supersymmetric Decays of the Z' Boson*, *JHEP* **1109** (2011) 058, [arXiv:1107.1133].

[175] **ATLAS** Collaboration, G. Aad et al., *Search for high-mass dilepton resonances in pp collisions at $\sqrt{s} = 8$ TeV with the ATLAS detector*, *Phys.Rev.* **D90** (2014), no. 5 052005, [arXiv:1405.4123].

[176] **CMS** Collaboration, V. Khachatryan et al., *Search for physics beyond the standard model in dilepton mass spectra in proton-proton collisions at $\sqrt{s} = 8$ TeV*, *JHEP* **1504** (2015) 025, [arXiv:1412.6302].

[177] **Super-Kamiokande** Collaboration, Y. Fukuda et al., *Evidence for oscillation of atmospheric neutrinos*, *Phys. Rev. Lett.* **81** (1998) 1562–1567, [hep-ex/9807003].

[178] **MEG Collaboration** Collaboration, J. Adam et al., *New constraint on the existence of the $\mu^+ \to e^+\gamma$ decay*, *Phys.Rev.Lett.* **110** (2013), no. 20 201801, [arXiv:1303.0754].

[179] A. Baldini, F. Cei, C. Cerri, S. Dussoni, L. Galli, et al., *MEG Upgrade Proposal*, arXiv:1301.7225.

[180] A. Blondel, A. Bravar, M. Pohl, S. Bachmann, N. Berger, et al., *Research Proposal for an Experiment to Search for the Decay $\mu \to eee$*, arXiv:1301.6113.

[181] The PRIME working group, *Search for the $\mu \to e$ Conversion Process at an Ultimate Sensitivity of the Order of 10^{-18} with PRISM*, *j-parc.jp/researcher/Hadron/en/pac_0606/pdf/p20-Kuno.pdf*.

[182] **BaBar Collaboration** Collaboration, B. Aubert et al., *Searches for Lepton Flavor Violation in the Decays tau+- -> e+- gamma and tau+- -> mu+- gamma*, *Phys.Rev.Lett.* **104** (2010) 021802, [arXiv:0908.2381].

[183] T. Aushev, W. Bartel, A. Bondar, J. Brodzicka, T. Browder, et al., *Physics at Super B Factory*, arXiv:1002.5012.

[184] **SINDRUM Collaboration** Collaboration, U. Bellgardt et al., *Search for the Decay mu+ -> e+ e+ e-*, *Nucl.Phys.* **B299** (1988) 1.

[185] K. Hayasaka, K. Inami, Y. Miyazaki, K. Arinstein, V. Aulchenko, et al., *Search for Lepton Flavor Violating Tau Decays into Three Leptons with 719 Million Produced Tau+Tau- Pairs*, *Phys.Lett.* **B687** (2010) 139–143, [arXiv:1001.3221].

[186] **SINDRUM II Collaboration.** Collaboration, C. Dohmen et al., *Test of lepton flavor conservation in mu –> e conversion on titanium*, *Phys.Lett.* **B317** (1993) 631–636.

[187] **SINDRUM II Collaboration** Collaboration, W. H. Bertl et al., *A Search for muon to electron conversion in muonic gold*, *Eur.Phys.J.* **C47** (2006) 337–346.

[188] **DeeMe Collaboration** Collaboration, M. Aoki, *An experimental search for muon-electron conversion in nuclear field at sensitivity of 10**-14 with a pulsed proton beam*, *AIP Conf.Proc.* **1441** (2012) 599–601.

[189] E. Arganda and M. J. Herrero, *Testing supersymmetry with lepton flavor violating tau and mu decays*, *Phys.Rev.* **D73** (2006) 055003, [hep-ph/0510405].

[190] A. Ilakovac and A. Pilaftsis, *Flavor violating charged lepton decays in seesaw-type models*, *Nucl.Phys.* **B437** (1995) 491, [hep-ph/9403398].

[191] J. Bernabeu, A. Santamaria, J. Vidal, A. Mendez, and J. Valle, *Lepton Flavor Nonconservation at High-Energies in a Superstring Inspired Standard Model*, *Phys.Lett.* **B187** (1987) 303.

[192] F. Deppisch and J. Valle, *Enhanced lepton flavor violation in the supersymmetric inverse seesaw model*, *Phys.Rev.* **D72** (2005) 036001, [hep-ph/0406040].

[193] M. Hirsch, F. Staub, and A. Vicente, *Enhancing $l_i \to 3l_j$ with the Z^0-penguin*, *Phys.Rev.* **D85** (2012), no. 5 113013, [arXiv:1202.1825].

[194] A. Abada, D. Das, A. Vicente, and C. Weiland, *Enhancing lepton flavour violation in the supersymmetric inverse seesaw beyond the dipole contribution*, *JHEP* **1209** (2012) 015, [arXiv:1206.6497].

[195] M. E. Krauss, W. Porod, F. Staub, A. Abada, A. Vicente, et al., *Decoupling of heavy sneutrinos in low-scale seesaw models*, *Phys.Rev.* **D90** (2014) 013008, [arXiv:1312.5318].

[196] A. Abada, M. E. Krauss, W. Porod, F. Staub, A. Vicente, et al., *Lepton flavor violation in low-scale seesaw models: SUSY and non-SUSY contributions*, *JHEP* **1411** (2014) 048, [arXiv:1408.0138].

[197] J. Casas and A. Ibarra, *Oscillating neutrinos and muon –> e, gamma*, *Nucl.Phys.* **B618** (2001) 171–204, [hep-ph/0103065].

[198] L. Basso, A. Belyaev, D. Chowdhury, M. Hirsch, S. Khalil, et al., *Proposal for generalised Supersymmetry Les Houches Accord for see-saw models and PDG numbering scheme*, *Comput.Phys.Commun.* **184** (2013) 698–719, [arXiv:1206.4563].

[199] A. Abada, D. Das, A. Teixeira, A. Vicente, and C. Weiland, *Tree-level lepton universality violation in the presence of sterile neutrinos: impact for R_K and R_π*, *JHEP* **1302** (2013) 048, [arXiv:1211.3052].

[200] B. Pontecorvo, *Mesonium and anti-mesonium*, *Sov. Phys. JETP* **6** (1957) 429. [Zh. Eksp. Teor. Fiz.33,549(1957)].

[201] Z. Maki, M. Nakagawa, and S. Sakata, *Remarks on the unified model of elementary particles*, *Prog. Theor. Phys.* **28** (1962) 870–880.

[202] D. Forero, M. Tortola, and J. Valle, *Neutrino oscillations refitted*, *Phys.Rev.* **D90** (2014), no. 9 093006, [arXiv:1405.7540].

[203] D. Forero, M. Tortola, and J. Valle, *Global status of neutrino oscillation parameters after Neutrino-2012*, *Phys.Rev.* **D86** (2012) 073012, [arXiv:1205.4018].

[204] M. Gonzalez-Garcia, M. Maltoni, J. Salvado, and T. Schwetz, *Global fit to three neutrino mixing: critical look at present precision*, *JHEP* **1212** (2012) 123, [arXiv:1209.3023].

[205] F. Capozzi, G. Fogli, E. Lisi, A. Marrone, D. Montanino, et al., *Status of three-neutrino oscillation parameters, circa 2013*, *Phys.Rev.* **D89** (2014) 093018, [arXiv:1312.2878].

[206] W. Porod, F. Staub, and A. Vicente, *A Flavor Kit for BSM models*, *Eur.Phys.J.* **C74** (2014), no. 8 2992, [arXiv:1405.1434].

[207] T. Hahn and M. Perez-Victoria, *Automatized one loop calculations in four-dimensions and D-dimensions*, *Comput.Phys.Commun.* **118** (1999) 153–165, [hep-ph/9807565].

[208] T. Hahn, *Generating Feynman diagrams and amplitudes with FeynArts 3*, *Comput.Phys.Commun.* **140** (2001) 418–431, [hep-ph/0012260].

[209] T. Hahn, *Automatic loop calculations with FeynArts, FormCalc, and LoopTools*, *Nucl.Phys.Proc.Suppl.* **89** (2000) 231–236, [hep-ph/0005029].

[210] T. Hahn, *New features in FormCalc 4*, *Nucl.Phys.Proc.Suppl.* **135** (2004) 333–337, [hep-ph/0406288].

[211] H. Dreiner, K. Nickel, F. Staub, and A. Vicente, *New bounds on trilinear R-parity violation from lepton flavor violating observables*, *Phys.Rev.* **D86** (2012) 015003, [arXiv:1204.5925].

[212] M. Hirsch, F. Staub, and A. Vicente, *Erratum: Enhancing $l_i \to 3l_j$ with the Z^0-penguin [phys.rev. **D85** , 113013 (2012)]*, *Phys.Rev.* **D91** (2015) 059902.

[213] A. Ilakovac and A. Pilaftsis, *Supersymmetric Lepton Flavour Violation in Low-Scale Seesaw Models*, *Phys.Rev.* **D80** (2009) 091902, [arXiv:0904.2381].

[214] R. Alonso, M. Dhen, M. Gavela, and T. Hambye, *Muon conversion to electron in nuclei in type-I seesaw models*, *JHEP* **1301** (2013) 118, [arXiv:1209.2679].

[215] D. Dinh, A. Ibarra, E. Molinaro, and S. Petcov, *The $\mu - e$ Conversion in Nuclei, $\mu \to e\gamma, \mu \to 3e$ Decays and TeV Scale See-Saw Scenarios of Neutrino Mass Generation*, *JHEP* **1208** (2012) 125, [arXiv:1205.4671].

[216] A. Ilakovac, A. Pilaftsis, and L. Popov, *Charged lepton flavor violation in supersymmetric low-scale seesaw models*, *Phys.Rev.* **D87** (2013), no. 5 053014, [arXiv:1212.5939].

[217] **Particle Data Group** Collaboration, J. Beringer et al., *Review of Particle Physics (RPP)*, *Phys.Rev.* **D86** (2012) 010001.

[218] V. De Romeri and M. Hirsch, *Sneutrino Dark Matter in Low-scale Seesaw Scenarios*, *JHEP* **1212** (2012) 106, [arXiv:1209.3891].

[219] J. Hisano, T. Moroi, K. Tobe, and M. Yamaguchi, *Lepton flavor violation via right-handed neutrino Yukawa couplings in supersymmetric standard model*, *Phys.Rev.* **D53** (1996) 2442–2459, [hep-ph/9510309].

[220] E. Arganda. Private communication.

[221] Y. Kuno and Y. Okada, *Muon decay and physics beyond the standard model*, *Rev.Mod.Phys.* **73** (2001) 151–202, [hep-ph/9909265].

[222] E. Arganda, M. Herrero, and A. Teixeira, *mu-e conversion in nuclei within the CMSSM seesaw: Universality versus non-universality*, *JHEP* **0710** (2007) 104, [arXiv:0707.2955].

[223] J. Vergados, *The Neutrino Mass and Family, Lepton and Baryon Nonconservation in Gauge Theories*, *Phys.Rept.* **133** (1986) 1.

[224] J. Bernabeu, E. Nardi, and D. Tommasini, *μ - e conversion in nuclei and Z' physics*, *Nucl.Phys.* **B409** (1993) 69–86, [hep-ph/9306251].

[225] A. Faessler, T. Kosmas, S. Kovalenko, and J. Vergados, *Constraints on R-parity violating supersymmetry from muon electron nuclear conversion*, hep-ph/9904335.

[226] R. Kitano, M. Koike, and Y. Okada, *Detailed calculation of lepton flavor violating muon electron conversion rate for various nuclei*, *Phys.Rev.* **D66** (2002) 096002, [hep-ph/0203110].

[227] A. Crivellin, M. Hoferichter, and M. Procura, *Improved predictions for $\mu \to e$ conversion in nuclei and Higgs-induced lepton flavor violation*, *Phys.Rev.* **D89** (2014) 093024, [arXiv:1404.7134].

[228] H. Chiang, E. Oset, T. Kosmas, A. Faessler, and J. Vergados, *Coherent and incoherent (mu-, e-) conversion in nuclei*, *Nucl.Phys.* **A559** (1993) 526–542.

[229] T. Kosmas, S. Kovalenko, and I. Schmidt, *Nuclear muon- e- conversion in strange quark sea*, *Phys.Lett.* **B511** (2001) 203, [hep-ph/0102101].

[230] E. Arganda, M. J. Herrero, and J. Portoles, *Lepton flavour violating semileptonic tau decays in constrained MSSM-seesaw scenarios*, *JHEP* **06** (2008) 079, [arXiv:0803.2039].

[231] E. Arganda, A. M. Curiel, M. J. Herrero, and D. Temes, *Lepton flavor violating Higgs boson decays from massive seesaw neutrinos*, *Phys.Rev.* **D71** (2005) 035011, [hep-ph/0407302].

DANKSAGUNG

An dieser Stelle ist es an der Zeit, ‘Danke’ zu sagen.

Allen voran sind hier zwei Personen zu nennen: mein Dank geht an meinem Doktorvater Werner Porod für die Möglichkeit, diese Dissertation zu schreiben sowie seine exzellente Betreuung. Besonders wertvoll war die stets enge Zusammenarbeit und sein immer offenes Ohr, wenn ich Hilfe oder Ratschlag benötigt habe. Trotz seines immensen bürokratischen Aufwands als Studiendekan findet er für jeden seiner Studenten die Zeit, über die jeweiligen Projekte zu diskutieren, Denkanstöße zu geben und neue, interessante Fragestellungen aufzuwerfen. Desweiteren war es ein Privileg, mit Florian Staub zusammenzuarbeiten. Ohne lange zu zögern, nimmt er Angelegenheiten direkt in die Hand und ist hierbei auch noch enorm effektiv. Insbesondere für die ständige Hilfestellung in Fragen zu `SARAH` bin ich sehr dankbar.

Außerdem möchte ich mich bedanken bei Ansgar Denner für die Möglichkeit, diese Arbeit an seinem Lehrstuhl durchzuführen, bei meinen verschiedensten Kollaborateuren für die erfolgreiche Zusammenarbeit, bei Ben O’Leary für die vielen Diskussionen und Erklärungen über Vakuumstabilität sowie bei Brigitte Wehner, der guten Seele des Lehrstuhls, die uns allen die Bürokratie vom Leibe hält. Für die finanzielle Unterstützung danke ich der DFG im Rahmen des Projekts Nr. PO-1337/3-1 sowie des Graduiertenkollegs GRK 1147. Erst hierdurch war u. a. so manche Reise im Rahmen einer internationalen Konferenz oder Schule möglich.

Das Dotorandendasein in Würzburg wird erheblich versüßt durch den Umgang mit den Kollegen sowie den täglichen Ritualen wie der 11-Uhr Mensa oder der nachmittäglichen Kaffepause und den zugehörigen (mal mehr, mal weniger anspruchsvollen) Diskussionen. Sehr wichtig hierfür sind Leader wie Jean-Nicolas Lang und Chrostoph Uhlemann, die insbes. die Mensa-Zeit unnachgiebig verteidigen und um Punkt 11 die Leute aus ihren Büros scheuchen (bzw. um 11:05 Uhr meinen Namensvetter M. Krauß an der Ampel abholen). Insbesondere möchte ich mich bei dem immer hilfsbereiten Lukas Mitzka dafür bedanken, dass er sich für jede Frage Zeit nimmt, um mit seinem scheinbar unerschöpflichen Grundwissen Licht ins Dunkel zu bringen,[3] und für einige hilfreiche Kommentare zu meiner Arbeit. Vielen Dank auch an Thomas ‘D***head’ Garratt für das Durchlesen und Aufzeigen

[3] er scheint als Kind ein Quantenfeldtheorie-Buch verschluckt zu haben

einiger sprachlicher Aussetzer in meinem Entwurf. Besonderen Dank auch an Timon Emken für die tolle gemeinsame (leider viel zu kurze) Zeit als Bürokollegen.

Schließlich habe ich meinen Eltern und Freunden einen großes Dank auszusprechen für das Verständnis und die Unterstützung, auch wenn es manchmal mit mir "schwierich" war. Besonders meine Eltern haben mir hierbei ständig den Rücken freigehalten. Last but not least möchte ich Stefanie Damm danken für ihre Liebe und Geduld, dafür, mich trotz ihres eigenen Stress unterstützt und es immer wieder geschafft zu haben, meinen Kopf wieder freizumachen.